

70-11,815

HAFTEL, Michael Ivan, 1943-  
TWO-NUCLEON POTENTIALS AND NUCLEAR SATURATION.

University of Pittsburgh, Ph.D., 1969  
Physics, nuclear

University Microfilms, A XEROX Company , Ann Arbor, Michigan

TWO-NUCLEON POTENTIALS AND NUCLEAR SATURATION

By

Michael Ivan Haftel

B.S., The Pennsylvania State University, 1965

Submitted to the Graduate Faculty of  
Arts and Sciences in partial fulfillment  
of the requirements for the degree of  
Doctor of Philosophy

University of Pittsburgh

1969

UNIVERSITY OF PITTSBURGH

FACULTY OF ARTS AND SCIENCES

This dissertation was presented

by

Michael I. Haftel

It was defended on

October 16, 1969

and approved by

Dr. R. H. Pratt

Dr. R. M. Drisko

Dr. C. A. Hollingsworth

Dr. B. L. Cohen

Dr. F. Tabakin

Chairman

## FOREWORD

The author is very deeply indebted to Professor Frank Tabakin for suggesting this problem, for his guidance and for many helpful conversations. He also would like to thank Dr. David Clement and Mr. Frank Rybicki for invaluable assistance and advice in computer programming; to Professor M. Baranger and Mr. P. Kao for providing us with the motivation to examine the particle spectrum in nuclear matter; to Dr. R. Reid for clarifying the Coulomb corrections to his phase-shifts needed to check our computer codes; to Professor G. Breit for sending us his latest two-nucleon phase-shifts; and to Dr. B. Barrett for his assistance in proofreading this thesis. Special thanks are due to the author's wife, Donna, for typing the rough drafts of the manuscript.

The calculations in this thesis were performed at the University of Pittsburgh Computation Center. The research was supported by the National Science Foundation under Grant GP-9330. The financial support given to the author by the University of Pittsburgh in the form of an A. W. Mellon Fellowship, and by the National Science Foundation in the form of a N.S.F. Traineeship, is greatly appreciated.

A preliminary version of this work was presented to the Spring 1969 Meeting of the American Physical Society in Washington, D. C.

## TABLE OF CONTENTS

	Page
FOREWORD . . . . .	ii
I. INTRODUCTION . . . . .	1
II. THE TWO-BODY PROBLEM FOR NON-LOCAL POTENTIALS . . . . .	12
A. The Schroedinger Equation . . . . .	13
B. Partial Wave Decomposition of $V(\vec{k}, \vec{k}')$ . . . . .	14
C. Partial-Wave Expansion of the Schroedinger Equation for Scattering . . . . .	18
D. Solution of the Lippmann-Schwinger Equation - Failure of the Born Series . . . . .	24
E. Solution of the Lippmann-Schwinger Equation by Direct Matrix Inversion . . . . .	26
F. Evaluation of the Direct Matrix Inversion Technique . .	30
III. SOLUTION OF THE BETHE-GOLDSTONE EQUATION IN NUCLEAR MATTER .	35
A. Nuclear Matter . . . . .	36
B. The Rayleigh-Schroedinger Perturbation Series . . . . .	39
C. The Brueckner G Matrix and the Brueckner-Goldstone Expansion . . . . .	42
D. The Bethe-Goldstone Equation - Relative and Center-of-Mass Dependence . . . . .	44
E. Healing and the Convergence of the Brueckner-Goldstone Expansion . . . . .	47
F. Solution of the Bethe-Goldstone Equation - Elimination of Angular Dependence . . . . .	52

## Table of Contents Continued

	Page
1. Angle-Average Approximation . . . . .	52
2. The Effective Mass Approximation . . . . .	56
3. Self-Consistency . . . . .	57
G. Partial-Wave Decomposition of the Bethe-Goldstone Equation . . . . .	59
H. Solution of the Bethe-Goldstone Equation - Previous Methods . . . . .	62
I. The Direct Matrix Inversion Method of Solving the Bethe- Goldstone Equation . . . . .	64
J. Calculation of the Single-Particle Spectrum . . . . .	66
K. Calculation of the Binding Energy of Nuclear Matter . .	71
IV. A SMOOTH TRIPLET-EVEN POTENTIAL . . . . .	81
A. Smoothness and Tensor to Central Effects in the Two- Body and Many-Body Problems . . . . .	83
B. The Potential Model . . . . .	85
C. S-Wave Phase Shifts and Mixing Coefficient . . . . .	96
D. D-Wave Phase Shifts . . . . .	97
E. Forces A and B in the Nuclear Many-Body Problem . . .	99
V. NUCLEAR MATTER CALCULATIONS . . . . .	101
A. Smoothness Criteria . . . . .	102
B. Description of the Nuclear Matter Calculations . . . .	103
C. Results and Discussion . . . . .	105
1. Forces A and B . . . . .	105
2. Reid Soft-Core Potential . . . . .	120

Table of Contents Continued

	Page
3. The Bryan-Scott Potential . . . . .	128
a. Description of the Calculation and Results . . .	131
b. Classification of Mesons in the Bryan-Scott Potential for Nuclear Matter . . . . .	136
4. Appel Potential . . . . .	143
D. Summary and Explanation of the Importance of the Tensor Force . . . . .	144
E. A Canonical Transformation to Generate Phase-Shift- Equivalent Potentials . . . . .	153
F. Sensitivity of Binding Energies to the Particle Spectrum	160
VI. CONCLUSIONS . . . . .	172

APPENDICES

A1: ASYMPTOTIC FORM OF THE TWO-NUCLEON WAVE FUNCTION FOR SCATTERING . . . . .	177
A2: LAGUERRE INTEGRATION POINTS AND WEIGHTS FOR N > 15 . . .	183
B1: G MATRIX ELEMENTS FOR A SINGLE SEPARABLE POTENTIAL . .	190
B2: THE SINGLE-PARTICLE SPECTRUM . . . . .	193
B3: TOTAL BINDING ENERGY OF NUCLEAR MATTER . . . . .	199
C1: MATRIX ELEMENTS FOR GAUSSIAN POTENTIALS . . . . .	202
C2: EVALUATION OF THE RADIAL INTEGRALS NECESSARY FOR THE REID AND BRYAN-SCOTT POTENTIALS . . . . .	208
D1: CANCELLATION OF CERTAIN OPEP CONTRIBUTIONS . . . . .	212
D2: ELIMINATION OF ANGULAR DEPENDENCE IN THE ALTERED SINGLE-PARTICLE SPECTRUM . . . . .	216
REFERENCES . . . . .	219

## I. INTRODUCTION

The basic problem studied in this thesis is whether the binding energy of nuclei can be employed to fix the two nucleon interaction. In phenomenological treatments of the two-nucleon interaction, rather arbitrary decisions are made concerning the behavior of the interaction at short distances. This behavior can be described as either a local, strong repulsion, or as some form of nonlocality. In addition to the ambiguities concerning the behavior of the central force, there are ambiguities in the nature of the tensor force. The question then arises whether one can resolve these ambiguities in the description of the two-nucleon interaction on the basis of the binding energies of nuclei.

The main reason for employing non-local potentials in this thesis is that they provide a means of controlling the short-range correlations in the two-nucleon wave function. The types of nonlocalities used are suggested by meson theory<sup>1-6</sup> and by earlier phenomenological treatments.<sup>7,8</sup>

Since the elastic-scattering data does not uniquely fix the role of non-locality and of short-range correlations in the two-nucleon interaction, one must turn to alternate means of determining these properties. Since ultimately one desires to predict properties of nuclei from the two-nucleon interaction, the nuclear many-body problem offers one logical means to test the role of non-locality. This thesis, in particular, studies the role of non-locality and short-range correlations in infinite nuclear matter. The main goal is to determine whether smooth, non-local potentials<sup>9</sup> can produce nuclear saturation at nearly the correct energy and density. Such a determination is crucial for the validity of the Hartree-Fock technique as a means of calculating properties of nuclei.

Our motivation for employing infinite nuclear matter to test the sensitivity of nuclear binding energies to different forms of the two-nucleon interactions is twofold. First, Brueckner theory<sup>10-12</sup> allows us to calculate the binding energy and saturation density of nuclear matter for potentials of various smoothness. For infinite nuclear matter this calculation is much simpler than for finite nuclei. With Brueckner theory one generally avoids the convergence difficulties of Hartree-Fock theory. Second, while nuclear matter is not a real system, it does relate to finite nuclei through the volume term in the semi-empirical mass formula. Extrapolation of finite nuclei properties indicate that the correct binding energies of nuclear matter is -15.8 MeV per particle.<sup>13</sup> The correct density, as calculated by Brandow,<sup>14</sup> corresponds to a "Fermi momentum" of  $k_F = 1.36 F^{-1}$ . We use these numbers as a guide in determining what constraints nuclear matter places on the various forms of the two-nucleon interaction.

The principal technique we use to determine the role of non-locality is to employ potentials of varying smoothness. We might have found that nuclear-binding energies are relatively insensitive to the smoothness or non-local character of nuclear potentials. In this case, one might have, with confidence, proceeded to apply Hartree-Fock theory to smooth potentials to determine nuclear properties. However, we find that nuclear binding energies are sensitive to the smoothness of the nuclear force, which means that the Hartree-Fock procedure of predicting properties of nuclei has to be re-examined.

In our investigations we pay particular attention to the role of the tensor interaction. The tensor force causes convergence difficulties

in Hartree-Fock theory even for potentials having smooth, non-local, short-range repulsions.<sup>8,15,16</sup> We expect, therefore, that we will have to consider non-local tensor forces in a complete study of the role of non-locality.

A problem arises with respect to the tensor force. Most two-nucleon interactions used for Hartree-Fock calculations, such as the Tabakin interaction,<sup>16</sup> have strong enough tensor forces in the  $^3S_1 + ^3D_1$  eigenchannel so as to leave the question of convergence to second order unresolved. Therefore, we find it useful in our study of smoothness to develop a non-local potential model with a weak tensor force. We place two requirements on such a force. First, it must reproduce the two-body scattering data. Second, it must have sufficiently small off-energy-shell matrix elements for Hartree-Fock theory to converge with very small higher-order corrections. In particular, the off-energy-shell matrix elements of the tensor force in the  $^3S_1 + ^3D_1$  eigenchannel must be small. We expect that we will have to introduce non-local tensor forces to achieve such goals.

In developing a very smooth, non-local potential model, we anticipate that such a force will have a fairly complicated velocity dependence. We must be prepared to solve the two-body Schroedinger equation for general non-local potentials. We cannot use iteration of the Born series to solve the Schroedinger equation. Iteration fails in the  $^3S_1 + ^3D_1$  eigenchannel because of the deuteron-bound-state pole. We resolve this problem by solving the Schroedinger equation by direct inversion of the Lippman-Schwinger equation in momentum space. We are able to extend this technique to solving the Bethe-Goldstone equation for

nuclear matter. Momentum-space calculations enable us to handle the two-body problem and many-body problem in nuclear matter for any general non-local potential.

At this point a brief review of the two-nucleon interaction with respect to the many-body problem is helpful.

The first potentials developed to fit the scattering data in the 1950's were based on Jastrow's suggestion of employing an infinite hard core to account for the high-energy-scattering data.<sup>17</sup> The Gammel-Christian-Thaler<sup>18</sup> and Gammel-Thaler potentials<sup>19</sup> are examples of hard-core potentials of this period. These potentials are not suitable for the many-nucleon problem because they have infinite matrix elements. The Hartree-Fock approximation, which had been successful in atomic physics, could not be applied to hard core potentials having infinite matrix elements. With the advent of Brueckner theory,<sup>10,11</sup> hard-core potentials could be applied to calculate the properties of infinite nuclear matter. Brueckner theory handles the hard core by treatment of the singular potential in terms of a finite reaction matrix for scattering in a nuclear medium. An early calculation by Brueckner and Gammel,<sup>11</sup> which employed the Gammel-Thaler potentials, gave rough agreement with the volume term of the semi-empirical mass formula. However, a later calculation by Brueckner and Masterson<sup>12</sup> showed that phenomenological potentials give widely varying binding energies of nuclear matter. This result was not alarming because the potentials used also give different results in the two-body problem. However, the experimental two-body data of this period was not determined well enough to provide a basis for determining the best phenomenological potential.

While Brueckner theory is relatively simple to apply to nuclear matter, it becomes a complicated procedure for finite-nuclei calculations. The need for nonsingular potentials for use in Hartree-Fock finite nuclei calculations became apparent. The first attempts to develop finite potentials which fit the scattering data were made by Green,<sup>7</sup> and Levinger et al.<sup>8</sup> in 1962. These potentials used a short-range repulsion that was quadratic in momentum to replace the infinite hard core. Although such potentials do have finite off-energy-shell matrix elements, they prove to be unsuitable for Hartree-Fock calculations. Higher-order corrections to Hartree-Fock theory are especially large in the  $^3S_1 + ^3D_1$  state where the tensor force enters.

In 1964 Tabakin proposed a two-term, separable, non-local potential for application to Hartree-Fock calculations.<sup>16</sup> The Tabakin potential has been used extensively for Hartree-Fock calculations of binding energies and single-particle energies of finite nuclei<sup>20-22</sup> and for shell-model calculations.<sup>23</sup> The calculations of Svenne, Kerman, and Villars;<sup>20</sup> and Kerman and Bassichis,<sup>21</sup> showed that with second-order corrections the Tabakin potential gives nearly the experimental binding energy for nuclei up to Ca<sup>40</sup>. The radii of nuclei up to Ca<sup>40</sup>, as calculated with the Tabakin potential, are slightly too small.<sup>20</sup>

In the above calculations the investigators terminated their calculations at second-order corrections. The justification for this termination was the convergence ratio of 17% of the second-order potential energy to the first-order Hartree-Fock energy. If one terminates the calculation of the binding energy of nuclear matter for the Tabakin potential at second order, the result is a binding energy of -15 MeV

per particle. This value is extremely close to the correct value. A recent calculation that employs the methods of Brueckner theory indicates that the binding energy of the Tabakin potential is about -22 MeV per particle.<sup>24</sup> This result implies that termination at second-order corrections is a questionable procedure. This result also suggests that smooth potentials may cause over-binding. This thesis attempts to determine whether over-binding is necessarily characteristic of smooth potentials.

While some investigators attempted to develop potentials suitable for Hartree-Fock calculations, others attempted to fit the scattering data with high precision using hard-core potentials. The Yale<sup>25</sup> and Hamada-Johnston<sup>26</sup> hard-core potentials achieve very good fits to the two-body data. More recently, Reid,<sup>27</sup> using a hard-core potential, achieved an excellent fit to the two-body data. A nuclear matter calculation by Razavy,<sup>28</sup> with the Hamada-Johnston potential in 1963, demonstrated that the Hamada-Johnston potential gives -7.8 MeV binding energy per particle. This result essentially agreed with the earlier work of Brueckner and Masterson<sup>12</sup> that showed the Yale potential to give -8.3 MeV per particle. These binding energies are well below the correct value of -15.8 MeV. Finite or "soft"-core potentials were introduced to possibly reduce this discrepancy with the semi-empirical mass formula. Two such finite-core potentials were proposed by Reid<sup>27</sup> and by Bressel et al.<sup>29</sup> Calculations by Sprung in 1967,<sup>30</sup> and by Kallio and Day<sup>31</sup> in 1968, gave binding energies of -8.6 MeV and -9.4 MeV per particle for the Reid soft-core potential. The same investigators got values of -7.8 MeV and -6.8 MeV for the Reid hard-core potential. Therefore, soft-core potentials do

not reduce the discrepancy with the correct binding energy to any great degree.

The strong short-range repulsion and the strong tensor force are usually given as the main reasons for the saturation obtained with the Reid potentials. However, the relative importance of these two factors has not been fully explored. Also, whether the discrepancy with the semi-empirical mass formula is due to the strong short-range repulsion, the strong tensor force, or possible ambiguities in the summation of the Breuckner-Goldstone expansion for nuclear matter, is not known. In our nuclear matter calculations, we concentrate on the roles of the short-range repulsion and the tensor force. We discover, however, that possible incorrect calculation techniques using Brueckner theory could be causing the approximately 6 MeV disagreement with the semi-empirical mass formula (See Section V-F).

The work of Tabakin and Davies<sup>32</sup> has helped elucidate the role of the short-range repulsion. With their singlet-state potential, Tabakin and Davies were able to qualitatively fit the singlet-state phase shifts up to 300 MeV for  $L \leq 2$  with an extremely smooth potential. They achieved smoothness by allowing the short-range repulsion to have an exponential momentum dependence. This momentum dependence greatly reduces off-energy-shell matrix elements and short-range correlations. In nuclear matter their potential gave a  $^1S_0$  potential-energy contribution that was close to that obtained with the Reid soft-core potential. Tabakin and Davies' result implies that a strong, static, repulsive core may not be necessary for nuclear saturation. However, in their calculation Tabakin and Davies neglected the important  $^3S_1 + ^3D_1$  eigenchannel because

of the difficulty of solving the Schrödinger equation for non-local potentials in eigenchannels with a bound state. We speculate that if appreciable differences in binding energies exist between potentials of various smoothness, the discrepancy may be due to the strength of the tensor force.

In addition to the types of phenomenological potentials we have previously mentioned, some authors<sup>1-6, 33-35</sup> have attempted to derive two-nucleon potentials from meson theory. These potentials are called one-boson-exchange potentials(OBEPs). In the non-relativistic approximation terms quadratic in momentum are retained in these potentials. In the potentials proposed by Ingber<sup>6</sup>, and by Green and Sawada<sup>5</sup> quadratic momentum dependence in the tensor force is included in the non-relativistic limit. In the full relativistic forms of these interactions complicated, non-local forms appear. An important aspect of the numerical methods we have developed to handle general non-local potentials in the two-body problem and nuclear matter is that these methods can be applied to both the relativistic and non-relativistic forms of meson-theoretic interactions. As a first step in that direction, we calculate the binding energy of nuclear matter for the non-relativistic form of the Bryan-Scott potential.<sup>1-3</sup> We include this potential as part of a larger study to investigate the roles of non-locality and smoothness in the central and tensor parts of the two-nucleon interaction. By studying the Bryan-Scott potential, we also hope to determine whether the one-boson-exchange theory of nuclear forces can account for nuclear saturation.

Two points are clear from the previous discussion. First, the applicability of the Hartree-Fock approximation depends sensitively on

the nature of the short-range repulsion and on the strength of the tensor force. Second, the strengths of the short-range repulsion or tensor force may be crucial factors in nuclear saturation. If, for example, a strong short-range repulsion or a strong tensor force is proven to be necessary for saturation, the validity of Hartree-Fock theory as a means of predicting the properties of nuclei is in jeopardy.

Before we are able to investigate the role of non-locality in the two-nucleon interaction, we must be able to solve the Schrödinger equation for non-local potentials. A method for solving the Schrödinger equation for general non-local potentials is presented in Section II of this thesis. The method is based on direct inversion of the Lippmann-Schwinger equation in momentum space and can be applied to any finite, short-range potential.

In Section III of this thesis nuclear matter and the Bethe-Goldstone equation are discussed. We extend the numerical methods of Section II to solve the Bethe-Goldstone equation in momentum space. The method we propose again applies to any finite, short-range potential. We avoid the intermediate step of a reference-spectrum calculation by direct inversion of the Bethe-Goldstone equation in momentum space.

In Section IV the methods of Section II are used to develop two extremely smooth potential models for the triplet-even states. These potentials have exponential velocity dependence in the tensor force. The introduction of this velocity dependence in the tensor force helps reduce the off-energy-shell matrix elements of the tensor force. At the same time we are able to reproduce the experimental  $^3S_1 + ^3D_1$  and  $^3D_2$  phase parameters for elastic scattering with reasonable accuracy. These

potential models were developed in order to determine whether extremely smooth potential models, which fit the two-nucleon phase shifts, can saturate nuclear matter at nearly the correct energy and density.

In Section V we calculate the binding energies and saturation densities of nuclear matter for forces of varying degree of non-locality and smoothness. As expected, the potentials with more complicated velocity dependence are found to be smoother. As a measure of smoothness we employ the wound integral  $\kappa$  as defined by Brandow.<sup>36</sup> The significance of  $\kappa$  is also discussed in Section III. The results of our calculations indicate that strong tensor forces are necessary for nuclear saturation to occur at the correct density. On the other hand, the strong short-range repulsion plays only a minor role in nuclear saturation. We also examine the binding energies of exactly-phase-shift-equivalent potentials by employing a short-ranged canonical transformation suggested to us by F. Coester.<sup>37</sup> The relation between smoothness and nuclear-binding energies in this calcuation is consistent with that of the other calculations of Section V. In all of our nuclear-matter calculations we employ the current assumption of a free-particle spectrum for particles outside the Fermi sea. Near the end of Section V we examine the sensitivity of nuclear-binding energies to alternate choices of the particle spectrum for particles with momentum between  $k_F$  and  $2k_F$ . The sensitivity to the particle spectrum is found to be very significant in the  $^3S_1 + ^3D_1$  eigen-channel because of properties of the tensor force that are discussed in Section V. Our results indicate that further investigations into the convergence of the Breuckner-Goldstone expansion are necessary to accurately determine the binding energy of nuclear matter.

In Section VI conclusions based on the results of the calculations of Section V are presented. The most important conclusion is that the requirement of nuclear saturation rules out potentials with weak tensor forces. This conclusion contradicts the basic assumption of the Hartree-Fock method for calculating properties of nuclei. In Section VI we also suggest some future problems that can be studied with the calculative techniques developed in this thesis.

## II. THE TWO-BODY PROBLEM FOR NON-LOCAL POTENTIALS

Before investigating the role of non-locality in the nuclear many-body problem, one faces the task of solving the two-body Schrödinger equation for non-local potentials. For a potential to be suitable for predicting the properties of nuclei, it should at least be able to predict the experimental two-body properties with reasonable accuracy. Furthermore, the techniques used to solve the Bethe-Goldstone equation in the nuclear-many-body problem are based on techniques for solving the two-body problem. In this section we review the nuclear-two-body problem with special emphasis on non-local potentials. We develop a method of solving the two-body scattering problem by direct inversion of the Lippmann-Schwinger equation in momentum space. This method applies equally well to local and non-local potentials as long as the potentials are finite and short ranged. We apply this method to develop smooth, non-local, triplet-even-state potentials in Section IV of this thesis. With some modifications we also apply the direct-inversion technique to nuclear matter in Sections III and V.

Let us begin our discussion of the two-body problem with a description of the time-independent, non-relativistic Schrödinger equation in relative coordinates. The scattering solutions are emphasized because we ultimately want to be able to obtain scattering phase shifts from non-local-potential models.

### A. The Schrödinger Equation

The time-independent Schrödinger equation describing the motion of two-nucleons with total relative energy  $E_n$  is given by

$$-\frac{\hbar^2}{M} \nabla_{\vec{r}}^2 \psi_n(\vec{r}) + \int d^3r' V(\vec{r}, \vec{r}') \psi_n(\vec{r}') = E_n \psi_n(\vec{r}) , \quad (2-1)$$

where  $M$  is the nucleon mass,  $\vec{r} = \vec{r}_1 - \vec{r}_2$  denotes the relative displacement of nucleons one and two,  $V(\vec{r}, \vec{r}')$  is the interaction between the two nucleons, and  $\psi_n(\vec{r})$  is the relative part of the two-nucleon wave-function with eigenvalue  $E_n$ . The set of solutions  $\{\psi_n(\vec{r})\}$  to Eq. (2-1) determine such physically observable quantities as scattering cross sections, bound-state energies, and bound-state electric-quadrupole and magnetic-dipole moments. Equation (2-1) expresses the Schrödinger equation in configuration space, where the interaction  $V(\vec{r}, \vec{r}')$  may be non-local.

In momentum space the relative Schrödinger equation becomes

$$-\frac{\hbar^2}{M} k^2 \tilde{\psi}_n(\vec{k}) + \int d^3k' V(\vec{k}, \vec{k}') \tilde{\psi}_n(\vec{k}') = E_n \tilde{\psi}_n(\vec{k}) , \quad (2-2)$$

where  $\vec{k} = \vec{p}/M$  and  $\vec{p} = \frac{\vec{p}_1 - \vec{p}_2}{2}$  is the relative momentum between nucleons one and two. The wave-function  $\tilde{\psi}_n(\vec{k})$  is simply the Fourier transform of  $\psi_n(\vec{r})$ , i.e.

$$\tilde{\psi}_n(\vec{k}) = 1/(2\pi)^{3/2} \int d^3r' e^{-ik \cdot \vec{r}'} \psi_n(\vec{r}') . \quad (2-3)$$

The potential matrix elements in momentum space obey the relation

$$V(\vec{k}, \vec{k}') = 1/(2\pi)^3 \int d^3r d^3r' e^{-ik \cdot \vec{r}} e^{ik' \cdot \vec{r}'} V(\vec{r}, \vec{r}') e^{ik' \cdot \vec{r}'} . \quad (2-4)$$

The two-body, relative wave-functions depend on spin and isospin coordinates as well as on spatial or momentum coordinates. Consequently,  $V(\vec{r}, \vec{r}')$  and  $V(\vec{k}, \vec{k}')$  are operators in spin-isospin space.

For local potentials  $V(\vec{r}, \vec{r}') = V(\vec{r})\delta(\vec{r}-\vec{r}')$ . In this case Equation (2-1) simplifies to the familiar differential equation

$$-\frac{\hbar^2}{M} \nabla_{\vec{r}}^2 \psi_n(\vec{r}) + V(\vec{r})\psi_n(\vec{r}) = E_n\psi_n(\vec{r}) . \quad (2-5)$$

Many numerical methods exist to solve differential equations accurately and rapidly on modern computers. The solution of the Schroedinger equation for local potentials, therefore, is quite straightforward and will not be discussed further.

For non-local potentials the Schroedinger equation (2-1) is a three-dimensional integro-differential equation. In momentum space the Schroedinger equation is a three-dimensional integral equation for either local or non-local potentials. Since integral equations are fairly simple to solve, and because this thesis explores the properties of non-local potentials, we concentrate on solving the Schroedinger equation in momentum space.

### B. Partial Wave Decomposition of $V(\vec{k}, \vec{k}')$

To facilitate the solution of the Schroedinger equation, we reduce the three-dimensional integral equation to a set of one-dimensional integral equations by employing a partial-wave decomposition of the Schroedinger equation (2-2). The first step in the partial-wave decomposition of the Schroedinger equation is to expand  $V(\vec{k}, \vec{k}')$  in

partial waves. This partial-wave expansion in momentum space is given by

$$V(\vec{k}, \vec{k}') = \frac{2}{\pi} \frac{\hbar^2}{M} \sum_{LL', \alpha MT_3}^{L'-L} V_{LL'}^{\alpha}(k, k') y_{L'}^{\alpha M}(\hat{k}) y_{L'}^{+\alpha M}(\hat{k}') \quad (2-6)$$

The corresponding expansion for  $V(\vec{r}, \vec{r}')$  in configuration space is given by

$$V(\vec{r}, \vec{r}') = \frac{\hbar^2}{M} \sum_{LL', \alpha MT_3} V_{LL'}^{\alpha M}(r, r') \tilde{y}_L^{\alpha M}(\hat{r}) \tilde{y}_L^{+\alpha M}(\hat{r}') \quad (2-7)$$

where  $\alpha$  stands for the quantum numbers  $J$ ,  $S$ , and  $T$ . In the expansion (2-7),  $\tilde{y}_L^{\alpha M}(\hat{r})$  is an eigenfunction of  $\vec{J}^2$  with eigenvalue  $J(J+1)\hbar^2$ , of  $J_z$  with eigenvalue  $M\hbar$ , of  $\vec{L}^2$  with eigenvalue  $L(L+1)\hbar^2$ , of  $\vec{S}^2$  with eigenvalue  $S(S+1)\hbar^2$ , and of isospin  $\vec{T}$  with magnitude  $(T(T+1))$  and  $z$  component  $T_3$ . Explicitly,

$$\tilde{y}_L^{\alpha M}(\hat{r}) = y_{LS}^{JM}(\hat{r}) |TT_3\rangle = \sum_{M_L M_S} \langle M_L M_S | C_{LS} | JM \rangle Y_{LML}(\hat{r}) |SM_S\rangle |TT_3\rangle ,$$

where  $Y_{LML}(\hat{r})$  is a Legendre function and an eigenfunction of orbital angular momentum  $\vec{L}$ . The  $\langle M_L M_S | C_{LS} | JM \rangle$  are Clebsch-Gordan coefficients. The expressions  $\tilde{y}_L^{\alpha M}(\hat{r}) y_L^{+\alpha M}(\hat{r}')$  are operators in spin-isospin space as well as functions of  $\vec{r}$  and  $\vec{r}'$ . The expansion (2-6) is a result of the plane-wave decomposition

$$e^{i\vec{k}_0 \cdot \vec{r}} / (2\pi)^{3/2} = (2/\pi)^{\frac{1}{2}} \sum_{LM} i^L j_L(k_0 r) Y_{LML}^*(\hat{k}_0) Y_{LML}(\hat{r})$$

where  $(2/\pi)^{\frac{1}{2}} j_L(k_0 r)$  is an eigenfunction of  $\vec{p}^2$  with eigenvalue  $\hbar^2 k_0^2 r^2$ .

The expansions (2-6) and (2-7) define the most general expansions for a potential that conserves total relative angular momentum  $\vec{J}$ , total spin magnitude  $\vec{S}^2$ , and total isospin  $\vec{T}$ . Conservation of angular momentum and of isospin follow from the rotational invariance, charge symmetry,

and charge independence of the two-nucleon interaction. Space reflection invariance implies that the interaction  $V$  cannot connect states of opposite parity. Therefore,  $v_{LL'}^S(k, k')$  vanishes unless  $(-1)^L = (-1)^{L'}$ . The Pauli-exclusion principle limits the basis of eigenstates of the two-body system to those eigenstates that are anti-symmetric under interchange of position, spin, and isospin coordinates of the two nucleons. The Pauli exclusion principle, therefore, implies that the allowed basis of eigenvectors is limited to those eigenstates for which  $(-1)^{L+S+T} = -1$ . This restriction, along with conservation of parity, tells us that the magnitude of the total spin  $S$  is a conserved quantity. In Table I the allowed eigenstates of the two-nucleon system are shown. Pairs of eigenstates for which the interaction  $V$  may couple orbital angular momentum have a plus sign between them. The notation is the usual spectroscopic notation.

In our future discussion we shall employ the terms "eigenstate" and "eigenchannel". The term "eigenstate" and "eigenchannel" are synonymous for cases in Table I for which  $V$  may not couple two states of different orbital angular momenta. If  $V$  can couple the orbital angular momentum of one eigenstate with that of another eigenstate, we refer to the pair collectively as an "eigenchannel". If a potential  $V$  always conserves orbital angular momentum, i.e.

$$v_{LL'}^S(k, k') = v_L^S(k, k') \delta_{LL'} ,$$

then the potential is said to be a central potential. A potential of the form  $V = V(r)$  is an example of a central potential. If a potential can connect eigenstates with different orbital angular momenta, the potential is said to be a non-central or a tensor potential. The potential

TABLE I

Allowed eigenstates of the two nucleon system for  $J \leq 7$ . States that may couple orbital angular momentum have a plus sign between them. The notation is the usual spectroscopic notation.

		$T = 0$		$T = 1$	
$S = 0$		$^1P_1$	$^1H_5$	$^1S_0$	$^1F_4$
$S = 1$	$^1F_3$	$^1J_7$		$^1D_2$	$^1H_6$
	$^3S_1 + ^3D_1$	$^3G_5 + ^3I_5$		$^3P_0$	$^3F_4 + ^3H_9$
	$^3D_2$	$^3I_6$		$^3P_1$	$^3H_5$
	$^3D_3 + ^3G_3$	$^3I_7 + ^3K_7$		$^3P_2 + ^3F_2$	$^3H_6 + ^3J_6$
	$^3G_4$			$^3F_3$	$^3J_7$

$V = V(r)S_{12}(\hat{r})$ , where  $S_{12}(\hat{r}) = 3(\vec{\sigma}_1 \cdot \hat{r})(\vec{\sigma}_1 \cdot \hat{r}) - (\vec{\sigma}_1 \cdot \vec{\sigma}_2)$  and  $\vec{\sigma}$  represents the Pauli spin matrix, is an example of a tensor potential.

The final restrictions we place on the interaction is that it be time reversal invariant and Hermitian. These restrictions imply that  $v_{LL}^{\alpha}(k, k')$  must be a real, symmetric matrix, i.e.

$$v_{LL}^{\alpha}(k, k') = v_{L'L}^{\alpha}(k', k) = v_{L'L}^{*\alpha}(k', k) .$$

The matrix  $v_{LL}^{\alpha}(k, k')$ , subject to the invariances and symmetries mentioned above, provides the most general form of the two-nucleon interaction.<sup>38</sup>

### C. Partial-Wave Expansion of the Schroedinger Equation for Scattering

Now that we have the most general partial-wave expansion for  $V(\vec{k}, \vec{k}')$ , we wish to apply a partial-wave expansion to the Schroedinger Equation (2-2). For the scattering problem, let us first write the Schroedinger equation in a form that assures correct boundary conditions. For outgoing spherical-wave boundary conditions, the Schroedinger equation in momentum space is

$$\hat{\psi}^{(+)}(\vec{k}) = \delta(\vec{k} - \vec{k}_0) |SM_S> |TT_3> - \frac{M}{n^2} \int \frac{d^3 k' v(\vec{k}, \vec{k}') \psi^{(+)}(\vec{k}')}{(k'^2 - k_0^2 - i\epsilon)} \quad (2-8)$$

where  $n$  labels the incoming momentum  $\vec{k}_0$  and the incoming spin-isospin states of the two-body system. For standing-wave boundary conditions the Schroedinger equation becomes

$$\tilde{\psi}_n(\vec{k}) = \delta(\vec{k} - \vec{k}_0) |SM_S> |TT_3> - \frac{M}{n^2} P \int \frac{d^3 k' v(\vec{k}, \vec{k}') \psi_n(\vec{k}')}{(k'^2 - k_0^2)} \quad (2-9)$$

where P stands for a principal value contour. For numerical reasons we find it more convenient to work with (2-9) than with (2-8). In the following discussion, therefore, we solve the standing wave equation.

We may reduce (2-9) to a set of one-dimensional integral equations by expanding  $\tilde{\psi}_n(k)$  in partial waves. The most general partial-wave expansion of  $\tilde{\psi}_n(k)$  is given by

$$\tilde{\psi}_n(k) = \sum_{\alpha MLL, T_3} i^{L-L'} \psi_{LL', (k)}^{\alpha} Y_{LM_L}^*(\hat{k}_o) < JM | C_{LS} | M_L M_S > y_L^{\alpha M}(\hat{k}) . \quad (2-10)$$

The configuration-space equivalent of (2-10) is

$$\psi_n(\vec{r}) = \left( \frac{2}{\pi} \right)^{\frac{1}{2}} \sum_{\alpha MLL, T_3} i^{L-L'} \psi_{LL', (r)}^{\alpha} Y_{LM_L}^*(\hat{k}_o) < JM | C_{LS} | M_L M_S > y_L^{\alpha M}(\hat{r}) \quad (2-11)$$

where

$$\psi_{LL', (k)}^{\alpha} = \frac{2}{\pi} \int_0^{\infty} r^2 dr j_{L'}(kr) \psi_{LL', (r)}^{\alpha} . \quad (2-12)$$

In expressions (2-10,11,12) we let the label  $\alpha$  include the incoming momentum  $\vec{k}_o$ .

With the partial-wave expression (2-10) the Schrödinger equation, in eigenchannel  $\alpha$ , reduces to

$$\psi_{LL', (k)}^{\alpha} = \frac{\delta(k-k_o)}{k_o^2} \delta_{LL'} - \frac{2}{\pi} P \sum_{L'} \int_0^{\infty} k'^2 dk' V_{L'L}^{\alpha}(k, k') \psi_{LL', (k')}^{\alpha} . \quad (2-13)$$

To relate the wave-function in momentum space to the scattering phase-shifts, we define the reaction or R matrix by

$$R_{LL', (k, k_o)}^{\alpha} = \sum_{L'} \int_0^{\infty} k'^2 dk' V_{L'L}^{\alpha}(k, k') \psi_{LL', (k')}^{\alpha} . \quad (2-14)$$

The R matrix is related to the wave functions in momentum or configuration space by

$$\psi_{LL'}^{\alpha}(k) = \frac{\delta(k-k_o)}{k^2} \delta_{LL'} - \frac{2}{\pi} P \int_0^\infty \frac{dk' R_{LL'}^{\alpha}(k', k_o) \delta(k'-k_o)}{(k'^2 - k_o^2)} \quad (2-15)$$

and

$$\psi_{LL'}^{\alpha}(r) = j_L(k_o r) \delta_{LL'} - \frac{2}{\pi} P \int_0^\infty \frac{k'^2 dk' R_{LL'}^{\alpha}(k', k_o) j_{L'}(k' r)}{(k'^2 - k_o^2)} . \quad (2-16)$$

Furthermore, by application of (2-14) to (2-15) we may derive the one-dimensional Lippmann-Schwinger equation for R

$$R_{LL'}^{\alpha}(k, k_o) = V_{LL'}^{\alpha}(k, k_o) - \frac{2}{\pi} P \sum_L \int_0^\infty \frac{k'^2 dk' V_{LL'}^{\alpha}(k, k') R_{LL'}^{\alpha}(k', k_o)}{(k'^2 - k_o^2)} . \quad (2-17)$$

Since the scattering phase-shifts depend on the asymptotic form of  $\psi_{LL'}^{\alpha}(r)$  for  $r \rightarrow \infty$ , we evaluate (2-16) in the asymptotic limit in Appendix A1. The result is

$$k_o r \psi_{LL'}^{\alpha}(r) \xrightarrow[r \rightarrow \infty]{} \sin(k_o r - \frac{L\pi}{2}) \delta_{LL'} - k_o R_{LL'}^{\alpha}(k_o, k_o) \cos(k_o r - \frac{L'\pi}{2}) .$$

The scattered-wave part of the two-body wave function at large distances arises solely from the singularity at  $k' = k_o$  in the integrand of (2-16). With the asymptotic form of  $\psi_{LL'}^{\alpha}(r)$  we may evaluate the scattering phase-shifts. For uncoupled channels, the asymptotic wave function is proportional to  $\sin[k_o r - \frac{L\pi}{2} + \delta_L^{\alpha}(k_o)]$ ; therefore, the phase-shift

$\delta_L^\alpha(k_0)$  is given by

$$-\tan \delta_L^\alpha(k_0)/k_0 = R_{LL}^\alpha . \quad (2-18)$$

The shortened notation  $R_{LL}^\alpha$ , indicates the on-energy-shell matrix element  $R_{LL}^\alpha(k_0, k_0)$ . An important feature of the relation (2-18) is that, even for infinite hard-core potentials, the phase-shifts are finite.

Consequently, the R matrix is a finite quantity even for infinite hard-core potentials. The reduction of a singular potential to a finite reaction matrix is also the basis of Brueckner theory for the nuclear many-body problem.

For coupled channels the relations between the R matrix and the phase parameters are more complicated. In the Blatt-Biedenharn parametrization<sup>39</sup> the relations between the R matrix, the eigenphase-shifts, and mixing coefficients are given by

$$\tan \delta_{J-1}^\alpha(k_0) = -\frac{k_0}{2} \left[ R_{J-1,J-1}^\alpha + R_{J+1,J+1}^\alpha + \frac{R_{J-1,J-1}^\alpha - R_{J+1,J+1}^\alpha}{\cos 2\alpha} \right]$$

$$\tan \delta_{J+1}^\alpha(k_0) = -\frac{k_0}{2} \left[ R_{J-1,J-1}^\alpha + R_{J+1,J+1}^\alpha - \frac{R_{J-1,J-1}^\alpha - R_{J+1,J+1}^\alpha}{\cos 2\alpha} \right]$$

$$\tan 2\alpha(k_0) = \frac{2R_{J-1,J+1}^\alpha}{R_{J-1,J-1}^\alpha - R_{J+1,J+1}^\alpha} . \quad (2-19)$$

For the definition of these phase parameters in terms of the asymptotic wave functions, see Appendix A1.

A few observations on the significance of the R matrix are now useful. First, the on-energy-shell R matrix elements completely specify the scattering phase parameters from which one may construct the elastic-scattering cross sections. Second, the R matrix contains as much information as the two-nucleon wave function. By Equation (2-16) the off-energy-shell R matrix elements, i.e.  $R_{LL}^{\alpha}(k, k_0)$  for  $k \neq k_0$ , determine the wave function at finite distances. In particular, the second term on the right hand side of Eq. (2-16) gives the distortion in the two-nucleon wave function at finite distances. The magnitude of the off-energy-shell R matrix elements determine the short-range correlations or smoothness of the two-nucleon wave function. Because the off-energy-shell behavior of R and V are related by (2-17), strong short-range correlations ultimately result from large off-energy-shell V matrix elements. A third important point is that R satisfies a one-dimensional integral equation in each eigenchannel.<sup>40</sup> One may just as easily solve for the R matrix as for the wave functions  $\psi_{LL}^{\alpha}(k)$  for non-local potentials. Thus, our procedure will be to solve for the R matrix from which we can extract the elastic-scattering phase shifts.

From the R matrix we can also construct the standing wave solutions  $\tilde{\psi}_n(k)$  of the wave equation (2-9). These solutions are

$$\tilde{\psi}_n(k) = \delta(k - k_0) |S_M> |T_{T_3}> - \frac{M}{\pi^2} P \int \frac{d^3 k' R(k', k_0) \delta(k' - k_0)}{k'^2 - k_0^2} |S_M> |T_{T_3}>$$
(2-20)

where  $R(k', k_0)$  has the same partial-wave decomposition with respect to  $R_{LL}^{\alpha}(k', k_0)$  as  $V(k', k_0)$  has to  $V_{LL}^{\alpha}(k', k_0)$ . Furthermore,  $R(k', k_0)$  satisfies the well-known Lippmann-Schwinger equation

$$R(\vec{k}', \vec{k}_o) = V(\vec{k}', \vec{k}_o) - \frac{M}{\pi^2} P \int \frac{d^3 k' V(\vec{k}', \vec{k}) R(\vec{k}, \vec{k}_o)}{k'^2 - k_o^2}. \quad (2-21)$$

We do not employ Eq. (2-21) directly; however, in Section III we encounter a very similar integral equation for the Brueckner G matrix for nuclear matter. We then apply the technique of a partial-wave decomposition to solve for the G matrix.

In our previous discussion we could have solved the Schroedinger equation for the outgoing wave solution  $\downarrow_{LL}^{\alpha}(k)$ . The resulting reaction matrix would be  $T_{LL}^{\alpha}(k, k_o)$  where

$$T_{LL}^{\alpha}(k, k_o) = V_{LL}^{\alpha}(k, k_o) - \frac{2}{\pi} \sum_l \int \frac{k'^2 dk' V_{Ll}^{\alpha}(k, k') T_{ll}^{\alpha}(k', k_o)}{(k'^2 - k_o^2 - i\epsilon)}. \quad (2-22)$$

Equation (2-22) involves complex numbers. To facilitate numerical calculations, we solve (2-17) instead for the real matrix R.

The Lippmann-Schwinger equation (2-17) is a set of one-dimensional integral equations with one equation for each eigenchannel.<sup>40</sup> For short-range potentials, one may construct the two-body wave functions and elastic-scattering cross-sections by solving the Lippmann-Schwinger equation for a finite number of eigenchannels. The argument for this truncation is that two particles with high relative angular momentum never approach each other closely enough to feel the nuclear force. This argument holds as long as the potential between the particle falls off rapidly at large distances, i.e., it is short-ranged.

For short-ranged forces the easiest way of constructing the two-body wave functions and elastic-scattering cross-sections for non-local

potentials is to solve Eq. (2-17). Our main objective for the two-body problem, therefore, becomes to solve (2-17) for non-local potentials.

#### D. Solution of the Lippmann-Schwinger Equation -

##### Failure of the Born Series

One method of solving the Lippmann-Schwinger equation is to iterate on the right hand side of Eq. (2-17) in  $V$ . The resulting series is the Born series. Formally, the Lippmann-Schwinger equation can be written

$$R(\omega) = V + V \frac{P}{\omega - H_0} R(\omega) \quad (2-23)$$

where  $H_0$  is the unperturbed Hamiltonian. The Born series for  $R(\omega)$  becomes

$$R(\omega) = V + V \frac{P}{\omega - H_0} V + V \frac{P}{\omega - H_0} V \frac{P}{\omega - H_0} V + \dots \quad (2-24)$$

If  $V$  is singular or if  $V$  has large off-energy-shell matrix elements, the Born series diverges. The Born series, therefore, is inapplicable for strong potentials.

The Born series also fails if the Hamiltonian has bound states. The failure of the Born series follows from the formal solution

$$R(\omega) = V + V \frac{P}{\omega - H} V \quad (2-25)$$

of the Lippmann-Schwinger equation. One may expand the second term on the right hand side of (2-25) in terms of intermediate eigenstates of the

Hamiltonian  $H$ . The bound state contribution to the right hand side of (2-25) simply becomes the summation

$$\sum_m V|m > \frac{1}{\omega - E_m} < m|V$$

where the  $E_m$  are bound state eigenvalues. For  $\omega$  equal to any of the bound state eigenvalues, the  $R$  matrix becomes infinite. The Born series must diverge in such cases because the individual terms of the Born series are finite.

The failure of the Born series for potentials with bound states is also apparent from Levinson's theorem.<sup>41</sup> Levinson's theorem states

$$\frac{\delta_0(\infty) - \delta_0(0)}{\pi} = n$$

where  $\delta_0(k_0)$  is the S wave phase-shift and  $n$  is the number of bound states. For  $n > 0$ ,  $\delta_0$  must pass through  $\pi/2$  or odd multiples of  $\pi/2$  at least once. At energies for which  $\delta_0(k_0)$  is  $\pi/2$ ,  $R_{00}^\alpha(k_0, k_0)$  is infinite because the tangent of the phase-shift is infinite. We conclude that the Born series diverges near the energies at which  $\delta_0(k_0)$  passes through  $\pi/2$  or odd multiples of  $\pi/2$ .

Because of the inapplicability of the Born series to strong potentials or to potentials with a bound state, we have to resort to other methods of solving the Lippmann-Schwinger equation for non-local potentials. Numerical inversion of the Lippmann-Schwinger equation in momentum space provides the solution method we need.<sup>42</sup>

### E. Solution of the Lippmann-Schwinger Equation by Direct Matrix Inversion

To numerically invert the Lippmann-Schwinger equation in momentum space, we follow the suggestion made by several authors<sup>43-45</sup> to reduce the equation (2-17) to a set of simultaneous linear equations. The technique we employ to eliminate the singularity in the numerical solution of (2-17) permits us to solve the Lippmann-Schwinger equation directly and rapidly by computer.<sup>46</sup>

The first step to reduce (2-17) to linear equations is to remove the principal value in (2-17). With application of the identity

$$P \int_0^\infty \frac{dk' F(k')}{k'^2 - k_0^2} = \int_0^\infty dk' \frac{[F(k') - F(k_0)]}{k'^2 - k_0^2},$$

Eq. (2-17) becomes, for uncoupled channels,

$$R_{LL}^\alpha(k, k_0) = V_{LL}^\alpha(k, k_0) - \frac{2}{\pi} \int_0^\infty dk' \frac{[k'^2 V_{LL}^\alpha(k, k') R_{LL}^\alpha(k', k_0) - k_0^2 V_{LL}^\alpha(k, k_0) R_{LL}^\alpha(k_0, k_0)]}{k'^2 - k_0^2} \quad (2-26)$$

The value of the integrand in (2-26) in the limit  $k' \rightarrow k_0$  becomes

$$\frac{2k_0 V_{LL}^\alpha(k, k_0) R_{LL}^\alpha(k_0, k_0) - k_0^2 V_{LL}^\alpha(k_0, k_0) R_{LL}^\alpha(k_0, k_0) - k_0^2 V_{LL}^\alpha(k_0, k_0) R_{LL}^\alpha(k_0, k_0)}{2k_0} \quad (2-27)$$

where

$$V_{LL}^{\alpha'}(k_0, k_0) = \partial/\partial k' [V_{LL}^\alpha(k_0, k')] \Big|_{k'=k_0}$$

and

$$R_{LL}^{\alpha'}(k_o, k_o) = \partial/\partial k' [R_{LL}^{\alpha}(k', k_o)] \Big|_{k'=k_o} .$$

The limit (2-27) indicates that the integrand in (2-26) is a finite, well-defined function of  $k'$  and  $k_o$  even in the limit  $k' \rightarrow k_o$ . Consequently, the integral in (2-26) is well-defined. We may therefore apply the following numerical techniques to solve (2-26).

By the application of an  $N$  point Laguerre infinite integration formula

$$\int_0^\infty dk f(k) \approx \sum_{j=1}^N f(k_j) W_j ,$$

Eq. (2-26) becomes

$$R_{LL}^{\alpha}(k, k_o) \approx V_{LL}^{\alpha}(k, k_o) - \frac{2}{\pi} \sum_{j=1}^N k_j^{-2} \frac{V_{LL}^{\alpha}(k, k_j) R_{LL}^{\alpha}(k_j, k_o) W_j}{k_j^{-2} k_o^{-2}} \\ + \frac{2}{\pi} \left( \sum_{m=1}^N \frac{W_m}{k_m^{-2} - k_o^{-2}} \right) k_o^{-2} V_{LL}^{\alpha}(k, k_o) R_{LL}^{\alpha}(k_o, k_o) . \quad (2-28)$$

The  $k_j$  are called the grid points and the  $W_j$  are called the weights of the Laguerre integration formula. Because the standard tables<sup>47</sup> list the Laguerre points and weights only for  $N \leq 15$ , we calculated the Laguerre points and weights numerically for selected values of  $N$  for  $N > 15$ . These grid points and weights appear in Appendix A2. The application of infinite integration formulas other than the Laguerre formula are also valid. The best integration formula will vary from potential to potential. The Laguerre formula gives the best results when the integrand in Eq. (2-26) decays exponentially with  $k'$ . For a less rapid

decay, as occurs for the Reid-soft core potential, the Gaussian formula

$$\int_0^1 f(y) dy = \sum_{i=1}^N f(y_i) w_i$$

with the mapping

$$k_i = \tan \frac{\pi}{2} y_i$$

$$w_i = \frac{\pi}{2} w_i \sec^2 y_i$$

gives somewhat better precision than the Laguerre formula for a fixed  $N$ . For a large enough number of points, of course, the results obtained by either integration formula should converge to a common value.

To reduce Eq. (2-28) to a finite number of simultaneous linear equations, we evaluate (2-29) at  $k = k_i$ ,  $i = 1, \dots, N$ . We also evaluate (2-28) at  $k = k_{N+1} \equiv k_o$ . The resulting set of  $N + 1$  equations for the  $N + 1$  unknowns

$$R_{LL}^\alpha(k_i, k_o) \quad i = 1, \dots, N+1$$

is given by

$$R_{LL}^\alpha(k_i, k_o) = v_{LL}^\alpha(k_i, k_o) - \frac{2}{\pi} \sum_{j=1}^N \frac{k_j^2 w_j v_{LL}^\alpha(k_i, k_j) R_{LL}^\alpha(k_j, k_o)}{k_j^2 - k_o^2} \\ + \frac{2}{\pi} \left( \sum_{m=1}^N \frac{w_m}{k_m^2 - k_o^2} \right) k_o^2 v_{LL}^\alpha(k_i, k_o) R_{LL}^\alpha(k_{N+1}, k_o) \quad (2-29)$$

$$i = 1, \dots, N + 1 .$$

The only restriction we must place on the set of equations (2-29) is that  $k_o$  is not equal or extremely close in value to one of the grid

points of the integration formula. We thereby avoid unreasonably large numbers in our computer code. For any arbitrary value for  $k_o$ , except for the finite set of values corresponding to the  $N$  grid points, the set of equations (2-29) has consistent solutions. Since none of the denominators of (2-29) vanish, the derivatives of  $V$  and  $R$  do not enter into the numerical solution of (2-29). Our choice of  $k_{N+1} = k_o$  enables us to solve for the on-energy shell matrix elements  $R_{LL}^\alpha(k_o, k_o)$  for almost any value of incoming momentum  $k_o$ . We may then directly extract the phase parameters for elastic scattering. The elimination of the singularity in the integrand of (2-17) by the equation (2-26), and the choice of evaluating (2-27) at  $k_{N+1} = k_o$ , are the principal differences between our method and those proposed previously.<sup>48</sup>

To solve (2-29) we define  $w'_j$  by

$$w'_j = \frac{2}{\pi} \frac{k_j^2 w_j}{(k_j^2 - k_o^2)} \quad j = 1, \dots, N$$

$$w'_{N+1} = -\frac{2}{\pi} \left( \sum_{m=1}^N \frac{w_m}{k_m^2 - k_o^2} \right) k_o^2 .$$

The set of equations (2-29) then becomes

$$R_{LL}^\alpha(k_i, k_o) = V_{LL}^\alpha(k_i, k_o) - \sum_{j=1}^{N+1} V_{LL}^\alpha(k_i, k_j) w'_j R_{LL}^\alpha(k_j, k_o) . \quad (2-30)$$

With the definition

$$F_{ij} = \delta_{ij} + w'_j V_{LL}^\alpha(k_i, k_j) ,$$

Eq. (2-30) can be rewritten in the relatively simple form

$$\sum_{j=1}^{N+1} F_{ij} R_{LL'}^{\alpha}(k_j, k_o) = v_{LL'}^{\alpha}(k_j, k_o) \quad i = 1 \dots N+1 \quad . \quad (2-31)$$

Equation (2-31) is solved by numerical inversion of the matrix F.

For coupled channels the solution of the Lippmann-Schwinger equation proceeds in a similar fashion. The unknowns are the  $(2N+2)$  quantities  $R_{J-1,L'}^{\alpha}(k_i, k_o)$  and  $R_{J+1,L'}^{\alpha}(k_i, k_o)$ ,  $i = 1 \dots N+1$ , for a fixed  $L'$ ,  $\alpha$ , and  $k_o$ . Solution is again by the numerical inversion of the  $(2N+2)$  dimensional coefficient matrix F where

$$F = \begin{pmatrix} & & \\ & F^{J-1,J-1} & F^{J-1,J+1} \\ & & \\ F^{J+1,J-1} & & F^{J+1,J+1} \end{pmatrix}$$

and  $F_{ij}^{LL'} = v_{LL'}^{\alpha}(k_i, k_j) w_j + \delta_{LL'} \delta_{ij}$ . The only difference from the uncoupled case is that the matrix size is enlarged to include the L and  $L'$  labels.

#### F. Evaluation of the Direct Matrix Inversion Technique

To judge the accuracy of the direct-matrix-inversion technique, we chose two test potentials — a  ${}^1S_0$  finite-core potential and the Reid soft-core  ${}^1S_0$  potential.<sup>27</sup> The finite-core potential chosen has a square-well repulsion of strength 100 MeV and a range of .4 Fermis. To this repulsion we added a square-well attraction of depth 50 MeV and range of 2.5 Fermis, which gives the finite-core potential a  ${}^1S_0$  bound state. This finite-core potential provides an excellent test of the direct-matrix-

inversion technique because the potential has an extremely strong short-range repulsion and a bound state. Furthermore, we may check the accuracy of the direct-matrix-inversion method because the phase-shifts for this potential are known analytically. The Reid-soft-core potential is also considered because it is another potential with large matrix elements for which the phase-shifts are accurately known. The results of these test calculations appear in Tables II and III.

The results in Tables II and III demonstrate that direct matrix inversion provides an excellent means of solving the Schroedinger equation in the scattering problem for finite potentials. The direct-matrix-inversion method gives excellent precision even when the potential has large matrix elements. For the Reid  $^1S_0$  soft-core potential, the computer time required is only 11 seconds for seven energies and 24 grid points on the 7090 computer. The precision obtained is better than .001 radians for the Reid  $^1S_0$  soft-core potential with 24 Gaussian points. The precision for the bound-state, finite-core potential is .003 radians for 25 Laguerre points. These small numerical errors in our calculations are negligible compared to the errors in the experimental determination of the two-nucleon phase-shifts. Furthermore, the calculated phase-shifts are stable as one increases the number of grid points.<sup>49</sup> Stability with increasing number of grid points is an important requirement for the direct-matrix-inversion method to be reliable.

Since direct matrix inversion is very successful in solving the two-body problem for general finite potentials, the next logical step is to extend the matrix-inversion technique to the nuclear-many-body problem. The next section of this thesis deals with the description of Brueckner

TABLE II

Comparison of matrix inversion  $^1S_0$  phase-shifts and analytic  $^1S_0$  phase-shifts for a finite-core plus square-well potential. Laguerre integration routines are used. All phase-shifts are in radians.

Lab Energy (MeV)	N = 15	N = 25	Analytic
2.00	2.61207	2.61298	2.61284
20.75	1.61056	1.62751	1.62413
100.00	.50375	.50486	.50385
140.27	.25500	.25821	.25851
200.00	.04529	.04903	.04984
300.00	- .10612	- .10831	- .10694

TABLE III

Comparison of matrix inversion  $^1S_0$  phase-shifts and real  $^1S_0$  phase-shifts for the Reid soft-core potential. Real phase-shifts are taken from reference 27. We adjust the phase-shifts in Reference 27, which include the Coulomb interaction, to nuclear phase-shifts according to the Coulomb corrections also listed in Reference 27. Gaussian integration routines are used. All phase-shifts are in radians.

Lab Energy (MeV)	N = 16	N = 24	Real
24	.86182	.86071	.86055
48	.68560	.68466	.68459
96	.44111	.44080	.44019
144	.26395	.26310	.26303
208	.08135	.08040	.08033
352	-.21511	-.21630	-.21638

theory and nuclear matter. We show there how to apply the direct-matrix-inversion technique to solve the Bethe-Goldstone equation for nuclear matter.

### III. SOLUTION OF THE BETHE-GOLDSTONE EQUATION IN NUCLEAR MATTER

To study the influence of the various aspects of the two-nucleon interaction on nuclear-binding energies, one must first develop a valid technique of calculating the binding energy of the many-nucleon system. The linked-cluster Rayleigh-Schroedinger perturbation theory expansion for the ground-state energy of the many-nucleon system provides the basis for calculations of nuclear binding energies. The Rayleigh-Schroedinger perturbation expansion is essentially an expansion in powers of  $V$ , where  $V$  denotes the two-nucleon interaction. Since many modern potential models employ a singular, or nearly singular short-range repulsion, or have strong tensor forces, an expansion in  $V$  does not converge. To remedy this convergence difficulty, Brueckner<sup>10,11</sup> grouped selected terms in the perturbation expansion and summed them to obtain a reaction matrix  $G$ . The Brueckner-Goldstone<sup>50</sup> expansion quantitatively relates the ground-state energy of the many-body system to the finite  $G$  matrix. The  $G$  matrix plays the role of an effective interaction of two particles in a nuclear medium. By the definition of the  $G$  matrix, which we shall shortly present,  $G$  is finite even for singular potentials in much the same way that the reaction  $R$  matrix for free scattering is finite for singular potentials. In fact, the equation that defines  $G$ , the Bethe-Goldstone equation, resembles the Lippmann-Schwinger equation for  $R$ . Because of the finiteness of  $G$ , the Brueckner-Goldstone expansion for the ground-state energy converges much more rapidly than the Rayleigh-Schroedinger perturbation expansion in  $V$ .

While Brueckner theory is relatively difficult to apply to finite nuclei, infinite nuclear matter provides a simple means of applying the

methods of Brueckner theory to the many-nucleon problem. Nuclear matter serves as a testing ground for the applicability of Brueckner theory. Thus, the main goals of this section are to study the properties of nuclear matter in terms of the Brueckner G matrix and to solve the Bethe-Goldstone equation. One of the results of this section is that the technique of direct matrix inversion is applicable to the solution of the Bethe-Goldstone equation for general non-local potentials. We shall make use of this technique to study the properties of non-local potentials in nuclear matter.

#### A. Nuclear Matter

Nuclear matter is a hypothetical system consisting of an equal number of protons and neutrons. The Coulomb interaction is absent and the number of particles, A, approaches infinity. Translational invariance of nuclear matter implies that the particle density  $\rho$  is constant and the single-particle wave functions, or "orbitals", are plane waves. In configuration space the single-particle orbitals,  $\phi_\mu(\vec{r}_1)$ , are given by

$$\phi_\mu(\vec{r}_1) = \langle \vec{r}_1 | \mu \rangle = \frac{e^{i\vec{k}_\mu \cdot \vec{r}_1}}{\Omega^{\frac{1}{2}}} | s_\mu t_\mu \rangle \quad (3-1)$$

where  $s_\mu$  labels the spin state of the nucleon, and  $t_\mu$  is the iso-spin label ( $+\frac{1}{2}$   $\rightarrow$  proton,  $-\frac{1}{2}$   $\rightarrow$  neutron). The volume that encloses the nucleons,  $\Omega$ , appears in Eq. (3-1) to normalize the single-particle orbitals. For an infinite system, both A and  $\Omega$  approach infinity, but the particle density  $\rho = A/\Omega$  remains finite.

In the ground state of nuclear matter the A particles fill the lowest available single-particle orbitals consistent with the Pauli exclusion principle and the periodic boundary conditions on the plane waves. These boundary conditions are  $\vec{k}_\mu = 2\vec{n}_\mu \pi/\Omega^{1/3}$ , where  $\vec{n}_\mu$  is a vector with integer components. For an infinite system, the number of particles, A, becomes infinite, and the single-particle orbitals have a continuous distribution in momentum up to a maximum momentum of  $k_F$  — the Fermi momentum. In addition, half of the particles of each type (protons and neutrons) have spin up, and half have spin down. The unperturbed many-body wave function for such a system is

$$\phi_0(\vec{r}_1, \dots, \vec{r}_A) = \mathcal{A} \prod_{\mu=1}^A \psi_\mu(\vec{r}_\mu) .$$

The antisymmetrization operator  $\mathcal{A}$  assures that  $\phi_0$  is normalized and antisymmetric upon interchange of any pair of particles. In the limit of A and  $\Omega$  becoming infinite, the summation  $\sum_{\mu=1}^A$  becomes

$$\sum_{\mu=1}^{\frac{1}{2}} s_\mu t_\mu \quad \Omega/(2\pi)^3 \int_{k_\mu < k_F} d^3 k_\mu . \quad (3-2)$$

As a consequence of (3-2), the total kinetic energy, T, of the system becomes  $T = \frac{3\pi^2 k_F^2 A}{5M}$ , and the particle density  $\rho$  is  $\rho = 2k_F^3/(3\pi^2)$ .

The basic assumption one makes in nuclear-matter calculations is that the energy per particle corresponds to the volume term,  $C_1$ , which is the only surviving term in the infinite limit of the semi-empirical mass formula  $\frac{E}{A} \approx C_1 + C_2/A^{1/3} + C_3 Z^2/A + C_4 (N-Z)^2/A^2$ .

Here A, N, and Z denote the numbers of nucleons, neutrons, and protons, respectively. Nuclear-matter calculations thereby exclude the effects of the surface term,  $C_2 A^{-1/3}$ , and the Coulomb term,  $C_3 A^2/A$ . The symmetry term,  $C_4 (N-Z)^2/A^2$ , simply indicates that, in the absence of the Coulomb repulsion, the number of protons and neutrons should be equal.

While nuclear matter is not a real system, it does relate to finite nuclei through the volume term of the semi-empirical mass formula. Furthermore, the central regions of complex nuclei are expected to resemble nuclear matter.

The main goal of nuclear-matter calculations is to calculate the binding energies of nuclear matter as a function of density. The density at which the binding energy per particle is a minimum, or the saturation density, is the density at which nuclear matter should constitute a stable configuration. The basic criterion one places on a potential model in nuclear-matter calculations is that the potential produces saturation at the correct binding energy and density. This expected binding energy, as given by the semi-empirical mass formula, is  $E/A = C_1 = -15.8 \text{ MeV/particle}$ .<sup>13</sup> The equilibrium density of nuclear matter, according to Brandow's analysis,<sup>14</sup> corresponds to a Fermi momentum of  $k_F = 1.36 F^{-1}$ . This value results from the study of the interior density of finite nuclei after Coulomb and surface effects have been accounted for.

By considering nuclear matter, we eliminate one of the most difficult problems of finite nucleus Brueckner-Hartree-Fock calculations — the self-consistent determination of the single-particle orbitals. The

elimination of this problem allows us to apply Brueckner theory to nuclear matter with relative ease. Our ultimate goal is to use Brueckner theory to study nuclear saturation. We now describe Brueckner theory as applied to nuclear matter. We begin with a discussion of Rayleigh-Schroedinger perturbation theory.

### B. The Rayleigh-Schroedinger Perturbation Series

The Rayleigh-Schroedinger perturbation series expresses the ground-state energy of the many-nucleon system in powers of the perturbation Hamiltonian  $H_1$ , where the total Hamiltonian  $H$  is  $H = H_0 + H_1$  and  $H_0$  is the unperturbed Hamiltonian. In addition to kinetic energy, the unperturbed Hamiltonian may include a sum of single-particle potentials,  $U = \sum U_i$ , where  $U_i$  represents an "average" single-particle potential. In nuclear matter translational invariance requires that  $U$  be diagonal in the plane-wave single-particle basis. Furthermore, since nuclear matter is rotationally invariant as well, we should expect  $U$  to be independent of the direction of the single-particle momentum. While  $U$  is arbitrary, clearly a good choice of  $U$  is such as to make the perturbation Hamiltonian small. In Hartree-Fock theory the best choice of  $U$  is specified by the relation

$$\langle \mu | U_{HF} | \mu \rangle = \sum_{\alpha=1}^A \langle \mu\alpha | V | \mu\alpha - \alpha\mu \rangle .$$

For Brueckner theory, Bethe, Brandow, and Petschek<sup>51</sup> specify the best choice of  $U$  in a related manner. We shall return to this point later.

If the total Hamiltonian is denoted by

$$H = \sum_{i=1}^A T_i + \frac{1}{2} \sum_{i,j < A} V_{ij},$$

where  $V_{ij}$  denotes the two-nucleon interaction between particles  $i$  and  $j$ , the perturbation Hamiltonian becomes

$$H_1 = \frac{1}{2} \sum_{i,j < A} V_{ij} - \sum_{i=1}^A U_i.$$

The zero, first, and second-order terms in the Rayleigh-Schroedinger perturbation series for the ground-state energy are given by

$$E^{(0)} = \frac{3\pi^2 k_F^2 A}{5M} + \sum_{\mu=1}^A \langle \mu | U | \mu \rangle \quad (3-3)$$

$$E^{(1)} = \langle \phi_0 | H_1 | \phi_0 \rangle = \frac{1}{2} \sum_{\mu, \nu < A} \langle \mu \nu | V | \mu \nu - \nu \mu \rangle - \sum_{\mu=1}^A \langle \mu | U | \mu \rangle \quad (3-4)$$

$$\begin{aligned} E^{(2)} &= \langle \phi_0 | H(E_0 - H_0)^{-1} P H_1 | \phi_0 \rangle \\ &= \frac{1}{2} \sum_{\substack{\mu, \nu < A \\ \alpha, \beta > A}} \langle \mu \nu | V | \alpha \beta \rangle (E_\mu + E_\nu - E_\alpha - E_\beta)^{-1} \langle \alpha \beta | V | \mu \nu - \nu \mu \rangle. \end{aligned} \quad (3-5)$$

In the above expressions  $\phi_0$  is the unperturbed ground-state Slater determinant for the system,  $E^{(0)}$  is the unperturbed ground-state energy, and  $P$  is a projection operator that projects out any intermediate many-body state that is equal to  $\phi_0$ . The  $E_\alpha$  are the single-particle energies.

The cancellation of U terms up to second order necessitates the consideration of at least third-order terms to intelligently choose the best single-particle potential. The antisymmetrized kets  $|\mu\nu - \nu\mu\rangle$  that appear in Equations (3-4,5) result from the Pauli exclusion principle. Only intermediate two-body states with both momenta above the Fermi sea ( $k_\alpha, k_\beta > k_F$ ) appear in (3-5). The corresponding many-body intermediate states, ones for which two "hole" state particles ( $k_\mu, k_\nu < k_F$ ) are excited to two "particle" states ( $k_\alpha, k_\beta > k_F$ ), are the only intermediate many-body states that conserve total momentum for nuclear matter and obey the Pauli-exclusion principle. The projection operator P, which projects out any many-body states equal to the original Slater determinate, prevents any second-order U terms from appearing.

Formally, the perturbation expansion to second order becomes

$$E = T + \frac{1}{2} \sum_{\mu, \nu < A} \langle \mu\nu | V + V \frac{Q}{e} V | \mu\nu - \nu\mu \rangle , \quad (3-6)$$

where

$$\frac{1}{e} |\gamma\delta\rangle = \frac{1}{\omega - E_\gamma - E_\delta} |\gamma\delta\rangle$$

and

$$\begin{aligned} Q|\gamma\delta\rangle &= |\gamma\delta\rangle \text{ if } k_\gamma, k_\delta > k_F \\ &= 0 \text{ otherwise.} \end{aligned}$$

For the terms we have considered so far  $\omega = E_\mu + E_\nu$ . The Q operator in Eq. (3-6) is a direct consequence of the Pauli-exclusion principle.

Terms of the form (3-6) appear not only up to second order, but in all orders of the perturbation expansion. In fact, infinite sequences of the form

$$\langle \alpha\beta | V + V \frac{Q}{e} V + V \frac{Q}{e} V \frac{Q}{e} V + \dots | \gamma\delta \rangle, \text{ where } e = \omega - H_0 \quad (3-7)$$

appear repeatedly in the perturbation expansion. To sum the Rayleigh-Schroedinger perturbation series in terms of the infinite sequences (3-7), we must first consider the possible causes for divergences of the perturbation expansion.

Two types of divergences arise in the Rayleigh-Schroedinger perturbation expansion. The first is a divergence in the number of particles. This divergence arises from the presence of the so-called "unlinked cluster diagrams". The contribution of each type of these diagrams, in the limit  $A \rightarrow \infty$ , is proportional to  $A^2$ .<sup>52</sup> The energy per particle, therefore, becomes infinite. Goldstone<sup>50</sup> demonstrated that the contributions from unlinked cluster diagrams of all types exactly summed to zero in each order of the perturbation series. Therefore, the energy per particle remains finite. Moreover, we need consider only the "linked cluster" expansion.. The infinite sequences (3-7) are encountered in this linked cluster expansion.

The second divergence occurs if  $V$  is singular or has large off-energy-shell matrix elements. In this case the individual terms in (3-7) are large and the "linked cluster", or Goldstone expansion,<sup>50</sup> diverges. This is the divergence Brueckner theory was designed to handle.

### C. The Brueckner G Matrix and the Brueckner-Goldstone Expansion

Brueckner<sup>10,11</sup> handled the divergence of (3-7) by defining a reaction matrix  $G$  by the operator equation

$$G(\omega) = V + V \frac{Q}{e} G(\omega) . \quad (3-8)$$

Iteration of the right-hand side of (3-8) in powers of  $V$  reproduces the infinite sequence (3-7), which shows that the  $G$  matrix represents a sum of the so-called ladder diagrams.

The above definition of  $G(\omega)$  resembles the operator equation for the  $R$  matrix,  $R(\omega) = V + V \frac{1}{\omega - H_0} R(\omega)$ . The Born series for  $R$ , in turn, resembles the infinite sequence (3-7). We recall from Section II that  $R$  is finite even if  $V$  is singular. Likewise, we expect that  $G(\omega)$  is finite for singular potentials.

With the definition (3-8) we can now regroup the perturbation expansion for the ground-state energy in terms of the appropriate  $G$  matrix elements. The resulting Brueckner-Goldstone expansion expresses the ground-state energy of nuclear matter in powers of  $G$ . To lowest order in  $G$  the ground-state energy of nuclear matter becomes<sup>53</sup>

$$E \approx T + \frac{1}{2} \sum_{\mu\nu<A} <\mu\nu|G(E_\mu+E_\nu)|\mu\nu - v_\mu> . \quad (3-9)$$

The evaluation of (3-9) is straightforward once the on-energy-shell  $G$  matrix is known. Indeed, Equation (3-9) states that the ground-state energy of nuclear matter is simply obtained from pair-interaction energies summed over all pairs in the Fermi sea. These interactions are represented by the diagonal  $G$  matrix elements. The  $G$  matrix approximately takes into account the presence of the other particles through the  $Q$  operator and the single-particle spectrum. Since the on-energy-shell  $G$  matrix satisfies an equation similar to the Lippmann-Schwinger equation for free scattering, the problem of determining the ground-state energy of nuclear matter becomes similar to solving a two-body problem. Thus, the previously described techniques for solving the

two-body problem should be applicable for solving for the G matrix. We now discuss the reduction of the Bethe-Goldstone equation to an integral equation. We also discuss the validity of Equation (3-9).

#### D. The Bethe-Goldstone Equation—Relative and Center-of-Mass Dependence

Explicitly, in terms of two-body matrix elements, the Bethe-Goldstone equation is

$$\langle \alpha\beta | G(\omega) | \mu\nu \rangle = \langle \alpha\beta | V | \mu\nu \rangle + \sum_{\gamma\delta>A} \langle \alpha\beta | V | \gamma\delta \rangle (\omega - E_\gamma - E_\delta)^{-1} \langle \gamma\delta | G(\omega) | \mu\nu \rangle . \quad (3-10)$$

To cast Equation (3-10) in an integral-equation form similar to the Lippmann-Schwinger equation, we define the relative and center-of-mass quantities

$$\begin{aligned} \vec{k}_{\mu\nu} &= (\vec{k}_\mu - \vec{k}_\nu)/2 & \vec{r} &= \vec{r}_1 - \vec{r}_2 \\ \vec{K}_{\mu\nu} &= (\vec{k}_\mu + \vec{k}_\nu)/2 & \vec{R} &= (\vec{r}_1 + \vec{r}_2)/2, \end{aligned}$$

where  $k_\mu$  and  $k_\nu$  label the momentum of the single-particle orbitals, and  $\vec{r}_1$  and  $\vec{r}_2$  label the single-particle coordinates for a pair 1,2.

With these coordinates the unperturbed two-body wave function  $\phi_{\mu\nu}$  is expressed, in configuration space, as

$$\begin{aligned} \phi_{\mu\nu}(\vec{r}_1, \vec{r}_2) &= \langle \vec{r}_1 \vec{r}_2 | \mu\nu \rangle = e^{i\vec{k}_\mu \cdot \vec{r}_1} e^{i\vec{k}_\nu \cdot \vec{r}_2/\Omega} | s_\mu t_\mu \rangle | s_\nu t_\nu \rangle \\ &= e^{i2\vec{K}_{\mu\nu} \cdot \vec{R}} e^{i\vec{k}_{\mu\nu} \cdot \vec{r}/\Omega} | s_\mu t_\mu \rangle | s_\nu t_\nu \rangle . \end{aligned}$$

To derive a useful integral equation for  $G$  we define the operator  $G_\omega (K_{\mu\nu}; k_{\mu'} v', k_{\mu\nu})$  by the equation

$$\langle \mu' v' | G(\omega) | \mu v \rangle = \langle s_\mu' t_\mu' s_v' t_v' | \delta_{\vec{K}_{\mu'} v', \vec{K}_{\mu v}} \frac{(2\pi)^3}{\Omega} G_\omega (K_{\mu\nu}; k_{\mu'} v', k_{\mu\nu})$$

$$| s_\mu t_\mu s_v t_v \rangle . \quad (3-11)$$

The Kronecker delta appears in Eq. (3-11) instead of the Dirac delta because the single-particle orbitals in nuclear matter are normalized in a finite volume  $\Omega$ . The factor  $(2\pi)^3/\Omega$  appears because we wish to evaluate  $G$  between relative states of the form  $e^{i\vec{K} \cdot \vec{r}}/(2\pi)^{3/2}$  as is done for the  $R$  matrix.

The center-of-mass momentum dependence of  $G_\omega$  arises because the eigenvalues of the operators  $Q$  and  $e$ , when operating on a two-body state  $|\mu v\rangle$ , depend not only on the magnitudes of  $\vec{K}_{\mu v}$  and  $\vec{k}_{\mu v}$ , but also on the angle between them. Consequently, while  $G_\omega$  cannot connect two-body states with different total momentum,  $G_\omega$  depends on the magnitude and direction of the total momentum.

In our future discussion we shall omit the single-particle labels from the relative and center-of-mass momenta. Unless otherwise indicated,  $\vec{k}_0$  refers to the incident relative momentum,  $\vec{k}'$  refers to the intermediate-state relative momentum,  $\vec{k}$  refers to the final-state relative momentum, and  $\vec{K}$  refers to the center-of-mass momentum, which must be conserved. The single-particle momenta retain their single-particle labels. The starting energy  $\omega$  will always be calculated on the energy shell<sup>53</sup> unless otherwise indicated.

If we substitute Eq. (3-11) into (3-10), and replace the summation over intermediate states with an integration over intermediate-state relative momentum, the integral equation

$$G(\vec{k}; \vec{k}, \vec{k}_o) = v(\vec{k}, \vec{k}_o) - \int \frac{d^3 k' v(\vec{k}, \vec{k}') Q(\vec{k}, \vec{k}') G(\vec{k}, \vec{k}', \vec{k}_o)}{E(\vec{k}', \vec{k}) - E(\vec{k}_o, \vec{k})} \quad (3-12)$$

results. The function  $Q(\vec{k}', \vec{k})$  is simply the eigenvalue of  $Q$  when it operates on a two-body intermediate state with center-of-mass momentum  $\vec{k}$  and relative momentum  $\vec{k}'$ . The function  $Q(\vec{k}', \vec{k})$  excludes  $\vec{k}'$  from the domain of integration unless  $|\vec{k}' \pm \vec{k}| \geq k_F$ . The energies  $E(\vec{k}', \vec{k})$  and  $E(\vec{k}_o, \vec{k})$  are simply the sum of single-particle energies for two-particle states that have relative and center-of-mass momenta  $\vec{k}', \vec{k}$  and  $\vec{k}_o, \vec{k}$ , respectively.

One very important feature of Eq. (3-12) is that  $Q(\vec{k}', \vec{k})$  excludes  $\vec{k}' = \vec{k}_o$  from the domain of integration. A non-singular integrand results. This lack of singularity leads to the "healing" property of the "nuclear" wave function. This healing property is very important for the validity of Equation (3-9). The healing property also allows one to define a smallness parameter  $\kappa$ . This smallness parameter is of extreme importance because it largely determines the convergence of the Brueckner-Goldstone expansion. As we shall see, the smallness parameter  $\kappa$  is a measure of the short-range correlations in nuclear matter. In this thesis we repeatedly refer to  $\kappa$  as a measure of the smoothness of the two-nucleon interaction.

### E. Healing and the Convergence of the Brueckner-Goldstone Expansion

The idea of "healing" is understood most physically by considering a two-body-correlated nuclear wave function  $\psi_{\mu\nu}^N(\vec{r})$ . We define  $\psi_{\mu\nu}^N(\vec{r})$  by the equation

$$\psi_{\mu\nu}^N(\vec{r}) = \varphi_{\mu\nu}(\vec{r}) - \int \frac{d^3k' G(\vec{k}; \vec{k}', \vec{k}_o) e^{i\vec{k}' \cdot \vec{r}}}{E(\vec{k}, \vec{k}') + E(\vec{k}_o, \vec{k})} Q(\vec{k}, \vec{k}') |SM_S> |TT_3>, \quad (3-13)$$

where

$$\varphi_{\mu\nu}(\vec{r}) = e^{ik_o \cdot \vec{r}} / (2\pi)^{3/2} |SM_S> |TT_3> .$$

The spins and isospins are coupled to  $S$ ,  $M_S$ ,  $T$ ,  $T_3$ , as in the free scattering problem. The correlated wave function is related to the  $G$  matrix ( $G\psi = V\psi^N$ ) in a similar fashion as the free-scattering wave function is related to the  $R$  matrix ( $R\psi = V\psi$ ). One may regard the correlated nuclear wave function as a wave function that describes the interaction of two-nucleons in the nuclear medium. One very important difference exists between the nuclear wave function and the free-scattering wave function. Namely, the asymptotic form of the nuclear wave function approaches that of the plane wave, i.e.  $\psi_{\mu\nu}^N(\vec{r}) \xrightarrow[r \rightarrow \infty]{} \varphi_{\mu\nu}(\vec{r})$ . Mathematically, this property, called "healing"<sup>54</sup>, results from the non-singular integrand in Eq. (3-13). Physically, healing is a consequence of the Pauli exclusion principle.

Because of the healing property, correlations in the nuclear wave-function are limited to short distances. True scattering does not occur in a nuclear medium because the nuclear wave function does not contain a scattered wave in the asymptotic limit.

To measure the correlations in the nuclear wave function, we define a wave-function defect  $\xi_{\mu\nu}^N$  where

$$\xi_{\mu\nu}^N(\vec{r}) = \phi_{\mu\nu}(\vec{r}) - \psi_{\mu\nu}^N(\vec{r}).$$

Due to the healing of  $\psi_{\mu\nu}^N(\vec{r})$ , the wave-function defect vanishes in the asymptotic limit and, thus, measures the short-range correlations only.

In Figure 1 we present typical plots of the  $^1S_0$  part of  $\psi_{\mu\nu}^N(\vec{r})$ ,  $\phi_{\mu\nu}(\vec{r})$  and  $\xi_{\mu\nu}^N(\vec{r})$  for a hard-core potential. As seen in Figure 1, strong correlations are mainly limited to distances less than 1 Fermi. In nuclear matter the average internucleon distance is about 1.8 Fermis. Since two-body correlations are mainly limited to distances considerably shorter than the average internucleon distance, the probability that three nucleons approach each other closely enough to cause significant three-body correlations becomes fairly small. The importance of this property will become evident shortly.

One overall measure of the short-range correlations in nuclear matter is the smallness parameter, or wound integral,  $\kappa$ . The wound integral  $\kappa$  is defined as

$$\kappa = \frac{(2\pi)^3}{8} \rho \sum_{SM_{STT3}} \int d^3r |\xi_{\mu\nu}^N(\vec{r})|^2 .$$

Physically, the wound integral  $\kappa$  measures the probability of exciting two incident particles in the Fermi sea to momenta above the Fermi sea. Since the magnitude of  $\kappa$  indicates the degree of short-range correlations and how quickly the nuclear wave function heals,  $\kappa$  also indicates how important three-body correlations may be.

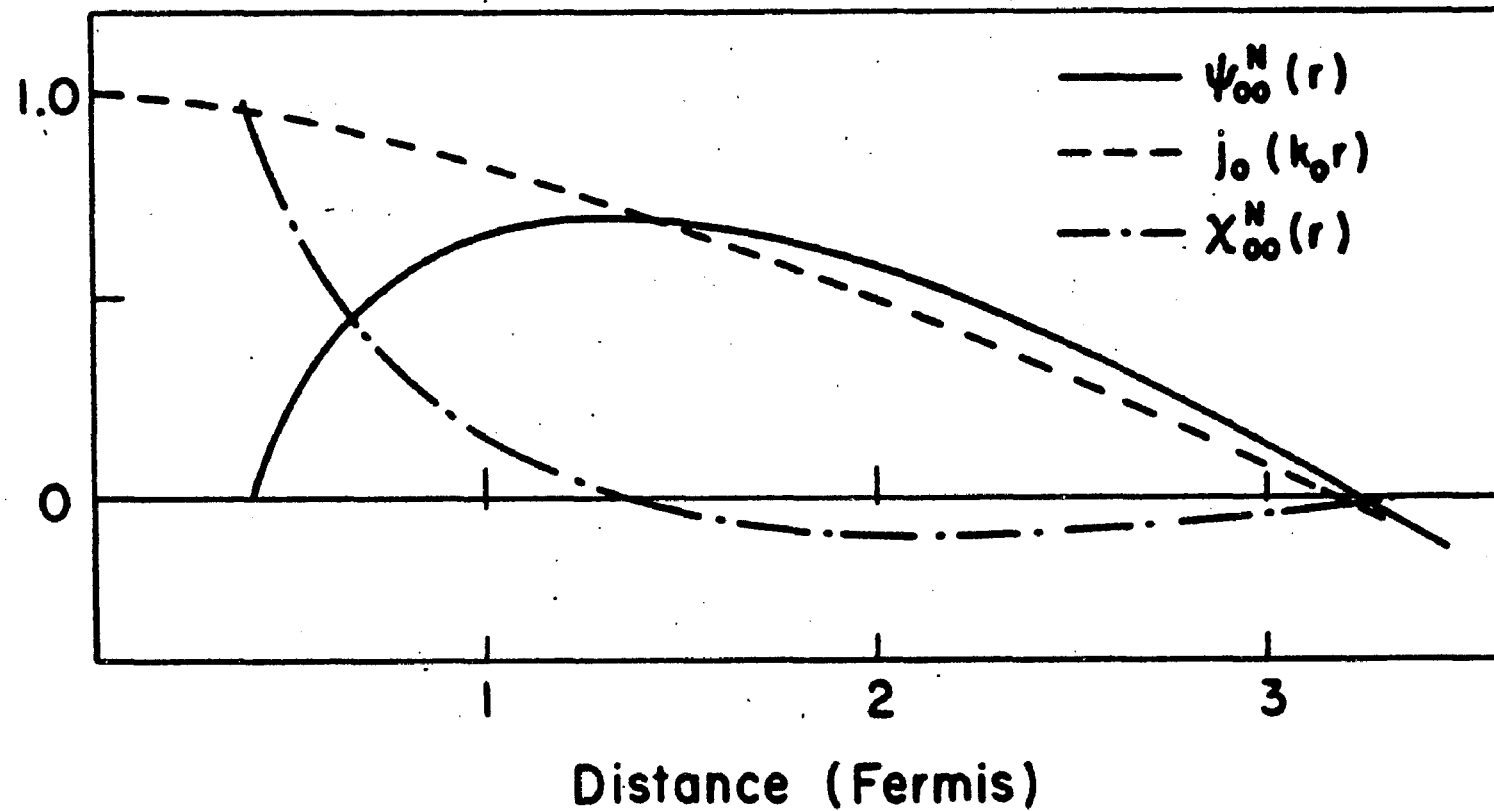


Figure 1. The relative two-body  $^1S$  nuclear wave function ( $\psi_{00}^N(r)$ ), unperturbed wave function ( $j_0(k_0r)$ ), and wave-function defect ( $X_{00}^N(r)$ ) for a hard-core plus attractive potential with a core radius of .4 Fermis: For these plots  $k_F \approx 1.5F^{-1}$  and  $k_0 \approx .9F^{-1}$ .

The importance of the value of  $\kappa$  has been demonstrated by the discovery that the Brueckner-Goldstone expansion converges rapidly if one groups the diagrams of this expansion according to the number of hole-lines instead of orders of  $G$ .<sup>36,55-57</sup> It has been shown<sup>36</sup> that the convergence of this grouping is roughly governed by the value of  $\kappa$ . The two-hole-line diagrams in this grouping correspond to the  $G$ -matrix elements that appear in Eq. (3-9). The three-hole-line diagrams are of many types and, to sum them, one must employ the three-body Faddeev equation techniques<sup>58</sup> described by Bethe.<sup>56</sup> Since the magnitude of three-body diagrams depend on the importance of three-body correlations, it is not surprising that  $\kappa$  approximately determines the ratio of the magnitudes of three-hole-line diagrams to those of two-hole-line diagrams.

For most hard- and soft-core potentials,  $.15 \leq \kappa \leq .20$ .<sup>59</sup> These values of  $\kappa$  are small enough to assure the rapid convergence of the Brueckner-Goldstone expansion when classified according to the number of hole-lines. These values of  $\kappa$ , however, indicate that three-body diagrams are not altogether negligible. Indeed, for some time it was believed that three-body diagrams contributed significantly to the ground-state energy of nuclear matter. However, actual calculations of three-body diagrams show that they give a total contribution only of the order of 1 MeV for hard-core potentials.<sup>60,61</sup> These calculations demonstrate that the three-body diagrams are individually appreciable, but, when summed together, their total contribution is quite small.

Since the "best" choice of the particle spectrum, i.e.,  $U(k_\gamma)$  for  $k_\gamma > k_F$ , is related to the evaluation of three-body diagrams, the present choice of  $U(k_\gamma)$  for  $k_\gamma > k_F$  is zero. The justification for this choice

is that the total three-body contribution is so small that it does not have to be cancelled by a non-zero  $U$ .

As we have seen,  $\kappa$  is a handy measure of the short-range correlations in nuclear matter. Accordingly, we employ  $\kappa$  to measure the smoothness of various two-nucleon interactions. If  $\kappa$  is small ( $\kappa \lesssim .03$ ), the nuclear and unperturbed wave functions differ only slightly. In this case Hartree-Fock theory is applicable because  $G \approx V$ . For slightly larger values of  $\kappa$  ( $.03 \lesssim \kappa \lesssim .2$ ), the correlations are large enough that Hartree-Fock theory is inapplicable; however, for potentials with  $\kappa \approx .2$ , the Brueckner-Goldstone expansion converges rapidly.<sup>55,56</sup> With the assumption that the sum of three-body contributions is small, Equation (3-9) should be valid. All of the potentials this thesis deals with have wound integrals smaller than .2. Therefore, we assume Equation (3-9) is valid.

For some physical systems, such as liquid He<sup>3</sup>, healing does not occur rapidly enough for correlations to be small by the average inter-particle distance. The wound integrals in these cases are typically greater than .2.<sup>62</sup> For these strong interactions, three-body correlations are probably significant. Equation (3-9) would not be adequate to compute the ground-state energy in these instances. In our calculations, however, we do not encounter interactions so strong that  $\kappa > .2$ .

Having discussed the importance of healing, we now return to our basic problem --- to solve for  $G$  and determine the ground-state energy of nuclear matter. To do this we return to Equation (3-13).

## F. Solution of the Bethe-Goldstone Equation—

### Elimination of Angular Dependence

The Bethe-Goldstone equation differs from the Lippmann-Schwinger equation because the  $Q$  operator in Equation (3-12) depends on the direction of the center-of-mass momentum. A partial-wave expansion applied to the Bethe-Goldstone equation, consequently, fails because of this extra angular dependence. The angular dependence of  $G$  on the direction of the center-of-mass momentum also implies that  $G$  does not conserve total relative angular momentum  $\vec{J}$ .

However, Irwin, in his Cornell thesis<sup>63</sup> examined the role of  $J$  coupling in nuclear matter and found that the effects of  $J$  coupling on nuclear binding energies are less than .1 MeV. Neglecting this small effect of  $J$  coupling, one feels justified in replacing the exact  $Q$  operator with an angle-averaged  $Q$  operator. The angle averaging of  $Q$ , along with the choice of a single-particle spectrum without angular dependence on  $\vec{K}$ , eliminates the  $J$  coupling problem from the Bethe-Goldstone equation. The ordinary partial-wave decomposition procedure can then be used. A discussion of the angle-average approximation follows.

#### 1. Angle-Average Approximation

The eigenvalues of the  $Q$  operator depend not only on the magnitudes of  $\vec{K}$  and  $\vec{k}'$ , but also on the angle between  $\vec{K}$  and  $\vec{k}'$ . We may express  $Q(\vec{k}', \vec{K})$  as a function of  $k'$ ,  $K$  and  $\cos\theta_{\vec{k} \vec{K}}$  where

$$\cos\theta_{\vec{k} \vec{K}} = \frac{\vec{k}' \cdot \vec{K}}{k' K} .$$

Given the conditions for a non-zero  $Q(\vec{k}', \vec{K})$

$$|\vec{k}'_\mu|^2 = |\vec{K} + \vec{k}'|^2 = k^2 + k'^2 + 2\vec{K} \cdot \vec{k}' > k_F^2$$

and

$$|\vec{k}'_\nu|^2 = |\vec{K} - \vec{k}'|^2 = k^2 + k'^2 - 2\vec{K} \cdot \vec{k}' > k_F^2 ,$$

the angular condition for  $Q(\vec{k}', \vec{K})$  to be non-zero becomes

$$|\cos\theta_{\vec{k}' \vec{K}}| < \frac{k'^2 + k^2 - k_F^2}{2k'k} .$$

For  $|\vec{k}' - \vec{K}| > k_F$ , the angular domain of integration includes all values of  $\cos\theta_{\vec{k}' \vec{K}}$  from -1 to +1. The  $Q$  operator in this case is unity. For  $k'^2 + k^2 < k_F^2$ , the  $Q$  operator excludes all values of  $\cos\theta_{\vec{k}' \vec{K}}$  from the domain of integration and  $Q(\vec{k}', \vec{K}) = 0$ . If  $k_F^2 - k^2 \leq k'^2 \leq (k_F + k)^2$ , then the angular domain of integration includes all values of  $\cos\theta_{\vec{k}' \vec{K}}$  from

$$- \left( \frac{k'^2 + k^2 - k_F^2}{2k'k} \right) \text{ to } + \left( \frac{(k'^2 + k^2 - k_F^2)}{2k'k} \right) .$$

Figure 2a shows  $Q(\vec{k}', \vec{K})$  as a function of  $\cos\theta_{\vec{k}' \vec{K}}$  in the last case.

The angle-average approximation replaces the exact  $Q$  shown in Figure 2a with a constant over the entire angular domain of integration for a given  $k', K$ . This constant,  $Q(k', K)$ , is the mean value of  $Q(\vec{k}', \vec{K})$  over  $\cos\theta_{\vec{k}' \vec{K}}$ . Figure 2b shows the angle-average  $Q$  operator as a function of  $\cos\theta_{\vec{k}' \vec{K}}$ . The area under figures 2a and 2b are equal. The full definition of the angle-average  $Q$  operator  $Q(k', K)$ , which replaces  $Q(\vec{k}', \vec{K})$  in Eq. (3-12), is given by

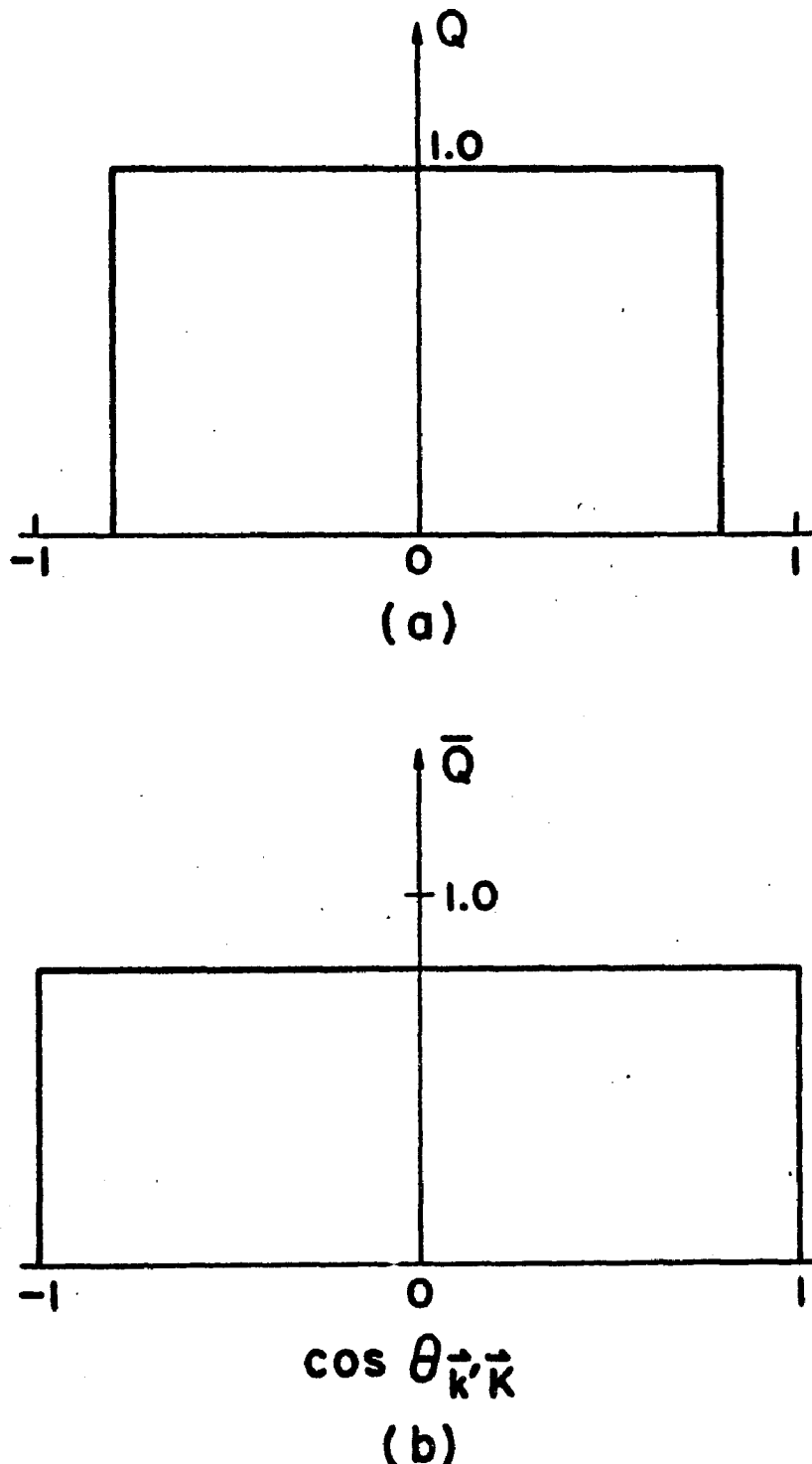


Figure 2. The Pauli  $Q$  operator and angle averaged  $Q$  operator as functions of  $\cos \theta_{\vec{k}', \vec{K}}$ . Figure 2(a) represents  $Q(\vec{k}', \vec{K})$  (denoted by  $Q$ ) for  $k_F^2 - K^2 \leq k'^2 \leq (k_F + K)^2$ .

Figure 2(b) represents the angle averaged  $Q(\vec{k}', \vec{K})$  (denoted by  $\bar{Q}$ ) for  $k_F^2 - K^2 \leq k'^2 \leq (k_F + K)^2$ . Both Figures 2(a) and 2(b) correspond to  $k_F = 1.5F^{-1}$ ,  $k' = 2.0F^{-1}$  and  $K = .7F^{-1}$ . The areas under 2(a) and 2(b) are equal.

$$\begin{aligned}
 Q(k', K) &= 0 && \text{if } k'^2 \leq k_F^2 - K^2 \\
 &= 1 && \text{if } k' \geq k_F + K \\
 &= \frac{K^2 + k'^2 - k_F^2}{2Kk'} && \text{if } k_F^2 - K^2 < k'^2 < (k_F + K)^2 .
 \end{aligned}
 \tag{3-15}$$

Another way of regarding the  $Q$  operator is to expand  $Q(\vec{k}', \vec{K})$  as a series of Legendre polynomials in  $\cos\theta_{\vec{k}' \vec{K}}$ . The resulting expansion, as given by McMillan and Lomon,<sup>64</sup> becomes

$$Q(\vec{k}', \vec{K}) = \sum_{L(\text{even})} A_L(k', K) P_L(\cos\theta_{\vec{k}' \vec{K}}) ,$$

where

$$A_L(k', K) = \frac{2L+1}{2} \int_{-1}^1 d(\cos\theta_{\vec{k}' \vec{K}}) Q(\vec{k}', \vec{K}) P_L(\cos\theta_{\vec{k}' \vec{K}}) .$$

The coefficients  $A_L(k', K)$  are given by

$$\begin{aligned}
 A_0(k', K) &= 1 && \text{if } |k' - K| > k_F \\
 &= 0 && \text{if } k'^2 + K^2 < k_F^2 \\
 &= \frac{K^2 + k'^2 - k_F^2}{2k'K} && \text{otherwise} \\
 A_L &= P_{L+1} \left( \frac{K^2 + k'^2 - k_F^2}{2k'K} \right) - P_{L-1} \left( \frac{K^2 + k'^2 - k_F^2}{2k'K} \right) \text{ if} \\
 &&& (k' - K)^2 \leq k_F^2 \leq k'^2 + K^2 \\
 &&& \text{and } L \text{ even} \\
 &= 0 && \text{otherwise} .
 \end{aligned}$$

The angle-average  $Q$  operator is the  $L = 0$  part of the partial-wave expansion of the exact  $Q$  operator. Since the angle-average  $Q$  operator has only an  $L = 0$  part, it cannot change the angular momentum when operating on eigenfunctions of  $J$ . The full  $Q$  operator has components with  $L > 0$  and may change the angular momentum when operating on eigenfunctions of  $J$ . Since we employ the angle-average  $Q$  operator, we neglect components of  $Q$  for  $L > 0$ .

The angle averaging of  $Q$  eliminates one source of angular dependence in the Bethe-Goldstone equation. Another source of angular dependence is the energy denominators of the Bethe-Goldstone equation. To eliminate angular dependence on the direction of the center-of-mass momentum in the energy denominators, we use the effective-mass approximation.

## 2. The Effective-Mass Approximation

The only requirement that nuclear matter places on the single-particle potential-energy operator  $U$  is that  $U$  must be diagonal between single-particle, plane-wave orbitals. The Brueckner-Goldstone expansion is valid for any choice of  $U$ . A poor choice of  $U$ , however, may necessitate the retention of higher-order terms in the Brueckner-Goldstone expansion to compute the binding energy accurately.

In nuclear matter,  $U$  is a function of only the magnitude of the single-particle momentum. With this assumption one may write the single-particle energy as

$$E_\alpha = E(k_\alpha) = \frac{\pi^2 k_\alpha^2}{2M} + U(k_\alpha) .$$

The energy denominators in the Bethe-Goldstone equation (3-12) become

$$E(\vec{k}', \vec{K}) - E(\vec{k}_0, \vec{K}) = \frac{\hbar^2}{M} (k'^2 - k_0^2) + U(|\vec{K} + \vec{k}'|) + U(|\vec{K} - \vec{k}'|) - U(|\vec{K} + \vec{k}_0|) - U(|\vec{K} - \vec{k}_0|) . \quad (3-16)$$

The energy denominators have angular dependence because the  $U$  terms in Eq. (3-16) depend on the angles between  $\vec{K}$  and  $\vec{k}'$ , and  $\vec{K}$  and  $\vec{k}_0$  as well as on the magnitudes of  $\vec{K}$ ,  $\vec{k}_0$  and  $\vec{k}'$ . In the effective-mass approximation one chooses the single-particle energies to have the quadratic form

$$E(k_\alpha) = \frac{\hbar^2 k_\alpha^2}{2M^*} - U_0 \quad \text{for } k_\alpha \leq k_F \\ = \frac{\hbar^2 k_\alpha^2}{2M} \quad \text{for } k_\alpha > k_F , \quad (3-17)$$

where  $M^*$  is called the "effective mass". With this choice of the single-particle spectrum, the angular dependence disappears from  $E(\vec{k}', \vec{K})$  and  $E(\vec{k}_0, \vec{K})$ . The resulting expressions for  $E(\vec{k}', \vec{K})$  and  $E(\vec{k}_0, \vec{K})$  become

$$E(\vec{k}', \vec{K}) = \frac{\hbar^2}{M} (K^2 + k'^2) \equiv E^>(\vec{k}', \vec{K})$$

$$E(\vec{k}_0, \vec{K}) = \frac{\hbar^2}{M^*} (K^2 + k_0^2) - U_0 \equiv E^<(\vec{k}_0, \vec{K}) .$$

The symbols  $E^<$  and  $E^>$  stand for energies for two particles below the Fermi sea and for energies for two particles above the Fermi sea, respectively.

### 3. Self-Consistency

In the effective-mass approximation one assumes the existence of a quadratic single-particle spectrum of the form (3-17) that approximates the "best" choice of the single-particle spectrum. The best choice of the hole spectrum, according to BBP,<sup>51</sup> is given by the relation

$$\langle \mu | U | \mu \rangle = U(k_F) = \sum_{\nu < A} \langle \mu \nu | G(E_\mu + E_\nu) | \mu \nu - \nu \mu \rangle \text{ for } \mu < A. \quad (3-18)$$

The BBP theorem states that the choice (3-18) allows a class of third-order terms, or diagrams, with two G-matrix elements and one U insertion to cancel a whole class of three-hole-line diagrams.<sup>65</sup>

The present popular choice for the potential energies for particles above the Fermi sea is zero. This choice rests on the results of the calculations of Bethe and Rajaraman<sup>60</sup> that show that the three-body cluster diagrams sum to only -1 MeV. This -1 MeV figure, in turn, rests on the assumption of a hard-core potential and on certain approximations made about the tensor force.<sup>66</sup> Therefore, the questions of the three-body-cluster diagrams and the particle spectrum are not yet fully resolved. The sensitivity of nuclear-binding energies to the choice of the particle spectrum is an interesting problem in itself. We return to this problem in Section V.

The choice of the hole spectrum, as given by Eq. (3-18), presents a self-consistency problem since (3-10) determines U from G. The determination of G, however, depends on the original choice of U. Ideally, the calculation of U by (3-18) should reproduce the original choice of U used to calculate G. To make U as self-consistent as possible in the effective-mass approximation, one should choose initial values of  $M^*$  and  $U_0$  to calculate G. With this G one should calculate a new  $U(0)$  and  $U(k_F)$  (or U at any two energies below the Fermi sea) according to (3-18). The two values  $U(0)$  and  $U(k_F)$  then determine new values for the parameters  $M^*$  and  $U_0$ . The new hole-spectrum parameters,  $M^*$  and  $U_0$ , determine a new G, which, in turn, determines new values of  $U(0)$  and  $U(k_F)$  according to (3-18).

Iteration of this procedure continues until  $M^*$  and  $U_0$  change very little between successive iterations. With reasonable starting values for  $M^*$  and  $U_0$ , two or three iterations are usually sufficient to determine  $M^*$  and  $U_0$  fairly self-consistently. We employ this procedure in our calculations.

The calculation of binding energies and self-consistent single-particle energies depend on the ability to solve the Bethe-Goldstone equation. Even with the removal of the angular-dependence problem, (3-12) is still a three-dimensional integral equation. Utilization of a partial-wave decomposition of  $G(\vec{K}; \vec{k}, \vec{k}_0)$  reduces (3-12) to a set of one-dimensional integral equations just as in the case of the Lippmann-Schwinger equation.

#### G. Partial-Wave Decomposition of the Bethe-Goldstone Equation

With the angle-average  $Q$  and effective-mass approximations, the Bethe-Goldstone equation becomes

$$G(\vec{K}; \vec{k}, \vec{k}_0) = V(\vec{k}, \vec{k}_0) - \int \frac{d^3 k' V(\vec{k}, \vec{k}') Q(k', K) G(K; \vec{k}', \vec{k}_0)}{E(k', K) - E(k_0, K)} . \quad (3-19)$$

Since neither  $Q$  nor the energy denominators in (3-19) now depend on the direction of  $\vec{K}$ ,  $G$  does not depend on the direction of  $\vec{K}$ . Accordingly we omit the direction of  $\vec{K}$  from (3-19).

To reduce (3-19) to a set of one-dimensional integral equations we can now employ the partial-wave decomposition

$$G_{LL}^{\alpha}(K; \vec{k}, \vec{k}_0) = \frac{2}{\pi} \frac{n^2}{M} \sum_{LL} \sum_{\alpha M T} \sum_3^{L-L} G_{LL}^{\alpha}(K; k, k_0) \tilde{y}_L^{\alpha M}(\vec{k}) \tilde{y}_L^{+\alpha M}(\vec{k}_0) \quad (3-20)$$

The resulting one-dimensional Bethe-Goldstone equation becomes, in the eigenchannel  $\alpha$ ,

$$G_{LL'}^{\alpha}(K; k, k_0) = v_{LL'}^{\alpha}(k, k_0) - \frac{2}{\pi} \sum_L \int_0^\infty \frac{k'^2 dk' Q(k', K) V_{LL'}^{\alpha}(k, k') G_{LL'}^{\alpha}(K; k', k_0)}{e^>(k', K) - e^<(k_0, K)}, \quad (3-21)$$

where

$$e^>(k', K) = \frac{M}{h^2} E^>(k', K)$$

$$e^<(k_0, K) = \frac{M}{h^2} E^<(k_0, K).$$

The partial-wave expansion for the correlated nuclear wave function  $\psi_{\mu\nu}^N(\vec{r})$  is similar to the partial-wave expansion for the free-scattering two-body wave function. The wave functions that result,  $\downarrow_{LL'}^{N\alpha}(r)$  and  $\downarrow_{LL'}^{N\alpha}(k)$ , are related to the  $G$  matrix by

$$\downarrow_{LL'}^{N\alpha}(r) = j_L(k_0 r) \delta_{LL'} - \frac{2}{\pi} \int_0^\infty \frac{k'^2 dk' Q(k', K) G_{LL'}^{\alpha}(K; k', k_0) j_L(k' r)}{e^>(k', K) - e^<(k_0, K)} \quad (3-22)$$

and

$$\downarrow_{LL'}^{N\alpha}(k) = \frac{\delta(k-k_0)}{k^2} \delta_{LL'} - \frac{2}{\pi} \frac{Q(k, K) G_{LL'}(K; k, k_0)}{e^>(k, K) - e^<(k_0, K)}. \quad (3-23)$$

Since the wave-function defect provides a means of exhibiting the healing property, we also wish to expand  $\xi_{\mu\nu}^N$  in partial waves. The wave

functions that results,  $\chi_{LL}^{N\alpha}(r)$  and  $\chi_{LL}^{N\alpha}(k)$ , are related to the G matrix by

$$\chi_{LL}^{N\alpha}(r) = \frac{2}{\pi} \int \frac{k'^2 dk' Q(k', K) G_{L'L}^{\alpha}(k; k', k_0) j_{L'}(k' r)}{e^>(k', K) - e^<(k_0, K)} \quad (3-24)$$

and

$$\chi_{LL}^{N\alpha}(k) = \frac{2}{\pi} \frac{Q(k, K) G_{L'L}^{\alpha}(k, k_0)}{e^>(k, K) - e^<(k_0, K)} . \quad (3-25)$$

The wound integral  $\kappa$ , which is a measure of the strength of the two-nucleon interaction, is now expanded in terms of the  $\chi_{LL}^{N\alpha}$ . The resulting expression for  $\kappa$  is given by

$$\kappa = \frac{\pi}{2} \rho \sum_{LL' \alpha} (2J+1)(2T+1) \int_0^\infty r^2 dr |\chi_{LL}^{N\alpha}(r)|^2 . \quad (3-26)$$

The definition  $\kappa \equiv \sum_{LL' \alpha} \kappa_{LL}^{\alpha}$ , where

$$\kappa_{LL}^{\alpha} = \frac{\pi}{2} \rho (2J+1)(2T+1) \int r^2 dr |\chi_{LL}^{N\alpha}(r)|^2 , \quad (3-27)$$

allows us to identify how much each partial wave contributes to the strength of the two-nucleon interaction. The wound integrals  $\kappa_{LL}^{\alpha}$ , may also be expressed in terms of the G matrix with the result

$$\kappa_{LL}^{\alpha} = \frac{2}{3\pi^2} k_F^3 (2J+1)(2T+1) \int_0^\infty \frac{k'^2 dk' Q^2(k', K) |G_{L'L}^{\alpha}(k', k_0)|^2}{[e^<(k_0, K) - e^>(k', K)]^2} . \quad (3-28)$$

The contribution from each partial wave depends on the off-diagonal G matrix elements. The magnitude of the off-diagonal G matrix elements, in turn, ultimately depend on the behavior of V off the energy shell. Thus,  $\chi_{LL}^{\alpha}$ , is a useful measure of the correlations present in the eigenchannel  $\alpha$ .

For  $L = L'$ , the wound integral  $\chi_{LL}^{\alpha}$  indicates the strength of the central interaction in eigenchannel  $\alpha$ . For  $L \neq L'$ , the wound integral  $\chi_{LL'}^{\alpha}$ , indicates the strength of the tensor interaction in eigenchannel  $\alpha$ . We shall find in Section V that the value of  $\chi_{02}^{\alpha}$  is of extreme importance to the saturation of nuclear matter.

The determination of nuclear binding energies, wave-function defects, and wound integrals ultimately depend on the evaluation of the G matrix. Solution of (3-21) for  $G_{LL'}^{\alpha}(K; k, k_0)$  now becomes the crucial step in determining nuclear binding energies.

#### H. Solution of the Bethe-Goldstone Equation — Previous Methods

The Bethe-Goldstone equation is very similar to the Lippmann-Schwinger equation after partial-wave decomposition. The form of (3-21) suggests that the technique of direct matrix inversion should be applicable in solving the Bethe-Goldstone equation. Indeed, we shall discover that the direct-matrix-inversion technique solves the Bethe-Goldstone equation accurately and is applicable for general non-local potentials.

Before we describe the details of the direct-matrix-inversion technique, we should mention that several reliable techniques exist for solving the Bethe-Goldstone equation for local potentials. The oldest method - the Brueckner-Gammel (BG) method<sup>11, 67</sup> - relies on solving for G by a

Green's function type of integral equation in configuration space for local potentials. For non-local potentials this integral equation involves a double integral and the method becomes impractical.

The reference-spectrum method (RSM) of BBP approximates the Bethe-Goldstone propagator  $Q/e$  by the "reference" propagator  $1/e^R$ . The reference propagator  $e^R$  is chosen so that the resulting reference wave functions have the healing property of the nuclear wave function. One then employs an iterative procedure to determine the  $G$  matrix from the reference  $G$  matrix,  $G^R$ . The RSM is especially adaptable to local potentials, because one may use differential-equation techniques to obtain the reference wave functions.

Another method, the Moszkowski-Scott (MS) separation method,<sup>51, 68, 69</sup> also simulates the healing property of nuclear wave functions. One obtains healing in the MS method by solving the two-body-scattering problem for that part of the potential (the short-range part  $V_S$ ) that gives zero phase-shift. One then determines the full  $G$  matrix by an iterative procedure on the long-range part of the potential ( $V_L$ ) and on the short-range  $R$  matrix ( $R_S$ ). The MS method is applicable only to local potentials because the separation of the potential into a long and short-range part is made most simply in configuration space.

Dahll, Ostgaard and Brandow<sup>59</sup> analyzed the methods mentioned above. For further details on the relative merits of these methods, one should consult this reference.

The methods mentioned above are useful techniques for solving the Bethe-Goldstone equation for local potentials. We now describe a method to solve the Bethe-Goldstone equation for general non-local potentials.

I. The Direct Matrix Inversion Method of Solving  
the Bethe-Goldstone Equation

Success in solving the Lippmann-Schwinger equation by direct matrix inversion in Section II implies that the same technique should apply in solving the Bethe-Goldstone equation (3-21). Direct matrix inversion avoids the iterative procedures employed in the reference spectrum of the Moszkowski-Scott methods. The chief goal of RSM and MS methods is to obtain reasonable approximations to  $G$  and iterate on these approximations. In Section II we showed that the direct-matrix-inversion technique is very reliable in solving for  $R$ , even for nearly singular potentials. We speculate that direct matrix inversion should accurately solve for the  $G$  matrix.

The direct-matrix-inversion technique for solving the Bethe-Goldstone equation is very similar to that employed in solving the Lippmann-Schwinger equation. We apply an  $N$ -point integration formula to the integral in (3-21) and evaluate (3-21) at  $k = k_i$ ,  $i = 1, \dots, N$ , and at  $k = k_{N+1} = k_o$ , where the  $k_i$  for  $i = 1, N$  are the  $N$  "grid" points of the integration formula. These two steps reduce (3-21) (for uncoupled channels) to  $N + 1$  simultaneous, linear equations for the  $N + 1$  unknowns

$$G_{LL}^{\alpha}(K; k_i, k_o) \quad i = 1, \dots, N+1 \\ \text{for a fixed } L, \alpha, K \text{ and } k_o.$$

Following the same steps as in Section II, we solve for  $G$  by inverting the matrix  $F$

$$F_{ij} = \delta_{ij} + w' j V_{LL}^{\alpha}(k_i, k_j) ,$$

where

$$W'_{j} = \frac{2}{\pi} k_j^2 Q(k_j, K) W_j / [e^>(k_j, K) - e^<(k_o, K)]$$

$$W'_{N+1} = 0,$$

and  $W_j$  is defined in Section II.

The difference between the coefficient matrix  $F$  in the solution of the Bethe-Goldstone equation and  $F$  in the solution of the Lippmann-Schwinger equation stems from the lack of singularities, the different energy denominators, and the presence of the  $Q$  operator in the Bethe-Goldstone equation.

For coupled channels the coefficient matrix  $F$  becomes

$$F_{ij}^{LL'} = \delta_{ij} \delta_{LL'} + W'_j V_{LL'}^{\alpha}(k_i, k_j).$$

The procedure for solving  $G$  then follows that of solving for  $R$  in Section II.

To test the accuracy of the direct-matrix-inversion technique, we calculated the  $G$  matrix elements for a very strong  ${}^1S_0$  single-separable potential. The potential we chose had the form

$$V_{OO}(k, k') = -g_O(k)g_O(k') \quad (3-29)$$

where

$$g_O(k) = \frac{\alpha}{k^2 + a^2} \quad \text{and}$$

$$\alpha = 3.6F^{-3/2}$$

$$a = 1.2F^{-1} .$$

Analytically, the  $G$  matrix elements for the above potential, in the angle average and effective-mass approximations, are given by

$$G_{00}^{\alpha}(k; k, k_0) = -g_0(k)g_0(k_0) \left[ 1 - 2/\pi \int_0^{\infty} \frac{k'^2 dk' g_0^2(k') Q(k', K)}{e(k', K) - e(k_0, K)} \right]^{-1} \quad (3-30)$$

For the potential (3-29) the analytic form of (3-30) appears in Appendix B1.

Figure 3 shows some of the G matrix elements obtained by 15-point Laguerre matrix inversion compared to the analytic values of G. Accuracy of the direct-matrix-inversion method improves with increasing center-of-mass momentum K. The reason for the improved accuracy at higher center-of-mass momenta is because the magnitudes of the discontinuities in the first derivatives of Q(k', K) at  $k' = \sqrt{k_F^2 - K^2}$  and at  $k' = k_F + K$  decrease with increasing K. These discontinuities introduce a small imprecision in the numerical integration routines used in the matrix inversion. Because of approximations we make later on the center-of-mass momentum, the imprecision at small K leads to only small errors (less than 2%) in the computations of total nuclear binding energies.

Since our ultimate goal is to determine nuclear binding energies, the most crucial test of matrix inversion is whether the G matrix elements obtained by this technique give accurate binding energies for a given two-nucleon interaction. The first step in the calculation of nuclear binding energies is to calculate the self-consistent single-particle spectrum. A description of our calculation of the single-particle spectrum, and a test case, follows.

#### J. Calculation of the Single-Particle Spectrum

According to the prescription of BBP the single-particle potential operator U should satisfy the relation

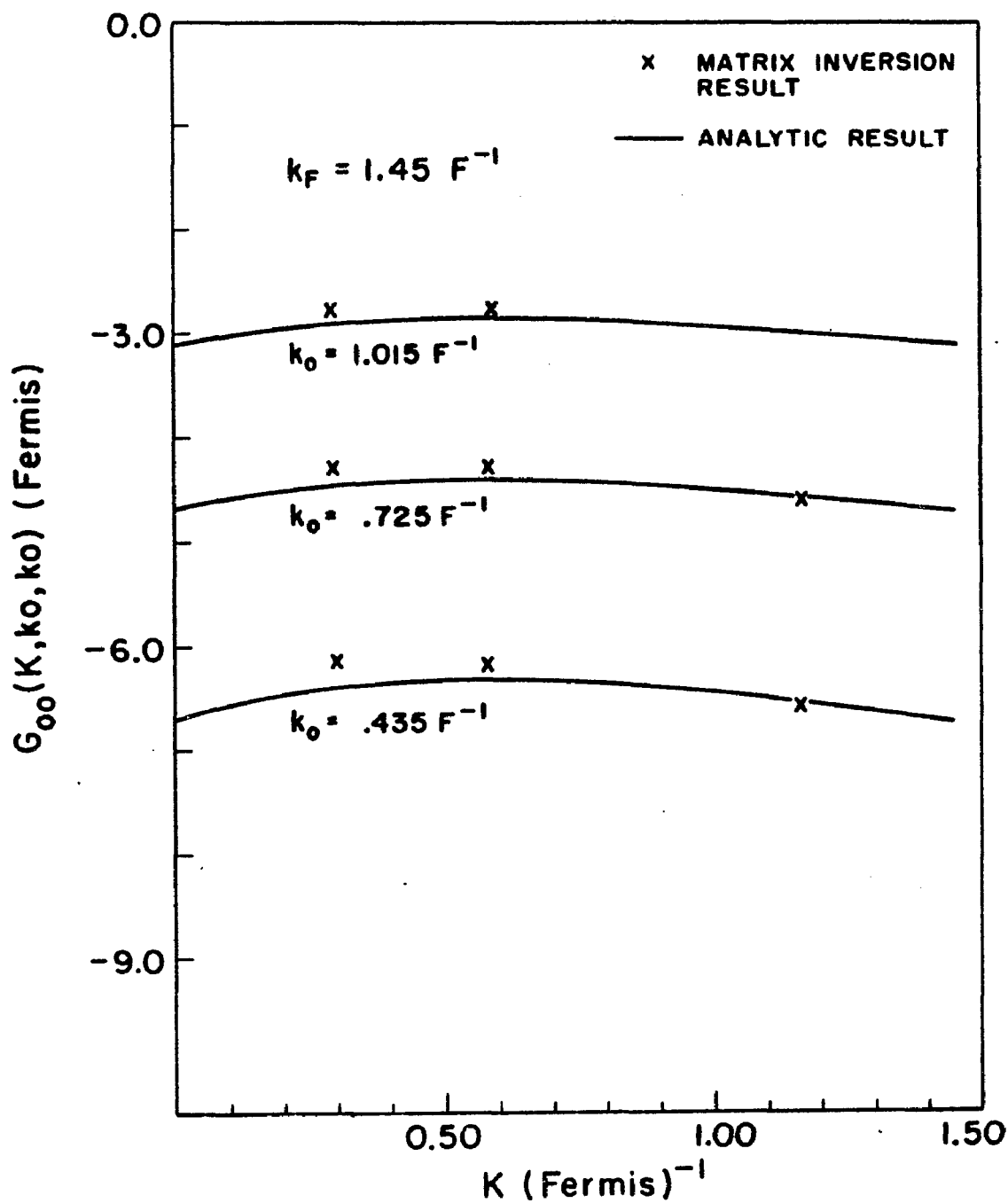


Figure 3. The diagonal  $G$  matrix elements obtained by matrix inversion compared to the analytic solutions for a strong separable potential. Here  $M^*/M = .8$ ,  $U_0 = 80 \text{ MeV}$ .

$$\langle \mu | U | \mu \rangle = \sum_{\nu < A} \langle \mu \nu | G(E_\mu + E_\nu) | \mu \nu - \nu \mu \rangle \quad \text{for } \mu < A,$$

self-consistently. Application of the Equations (3-11) and (3-20) reduces the BBP prescription to

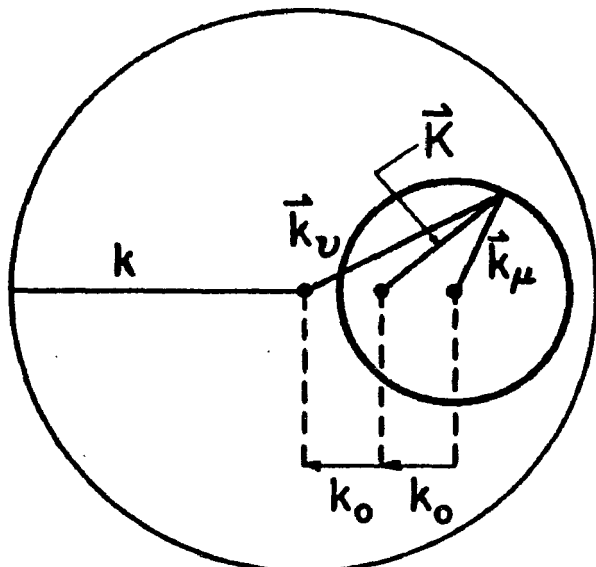
$$\begin{aligned} \langle \mu | U | \mu \rangle &= U(k_\mu) \\ &= \frac{4\pi^2}{\pi k_\mu^M} \sum_{I\alpha} (2J+1)(2T+1) \left[ \int_0^{\frac{k_F-k_\mu}{2}} k_o dk_o \frac{k_\mu+k_o}{|k_\mu-k_o|} KdK G_{LL}^\alpha(K; k_o, k_o) \right. \\ &\quad \left. + \int_{\frac{k_F-k_\mu}{2}}^{\frac{k_F+k_\mu}{2}} k_o dk_o \frac{\sqrt{\frac{k_F^2+k_\mu^2}{2} - k_o^2}}{|k_\mu-k_o|} KdK G_{LL}^\alpha(K; k_o, k_o) \right]. \end{aligned} \quad (3-31)$$

The details of the steps leading to (3-31) appear in Appendix B2. The limits of integration in (3-31) are determined by close examination of Figure 4.

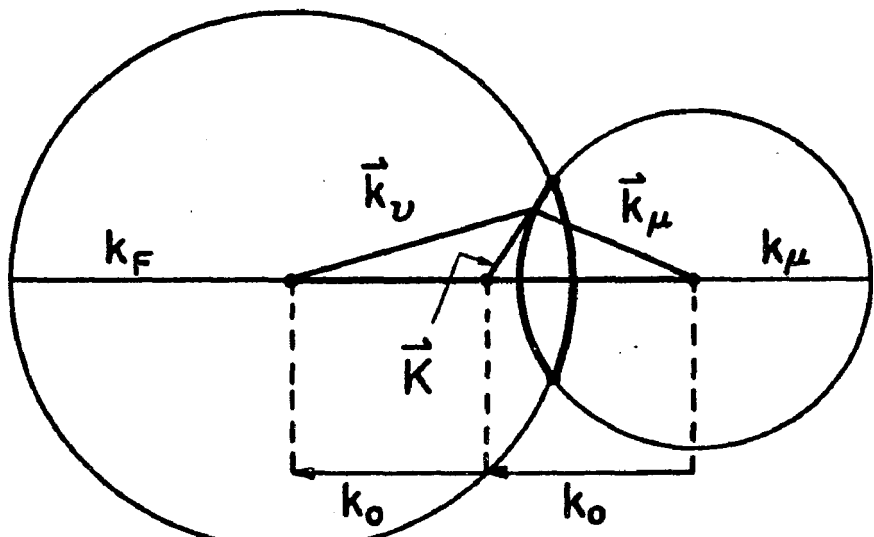
Equation (3-31) requires a double integration. To reduce the dimension of the integral and the number of G matrix elements involved in the computation of U, we make the further approximation that

$$G_{LL}^\alpha(K; k_o, k_o) \approx G_{LL}^\alpha(K_{AVE}; k_o, k_o). \quad (3-32)$$

We choose  $K_{AVE}$  to be the root-mean-square value of K for two particles in the Fermi sea with the constraints that one of the particles has momentum  $\vec{k}_\mu$  and the relative momentum has magnitude  $k_o$ . The resulting rms center-of-mass momentum is given by



(a)



(b)

Figure 4. The allowed values for  $\vec{K}$  in calculating the single particle spectrum: The heavy arc represents the intersection of a Fermi sphere and the surface of a sphere with radius  $k_\mu$ . The heavy arc indicates the allowed values of  $\vec{K}$  for a fixed  $k_o$  and  $k_\mu$  for  $\vec{k}_v$  to be in the Fermi sphere. Figure 4(a) is for  $k_o \leq \frac{k_F + k_\mu}{2}$  and Figure 4(b) is for

$$k_o \leq \frac{k_F + k_\mu}{2}$$

$$\frac{k_F - k_\mu}{2} \leq k_o \leq \frac{k_F + k_\mu}{2}$$

$$K_{\text{AVE}}^2 = k_\mu^2 + k_o^2 \quad \text{for } k_o \ll (k_F - k_\mu)/2$$

and

$$K_{\text{AVE}}^2 = k_\mu^2 + k_o^2 - \frac{1}{2}(k_\mu + 2k_o - k_F)(k_\mu + 2k_o + k_F) \quad \text{for}$$

$$(k_F - k_\mu)/2 \leq k_o \leq (k_F + k_\mu)/2 \quad . \quad (3-33)$$

With the approximation (3-32) the expression for  $U(k_\mu)$  simplifies to

$$\begin{aligned} U(k_\mu) \approx & \frac{8\hbar^2}{M} \sum_{J,T} (2J+1)(2T+1) \left[ \int_0^{\frac{k_F - k_\mu}{2}} k_o^2 dk_o G_{LL}^\alpha(K_{\text{AVE}}; k_o, k_o) \right. \\ & + \frac{1}{2k_\mu} \left. \int_{\frac{k_F - k_\mu}{2}}^{\frac{k_F + k_\mu}{2}} k_o dk_o [ \frac{1}{2}(k_F + k_\mu)(k_F - k_\mu) - k_o(k_o - k_\mu) ] G_{LL}^\alpha(K_{\text{AVE}}; k_o, k_o) \right] . \end{aligned} \quad (3-34)$$

We evaluate (3-34) numerically by Simpson's rule. Typically the integration mesh in  $k_o$  consist of 10 equally spaced intervals from  $k_o = 0$  to  $k_o = k_F$ . The values of  $k_\mu$  for which we calculate  $U(k_\mu)$  are such that both  $\frac{k_F - k_\mu}{2}$  and  $\frac{k_F + k_\mu}{2}$  fall at one of the end points of one of the intervals. A 10-interval Simpson's rule mesh suffices to evaluate (3-34). If we double the interval to 20, the values of  $U(k_\mu)$  change only in the fourth or fifth significant figure. In practice we usually evaluate only  $U(0)$  and  $U(k_F)$  to fix the parameters  $M^*$  and  $U_o$  for the effective-mass approximation.

The validity of the average center-of-mass approximation depends on  $G$  having only a weak dependence on center-of-mass momentum. For most realistic potentials,  $G_{LL}^\alpha(K; k_o, k_o)$  varies by at most 10% with  $K$  for a

given  $k_o$ . This property can be verified by inspection of Figure 3.

Because  $k_\mu$  is fixed, the actual variation of  $G$  with  $K$  is somewhat less than 10% for the matrix elements  $G_{LL}^\alpha(K; k_o, k_o)$  used to evaluate  $U(k_\mu)$ .

To evaluate the net precision of the direct-matrix-inversion method with the average center-of-mass-momentum approximation in computing the single-particle spectrum, we calculated the single-particle spectrum for the strong separable potential mentioned previously. Figure 5 compares the single-particle spectrum determined from the  $G$  matrix elements obtained by matrix inversion to that determined by analytic  $G$  matrix elements. The "analytic" calculation does not include the average-center-of-mass-momentum approximation. All calculations are for  $k_F = 1.45F^{-1}$ ,  $M^*/M = .8$  and  $U_o = 80$  MeV.

The deviations of the analytic single-particle potential energies from those obtained by matrix inversion with the average center-of-mass approximation range from 2% to 4% for 15 Laguerre point matrix inversion. Realizing that these calculations are for an extremely strong potential, we anticipate better accuracy for realistic potentials. Nevertheless, a 2-4% error in the single-particle spectrum has only a very small effect on the calculation of nuclear binding energies. Therefore, these calculations give us the confidence to apply the final test to our matrix-inversion method—its precision in calculating nuclear binding energies.

#### K. Calculation of the Binding Energy of Nuclear Matter

According to (3-9) the total ground-state energy of nuclear matter is given by

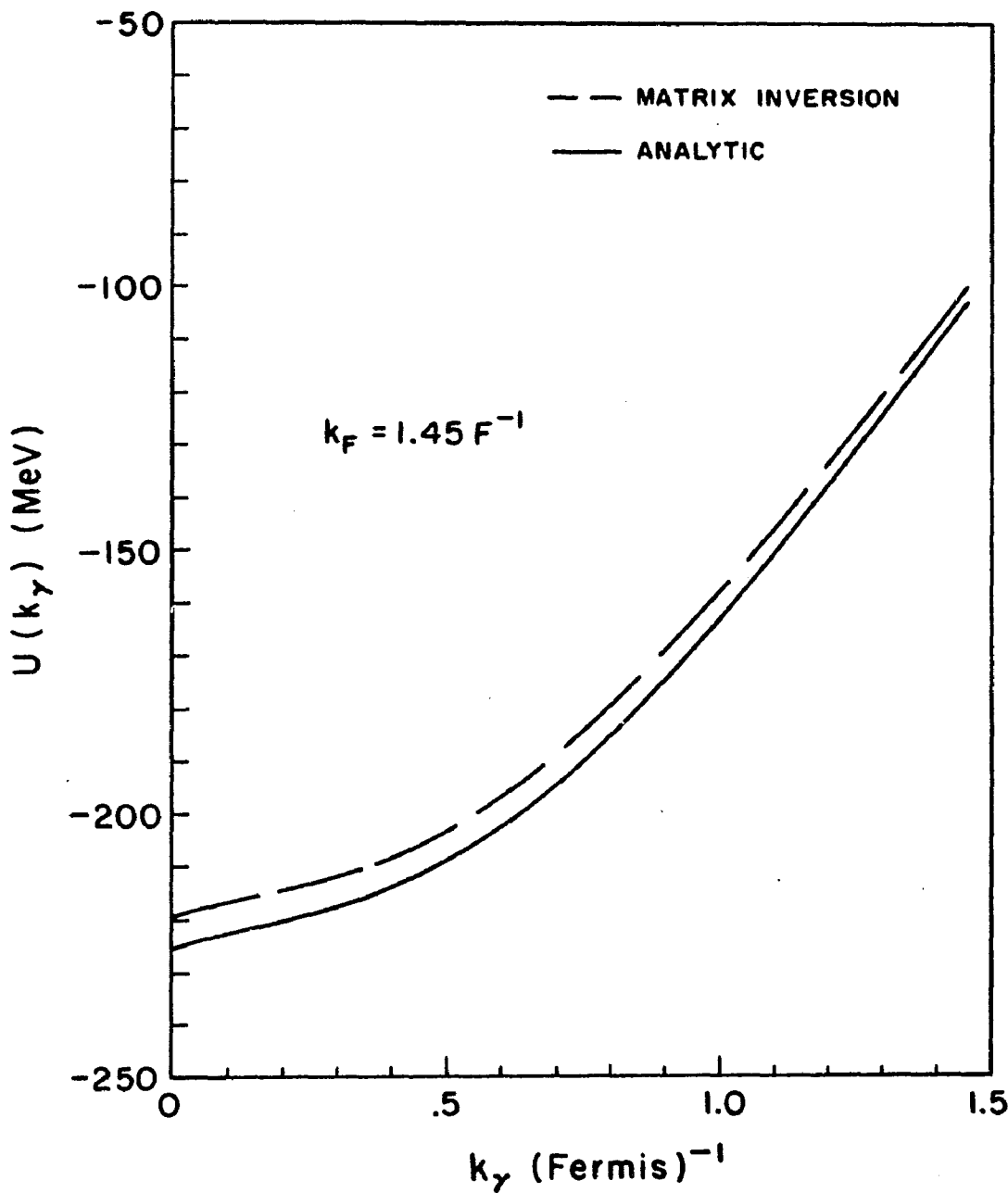


Figure 5. Comparison of the single-particle spectrum as obtained by matrix inversion to the analytic result: The analytic result is obtained without any approximations on the center-of-mass momentum. The results are for a strong separable potential. Hole spectrum parameters for the calculation of G are  $M^*/M = 0.8$ ,  $U_0 = 80$  MeV.

$$E = \frac{3}{5} \frac{\pi^2}{M} k_F^2 A + \frac{1}{2} \sum_{\mu\nu < A} \langle \mu\nu | G | \mu\nu - \nu\mu \rangle . \quad (3-9)$$

Application of the relation (3-11) and the partial-wave decomposition of  $G$  to (3-9) yields

$$E = \frac{3}{5} \frac{\pi^2}{M} k_F^2 A + \frac{3\pi^2 A}{\pi^2 M k_F^3} \sum_{L\alpha} (2J+1)(2T+1) \left[ 4\pi \int_0^{k_F} k_o^2 dk_o \int_0^{k_F - k_o} \right. \\ K^2 dK G_{LL}^\alpha(K; k_o, k_o) + 2\pi \int_0^{k_F} k_o^2 dk_o \int_{k_F - k_o}^{\sqrt{k_F^2 - k_o^2}} \left. K^2 dK \frac{(k_F^2 - K^2 - k_o^2)}{k_o K} \right] G_{LL}^\alpha(K; k_o, k_o) . \quad (3-35)$$

Appendix B3 contains the detailed derivation of this relation.

The limits of integration in (3-35) reflects that the integration is over all  $\vec{k}_o$  and  $\vec{K}$  for two particles in the Fermi sea. One may consult Figure 6 to verify these limits. The factor  $(k_F^2 - K^2 - k_o^2)/(k_o K)$  in the second integral results from the angular integration in  $\cos\theta_{\vec{k}_o \vec{K}}$ , since  $\cos\theta_{\vec{k}_o \vec{K}} < \frac{k_F^2 - K^2 - k_o^2}{2Kk_o}$  for two particles in the Fermi sea with relative momentum  $k_o$  and center-of-mass momentum  $K$ .

Following the same procedure as in the single-particle-spectrum case, we simplify (3-35) by the approximation

$$G_{LL}^\alpha(K; k_o, k_o) \approx G_{LL}^\alpha(K_{AVE}; k_o, k_o) . \quad (3-36)$$

Here  $K_{AVE}$  refers to the rms value of  $K$  for two particles below the Fermi sea with relative momentum  $k_o$ . The resulting rms center-of-mass momentum

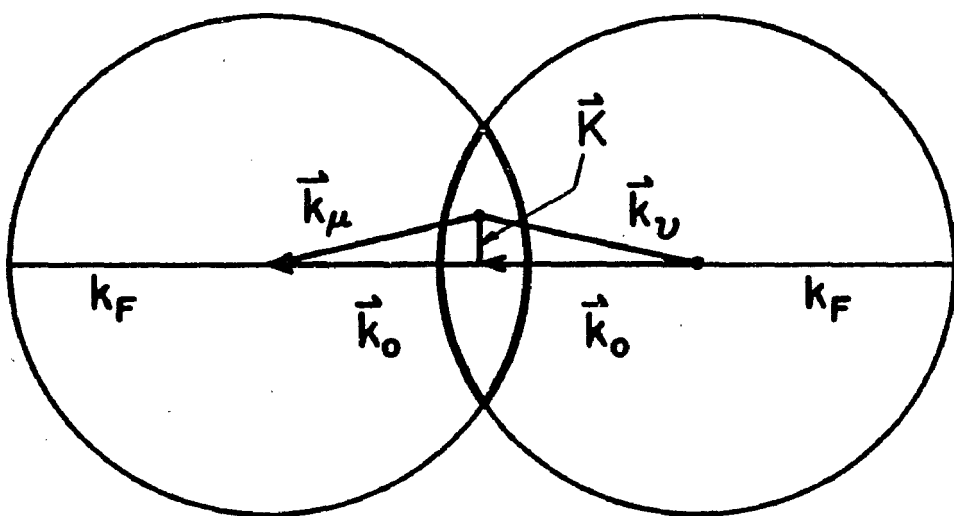


Figure 6. The allowed values of  $\vec{K}$  in calculating the total binding energy: The volume bounded by the heavy arcs represents the intersection of two Fermi spheres. The volume bounded by the heavy arcs indicates the allowed values of  $\vec{K}$  for a fixed  $\vec{k}_o$  for  $\vec{k}_\mu$  and  $\vec{k}_\nu$  to be inside a Fermi sphere.

is given by

$$K_{\text{AVE}}^2 = \frac{3}{5} k_F^2 (1 - k_o/k_F) \left( 1 + \frac{k_o^2/k_F^2}{3(2+k_o/k_F)} \right) . \quad (3-37)$$

This  $K_{\text{AVE}}$  should not be confused with the definition of  $K_{\text{AVE}}$  in the single-particle-spectrum case.

With the average-center-of-mass-momentum approximation, the expression for the ground-state energy per particle simplifies to

$$E/A \approx \frac{3}{5} \frac{n^2}{M} k_F^2 + \frac{4n^2}{mM} \sum_{LJ} (2J+1)(2T+1) \int_0^{k_F} k_o^2 dk_o \left( 1 - \frac{3}{2} \frac{k_o}{k_F} - \frac{1}{2} \frac{k_o^3}{k_F^3} \right) G_{LL}^\alpha(k_{\text{AVE}}; k_o, k_o) . \quad (3-38)$$

The ground-state energy of nuclear matter, according to (3-38), is simply the kinetic energy plus a summation of potential energies over the allowed eigenstates of the two-body system.

The numerical integration of (3-38) is by a 10 interval Simpson's rule. Again, doubling the intervals to 20 changes the numerical evaluation of the total nuclear binding energy by an insignificant amount (< .001 MeV).

Table IV gives the binding energy of nuclear matter determined from  $G$  matrix elements obtained by 10, 15 and 25 Laguerre-point matrix inversion. These values are also compared to the binding energy determined from analytic  $G$  matrix elements. The potential we employ for the results in Table IV is the very strong separable potential mentioned previously. The matrix inversion result comes to within 2 MeV out of 90 of

TABLE IV

Comparison of the  $^1S_0$  potential energy per particle determined from G matrix elements obtained by matrix inversion and analytic G matrix elements for a strong separable potential. All calculations are for  $k_p = 1.45F^{-1}$ ,  $M^*/M = .8$  and  $U_0 = 80$  MeV.

Laguerre Points	Potential Energy Per Particle (MeV)
$N = 10$	-91.86
$N = 15$	-88.04
$N = 25$	-89.52
Analytic	-89.98

the analytic result for 10 LaGuerre-point matrix inversion. For 25 Laguerre-point matrix inversion, the discrepancy is only .5 MeV. This accuracy is comparable to that obtained in the calculation of the single-particle spectrum. The improvement in precision as one increases the number of integration points from 10 to 25 indicates that the binding energy calculated by matrix inversion should converge to the analytic value for a sufficient number of integration points.

As a further check on the direct-matrix-inversion method, we calculated the binding energy of nuclear matter for the Reid soft-core potential and compared our results to those obtained by Sprung,<sup>30</sup> and by Kallio and Day.<sup>31</sup> In our calculations of the binding energy for the Reid soft-core potential, determination of self-consistent values of  $M^*$  and  $U_0$  preceded the computation of the total binding energy. Comparisons, state by state, of the binding energies obtained by 16 Gaussian-point matrix inversion to those determined by Sprung (reference-spectrum method) and Kallio and Day (an intro-differential equation method) appear in Table V. A more detailed calculation for the Reid soft-core potential appears in Section V, but we present some partial results in Table V for the sake of comparison. The binding energies in Table II are for  $k_F = 1.36F^{-1}$  with the self-consistent  $M^*$  and  $U_0$  that we calculate in Section V. The matrix-inversion binding energies agree extremely well with the binding energies obtained by Sprung, and by Kallio and Day, except for  $^3S_1$  state. Our calculations gave .6 MeV more binding in the  $^3S_1$  state than the calculation of Sprung, and .2 MeV more binding than the calculation of Kallio and Day. Kallio and Day infer that the disagreement between their binding energies and those of Sprung is due to the neglect of higher-order

TABLE V

State by state comparisons of the potential energies of the Reid soft - core potential as obtained by matrix inversion with the potential energies obtained by Sprung, and by Kallio and Day. In all cases  $k_F = 1.36F^{-1}$ . A Gaussian integration routine is used.

Potential Energy Per Particle (MeV)			
State	N = 16	Sprung <sup>b</sup>	Kallio and Day <sup>c</sup>
$^1S_0$	-15.57	-15.42	-15.52
$^1D_2$	- 2.55	- 2.54	- 2.56
$^1P_1$	2.39	2.40	2.38
$^3S_1$	-15.16	-14.50	-14.99
$^3D_1$	1.45	1.46	1.46
$^3D_2$	- 4.32	- 4.30	- 4.33
$^3P_0$	3.32	- 3.30	- 3.31
$^3P_1$	9.92	9.90	9.92
$^3P_2$	- 7.05	- 7.03	- 7.06
M*/M	.64 <sup>a</sup>		.60
$U_0$	79.05 <sup>a</sup>		81.00

<sup>a</sup>Our determination of the self consistent M\* and  $U_0$  includes effects of higher partial waves.

<sup>b</sup>Taken from Reference 30.

<sup>c</sup>Taken from Reference 31.

terms in the reference-spectrum calculation of Sprung. Kallio and Day claim that their results are more accurate. The slight error in our direct-matrix-inversion method probably results from the discontinuous derivatives of  $Q(k', K)$  in our integration grid. With the assumption that Kallio and Day's calculation is more accurate, the error due to discontinuous derivatives of  $Q(k', K)$  in our integration routines is about .2 MeV for the Reid soft-core potential. This error is negligible compared with the 6 MeV deviation between the binding energy of the Reid soft-core potential and the volume term of the semi-empirical mass formula. Consequently, we regard the results of our calculation to be in excellent agreement with those of Kallio and Day.<sup>70</sup>

From the results in Tables IV and V we conclude that the direct-matrix-inversion technique of solving the Bethe-Goldstone equation is quite accurate for computations of nuclear binding energies. Even with the very small error in our direct-matrix-inversion method, we achieve sufficient precision in computing nuclear binding energies for practical purposes.

The success of direct matrix inversion in our test cases indicates that perhaps the same technique may be applicable to finite-nucleus calculations. McCarthy and Kohler<sup>71,72</sup> use matrix inversion on the reference G matrix ( $G^R$ ) to calculate G for finite nuclei. Since the direct-matrix-inversion method gives accurate results in nuclear matter, the avoidance of the intermediate step of a reference-spectrum calculation seems to be possible in finite-nucleus calculations also. Although a finite-nucleus calculation is different from a nuclear-matter calculation in some respects, the applicability of the direct-matrix-inversion method to finite-nucleus calculations is worthy of investigation.

With the calculative techniques developed in the last two sections, we can now consider the two-body-scattering problem and the nuclear-many-body problem for finite, non-local potentials. We first apply the direct-matrix-inversion technique in the two-body problem to develop a smooth, non-local, potential model that fits the two-body phase-shifts in the triplet-even eigenchannels. Our future goal is to employ this potential model as part of a study of the properties of smooth potentials in nuclear matter. This goal requires the calculative techniques described in this section.

#### IV. A SMOOTH TRIPLET-EVEN POTENTIAL

Green,<sup>7</sup> and Levinger et al.<sup>8</sup> demonstrated that it was possible to fit the two-nucleon-scattering data with a potential that replaced the strong, static, repulsive core with a short-range repulsion that was quadratic in momentum. While the V matrix elements of these quadratic velocity-dependent potentials were finite, nuclear Hartree-Fock theory still did not readily converge for these potentials. The lack of convergence came mainly from the  $^3S_1 + ^3D_1$  eigenchannel in which the tensor force appears.

Tabakin and Davies<sup>32</sup> improved upon the convergence of the quadratic velocity-dependent potentials by introducing a velocity dependence of the form

$$V(r)C(p^2) + C(p^2)V(r)$$

where

$$V(r) = V_0 e^{-a^2 r^2} \quad \text{and}$$

$$C(p^2) = \frac{p^2}{h^2 a^2} e^{-p^2 s^2 / h^2} \quad (4-1)$$

The presence of the "smoothness parameter" s enabled Tabakin and Davies to further reduce the off-energy-shell V matrix elements over those of the earlier quadratic forms. Tabakin and Davies excluded the important triplet states from their potential because of the difficulty in solving the Schrödinger equation for non-local potentials in eigenchannels with a bound state.

Employing the matrix-inversion technique to solve the two-body problem, we extend the work of Tabakin and Davies to the triplet-even states. The results are two very smooth potential models that fit the scattering phase parameters in the  $^3S_1 + ^3D_1$  and  $^3D_2$  eigenchannels.

The introduction of the velocity dependence (4-1) helped Tabakin and Davies reduce the off-energy-shell matrix elements of the central force. Likewise, we are able to reduce the off-energy-shell matrix elements of the tensor force by introducing velocity dependence of the form (4-1) into the tensor interaction of our potential models. At the same time we achieve satisfactory fits to the scattering phase-shifts and mixing coefficients in the  $^3S_1 + ^3D_1$  and  $^3D_2$  eigenchannels. The ability to reduce the off-energy-shell matrix elements of the tensor force and yet fit the scattering data is the result of the increased freedom the velocity-dependent forms of the tensor force give one in reducing short-range correlations. In particular, velocity-dependent tensor forces allow us to fit the mixing coefficient  $\xi_1$  with tensor forces that have small off-energy-shell matrix elements. Therefore, we are able to produce wave functions that have the correct tensor coupling at large distances, yet do not have strong short-range correlations due to tensor coupling.

Up to now non-local tensor forces have not been widely used. The local tensor forces in most recent phenomenological potentials, even in those potentials that have non-static central forces, are responsible for the large higher-order corrections to Hartree-Fock calculations in the  $^3S_1 + ^3D_1$  eigenchannel. We shall see in Section V that our potential models, with their velocity-dependent tensor forces, give extremely small higher-order corrections in the binding energy of nuclear matter.

The theoretical justification for non-local tensor forces derives from the one-boson-exchange theory of nuclear forces. For example, the OBEPs proposed by Ingber<sup>6</sup> and by Green and Sawada<sup>5</sup> contain velocity-dependent tensor forces in the non-relativistic limit. Solution of the two-body problem in momentum space allows us to include general non-local tensor forces in the two-body scattering problem.

Our motivation in developing a very smooth potential model is to study the properties of smooth potentials in nuclear matter. By studying the properties of nuclear matter for forces of varying smoothness, we hope to determine what constraints nuclear saturation places on the smoothness of the two-nucleon interaction. Whether nuclear saturation rules out or fails to rule out smooth forces is a crucial factor for the validity of the Hartree-Fock technique of predicting properties of nuclei.

#### A. Smoothness and Tensor to Central Effects in the Two-Body and Many-Body Problems

The necessary conditions for smoothness in the  $^3S_1 + ^3D_1$  eigen-channel are small second-order corrections to the G matrix in the  $^3S_1$  state. The second-order correction to  $G_{00}^\alpha(K; k_o, k_o)$  is given by

$$- \frac{2}{\pi} \int_0^\infty \frac{k'^2 dk' Q(k', K) V_{00}^2(k_o, k')}{e^>(k', K) - e^<(k_o, K)} - \frac{2}{\pi} \int_0^\infty \frac{k'^2 dk' Q(k', K) V_{02}^2(k_o, k')}{e^>(k', K) - e^<(k_o, K)} . \quad (4-2)$$

Both terms in (4-2) are attractive. The second term is due to the tensor interaction. Consequently, the attraction in the  $^3S_1$  state in nuclear matter depends to a large degree on the magnitude of the off-energy-shell matrix elements of the tensor force. The intermediate-state momenta that

contribute to this attraction are those that are not suppressed by the Pauli Q operator. Smoothness requires small off-energy-shell matrix elements of the tensor force.

In the two-body free-scattering problem, the second-order correction to the R matrix  $R_{00}^\alpha(k_0, k_0)$  is given by

$$- \frac{2}{\pi} \int_0^\infty \frac{k'^2 dk' V_{00}^2(k_0, k')}{k'^2 - k_0^2} - \frac{2}{\pi} P \int_0^\infty \frac{k'^2 dk' V_{02}^2(k_0, k')}{k'^2 - k_0^2} . \quad (4-3)$$

Just as in nuclear matter, some of the attraction in the  $^3S_1$  state for two freely interacting nucleons depends on the magnitude of the off-energy-shell matrix elements of the tensor force. The contribution to the attraction in the  $^3S_1$  state due to the tensor force relative to the contribution of the central force, which acts in all orders, is sometimes referred to as the tensor-to-central ratio. Forces that rely on different tensor-to-central ratios to give the correct  $^3S_1$  phase-shifts may differ appreciably in their  $^3S_1$  potential-energy contributions to nuclear matter. This possibility results from the different effects the

propagators  $\frac{Q(k', k)}{e > - e <}$  and  $\frac{1}{k'^2 - k_0^2}$  have on the importance of higher-order corrections in the Bethe-Goldstone and Lippmann-Schwinger equations. In the Bethe-Goldstone equation, for instance, the Pauli Q operator suppresses the higher-order corrections due to intermediate states with low relative momenta  $k'$ . These different effects show up more strongly in the tensor force because the tensor force contributes for the first time in second order. The second-order contributions from the tensor force are usually large. Our calculations in Section V show that potentials with nearly the same

phase-shifts may have vastly different binding energies depending on the tensor force strengths.

### B. The Potential Model

For a given spin and isospin our potential model has the form

$$v^{ST}(\vec{r}, \vec{p}, \vec{\sigma}_1, \vec{\sigma}_2) = v_C + v_P + v_{SO} + v_T + v_{TP} + v_{TPP}$$

where the above terms stand for the following:

$v_C = v_C(r)$  gives the local, central interaction;

$v_P = \frac{1}{2}[v_P(r)c_P(p^2) + c_P(p^2)v_P(r)]$  gives the central, velocity - dependent interaction;

$v_{SO} = v_{SO}^J(r)\vec{L}\cdot\vec{S}$  gives the spin-orbit interaction, where the superscript J indicates that the spin-orbit interaction may be different in each eigenchannel;

$v_T = v_T(r)s_{12}(\hat{r})$ , where  $s_{12}(\hat{r}) = 3(\vec{\sigma}_1\cdot\hat{r})(\vec{\sigma}_2\cdot\hat{r}) - \vec{\sigma}_1\cdot\vec{\sigma}_2$ , gives the local-tensor interaction;

$v_{TP} = \frac{1}{2}[v_{TP}(r)s_{12}(\hat{r})c_{TP}(p^2) + c_{TP}(p^2)s_{12}(\hat{r})v_{TP}(r)]$  indicates the velocity-dependent tensor interaction in our potential model "B"; and

$v_{TPP} = \frac{1}{2}[v_{TPP}(r)s_{12}(\hat{p})c_{TPP}(p^2) + c_{TPP}(p^2)s_{12}(\hat{p})v_{TPP}(\hat{p})]$ , where  $s_{12}(\hat{p}) = 3(\vec{\sigma}_1\cdot\hat{p})(\vec{\sigma}_2\cdot\hat{p}) - \vec{\sigma}_1\cdot\vec{\sigma}_2$ , indicates the velocity-dependent-tensor interaction in our potential model "A". Okubo and Marshak<sup>38</sup> quote the S-matrix analysis of Puzikov et al.<sup>73</sup> that

indicates that the  $(\vec{\sigma}_1 \cdot \hat{p})(\vec{\sigma}_2 \cdot \hat{p})$  term in our model may be expressed in terms of the other forces that appear in our model, if one is interested only with the S matrix or on-energy-shell properties. Since we are interested in off-energy-shell properties of the two-nucleon interaction, we retain the  $V_{TPP}$  force. Okubo and Marshak<sup>38</sup> include the  $(\vec{\sigma}_1 \cdot \hat{p})(\vec{\sigma}_2 \cdot \hat{p})$  force in their "most general" two-nucleon interaction as well.

For the radial forms we choose Gaussians, i.e.  $V_i(r) = v_i e^{-a_i^2 r^2}$  except for the tensor interactions for which  $V_i(r) = v_i a_i^2 r^2 e^{-a_i^2 r^2}$ .

For the spin-orbit force, we allow the radial form to be state dependent with the possibility of two radial terms, i.e.,

$$V_{SO}^j(r) = v_{SO1}^j e^{-a_{SO1}^2 r^2} + v_{SO2}^j e^{-a_{SO2}^2 r^2}.$$

We find this necessary to fit both the  ${}^3D_1$  and  ${}^3D_2$  phase-shifts with weak tensor forces. We retain the velocity dependence of Tabakin and Davies

$$C_i(p^2) = \frac{p^2}{\hbar^2 a_i^2} e^{-p^2 s_i^2 / \hbar^2}.$$

This choice of velocity dependence helps reduce off-energy-shell matrix elements of the velocity-dependent terms.

We have two reasons for choosing Gaussian radial dependence. First, the matrix elements  $V_{LL}^\alpha(k, k')$  have analytic forms. These analytic forms appear in Appendix C1. Second, the matrix elements for both the central and tensor interactions decay as  $e^{-(k-k')^2/4a_i^2}$  off-the-

energy-shell. This exponential decay of the V matrix off-the-energy-shell is much more rapid than the decay off-the-energy-shell of potentials that possess the more common Yukawa radial dependence  $V(r) \propto e^{-\mu r}/r$ .

To fit the parameters of our potential model to the experimental phase parameters determined by the Yale group (YIV-1967),<sup>74</sup> we employed direct matrix inversion of the Lippmann-Schwinger equation in momentum space. The details of the direct-matrix-inversion technique appear in Section II of this thesis. We employed a 15-point La Guerre integration formula to numerically invert the Lippmann-Schwinger equation and to solve for the phase-shifts.

Initially we attempted to fit the phase parameters with a purely local, long-ranged, tensor force. Since the rate of decay of the V matrix elements off-the-energy-shell increases with the decreasing inverse range  $a_T$ , we limited this attempt to small values of  $a_T$ . This attempt failed. Invariably the mixing coefficient  $\mathcal{E}_1(k)$  changed sign within the energy region  $E_{LAB} < 330$  MeV. The experimental values of  $\mathcal{E}_1(k)$ , as determined by the Yale group, are always positive for  $E_{LAB} < 330$  MeV. We found that we could retain the long-range local tensor force if we added a short-ranged, velocity-dependent tensor force to prevent the sign change in  $\mathcal{E}_1(k)$ . The velocity-dependent part of the tensor force dominates the tensor interaction on-the-energy-shell at higher energies and is able to prevent the sign change in  $\mathcal{E}_1(k)$ . The long-ranged, local tensor force that we retained has small off-energy-shell matrix elements because the inverse range  $a_T$  is small. The velocity-dependent tensor force also has small off-energy-shell matrix elements because we employ the Tabakin-Davies exponential velocity dependence. In Figure 7 we illustrate the situation. Figure 7 qualitatively depicts the mixing

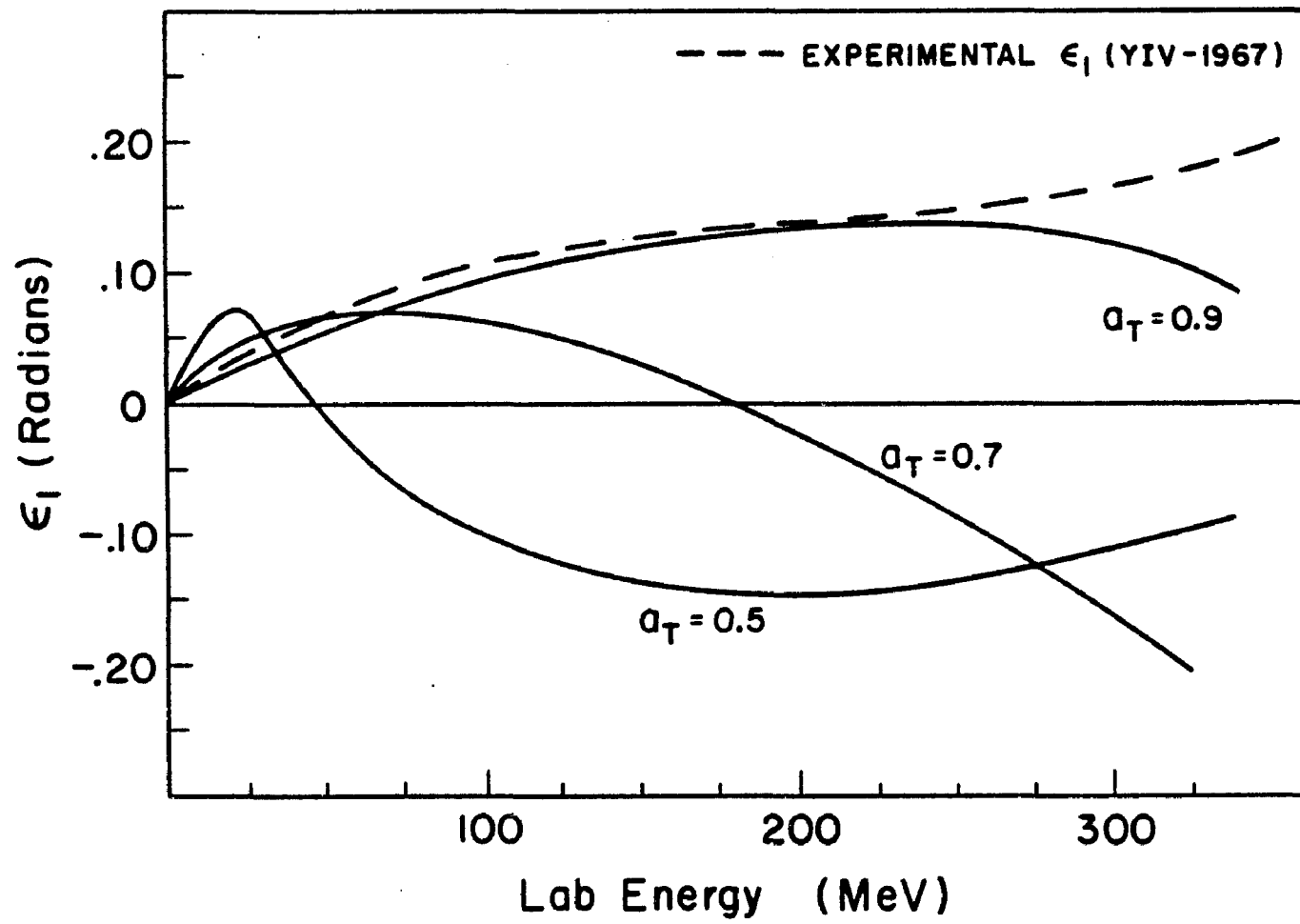


Figure 7. The behavior of the mixing coefficient  $\epsilon_1$  for local tensor forces of  $r^2 \times$  Gaussian radial dependence for various inverse ranges  $a_T$ .

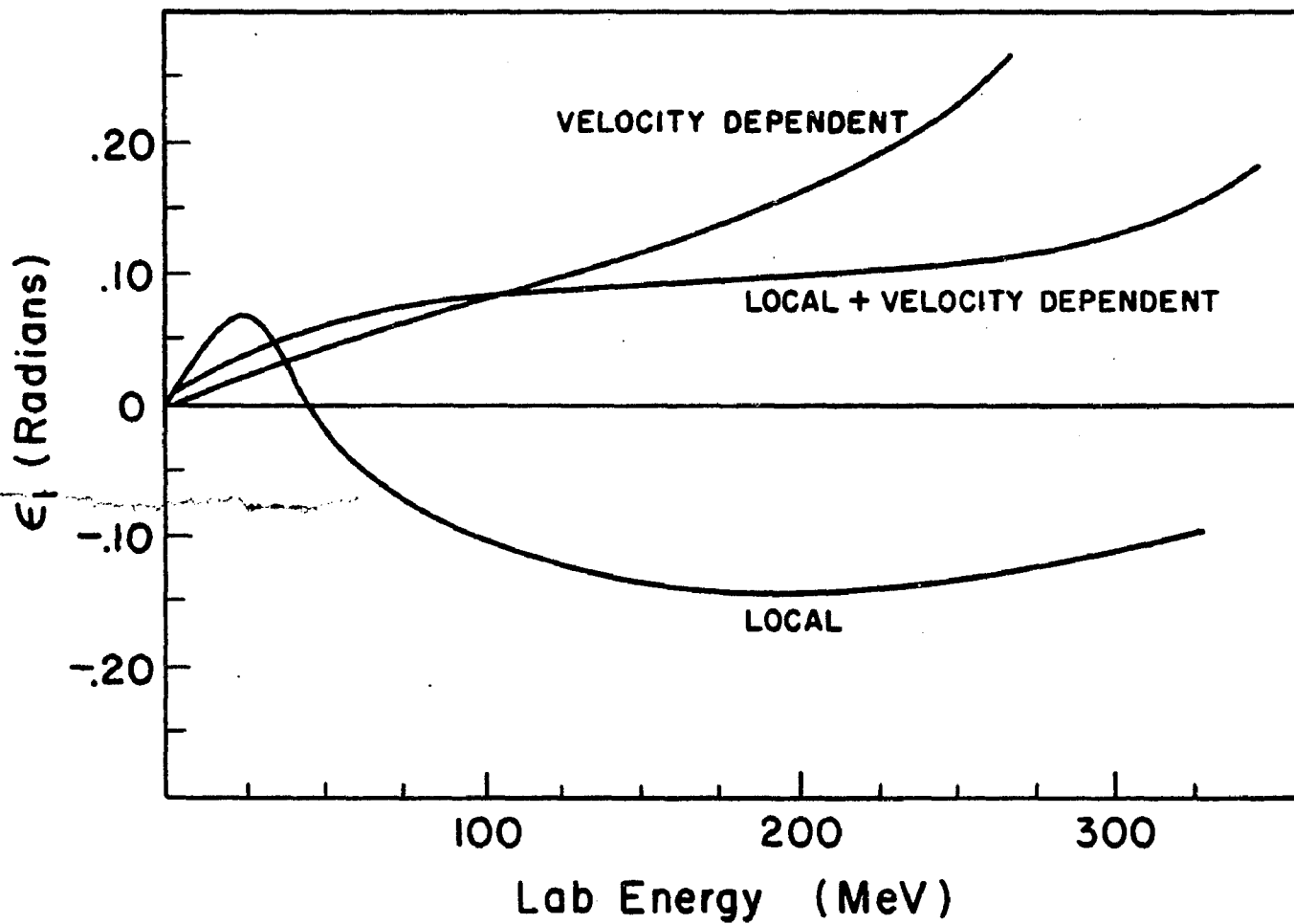


Figure 8. The behavior of the mixing coefficient  $\epsilon_1$  for a local long-range tensor force, a velocity dependent tensor force, and a combination of local and velocity-dependent tensor forces: The curve with the combination does not necessarily correspond to an equal combination.

coefficient  $\epsilon_1(k)$  resulting from local tensor forces of  $r^2$  times Gaussian radial dependence for various values of  $a_T$ . We rejected values of  $a_T > .8$  to avoid large off-energy-shell matrix elements. Figure 8 shows the resolution of our problem by qualitatively illustrating the mixing coefficients  $\epsilon_1(k)$  for various combinations of a long-ranged, local tensor force and a short-ranged, velocity-dependent tensor force.

With the utilization of velocity-dependent tensor forces, we obtained satisfactory fits to the  $^3S_1 + ^3D_1$  and  $^3D_2$  phase parameters for forces A and B. In Table VI we present the potential parameters employed to obtain the scattering phase parameters that appear in Figures 9 to 11. We employ the Blatt-Biedenharn parameterization.<sup>39</sup> We were also able to reproduce nearly the correct effective-range data and deuteron binding energy. These quantities, along with the deuteron electric-quadrupole moments and D-state probabilities, appear in Table VII. The deuteron electric-quadrupole moment,  $Q$ , is related to the low-energy mixing coefficient by the approximate relation<sup>75</sup>

$$\epsilon_1(k) \approx \sqrt{2} Q k^2 .$$

The electric-quadrupole moment, therefore, depends on the low energy, on-energy-shell behavior of the R matrix. We believe that the electric-quadrupole moment for force B could be improved without drastic alteration in the off-energy-shell behavior of our potential B. The low D-state probabilities in both forces are probably a necessary result of the weak tensor forces.

TABLE VI  
Potential parameters for forces A and B.

Force	(MeV)							
	$v_C$	$v_P$	$v_{SO1}^1$	$v_{SO1}^2$	$v_{SO2}^2$	$v_T$	$v_{TP}$	$v_{TPP}$
A	-186.0	7200.0	-423.0	28.0		5.55		1005.0
B	-97.6	7200.0	-6.3	.5.0	-1400.0	-25.0	-840.0	
(Fermis) <sup>-1</sup>								
	$a_C$	$a_P$	$a_{SO1}^1$	$a_{SO1}^2$	$a_{SO2}^2$	$a_T$	$a_{TP}$	$a_{TPP}$
A	1.00	2.80	1.10	0.53	1.60	0.44		2.20
B	0.79	2.80	0.40	0.34		0.73	1.80	
(Fermis) <sup>-1</sup>								
		$s_P$		$s_{TP}$		$s_{TPP}$		
A		0.530				0.785		
B		0.544		0.640				

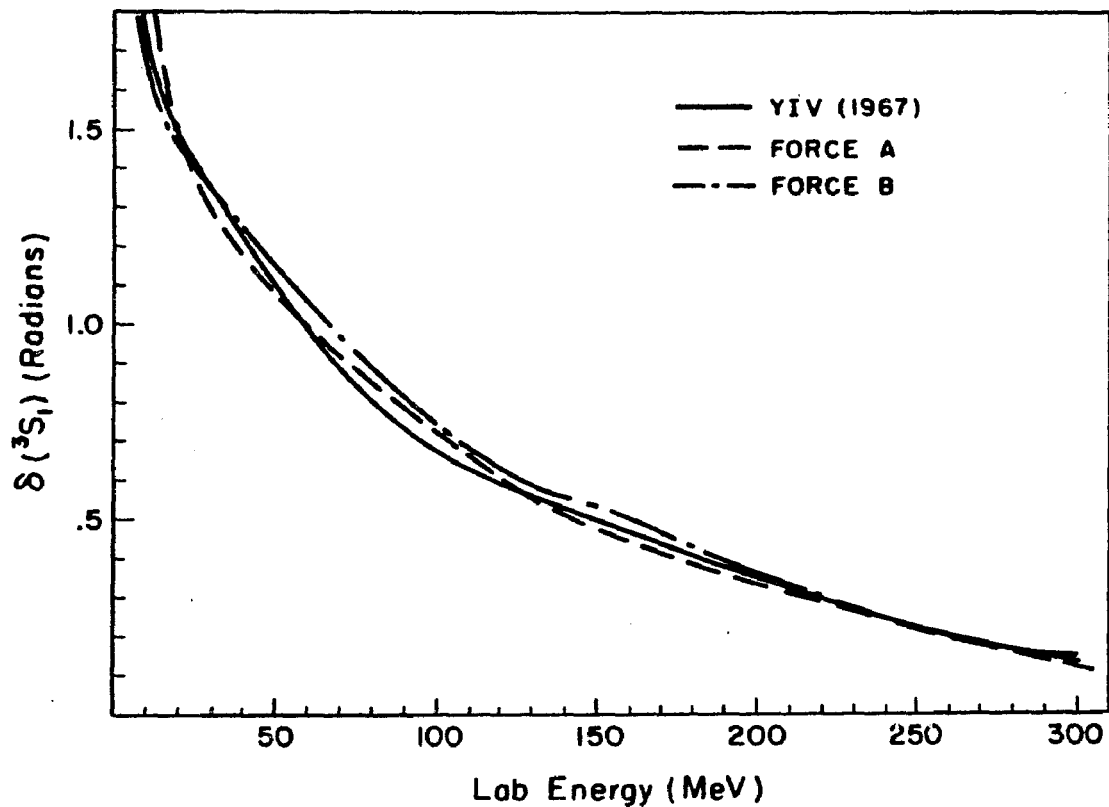


Figure 9. The  $^3S_1$  phase-shifts for forces A and B compared to Y-IV (1967).

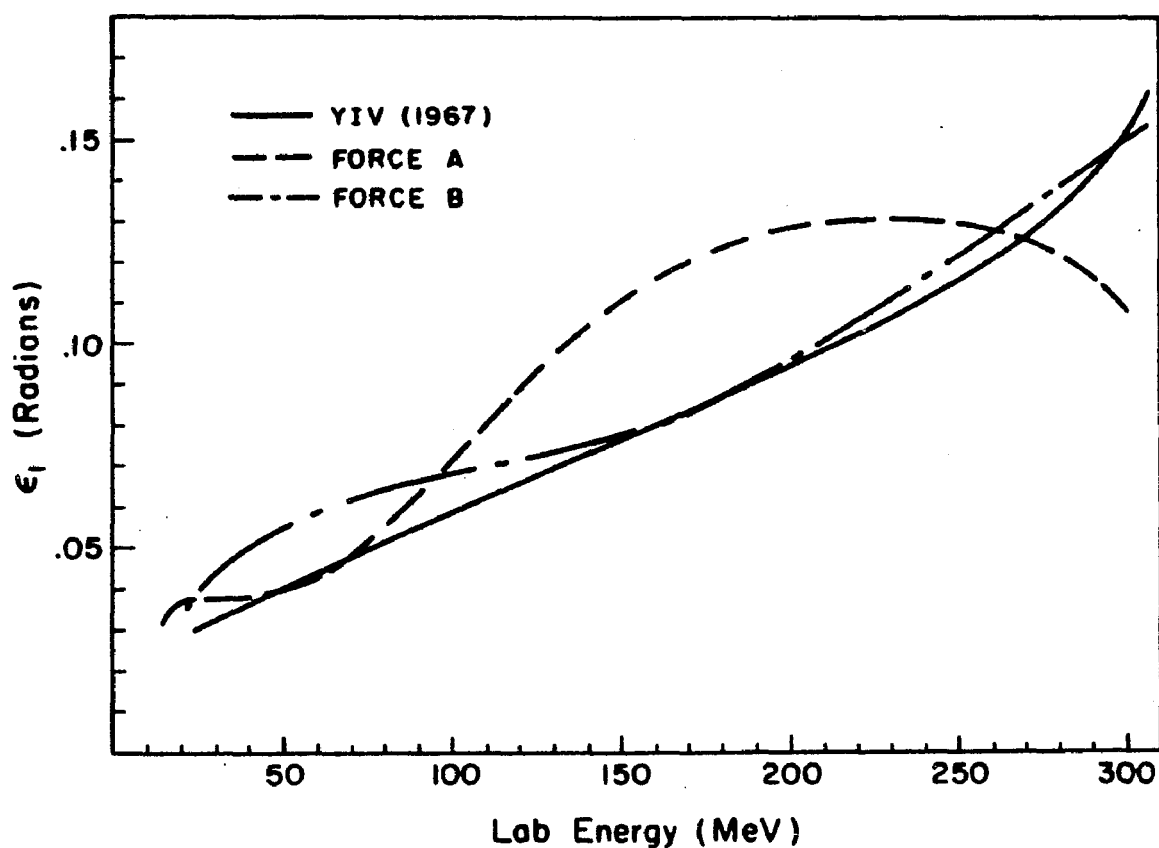


Figure 10. The mixing coefficient  $\epsilon_1$  for forces A and B compared to Y-IV (1967).

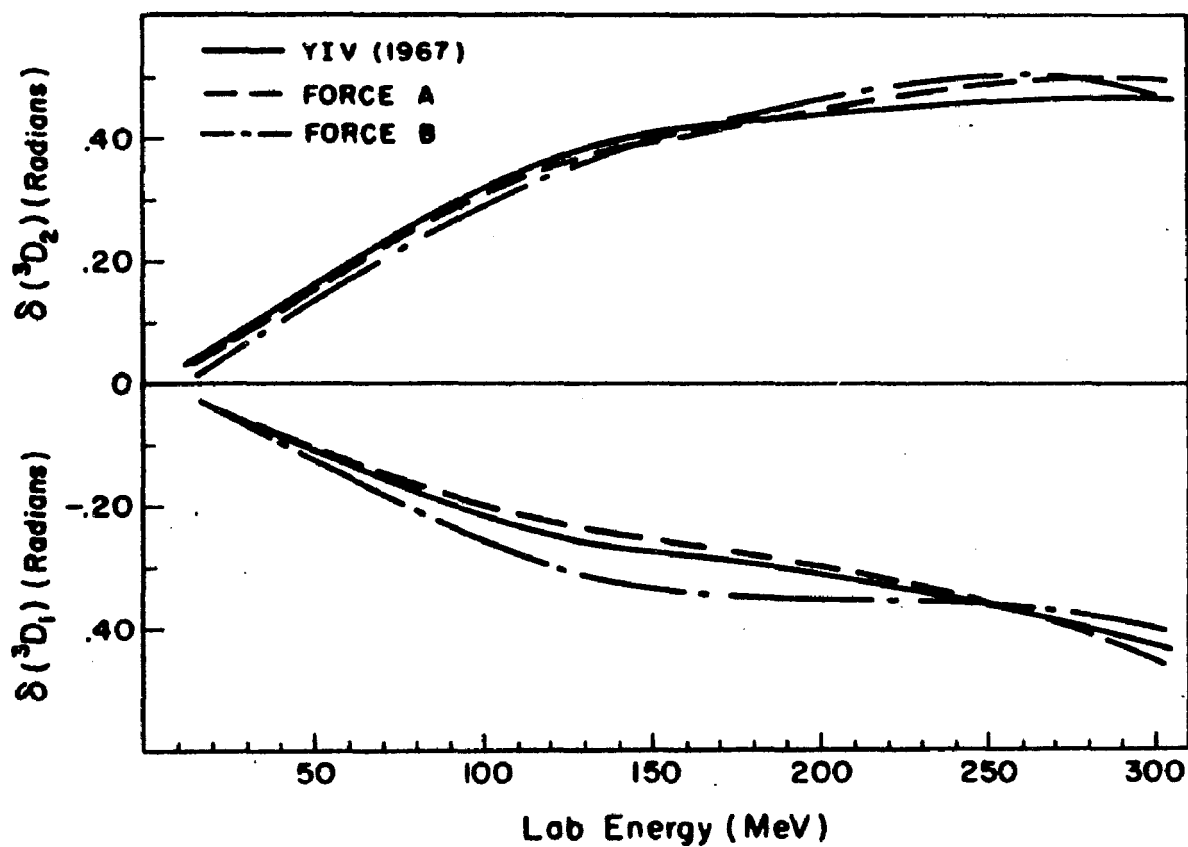


Figure 11. The  $^3D_1$  and  $^3D_2$  phase-shifts for forces A and B compared to Y-IV (1967).

TABLE VII

Effective range and deuteron data for forces A and B.

	A	B	Experiment
$a_T$ (F)	5.404	5.391	$5.392 \pm .006$
$r_{OT}$ (F)	1.738	1.731	$1.726 \pm .014$
$E_B$ (MeV)	2.28	2.28	2.22
$Q$ ( $F^2$ )	.265 <sup>a</sup>	.124 <sup>a</sup>	.278
$P_D$ (%)	2.00	2.01	4-8

<sup>a</sup>Calculated from the effective range formula  $\epsilon_1(k) \approx \sqrt{2} Qk^2$  for small k.

We evaluated this expression at  $E_{Lab} = 2$  MeV.

### C. S-Wave Phase Shifts and Mixing Coefficient

As mentioned earlier, some of the attraction in the  $^3S_1$  state in the two-body problem results from the tensor force acting in second-order and higher-order in the Born series. While both forces A and B match the experimental  $^3S_1$  phase-shifts well, force B, with a larger  $a_T$ , relies on a greater tensor-to-central ratio than that of force A. This result implies that the  $^3S_1 + ^3D_1$  phase parameters do not determine the tensor-to-central ratio to any great degree. Reid noted a similar situation in comparisons of the tensor-to-central ratios in his hard-and soft-core potentials. Because the phase parameters do not determine the central-to-tensor ratio, we are able to fit the experimental  $^3S_1 + ^3D_1$  phase parameters with potentials that have weak tensor forces.

The reason force B requires a shorter-ranged, stronger, local tensor force than that of force A follows from the low-energy behavior of the two types of tensor forces we employ. The strength of the on-energy-shell V matrix elements of  $V_{TP}$  at low energies are proportional to  $k^4$ . The matrix elements of  $V_{TPP}$  on-the-energy shell are proportional to  $k^2$  at low energies. The velocity-dependent tensor force  $V_{TPP}$ , therefore, has greater influence on the low and intermediate-energy mixing coefficients than  $V_{TP}$  does. The greater influence of  $V_{TPP}$  on  $\mathcal{E}_1$  allows us more freedom in fitting  $\mathcal{E}_1(k)$  and in reducing the off-energy-shell matrix elements of the tensor force. The tensor force that results in force A, in fact, is weaker than that of force B. The relative strengths of forces A and B are discussed further in Section V.

The mixing coefficients  $\mathcal{E}_1(k)$  in Figure 10 appear to be quite different for forces A and B. The mixing coefficient  $\mathcal{E}_1(k)$ , however, is

not experimentally well determined. The experimental errors in  $\epsilon_1$  at high energy ( $E_{LAB} \gtrsim 200$  MeV) are of the order of  $\pm .1$  radian.<sup>76</sup> Because of the large experimental errors in the measurement of  $\epsilon_1$ , we regard the fits of forces A and B to  $\epsilon_1$  as satisfactory.

#### D. D Wave Phase-Shifts

If we apply the same spin-orbit interaction in the  $^3D_2$  state as in the  $^3S_1 + ^3D_1$  eigenchannel for forces A and B, the resulting  $^3D_2$  phase-shifts appear in Figure 12. These phase-shifts are unsatisfactory, especially for force A. To correct these phase-shifts, we allow the spin-orbit interaction to be state dependent. We are then able to produce the satisfactory  $^3D_2$  phase-shifts that appear in Figure 11.

Our inability to fit the  $^3D_1$  and  $^3D_2$  phase-shifts with the same spin-orbit force is the result of the weak tensor forces we employ, especially in force A. The expectation value of  $S_{12}(\hat{r})$  and  $S_{12}(\hat{p})$  have the same magnitudes, but opposite signs, in the  $^3D_1$  and  $^3D_2$  states. This property causes a splitting in the  $^3D_1$  and  $^3D_2$  phase-shifts. Experimentally, the  $^3D_1$  and  $^3D_2$  phase-shifts are of approximately the same magnitude but of opposite signs. In force A, most of the strength of the tensor force resides in the short-ranged, velocity-dependent part. The D waves do not feel the short-ranged part of the tensor interaction. Because the long-ranged, local part of the tensor force is weak, the tensor force does not provide the necessary splitting of the  $^3D_1$  and  $^3D_2$  phase-shifts. A similar situation occurs for force B, but the situation improves at high energies.

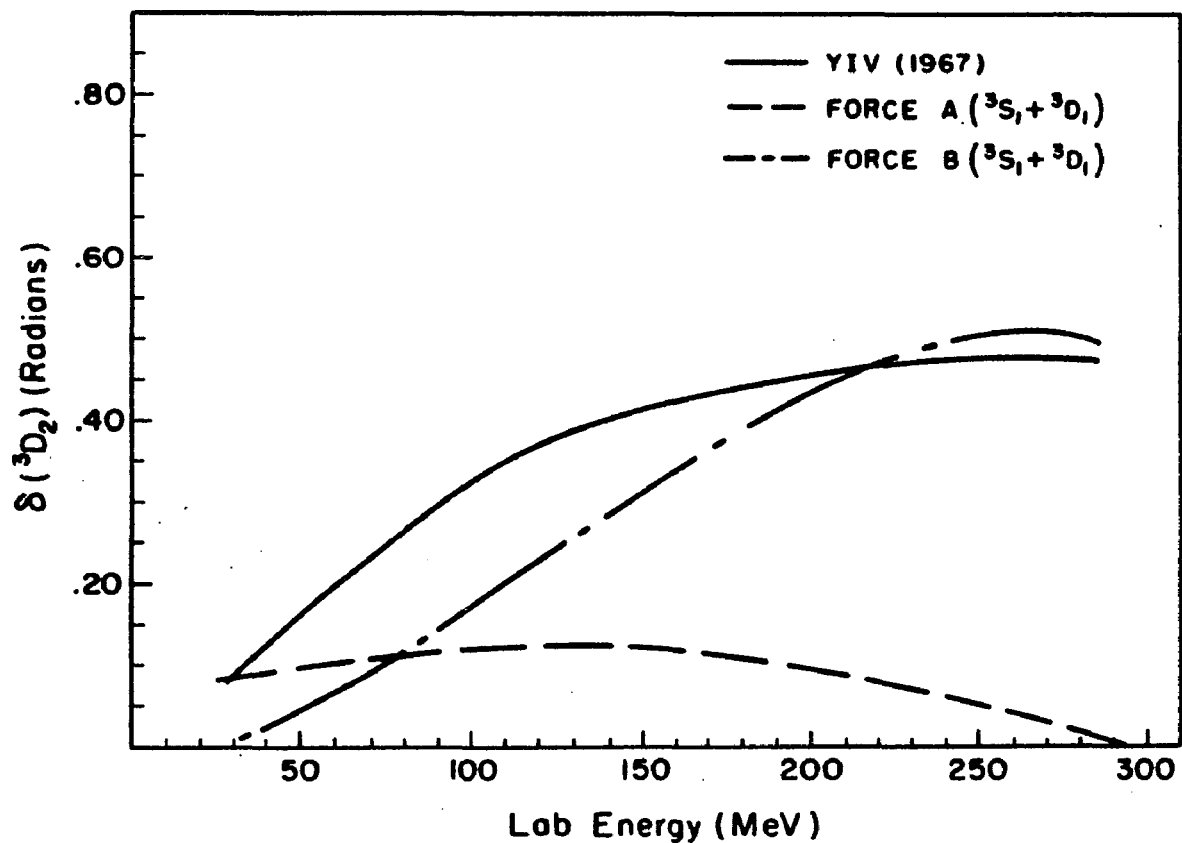


Figure 12. The  $^3D_2$  phase-shifts for forces A and B if these forces employ the same spin-orbit force in the  $^3D_2$  eigenchannel as they do in the  $^3S_1 + ^3D_1$  eigenchannel: Comparisons with Y-IV are shown.

We do not regard the state-dependent spin-orbit forces as serious deficiencies in our potential models. Forces A and B are purely phenomenological. In the phenomenological sense they are satisfactory because they produce nearly the correct on-energy-shell properties in the  $^3S_1 + ^3D_1$  and  $^3D_2$  eigenchannels. Thus we may apply forces A and B to nuclear matter to study the role of off-energy-shell behavior in nuclear saturation.

#### E. Forces A and B in the Nuclear Many-Body Problem

Having described the technical aspects of our smooth potential models in the two-body problem, we now indicate how these forces can be employed to study the nuclear many-body problem.

While our work and the work of Tabakin and Davies<sup>32</sup> demonstrate that the smooth velocity-dependent potentials are consistent with the two-body-scattering data, the properties of smooth potentials on nuclear saturation are relatively unknown. The smooth Tabakin-Davies potential gives qualitatively the same  $^1S_0$  potential energy in nuclear matter as the nearly-singular Reid soft-core potential.<sup>32</sup> This result implies that off-energy-shell behavior does not assume an important role in nuclear saturation. With the presence of the tensor force in the  $^3S_1 + ^3D_1$  eigenchannel, the story may be different. In fact, the results of nuclear-matter calculations in Section V show that the strength of the tensor force is the most critical factor in nuclear saturation.

Forces A and B are not complete two-nucleon interactions because these forces apply to only the  $^3S_1 + ^3D_1$  and  $^3D_2$  eigenchannels. To study the properties of smooth potentials in nuclear matter, we supplement

forces A and B with other previously developed smooth potentials. For the singlet states, we employ the Tabakin-Davies potential.<sup>32</sup> For the triplet-odd states, we employ one (force C) of a set of smooth potentials developed by Nestor, Krieger, Davies, and Baranger.<sup>77</sup> The details of the potential models we use may be found in the appropriate references. The inclusion of these potentials into our smooth potential models enables us to study nuclear matter with very smooth, velocity-dependent potentials. To study partial waves higher than D waves, we recommend using the one-pion exchange-potential (OPEP),<sup>78</sup> or the phase-shift approximation,<sup>10,79-81</sup> because the smooth potential models we employ fit the phase-shifts only up to D waves.

## V. NUCLEAR MATTER CALCULATIONS

In the previous section we have shown that it is possible to fit smooth potential models, with weak tensor forces, to the two-nucleon phase-shifts in the  $^3S_1 + ^3D_1$  eigenchannel. The question now arises as to whether smooth potential models, with weak tensor forces, can yield the correct binding energy of nuclei. The results of our nuclear-matter calculations in this section indicate that strong tensor forces, not strong short-range repulsions, are necessary for nuclear saturation to occur at nearly the correct density. The results of our calculations contradict the assumption that one may predict properties of nuclei with smooth forces. This assumption is the basic premise of nuclear-Hartree-Fock theory.

To detect a consistent relation between the smoothness of the two-nucleon interaction and nuclear saturation, we employ several potential models of varying smoothness and tensor-force strength. These potentials include the smooth potentials A and B of Section IV, the static Reid soft-core potential,<sup>27</sup> the Bryan-Scott OBEP,<sup>1-3</sup> and a velocity-dependent potential developed by Appel.<sup>82</sup> We include an OBEP in our study to test whether the one-boson-exchange theory of nuclear forces can account for nuclear saturation.

Of the potentials we study, only the Reid potential is static. The Bryan-Scott and Appel potentials have quadratic velocity dependence. The Appel potential, like forces A and B, includes a velocity-dependent tensor force.

All of the potentials we use give reasonably good fits to the two-body data. We are reasonably certain, therefore, that the differences

in binding energies among the potentials we consider are primarily due to off-energy-shell properties rather than to different fits to the two-body data. Later in this section we shall indicate how one may isolate off-energy-shell effects by generating exactly phase-shift equivalent potentials through a canonical transformation. We also briefly examine the sensitivity of nuclear-binding energies to the particle spectrum.

### A. Smoothness Criteria

To measure the strengths of the two-nucleon potentials mentioned previously, we employ the wound integral  $\kappa$  defined by Equation (3-14), and the partial-wave wound integrals  $\kappa_{LL}^{\alpha}$ , defined by (3-27). We concentrate our attention on  $\kappa_{00}$  for the  ${}^1S_0$  eigenchannel, and on  $\kappa_{00}$  and  $\kappa_{02}$  for the  ${}^3S_1 + {}^3D_1$  eigenchannel, because these quantities determine the strengths of the short-range repulsion and the tensor force for incident S waves. We find that  $\kappa_{02}$ , which measures the strength of the tensor force in the  ${}^3S_1 + {}^3D_1$  eigenchannel, plays an extremely crucial role in nuclear saturation.

Another important quantity is the Bessel transform,  ${}^{83}F_{LL}^{\alpha}(k)$ , of the wave-function defect. This Bessel transform is given by

$$\begin{aligned} F_{LL}^{\alpha}(k) &= k_o \int_0^{\infty} r^2 dr j_L^{\alpha}(kr) \kappa_{LL}^{\alpha}(r) \\ &= \frac{k Q(k, K) G_{LL}^{\alpha}(K; k, k_o)}{e^{-\langle k_o, K \rangle} - e^{-\langle k, K \rangle}} \end{aligned} \quad (5-1)$$

The quantity  $F_{LL}^{\alpha}(k)$  is a measure of the probability that an incident pair of particles with orbital angular momentum L, relative momentum  $k_o$ ,

and center-of-mass momentum  $K$  are excited to orbital angular momentum  $L'$  and relative momentum  $k$ . When we summarize our results later in this section, we analyze the role  $F_{OL'}^\alpha(k)$  plays in the saturation mechanism of nuclear matter. The importance of the tensor force, it turns out, results from the properties of  $F_{O2}^\alpha(k)$ .

To demonstrate how nuclear-binding energies and saturation densities depend on smoothness, we now present a description of our calculations and the results.

### B. Description of the Nuclear-Matter Calculations

The nuclear-matter calculations described in this section involve one basic numerical technique. Namely, the direct matrix inversion of the Bethe-Goldstone equation to solve for the  $G$  matrix. We employ the angle-average approximation, the effective-mass approximation, and the average center-of-mass momentum approximations described in Section III. A sixteen-point Gaussian integration formula replaces the infinite integrals in the Bethe-Goldstone equation for all potentials except for forces A and B. For forces A and B we use a fifteen-point Laguerre integration formula. We evaluate the finite integrals (3-34) and (3-38) needed to calculate the single-particle energies and the total binding energies by Simpson's Rule. The integration mesh is divided into ten equal intervals from  $k_0 = 0$  to  $k_0 = k_F$ . With the evaluation of these integrals, we calculate the binding energy as a function of  $k_F$ ; we also calculate self-consistent values of  $M^*$  and  $U_0$ . Discussions of the self-consistency problem occur for each potential individually. We calculate the wound integrals  $\kappa_{LL'}^\alpha$  by numerical integration of (3-28). We compute

$F_{OL}^{\alpha}(k)$  directly from the G matrix according to (5-1). The functions  $F_{OL}^{\alpha}(k)$  are presented later in the "Summary" part of this section.

In the Bryan-Scott OBEP calculation, we examine the role of each individual meson in addition to measuring the strengths of the short-range repulsion and tensor force. Since the meson masses and coupling constants between the meson and nucleon fields are employed as adjustable parameters in the Bryan-Scott OBEP, one of our goals is to determine which meson masses and coupling constants are important to nuclear saturation.

We include the Appel potential in our study to provide an example of a velocity-dependent tensor force other than those of forces A and B. The tensor force in the Appel potential is fairly weak ( $\kappa_{02} \approx .025$ ) but still considerably stronger than those of forces A ( $\kappa_{02} \approx .001$ ) and B ( $\kappa_{02} \approx .01$ ). The Appel potential, therefore, provides a helpful intermediate case for finding a relation between tensor-force strengths and nuclear-binding energies.

Of all the potentials mentioned previously, only the Reid potential is static. The Bryan-Scott and Appel potentials have quadratic momentum dependence, while forces A and B have more complicated momentum dependence. The velocity dependence of forces A, B, the Bryan-Scott potential, and the Appel potential do not present any special numerical problems, since the solution of the Bethe-Goldstone equation is in momentum space. The calculations are quite accurate and fairly rapid considering that we are dealing with non-local potentials. The calculation of the potential energy for one value of  $k_F$  for the  $^3S_1 + ^3D_1$  eigenchannel with a 16-point infinite integration formula takes about 1.5 minutes on the 7090 computer. About half of this time is used to calculate the matrix

elements  $V_{LL}^{\alpha}(k, k')$ , and slightly less than half the time to matrix invert.

### C. Results and Discussion

In our following discussion we shall refer to the total binding energy curve, the  $^1S_0$ ,  $^3S_1$ , total P-wave, and total D-wave potential-energy curves. These curves, which show these binding energies as a function of  $k_F$ , appear in Figures 13-17.<sup>84</sup> We also refer to the wound integrals  $\chi_{LL}^{\alpha}$ , that appear in Table VIII. The binding energies we obtain are also presented in tabular form, with state-by-state contributions, for each potential individually.

Let us begin our discussion with the results from forces A and B. We compare the binding energies of these forces with those of the Reid soft-core potential. The state-by-state contributions for forces A and B appear in Table IX, while the corresponding contributions for the Reid potential appear in Table XII (See Section V-C2).

#### 1. Results — Forces A and B

Only certain two-body states are explicitly included in our calculations of the binding energy and single-particle spectra for forces A and B. These states ( $^1S_0$ ,  $^1P_1$ ,  $^3S_1 + ^3D_1$ ,  $^3D_2$ ,  $^3P_0$ ,  $^3P_1$ ,  $^3P_2 + ^3F_2$ ) are the ones for which phase-shifts fits were achieved. For states other than the ones mentioned above, we use the potential energies from the Reid soft-core potential.

One of the consequences of the smoothness of forces A and B is the lack of sensitivity of the total binding energy of these forces on the hole-spectrum parameters  $M^*$  and  $U_0$ . Table X shows that a ten MeV

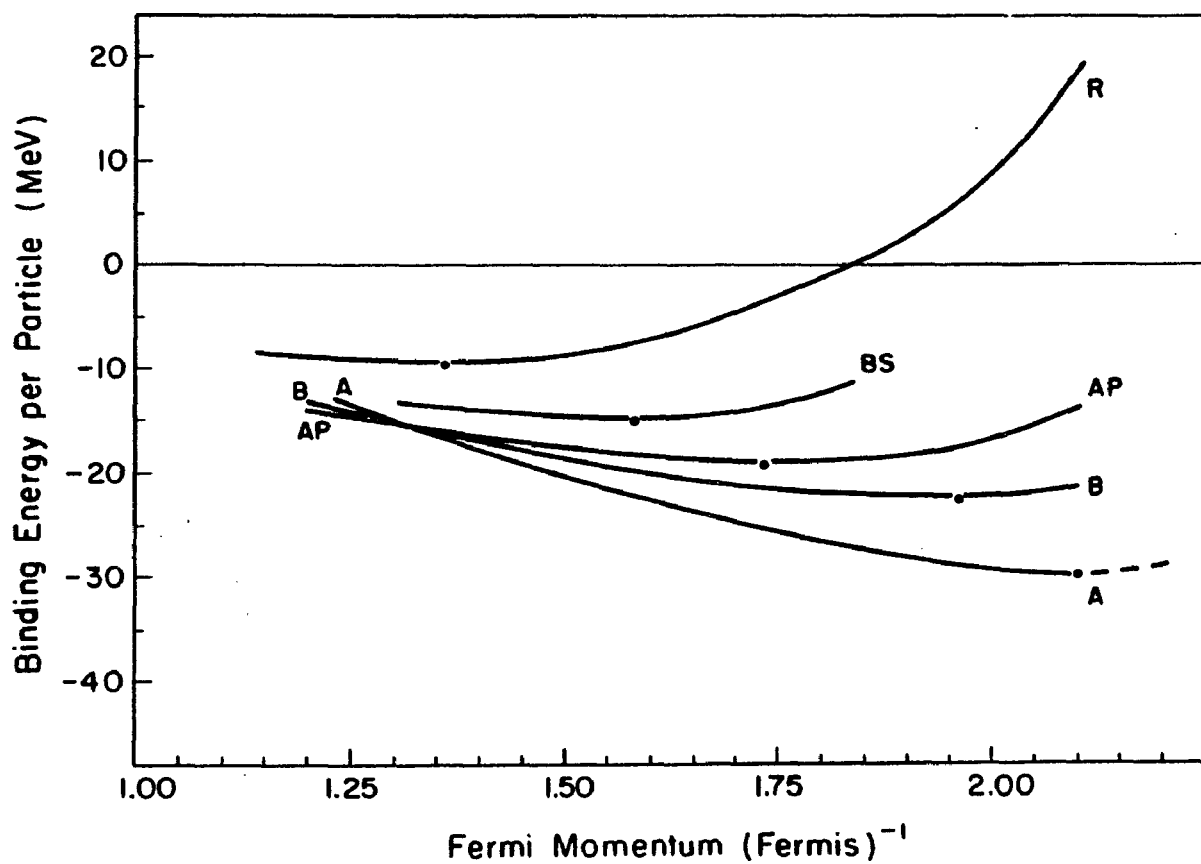


Figure 13. The total binding energy of nuclear matter: The dotted portion for force A is extrapolated from the calculated binding energies for  $k_F \leq 2.1 F^{-1}$ . The Appel potential totals include the  $^1S_0$ ,  $^1D_2$  and  $^3S_1 + ^3D_1$  potential energy contributions. Abbreviations are R-Reid, BS-Bryan-Scott, AP-Appel, B-Force B, A-Force A.

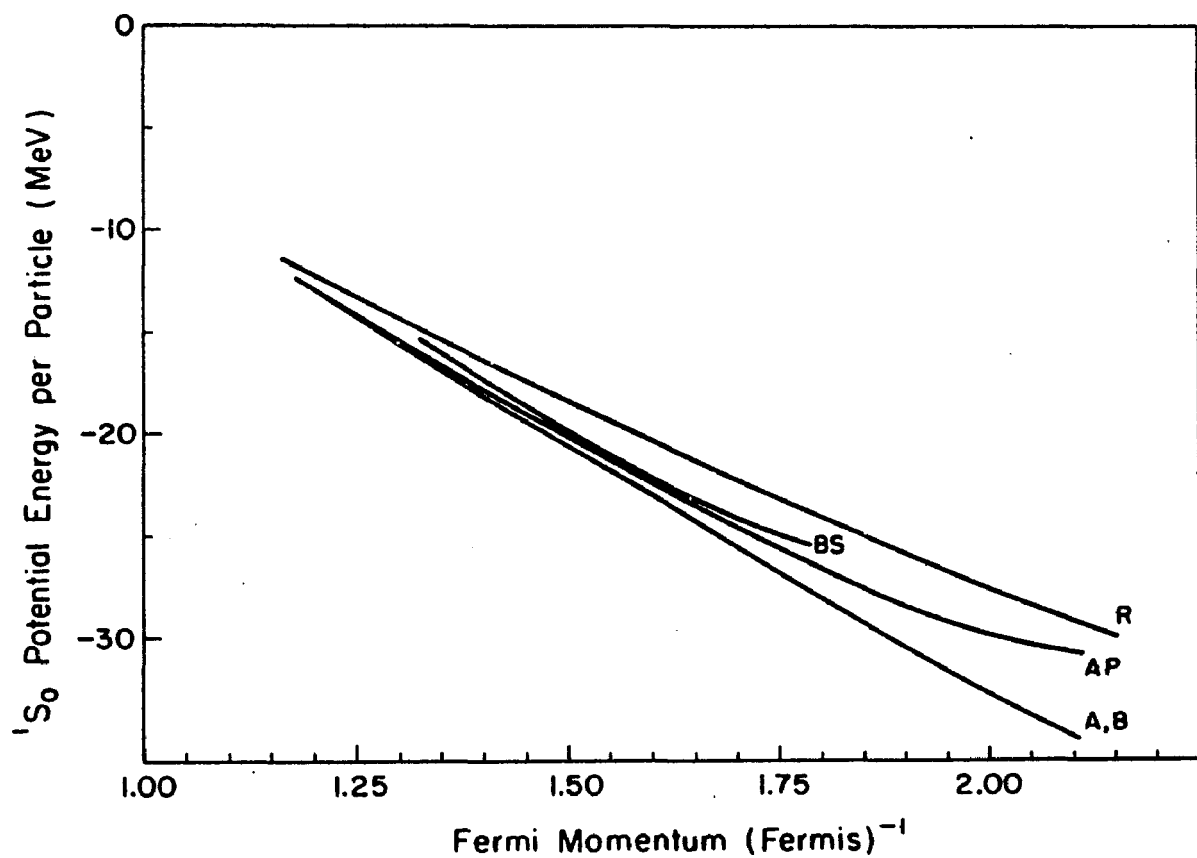


Figure 14. The  $^1S_0$  potential energy contributions in nuclear matter.

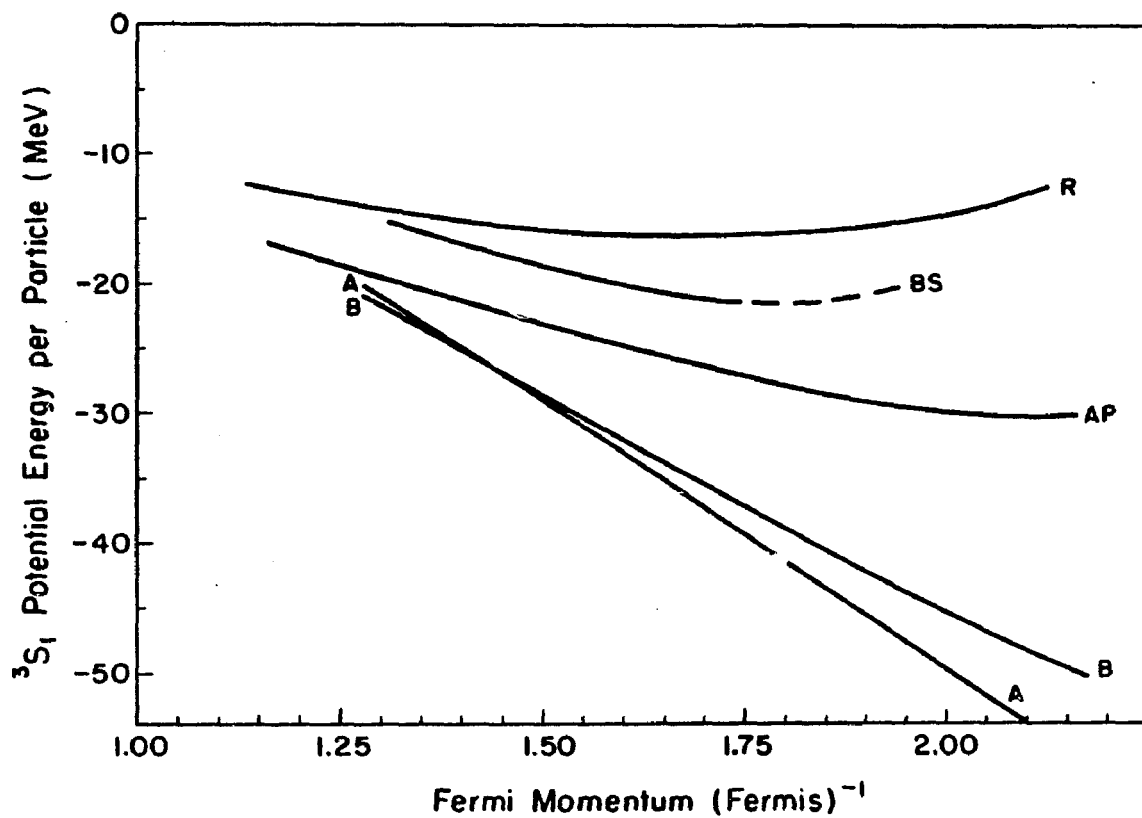


Figure 15. The  $^3S_1$  potential energy contributions in nuclear matter; The dotted portion for BS is extrapolated from the calculated potential energies for  $k_F \ll 1.74F^{-1}$ .

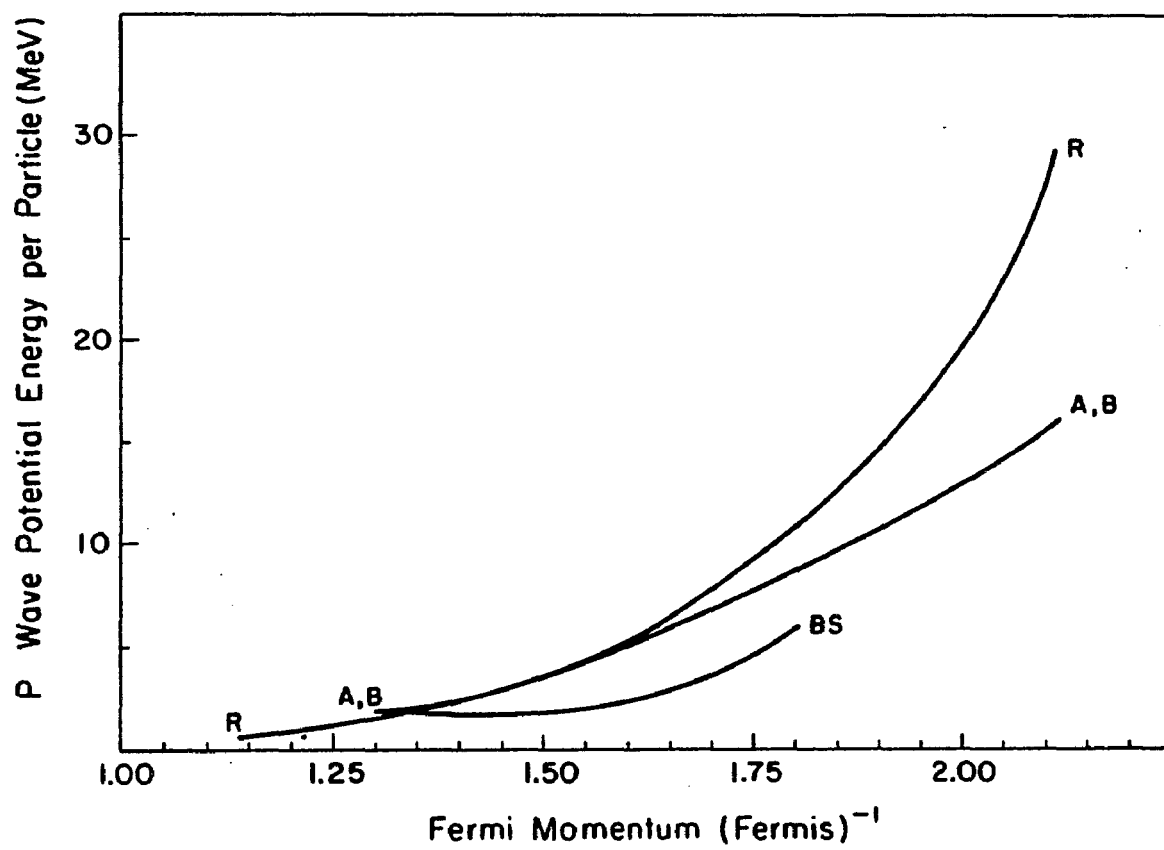


Figure 16. The total P-wave potential energy contributions in nuclear matter.

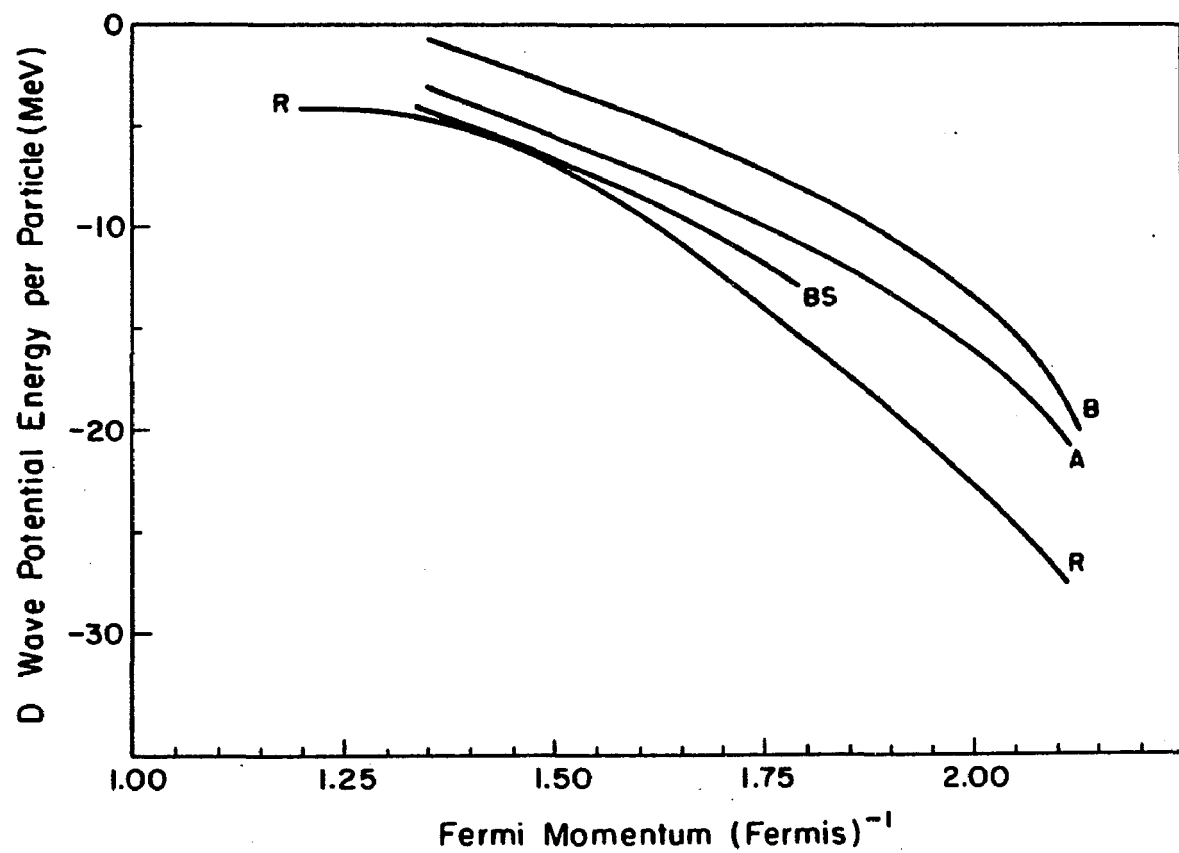


Figure 17. The total D-wave potential energy contributions in nuclear matter.

TABLE VIII

Wound integrals for potentials studied. Center of mass momentum used is  $\mathbf{k}_{\text{AVE}}$  defined by Eq. (3-37).

Wound Integral	Reid $k_o=0.9 \ k_F=1.5$	Bryan-Scott $k_o=.912 \ k_F=1.52$	Appel $k_o=0.9 \ k_F=1.5$	Force B $k_o=0.9 \ k_o=1.5$	Force A $k_o=0.9 \ k_o=1.5$
$^1S_0$	.0284	.0157	.0082	.0006	.0006
$^1D_2$	.0002	.0001	.0001	.0003	.0003
$^1P_1$	.0051	.0008		.0019	.0019
$^3S_1$	.0385	.0111	.0004	.0008	.0022
$^3S_1 + ^3D_1 (\kappa_{02})$	.0711	.0576	.0241	.0135	.0004
$^3S_1 + ^3D_1 (\kappa_{20})$	---	---	---	---	.0010
$^3D_1$	---	.0002	.0001	---	.0004
$^3D_2$	.0003	.0005	---	.0004	.0002
$^3P_0$	.0042	.0037	---	.0006	.0006
$^3P_1$	.0058	.0106	---	.0009	.0009
$^3P_2$	.0033	.0014	---	.0015	.0015
$^3P_2 + ^3F_2 (\kappa_{13})$	.0030	.0027	---	.0037	.0037
$^3P_2 + ^3F_2 (\kappa_{31})$	---	---	---	---	---
$^3F_2$	---	---	---	---	---
TOTAL	.1589	.1044	.0329	.0242	.0137

TABLE IX  
Binding energy of nuclear matter for forces A and B.

$k_F(F^{-1})$ State	FORCE A				FORCE B			
	1.36	1.50	1.80	2.10 (MeV)	1.36	1.50	1.80	2.10
$^1S_0$	- 17.00	- 20.58	- 28.21	- 34.85	- 17.01	- 20.58	- 28.22	- 34.88
$^1D_2$	- 1.09	- 1.92	- 5.21	- 11.34	- 1.09	- 1.92	- 5.21	- 11.35
$^1P_1$	2.92	4.62	9.98	17.09	2.91	4.62	9.96	17.07
$^3S_1$	- 23.55	- 28.89	- 41.43	- 54.08	- 23.91	- 28.79	- 39.08	- 48.23
$^3D_1$	1.81	2.72	5.73	10.79	2.28	3.40	6.66	11.01
$^3D_2$	- 4.21	- 6.27	- 12.47	- 21.25	- 3.29	- 5.10	- 10.95	- 19.72
$^3P_0$	- 3.15	- 4.12	- 6.12	- 7.57	- 3.15	- 4.12	- 6.12	- 7.58
$^3P_1$	11.20	15.94	29.27	46.80	11.20	15.93	29.26	46.78
$^3P_2$	- 8.84	- 12.83	- 24.44	- 40.53	- 8.86	- 12.85	- 24.48	- 40.59
$^3F_2$	- .17	- .29	- .62	- .70	- .17	- .29	- .62	- .71
$J \geq 3^a$	1.92	2.94	6.26	10.91	1.92	2.94	6.26	10.91
TOTALS								

<sup>a</sup>Taken from Reid values.

	FORCE A				FORCE B			
$k_F(F^{-1})$	1.36	1.50	1.80	2.10	1.36	1.50	1.80	2.10
S	- 40.55	- 49.47	- 69.64	- 88.93	- 40.92	- 49.37	- 67.30	- 83.12
P	2.11	3.60	8.79	15.80	2.10	3.57	8.72	15.68
D <sup>b</sup>	- 3.17	- 5.47	- 10.76	- 19.43	- 0.93	- 3.12	- 8.32	- 17.69
F <sup>c</sup>	1.06	3.06	6.39	11.66	1.06	3.06	6.39	11.66
$^3P_0 + ^3P_1 + ^3P_2$	- .81	- 1.02	- 1.19	- 1.29	- .81	- 1.05	- 1.25	- 1.39
P+D <sup>b</sup>	- 1.06	- 1.87	- 1.97	- 3.63	1.17	.45	.40	- 2.01
Total Potential Energy	- 40.17	- 50.69	- 67.26	- 84.73	- 39.19	- 46.78	- 62.56	- 78.29
Kinetic Energy	23.03	28.01	40.34	54.90	23.03	28.01	40.33	54.90
Total Binding Energy	- 17.14	- 20.68	- 26.92	- 29.82	- 16.16	- 18.76	- 22.21	- 22.38
M*/M	.60	.55	.48	.44	.57	.52	.49	.46
U <sub>o</sub>	105.0	130.4	194.0	265.0	103.0	128.3	183.3	242.0

<sup>b</sup>Includes Reid  $^3D_3$  contribution.

<sup>c</sup>Includes Reid  $^1F_3$ ,  $^3F_3$  and  $^3F_4$  contributions.

TABLE X.

Sensitivity of binding energies to hole spectrum parameters. All results are for  $k_F = 1.5F^{-1}$  with a 10 LaGuerre integration routine to invert the Bethe-Goldstone Equation.

Potential	M*	$U_0$ (MeV)	$^1S_0$	$^1D_2$	$^3S_1 + ^3D_1$
Reid	.592	92.56	-18.56	-3.88	-13.83
Reid	.592	100.00	-18.34	-3.88	-12.93
Reid	.610	92.56	-18.51	-3.88	-13.65
B	.522	128.37	-20.73	-1.91	-25.45
B	.522	138.37	-20.71	-1.91	-25.30

variation in  $U_0$  changes the  $^1S_0$  contributions to force B by .02 MeV and the  $^3S_1 + ^3D_1$  contribution by .15 MeV. The  $^1D_2$  contribution is unchanged. For the Reid soft-core potential a variation in  $U_0$  of about 7.5 MeV changes the  $^1S_0$ ,  $^3S_1 + ^3D_1$ , and  $^1D_2$  contributions by .22, 1.0, and zero MeV respectively. These results indicate that exact self-consistency is not so important for smooth forces as it is for stronger forces like the Reid soft-core potential. In fact, for smooth forces A and B, only one iteration is usually sufficient to achieve satisfactory self-consistent hole-spectrum parameters.

The results of our self-consistent calculations with force B indicate that this force saturates at about  $k_F = 1.97 F^{-1}$  with a binding energy of approximately -22.5 MeV. Force A fails to saturate for  $k_F < 2.1$ . Extrapolation of the binding-energy curve for force A indicates that saturation should take place at about  $k_F = 2.1 F^{-1}$  with a binding energy of about -30 MeV.

The most striking feature of the potential-energy curves for forces A and B is that the  $^3S_1$  potential energies (Figure 15) become extremely negative for high values of  $k_F$  compared with those of the Reid soft-core potential. At  $k_F = 1.8 F^{-1}$  the  $^3S_1$  potential energy of force A gives 22 MeV more attraction than the Reid  $^3S_1$  potential energy. In the  $^1S_0$  state (Figure 14), force A gives only 4 MeV more attraction than the Reid potential gives at  $k_F = 1.8 F^{-1}$ . The  $^1S_0$  Reid potential has a strong short-range repulsion, while the  $^3S_1 + ^3D_1$  Reid potential has a strong short-range repulsion and a strong tensor force. The possibility arises that the weak tensor forces, not the weak short-range repulsions, are responsible for the extreme overbinding of forces A and B in the  $^3S_1$  state. This point is further discussed in Section V-D.

The wound integrals, which appear in Table VIII, confirm that forces A and B are very smooth potentials. The wound integrals in Table VIII also confirm that the Reid potential is a very strong force. Comparisons of tensor-force strengths are especially significant. The wound integral  $\kappa_{02}^\alpha = .07$  accounts for the largest contribution to  $\kappa$  for the Reid soft-core potential. Forces A and B give values of  $\kappa_{02} = .0009$  and  $\kappa_{02} = .013$  respectively. The vast differences in tensor force strengths correlates significantly with the large differences in binding energies of the Reid potential and those of forces A and B.

We have not yet considered the role of P and D wave potential energies. We consider the effect of P and D waves later when we discuss the Reid potential. For now we simply state that the P and D-wave potential energies are not responsible for the overbinding of smooth potentials.

Figures 18 and 19, which illustrate the S-wave binding energies as calculated by Brueckner (G) and Hartree-Fock (V) theories, verify the smoothness of forces A and B. The results in Figures 18 and 19 should be compared with those of Figure 20, which shows the corresponding curves for the Reid potential. Figures 18 and 19 indicate that the total higher-order corrections in the  $^3S_1$  state are only 1 MeV for force A and 4 MeV for force B at  $k_F = 1.8 F^{-1}$ . Forces A and B exemplify the kind of potentials that Hartree-Fock theory is designed to handle. At the same time, the extreme overbinding of forces A and B contradicts the fundamental assumption of nuclear-Hartree-Fock theory. This assumption is that nuclear properties may be predicted from smooth potentials that fit the two-body data.

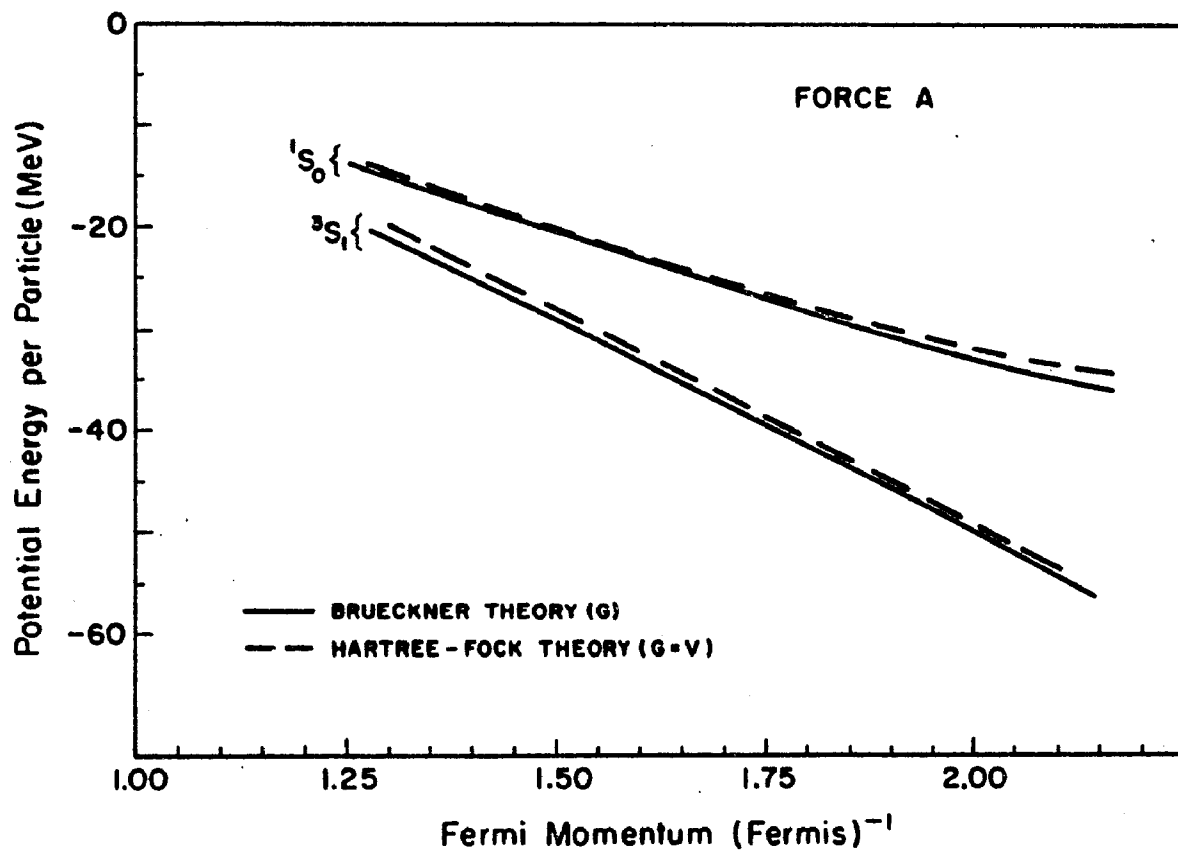


Figure 18. The S wave potential energy contributions in nuclear matter for force A as computed by Brueckner and Hartree-Fock theories.

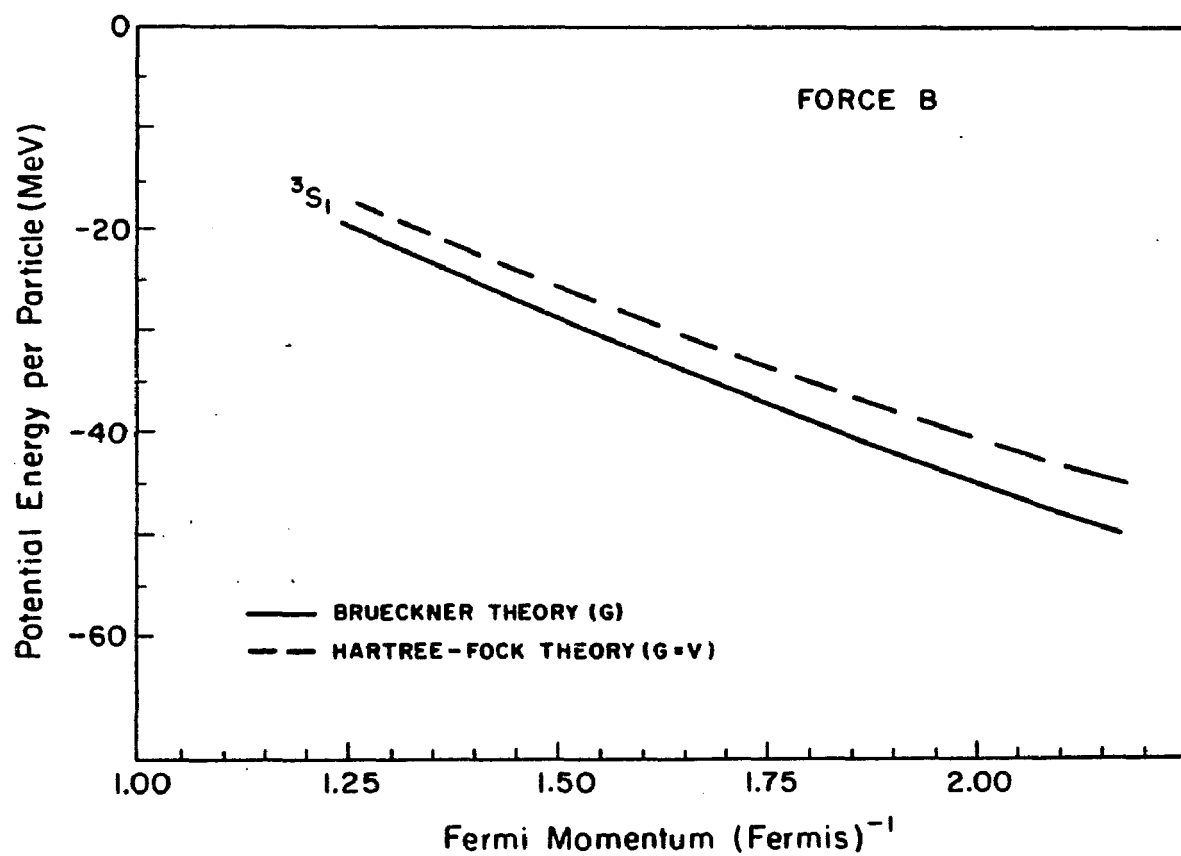


Figure 19. The  $^3S_1$  potential energy contributions in nuclear matter for force B as computed by Brueckner and Hartree-Fock theories.

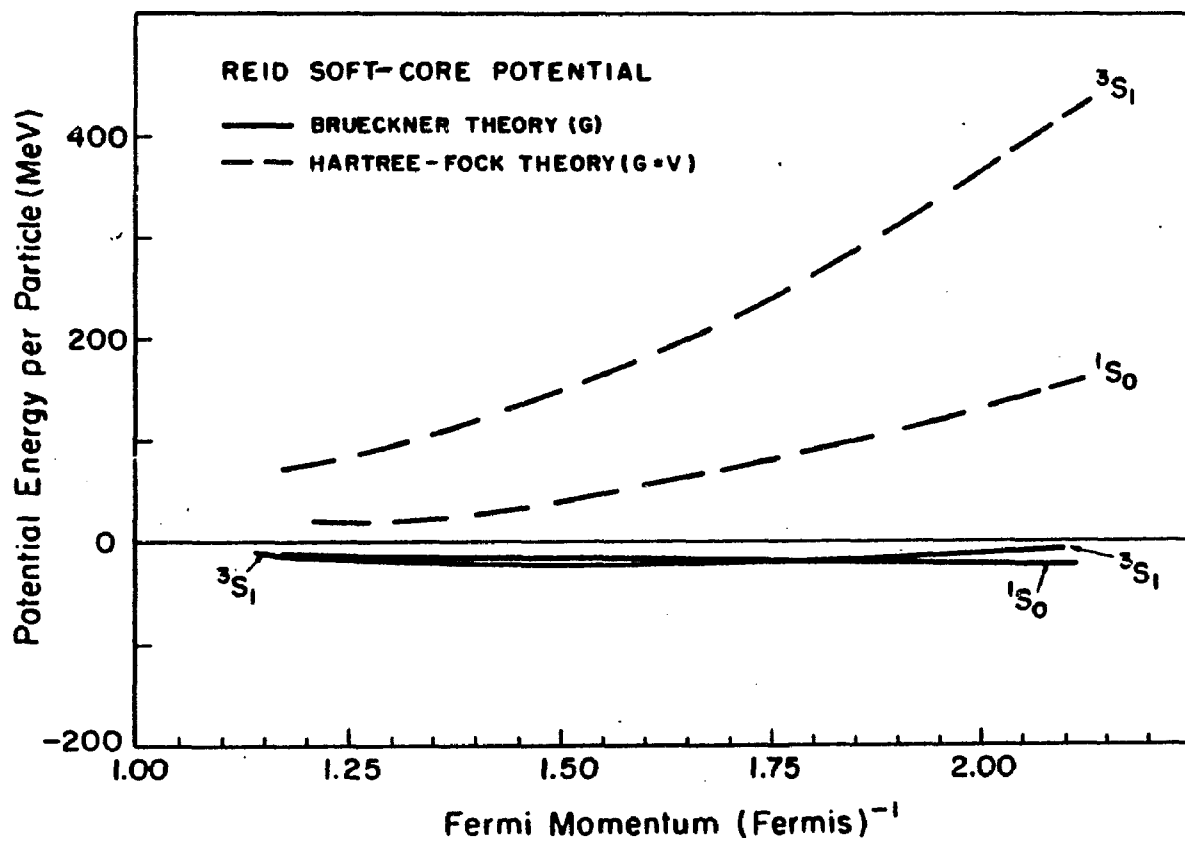


Figure 20. The S-wave potential energy contributions in nuclear matter for the Reid soft-core potential as computed by Brueckner and Hartree-Fock theories. Note the scale in this figure.

Examination of Table VIII reveals that forces A and B are the smoothest forces in our nuclear-matter studies. The Reid soft-core potential is the strongest force in our nuclear-matter studies. The following discussion describes our calculation and results for the Reid soft-core potential. Intermediate cases will be discussed later.

## 2. Results: Reid Soft-core Potential

Before we are able to calculate the binding energy of the Reid soft-core potential, we must decide how to handle higher partial waves. For  $J \geq 3$  the Reid potential is available in only the  $^1G_4$ ,  $^1F_3$ , and  $^3F_3$  eigenchannels.<sup>27</sup> The Reid potential, however, has a common OPEP tail for all states. This OPEP tail includes a short-range cut-off to eliminate the  $1/r^3$  singularity in the tensor force at the origin. The common OPEP employed in the Reid soft-core potential is given by

$$V_{\text{OPEP}} = \frac{V_\pi}{3} \vec{\tau}_1 \cdot \vec{\tau}_2 [\vec{\sigma}_1 \cdot \vec{\sigma}_2 + S_{12}(\hat{r})(1 + 3/x + 3/x^2)] \frac{e^{-x}}{x} - V_\pi S_{12}(\hat{r}) (4/x + 1/x^2) \frac{e^{-4x}}{x}, \quad (5-2)$$

where  $x = m_\pi r$ ,  $V_\pi = 10.463$  MeV, and  $m_\pi' = .70 F^{-1}$  and  $\tau_i = 2t_i$ . For  $J \geq 3$  we employ the Reid potential in the  $^1G_4$ ,  $^1F_3$  and  $^3F_3$  states. For other states up to  $L = 7$ , we employ the  $V_{\text{OPEP}}$  defined above.

Table XI presents the results of a first calculation of the contributions for some higher partial waves for  $J \geq 3$ . We calculate the potential energies with both the Brueckner ( $G$ ) and Hartree-Fock ( $V$ ) techniques. In all cases, except for the  $^3D_3$  state, the Hartree-Fock and Brueckner energies are in excellent agreement. Accordingly, in our full calculation for the Reid potential, we make the Hartree-Fock approximation

TABLE XI.

Binding energy per particle for higher partial waves - Brueckner (G) and Hartree-Fock (V) theories - for the Reid soft-core potential

Here  $k_F = 1.36F^{-1}$ .

State	Potential Energy Per Particle (MeV)	
	Brueckner Theory (G)	Hartree-Fock Theory (V)
$^1G_4$	- .47	- .47
$^1F_3$	.84	.84
$^1H_5$	.21	.21
$^3D_3$	.29	.53
$^3G_3$	.21	.21
$^3G_4$	- .72	- .72
$^3F_3$	1.55	1.56
$^3F_4$	- .22	- .21

$G \approx V$  for all  $J \geq 3$  eigenchannels except for the  $^3D_3 + ^3G_3$  eigenchannel.<sup>85</sup>

We neglect contributions for  $L > 7$ , because these account for only about .04 MeV at the saturation density, as we shall see later. The above procedure resolves the problem of how to accurately treat higher partial waves.

Another problem we face is self-consistency in choosing the hole-spectrum parameters. With the results of Table X as a guide, we iterate on  $M^*$  and  $U_0$  until the lack of self consistency would lead to an estimated error of less than .1 MeV in the total binding energy. In the last iteration we calculate the binding energy of nuclear matter for all states. We then estimate the self-consistent values of  $M^*$  and  $U_0$  from the values of these parameters after successive iterations. We then apply the self-consistent hole-spectrum parameters to a final calculation of the  $^3S_1 + ^3D_1$  potential energies. This procedure results in an error due to lack of self-consistency of about .02 MeV at  $k_F = 1.36F^{-1}$ . The error due to lack of self-consistency is small because we treat the  $^3S_1 + ^3D_1$  eigenchannel, which is most sensitive to  $M^*$  and  $U_0$ , as self-consistently as possible.

The results of our calculations, which appear in Table XII, indicate that the Reid potential saturates with -9.8 MeV binding at  $k_F = 1.36F^{-1}$ . The saturation density for the Reid soft-core potential matches the expected value. The wound integrals  $\kappa$ ,  $\kappa_{00}^{001}$ ,  $\kappa_{00}^{110}$ , and  $\kappa_{02}$  for the Reid potential are the largest of all the potentials we consider. The wound integral  $\kappa_{02}$  is the largest single contribution to  $\kappa$  and accounts for almost 50% of  $\kappa$ . Significantly, the Reid potential  $^3S_1$  curve is the only  $^3S_1$  curve of the potentials considered that possesses a

TABLE XII.

Binding energy of nuclear matter for the Reid soft-core potential.

$k_F(F^{-1})$	Potential Energy Per Particle (MeV)			
	1.20	1.36	1.50	1.80
State				
$^1S_0$	-12.25	-15.57	-18.43	-23.97
$^1D_2$	-1.48	-2.55	-3.88	-8.25
$^1G_4$	- .24	- .47	- .77	-1.86
$^1I_6$	- .05	- .11	- .19	- .54
$^1P_1$	1.29	2.39	3.88	9.36
$^1F_3$	.48	.84	1.28	2.67
$^1H_5$	.10	.21	.36	.91
$^1J_7$	.02	.05	.10	.32
$^3S_1$	-13.19	-15.16	-16.16	-15.84
$^3D_1$	.88	1.45	2.11	4.01
$^3D_2$	-2.58	-4.32	-6.36	-12.52
$^3D_3$	.17	.32	.52	1.18
$^3G_3$	.10	.21	.36	.95
$^3G_4$	- .36	- .72	-1.20	-2.95
$^3G_5$	.04	.09	.16	.45
$^3I_5$	.02	.04	.07	.22
$^3I_6$	- .07	- .16	- .30	- .87
$^3I_7$	.01	.16	.03	.12
$^3P_0$	-2.36	-3.32	-4.20	-5.74
$^3P_1$	6.14	9.93	14.37	28.19
$^3P_2$	-4.21	-7.05	-10.41	-20.84

$k_p (F^{-1})$	1.20	1.36	1.50	1.80
$^3P_2$	- 4.21	- 7.05	-10.41	- 20.84
$^3F_2$	- .30	- .55	- .89	- 2.02
$^3F_3$	.86	1.56	2.43	5.26
$^3F_4$	- .10	- .21	- .36	- .93
$^3H_4$	- .04	- .09	- .16	- .45
$^3H_5$	.16	.33	.59	1.58
$^3H_6$	- .02	- .04	- .07	- .22
$^3J_6$	- .01	- .02	- .03	- .11
$^3J_7$	.03	.08	.15	.49
$^3J_8$	- .002	- .01	- .02	- .06
<b>TOTALS</b>				
S	-25.45	-30.73	-34.59	- 39.81
P	.86	1.95	3.65	10.96
D	- 3.01	- 5.10	- 7.60	- 15.58
F	.94	1.63	2.46	4.99
G	- .46	- .89	- 1.46	- 3.42
H	.20	.41	.72	1.82
I	- .10	- .21	- .39	- .97
J	.05	.11	.21	.64
$J \geq 3$	1.10	1.92	2.94	6.26
$^3P_0 + ^3P_1 + ^3P_2$	- .43	- .44	- .23	1.60
P+D	- 2.15	- 3.15	- 3.95	- 4.62
Total Potential Energy	-26.99	-32.87	-37.09	- 41.95
Kinetic Energy	17.92	23.01	27.99	40.31
Total Binding Energy	- 9.07	- 9.86	- 9.10	- 1.14
M*/M	.70	.64	.60	.52
U <sub>o</sub>	62.2	79.0	94.2	122.2

minimum for  $k_F < 1.8F^{-1}$ . This shape of the  $^3S_1$  energy curve is a crucial factor in the saturation mechanism of the Reid potential.

Considerable concern exists because the Reid potential, which matches the two-body data almost perfectly, fails to reproduce the volume term of the semi-empirical mass formula. Several possible reasons exist for this failure to match experiment. First, the tensor force and/or the short-range repulsion may be too strong. Comparisons of the Reid  $^1S_0$  and  $^3S_1$  potential energies (Figures 14 and 15) to those of forces A and B suggest that the very strong tensor force is the more likely cause. The importance of the strong tensor force is evidenced by the minimum in the  $^3S_1$  curve.

Another reason for disagreement with experiment may be an incorrect treatment of higher partial waves. Our calculations show a total contribution of 1.96 MeV at  $k_F = 1.36F^{-1}$  from partial waves with  $J \geq 3$ . This value is similar to the 2.26 MeV value calculated by Bhargava and Sprung.<sup>86</sup> Most (.24 MeV) of the .3 MeV discrepancy arises from our correct utilization of the full G matrix in the  $^3D_3 + ^3G_3$  eigenchannel. The 2.26 MeV figure results from the Born approximation applied to OPEP for  $J \geq 3$ . The .3 MeV difference between the results of our calculation for  $J \geq 3$  and those of Reference 86 is negligible compared with the 6 MeV necessary to bring the binding energy of the Reid potential into agreement with the semi-empirical mass formula.<sup>87</sup>

If one examines the total potential energy contributed for each L value, a consistent pattern emerges for  $L > 2$ . Namely, the partial waves with orbital angular momentum L contribute in total about -0.5 times the total contribution of partial waves with orbital angular

momentum  $L = 1$ . This pattern allows us to estimate the error of neglecting partial waves for  $L > 7$ . This error amounts to approximately .04 MeV at  $k_F = 1.36 F^{-1}$ . Obviously, our neglect of partial waves for  $L > 7$  is insignificant compared to the 6 MeV necessary to bring the Reid potential into agreement with the correct value of -15.8 MeV.

Another interesting pattern emerges with respect to the contribution of higher partial waves. This pattern concerns cancellation or near cancellation of the potential energies contributed by the  $^3G_3 - ^3F_4$ ,  $^3H_4 - ^3G_5$  and  $^3J_6 - ^3I_7$  pairs. These cancellations are due to the form of the  $V_{OPEP}$  matrix elements. The explanation of these cancellations appears in Appendix D1.

As for P waves, comparisons of Tables IX and XII show that the sum of the  $^3P_{0,1,2}$  contributions are nearly zero for forces A, B, and the Reid potential. The individual contributions are large due to the large spin-orbit splitting of the P waves. However, the large repulsion of the  $^3P_1$  state is nearly cancelled by the attraction of the  $^3P_0$  and  $^3P_2$  states. In total, the P waves contribute a net repulsion nearly equal to the repulsion of the  $^1P_1$  state. This repulsion is small near the experimental density. The surprisingly small net potential energies of P waves results from the approximate Serber property of nuclear interactions. For a pure Serber force, states of odd relative angular momentum do not interact. The approximate Serber property, which implies near cancellation of P waves, holds for all the forces we study except for the Appel potential, for which the P waves do not even fit the two-body data. The differences in total P-wave energies between force A and the Reid potential (Figure 16) are not appreciable until very high densities

( $k_F > 1.9F^{-1}$ ). Most of the differences that do exist are primarily due to different fits to the two-body data.

The net effect of D waves (Figure 17) is attraction for all of the forces studied. The small differences that exist in D-wave energies among forces A, B, and the Reid potential are simply explained by the different fits to the two-body data. The net potential energies of the P and D waves, when summed together, do not vary by more than a few MeV from potential to potential — even at high densities. Thus, the principal reason for the large deviation in binding energies among the potentials studied so far is still a result of the behavior of the  $^3S_1$  energy curve. The behavior of this curve is related to the strength of the tensor force. The short-range repulsion, P waves, and D waves evidently play only a secondary role in nuclear saturation for forces that fit the scattering data.

So far in our discussions we have dealt with the two very smooth potentials — forces A and B, and one very strong force—the Reid potential. The smooth forces give too much binding compared with the semi-empirical mass formula, while the Reid potential does not give enough binding. We now consider two forces of intermediate smoothness—the Bryan-Scott OBEP and the Appel potential. We choose these forces to further test the validity of our previous statements concerning the importance of the tensor force and short-range repulsion in nuclear saturation. By considering these forces, we can get a better quantitative idea on how strong the tensor force should be to produce nuclear saturation near the correct energy and density. We discuss the Bryan-Scott OBEP first. This case also tests whether a meson-theoretic potential can produce nuclear saturation.

### 3. Results — The Bryan-Scott Potential

The Bryan-Scott OBEP, in its non-relativistic form, possesses a short-range repulsion that has both static and momentum dependent parts. The tensor force is local. Our main goal in considering the Bryan-Scott potential is to observe whether the strength of the tensor force and the short-range repulsion bear the same relation to nuclear binding energies as for the previously discussed potentials. We also want to determine how important a role each meson plays in the binding energy of the Bryan-Scott potential.

The Bryan-Scott potential can be written in the form  $V = \sum_i V_i$ , where  $V_i$  labels the potential contribution due to the exchange of the  $i^{\text{th}}$  meson. The mesons consist of two pseudo-scalar mesons ( $\pi$  and  $\eta$ ), and two vector mesons ( $\rho$  and  $\omega$ ). In addition, it is necessary to introduce two artificial scalar mesons ( $\sigma_0$  and  $\sigma_1$ ) to fit the scattering data.<sup>88</sup> The vector meson potentials are given by

$$\begin{aligned}
 v_i^{(V)}(\vec{r}, \vec{\nabla}, m_i) &= g_i^2 \frac{e^{-m_i r}}{r} + g_i^2 (1+f_i/g_i) \frac{m_i^2}{2M^2} \frac{e^{-m_i r}}{r} \\
 &- \frac{g_i^2}{2M^2} (\vec{\nabla}^2 \frac{e^{-m_i r}}{r} + \frac{e^{-m_i r}}{r} \vec{\nabla}^2) + \vec{L} \cdot \vec{S} \frac{g_i^2}{2M^2} (3/2 + 2f_i/g_i) \left( \frac{1}{r} \frac{d}{dr} \frac{e^{-m_i r}}{r} \right) \\
 &+ (\vec{\sigma}_1 \cdot \vec{\sigma}_2) (g_i + f_i)^2 \frac{m_i^2}{6M^2} \frac{e^{-m_i r}}{r} - S_{12}(r) \frac{(g_1 + f_1)^2}{4M^2} (m_1/3 + m_1/r + 1/r^2) \\
 &\times \frac{e^{-m_1 r}}{r}
 \end{aligned} \tag{5-3}$$

The scalar meson potentials are given by

$$v_i^{(S)}(\vec{r}, \vec{\nabla}, m_i) = -g_i^2(1-m_i^2/4M^2) \frac{e^{-m_i r}}{r} - \frac{g_i^2}{2M^2} (\vec{\nabla}^2 \frac{e^{-m_i r}}{r} + \frac{e^{-m_i r}}{r} \vec{\nabla}^2) \\ + \vec{L} \cdot \vec{S} \frac{g_i^2}{2M^2} \frac{1}{r} \frac{d}{dr} \frac{e^{-m_i r}}{r} . \quad (5-4)$$

The pseudo-scalar meson potentials are given by

$$v^{(PS)}(\vec{r}, \vec{\nabla}, m_i) = (\vec{\sigma}_1 \cdot \vec{\sigma}_2) \frac{g_1^2 m_i^2}{12M^2} + S_{12}(\vec{r}) \frac{g_i^2}{4M^2} (m_i^2/3 + m_i/r + 1/r^2) \frac{e^{-m_i r}}{r} . \quad (5-5)$$

The T=1 meson potentials ( $\pi$ ,  $\rho$ , and  $\sigma_1$ ) have an additional factor of  $\vec{\tau}_1 \cdot \vec{\tau}_2$ . The quantities  $m_i$ ,  $g_i$  and  $f_i$  are the mass of the  $i^{\text{th}}$  meson, the coupling constant of the  $i^{\text{th}}$  meson, and the coupling constant for the Pauli term of the  $i^{\text{th}}$  meson. Bryan and Scott employ the meson masses and coupling constants as adjustable parameters to fit the two-nucleon phase-shifts. The masses and coupling constants Bryan and Scott obtain appear in Table XIII.

In addition to the six mesons mentioned, a cut-off potential of mass  $\Lambda = 1500$  MeV is subtracted from each meson potential. This cut-off eliminates the  $1/r^3$  singularity in the potential at the origin. The potential for the  $i^{\text{th}}$  meson becomes

$$v_i(\vec{r}, \vec{\nabla}) = v_i(\vec{r}, \vec{\nabla}, m_i) - v_i(\vec{r}, \vec{\nabla}, \Lambda)$$

where  $v_i(\vec{r}, \vec{\nabla}, m_i)$  is defined by (5-3) through (5-5). Since it is not the purpose of this thesis to go into detail concerning the meson theoretic origin of the OBEP, we omit any further discussion concerning the origin

TABLE XIII.

Bryan-Scott potential parameters. The meson "mass"  $m_1$  in the last column is related to the "mass" in MeV by  $m_1 = (mc^2)/\hbar c \rightarrow (\text{Fermis})^{-1}$ .

Meson	T	Mass $(mc^2)$ (MeV)	$g^2$	f/g	$m_1(F^{-1})$
$\pi$	1	138.7	12.55	--	.703
$\eta$	0	548.7	2.60	--	2.781
$\sigma_1$	1	600.0	1.65	--	3.041
$\sigma_0$	0	550.0	8.19	--	2.787
$\rho$	1	763.0	1.81	1.13	3.867
$w$	0	782.8	17.26	--	3.967

of OBEP. We now proceed to calculate the binding energy of nuclear matter for the Bryan-Scott potential.

a. Description of the Calculation and Results. The procedure we use to determine the binding energy of nuclear matter for the Bryan-Scott potential is identical to the procedure for the Reid potential. We emphasize the density region corresponding to Fermi momenta of between  $k_F = 1.35F^{-1}$  and  $k_F = 1.74F^{-1}$ , because saturation should take place in this region. The results of our calculations appear in Table XIV. These results indicate that the Bryan-Scott potential saturates at  $k_F = 1.58F^{-1}$  with a total binding energy of -14.98 MeV. This binding energy is very close to the correct value and the density is slightly higher than the expected value of  $k_F = 1.36F^{-1}$ . These results are very encouraging, because they suggest that meson-theoretic potentials, which fit the two-nucleon phase-shifts with relatively few adjustable parameters, also predict reasonable binding energies and saturation densities for nuclear matter.

Our results with the Bryan-Scott potential confirm the previously discussed relation between wound integrals and nuclear-binding energies. The wound integral  $\kappa_{02} = .057$  for the Bryan-Scott potential falls between the values of  $\kappa_{02}$  for the Reid potential and force B. Correspondingly, the binding energy and saturation density fall between the Reid and force B values. The important  $^3S_1$  energy curve (Figure 15) fails to reach a minimum in the density region of our calculations; however, extrapolation of the  $^3S_1$  curve beyond  $k_F = 1.74F^{-1}$  suggests that a minimum may occur at about  $k_F = 1.80F^{-1}$ . The wound integral  $\kappa_{02} = .057$  gives the largest single contribution to the total wound integral  $\kappa$ . As with the Reid

TABLE XIV.

Binding energy of nuclear matter for the Bryan-Scott potential.

$k_F(F^{-1})$	1.35	1.52	1.58	1.62	1.74
State					
$^1S_0$	-16.32	- 20.31	- 21.66	- 22.53	- 25.12
$^1D_2$	- 2.12	- 3.49	- 4.09	- 4.52	- 6.03
$^1G_4$	- .37	- .68	- .82	- .92	- 1.29
$^1I_6$	- .09	- .19	- .23	- .27	- .40
$^1P_1$	2.86	4.13	4.65	5.03	6.27
$^1F_3$	.72	1.19	1.39	1.54	2.03
$^1H_5$	.18	.34	.42	.48	.69
$^1J_7$	.05	.10	.13	.15	.23
$^3S_1$	-16.90	- 19.33	- 19.99	- 20.41	- 21.49
$^3D_1$	1.40	2.32	2.72	3.02	4.04
$^3D_2$	- 3.59	- 5.83	- 6.80	- 7.51	- 9.90
$^3D_3$	.15	.25	.30	.34	.46
$^3G_3$	.18	.35	.43	.49	.70
$^3G_4$	- .62	- 1.16	- 1.41	- 1.60	- 2.27
$^3G_5$	.07	.14	.18	.21	.31
$^3I_S$	.03	.07	.09	.10	.16
$^3I_6$	- .14	- .29	- .37	- .42	- .64
$^3I_7$	.01	.03	.04	.05	.08
$^3P_0$	- 3.56	- 4.79	- 5.21	- 5.48	- 6.24
$^3P_1$	9.39	14.72	17.08	18.82	24.75
$^3P_2$	- 7.84	- 12.37	- 14.27	- 15.63	- 20.19
$^3F_2$	- .50	- .90	- 1.08	- 1.21	- 1.68

$k_F(F^{-1})$	1.35	1.52	1.58	1.62	1.74
$^3F_3$	1.35	2.33	2.77	3.09	4.22
$^3H_4$	- .30	- .62	- .79	- .92	- 1.40
$^3H_5$	.28	.56	.70	.80	1.17
$^3H_6$	- .03	- .08	- .10	- .12	- .18
$^3J_6$	- .01	- .03	- .04	- .05	- .08
$^3J_7$	.07	.15	.19	.23	.36
$^3J_8$	- .01	- .02	- .02	- .03	- .04
<b>TOTALS</b>					
S	-33.20	- 39.64	- 41.65	- 42.93	- 46.61
P	.85	1.65	2.22	2.74	4.59
D	- 4.25	- 6.75	- 7.87	- 8.66	- 11.43
F	1.27	2.00	2.29	2.51	3.17
G	- .74	- 1.35	- 1.62	- 1.83	- 2.56
H	.36	.67	.83	.95	1.34
I	- .18	- .38	- .46	- .54	- .80
J	.09	.20	.26	.29	.47
$J \geq 3$	1.45	2.29	2.68	2.93	4.06
$^3P_0 + ^3P_1 + ^3P_2$	- 2.01	- 2.48	- 2.43	- 2.29	- 1.68
P+D	- 3.40	- 5.10	- 5.65	- 5.92	- 6.84
Total Potential Energy	-35.72	- 43.32	- 45.98	- 47.50	- 51.82
Kinetic Energy	22.68	28.56	31.07	32.66	37.68
Total Binding Energy	-13.05	- 14.77	- 14.98	- 14.84	- 14.14
m*	.70	.63	.62	.60	.56
$U_o$	81.9	104.2	112.3	117.6	133.0

potential, most of the nuclear wave-function distortion results from the tensor force.

The  $^1S_0$  binding energies of the Bryan-Scott potential are qualitatively the same as those obtained for the Reid potential and force A. Again, appreciable differences between the binding energies of the Bryan-Scott potential and the other potentials studied arise from the  $^3S_1$  curve. The P-wave and the D-wave contributions of the Bryan-Scott potential, when summed together, qualitatively agree with the P and D-wave contributions of the other potentials studied. Inspection of the wound integrals in Table VIII shows that only a small part of the total wound integral comes from P and D waves for the Reid and Bryan-Scott potentials. Moreover, the differences in P and D wave potential energies among the potentials studied are again consistent with the different fits of the two-body phase-shifts. Thus, off-energy-shell effects play only a minor role in the P and D wave potential energies.

The wound integral  $x_{02}$  for the Bryan-Scott potential, while smaller than that of the Reid potential, still indicates a strong tensor force. Significantly, of the four forces considered, the two forces with strong tensor forces saturate at nearly the correct density while the two forces with weak tensor forces fail to saturate near the correct density. Of the two potentials with strong tensor forces (Reid and Bryan-Scott), the Reid potential saturates at the correct density and the Bryan-Scott potential saturates at the correct energy. Further refinements in summing the Brueckner-Goldstone expansion are necessary to determine whether the Bryan-Scott potential or the Reid potential can most satisfactorily reproduce the experimental properties of nuclear matter. In any case, saturation near the correct density seems to place a lower bound of about

.05 for  $\kappa_{02}$ . An important consequence of this lower bound is that potentials that produce nuclear saturation are not suitable for Hartree-Fock calculations.

The higher partial waves ( $J \geq 3$ ) contribute slightly less repulsion for the Bryan-Scott potential than for the Reid potential. One reason for this behavior may be the slightly weaker pion potential strength of the Bryan-Scott potential compared to that of the Reid potential. The strength of the pion part of the Bryan-Scott potential is

$$V_\pi = m_\pi c^2 \frac{(g_\pi m_\pi)}{2M} = 9.5 \text{ MeV} .$$

The corresponding  $V_\pi$  for the Reid potential is  $V_\pi = 10.463 \text{ MeV}$ . Another factor may be the presence of meson potentials other than the OPEP in the Bryan-Scott potential for higher partial waves. In the Reid potential the  ${}^3F_4$  potential energy nearly cancels the  ${}^3G_3$  potential energy, the  ${}^3G_5$  and  ${}^3H_4$  potential energies cancel, and the  ${}^3I_7$  and  ${}^3J_6$  potential energies cancel. These cancellations follow from the properties of the OPEP matrix elements. In the Bryan-Scott potential, the above pairs give a total attraction of -.28, -.01, and zero MeV respectively at  $k_F = 1.52 F^{-1}$ . The lack of cancellation in the Bryan-Scott potential gives about 0.3 MeV attraction, most of which comes from the  ${}^3F_4 - {}^3G_3$  pair. The difference between  $J \geq 3$  totals of the Reid and Bryan-Scott potentials at  $k_F \approx 1.5 F^{-1}$  is about .7 MeV. The weaker OPEP strength in the Bryan-Scott potential and differences in the forms of the Bryan-Scott and Reid potentials evidently account for the remaining 0.4 MeV difference at  $k_F \approx 1.5 F^{-1}$ .

In total, the different P and D wave potential energies and the different potential energy contributions for  $J \geq 3$  between the Reid and Bryan-Scott potentials fail to account for most of the 7 MeV difference in binding energies at  $k_F \approx 1.5F^{-1}$ . The greatest difference results from the  $^3S_1$  state, which accounts for 3 MeV. The  $^1S_0$  state accounts for about 1.5 MeV, while the P and D waves and  $J \geq 3$  contributions account for a total of 2.5 MeV. As density increases, the difference in  $^3S_1$  potential energies become much more important.

The results of our calculations with the Bryan-Scott potential indicate that the one-boson-exchange theory of nuclear forces has the crucial element necessary for nuclear saturation—a strong tensor force. We now wish to classify the meson potentials according to attraction, repulsion, and importance in nuclear matter. We also would like to determine the source of the strong tensor force so important to nuclear saturation. To determine the role of each meson in nuclear saturation, let us now see how the absence of each meson potential changes the binding energy of nuclear matter.

b. Classification of Mesons in the Bryan-Scott Potential for Nuclear Matter. For each meson (i) in the Bryan-Scott potential we calculate the binding energy of nuclear matter in the absence of the meson potential (i) and its cut-off, i.e.

$$v^{(i)}(\vec{r}, \vec{\nabla}) = v^{(BS)} - v_i(\vec{r}, \vec{\nabla}).$$

In the above expression  $v^{(i)}(\vec{r}, \vec{\nabla})$  is the potential employed in the  $i^{\text{th}}$  calculation,  $v^{(BS)}$  is the full Bryan-Scott potential, and  $v_i(\vec{r}, \vec{\nabla})$  is the potential contribution of the  $i^{\text{th}}$  meson including its cut-off. We

employ a suggestion of Bhargava and Sprung<sup>86</sup> and approximate the total potential energies of nuclear matter by the sum of the potential energy contributions from the  $^1S_0$ ,  $^1D_2$  and the  $^3S_1 + ^3D_1$  states.<sup>89</sup> Since extreme precision is not necessary for our present discussion, we employ a 10-point Laguerre formula to numerically invert the Bethe-Goldstone equation. The parameters  $M^*$  and  $U_0$  are constant throughout our calculations. These parameters are selected by interpolation or extrapolation from the self-consistent values given in Table XIV. The  $M^*$  and  $U_0$  we adopt are not self-consistent in the absence of one of the meson potentials.

We present the results of our calculations in Figures 21-23. Of the six mesons studied, three ( $\rho, \eta, \sigma_1$ ) have opposite influences in the  $^1S_0$  and  $^3S_1 + ^3D_1$  eigenchannels. The  $\rho$  meson is repulsive in the  $^1S_0$  eigenchannel but attractive in the  $^3S_1 + ^3D_1$  eigenchannel. The  $\eta$  and  $\sigma_1$  mesons are attractive in the  $^1S_0$  eigenchannel but repulsive in the  $^3S_1 + ^3D_1$  eigenchannel. In each case the characteristic of the  $^3S_1 + ^3D_1$  eigenchannel dominates.

Overall, the  $\eta$ ,  $\sigma$ , and  $\omega$  mesons give net repulsion, while the  $\pi$ ,  $\sigma_0$ , and  $\rho$  mesons give net attraction. While the two mesons of each type (scalar, Pseudoscalar, and vector) have the same kind of influence in the  $^1S_0$  channel, they have opposite influences in the  $^3S_1 + ^3D_1$  eigenchannel. This behavior arises from the factor  $\vec{\tau}_1 \cdot \vec{\tau}_2$  for the  $T = 1$  meson potentials ( $\pi, \rho, \sigma_1$ ). The operator  $\vec{\tau}_1 \cdot \vec{\tau}_2$  has eigenvalues of -3 for the  $T = 0$  states and 1 for the  $T = 1$  states. The  $T = 1$  meson potential of each type, therefore, has the opposite sign in the  $^3S_1 + ^3D_1$  eigenchannel than its  $T = 0$  counterpart.

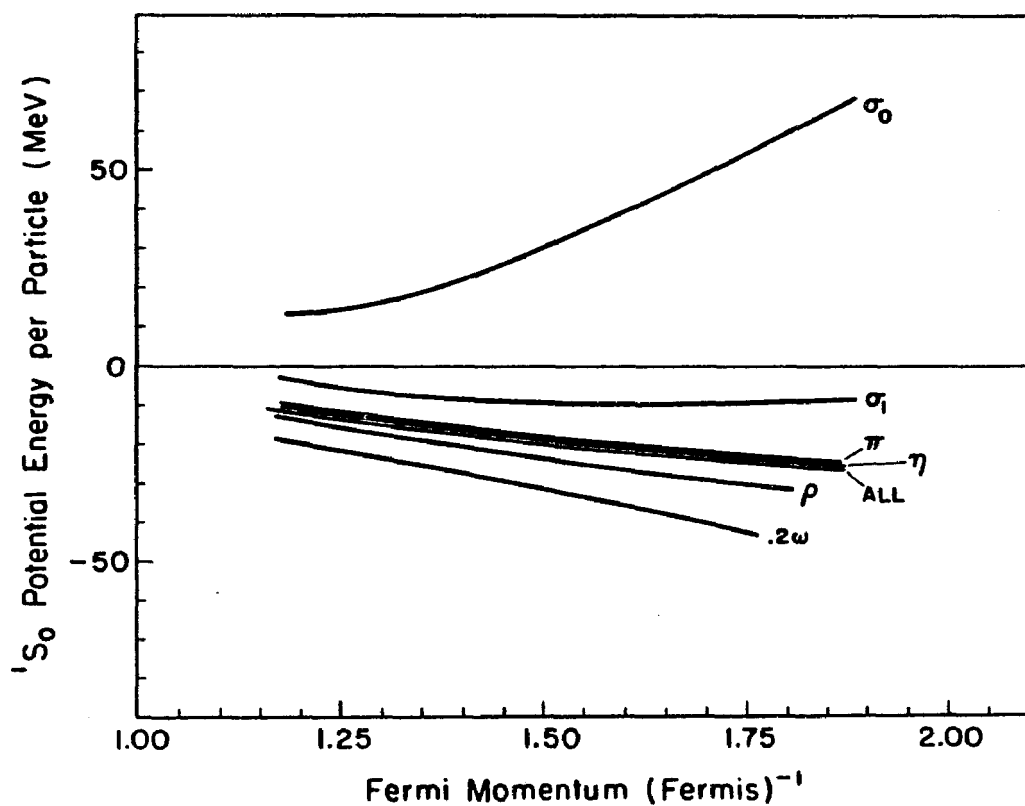


Figure 21. The  $^1S_0$  potential energy contributions in nuclear matter for the Bryan-Scott potential in the absence of each meson potential: The curve labeled "All" is the  $^1S_0$  potential energy contributions for the full Bryan-Scott potential. The curve labeled ". $2\omega$ " is for 20% of the  $\omega$  meson potential absent.

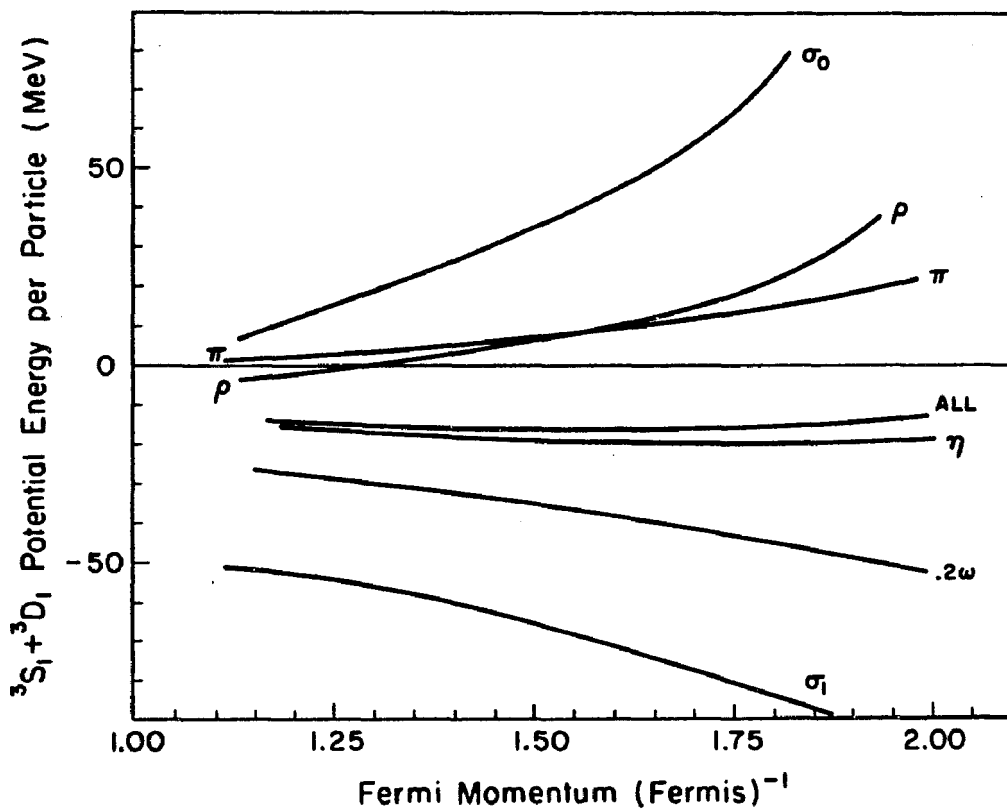


Figure 22. The  $^3S_1 + ^3D_1$  potential energy contributions in nuclear matter for the Bryan-Scott potential in the absence of each meson potential.

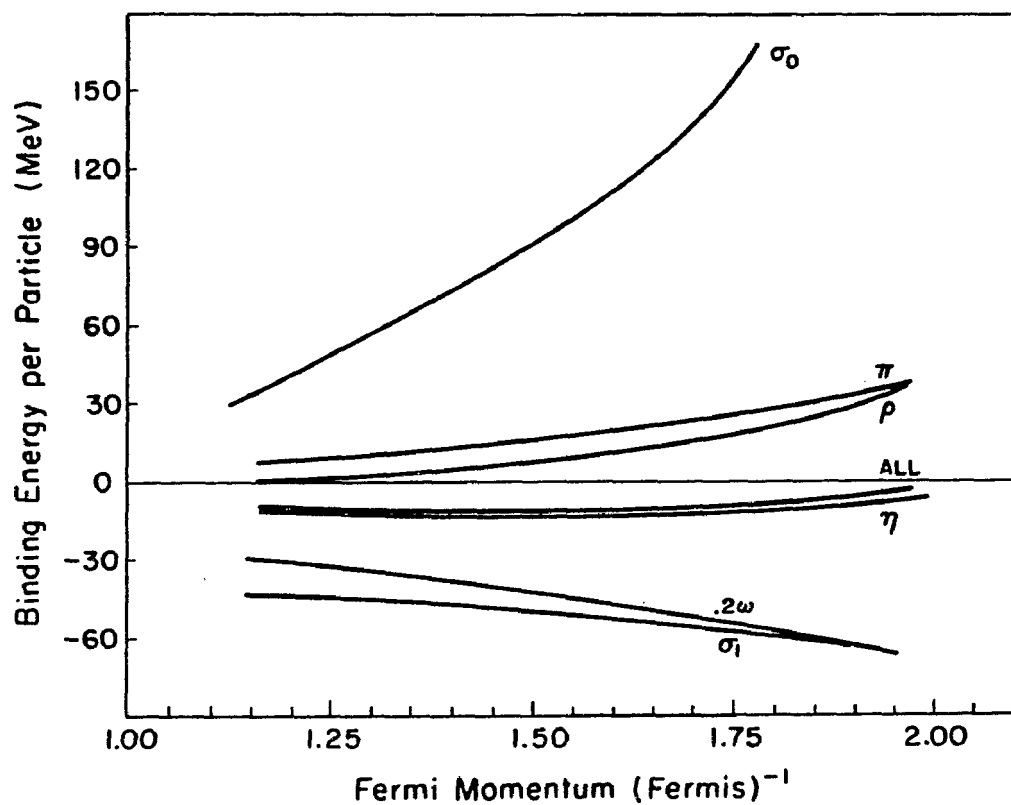


Figure 23. The total binding energy of nuclear matter for the Bryan-Scott potential in the absence of each meson potential; These totals include contributions from only the  $^1S_0$ ,  $^1D_2$ , and  $^3S_1 + ^3D_1$  eigenchannels.

Of the mesons that give net attraction, the  $\sigma_0$  is the most important. Absence of the  $\sigma_0$  meson accounts for about 100 MeV loss of binding at  $k_F = 1.50F^{-1}$ . The  $\pi$  and  $\rho$  mesons are of nearly equal importance, accounting for about 27 and 20 MeV respectively.

The  $\omega$  meson is the most important of the mesons that give net repulsion. In fact, the  $\omega$  meson provides almost all of the strong short-range repulsion in the  $^1S_0$  state. Without the  $\omega$  meson potential, the Bryan-Scott potential becomes almost purely attractive. Brueckner theory cannot handle strong, purely attractive potentials because many-body correlations become important and the wound integrals become extremely large. To make Brueckner theory applicable, we turned off only 20% of the  $\omega$  meson potential strength. Of the two remaining mesons, the  $\sigma_1$  is the more important meson, accounting for 37 MeV. The  $\eta$  meson accounts for an almost negligible 1 MeV.

The results in Figures 21-23 suggest that the absence of any meson, except the  $\eta$  meson, causes the nucleus to either collapse or fly apart. Except for the  $\omega$  meson, which contains the strong short-range repulsion employed to fit the high-energy scattering data, the masses and coupling constants of the scalar  $\sigma_0$  and  $\sigma_1$  mesons appear to be the most important. However, the  $\sigma_0$  and  $\sigma_1$  mesons have not been observed. Unfortunately, one cannot directly eliminate the  $\sigma_0$  and  $\sigma_1$  mesons from the Bryan-Scott model, because the  $\sigma_0$  and  $\sigma_1$  mesons supply most of the attraction for the  $^1S_0$  state. The  $\pi$  and  $\eta$  mesons supply very little attraction to the  $^1S_0$  state. If one changes the pion mass and coupling constant considerably, the higher partial-wave phase-shift fits, which depend almost exclusively on the pion parameters, will be ruined. More importantly, the pion mass and coupling constant should not be changed because they agree very well with the pion

mass and coupling constant determined from pion-nucleon scattering.<sup>90</sup> Therefore, the retention of the  $\sigma_0$  and  $\sigma_1$  mesons seems necessary to supply the attraction for the  $^1S_0$  state, both in the two-body and many-body cases.

The most notable feature in the  $^3S_1 + ^3D_1$  state contributions is the crossing of the  $\pi$  meson and  $\rho$  meson curves. At lower densities the  $\rho$  meson potential becomes more attractive than that of the  $\pi$  meson, but at higher densities the  $\rho$  meson potential becomes more attractive. This property implies that the  $\rho$  meson potential has a weak tensor force, while the  $\pi$  meson potential has a stronger tensor force. The wound integral  $\kappa_{02}$  for the Bryan-Scott potential is .057. With the absence of the  $\rho$  meson potential, the wound integral  $\kappa_{02}$  drops to .04. With the absence of the  $\pi$  meson potential, the wound integral  $\kappa_{02}$  drops to .001. These values of  $\kappa_{02}$  indicate that most of the tensor force strength of the Bryan-Scott potential resides in the pion potential. As we have seen earlier, nuclear saturation results from strong tensor forces. The  $\pi$  meson potential, therefore, contains the strong tensor force necessary for nuclear saturation.

So far in our nuclear matter studies, saturation, or lack of saturation, seems to depend on the strength of the tensor force, quantitatively embodied in the quantity  $\kappa_{02}$ . The Reid and Bryan-Scott potentials give large values ( $> .05$ ) for  $\kappa_{02}$ , while the smooth potentials A and B give very small values. A potential developed by Appel,<sup>82</sup> which includes quadratic momentum dependence in the tensor force, provides an example of a tensor force of intermediate strength.

#### 4. Results — Appel Potential

The Appel potential<sup>82</sup> is basically of the same form as force A, except the velocity dependence is quadratic. The radial forms are Gaussians for the velocity-dependent terms. The static terms have a Yukawa radial dependence with a short-range cut-off needed to eliminate the singularity at the origin. The most important feature of the Appel potential is the appearance of the velocity-dependent tensor force  $S_{12}(\hat{p})$ .

In our nuclear-matter calculation for the Appel potential we employ the approximation suggested by Bhargava and Sprung<sup>86</sup> and include only the contributions of the  $^1S_0$ ,  $^1D_2$ , and  $^3S_1 + ^3D_1$  eigenchannels. We omit the P waves from our study because the triplet-odd phase-shifts for the Appel potential are unsatisfactory. These approximations are consistent with our main goal—to study the role of the tensor force and short-range repulsion in nuclear binding energies.

The results of our nuclear-matter calculations with the Appel potential are included in Figures 13-15. The  $^3S_1$  energies for the Appel potential (Figure 15) fall between those of the Bryan-Scott potential and those of force B. Likewise, the wound integral  $\kappa_{02}$  falls between the Bryan-Scott and force B values. The calculated binding energy and saturation density of the Appel potential (Figure 13) are clearly too high compared to the correct values. Since the  $^1S_0$  energies (Figure 14) qualitatively agree with the results from the other potentials studied, the  $^3S_1$  curve is again chiefly responsible for the disagreement with the semi-empirical mass formula. These results confirm the previously observed pattern between nuclear binding energies and tensor force strengths. Overbinding and too high saturation densities occur for forces with weak

tensor forces. The sensitivity of nuclear-binding energies to the strength of the short-range repulsion is not too great because the  $^1S_0$  potential energy curves are in qualitative agreement for all of the potentials we have studied. Our study of the Appel potential shows that a wound integral of  $\kappa_{02} \approx .025$  does not indicate a strong enough tensor force for nuclear saturation to take place near the correct density.

#### D. Summary and Explanation of the Importance of the Tensor Force

In all of our nuclear-matter calculations a consistent relation emerges between nuclear binding energies and smoothness. This relation is that the smoother the potential, the greater the tendency toward overbinding and nuclear collapse. This overbinding for smooth potentials comes almost exclusively from the  $^3S_1$  state where the tensor force enters. We conclude that nuclear saturation requires strong tensor forces. The short-range repulsion seems only to play a secondary role because all of the  $^1S_0$  binding energies are in qualitative agreement.

In Figures 24-26 the above remarks are illustrated. The results in Figure 24 confirm that the saturation energies are more strongly correlated to the high density behavior of the  $^3S_1$  potential energies than to that of the  $^1S_0$  potential energies. Potentials with widely varying total binding energies have widely varying  $^3S_1$  potential energies. The  $^1S_0$  potential energies, however, are fairly constant. Figure 25 confirms the same relation for saturation densities. The results in Figure 26 indicate that the high density behavior of the  $^3S_1$  potential energies relate consistently with the wound integral  $\kappa_{02}$ . The  $^3S_1$  potential energies always become less attractive with increasing  $\kappa_{02}$ .

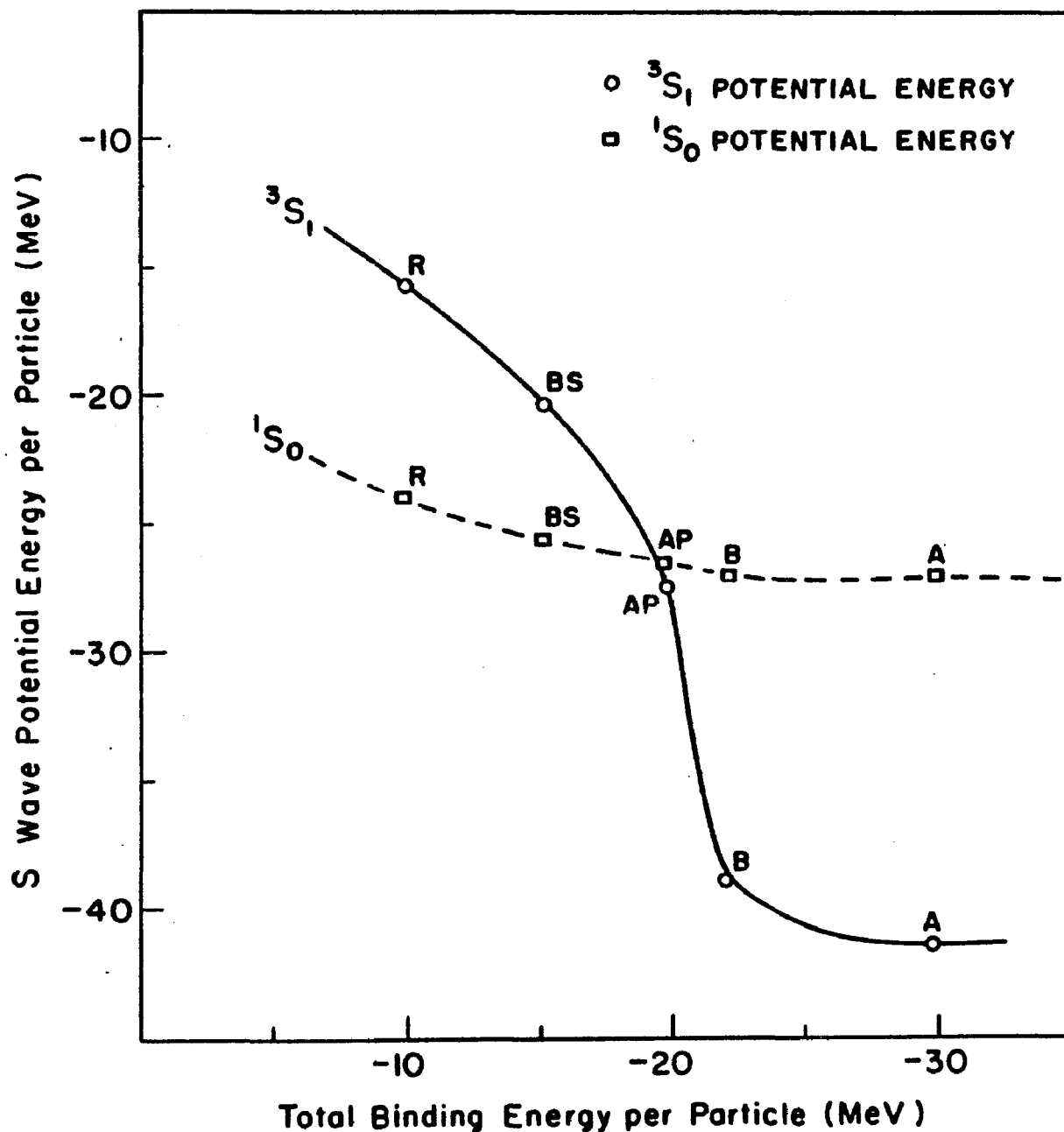


Figure 24. The high-density S-wave potential energies and the saturation densities for various potential models: The  $^1S_0$  and  $^3S_1$  potential energies are taken at  $k_F = 1.8F^{-1}$ . The total binding energies are taken at the saturation density for each potential.

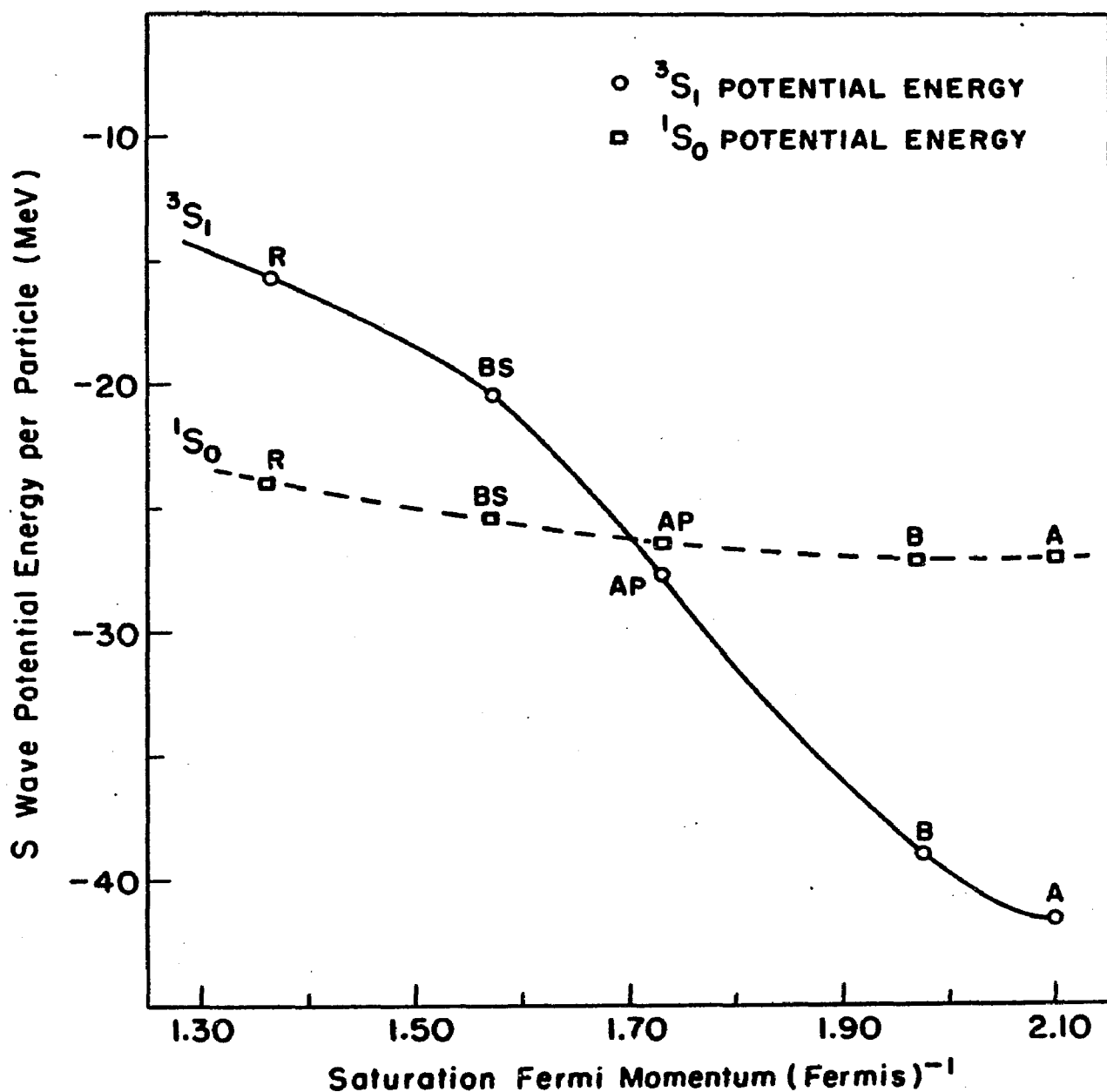


Figure 25. The high-density S-wave potential energies and the saturation densities for various potential models: The  $^1S_0$  and  $^3S_1$  potential energies are taken at  $k_F = 1.8\text{F}^{-1}$ .

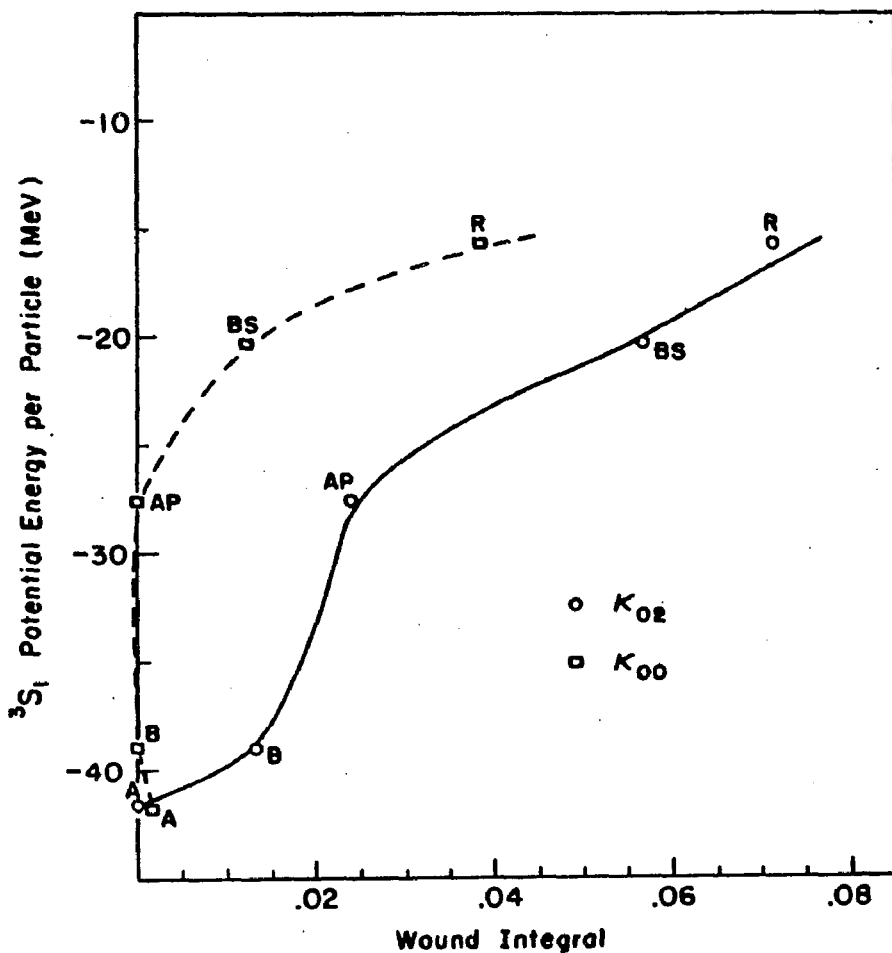


Figure 26. The high-density ( $k_F = 1.80F^{-1}$ )  $^3S_1$  potential energies and the wound integrals  $\kappa_{00}$ ,  $\kappa_{02}$  for various potential models: All wound integrals are calculated for  $k_F \approx 1.5F^{-1}$ ,  $k_0 \approx .9F^{-1}$ . The steepness of the line for  $\kappa_{00}$  does not indicate that the  $^3S_1$  potential energy is more sensitive to  $\kappa_{00}$  than to  $\kappa_{02}$  because from potential to potential on this line  $\kappa_{02}$  is varying.

The relation of the  $^3S_1$  energies to the strength of the central interaction,  $\kappa_{00}^{110}$ , is similar, but not nearly as consistent. Together, the results in Figures 24-26 indicate that nuclear saturation depends on strong tensor forces rather than on strong short-range repulsions. Quantitatively, a tensor force strength of  $.05 \leq \kappa_{02} \leq .07$  accompanies nuclear saturation at nearly the correct energy or density. These values of  $\kappa_{02}$  probably rule out the application of Hartree-Fock theory to potentials that give the correct energy or density of nuclear matter.

The saturation mechanism of the tensor force stems from the tendency of the tensor force to scatter to intermediate states with lower momenta than those to which the central force scatters. Examination of Figures 27 and 28, in which we present plots of  $F_{OL}^\alpha(k)$  for the Reid potential and for force B, confirms this behavior. The tensor coupled wave function defects,  $F_{02}^\alpha(k)$ , start to build up as soon as the Pauli principle allows and peak at about  $2.5 F^{-1}$ . The uncoupled part,  $F_{00}^\alpha(k)$ , does not begin to build up until about  $2.2 F^{-1}$  and peaks at about  $3.5 F^{-1}$ . The importance of the momentum distribution of  $F_{OL}^\alpha(k)$  to nuclear binding energies can be seen from the examination of second-order corrections to the R and G matrices.

To second order, the difference between the G matrix and the R matrix is given, in operator notation by

$$G - R \approx V \left( \frac{Q}{eN} - \frac{P}{e} \right) V , \quad (5-6)$$

where e refers to the free single-particle spectrum for elastic scattering and  $e^N$  refers to the nuclear spectrum. In our following discussion  $k_o$  denotes incident relative momentum,  $k'$  the intermediate-state relative

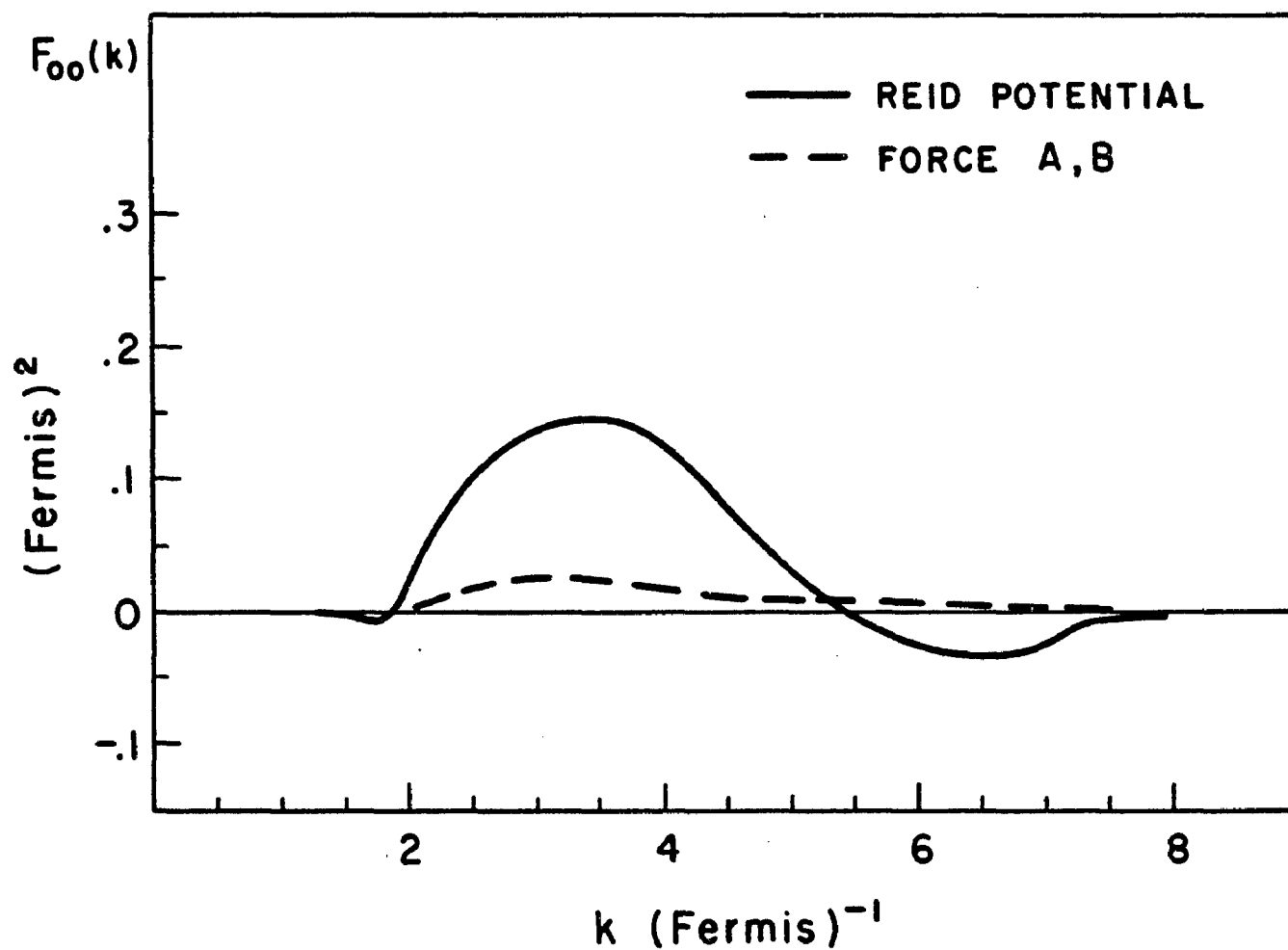


Figure 27.  $F_{00}^\alpha(k)$  for the  $^1S_0$  state for the Reid potential and for forces A,B: Here  $k_o = .9F^{-1}$ ,  $\frac{k}{F} = 1.5F^{-1}o$  and  $K = K_{\text{AVE}}$  as defined by Eq. ( 3-37 ).

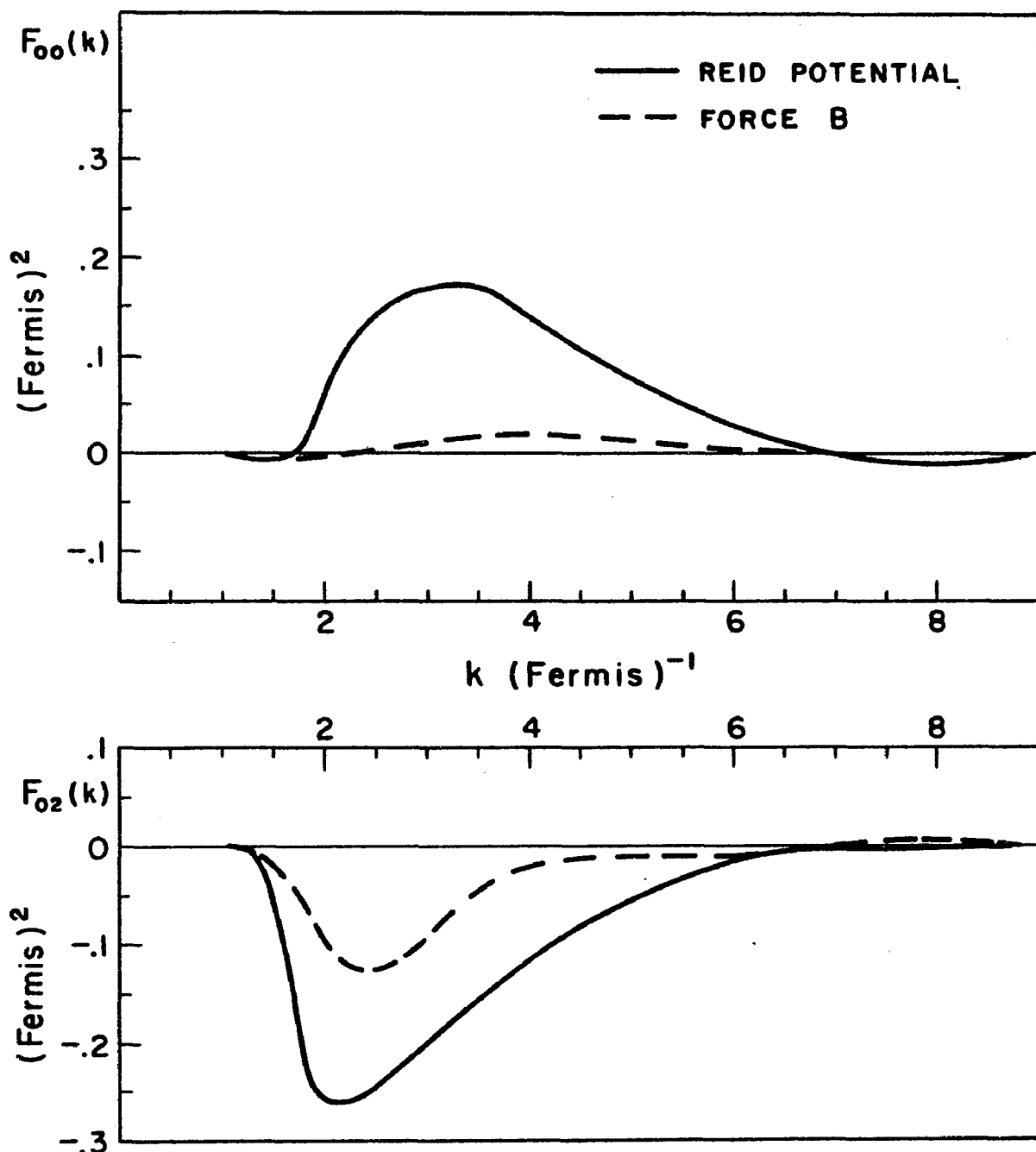


Figure 28.  $F_{00}^\alpha(k)$  and  $F_{02}^\alpha(k)$  for the  $^3S_1 + ^3D_1$  eigenchannel for the Reid potential and for force B. Here  $k_O = .9F^{-1}$ ,  $k_F = 1.5F^{-1}$ , and  $K = K_{\text{AVE}}$  as defined by Eq. (3-37).

momentum, and  $K$  the center-of-mass momentum. If we deal with nearly phase-shift-equivalent potentials, as we have done, the diagonal matrix elements of  $R$  are nearly constant from potential to potential. The right-hand side of (5-6) is always repulsive, if we consider diagonal elements of  $G$  and  $R$ , because the two  $V$  matrix elements involved are equal

$$V_{OL}^{\alpha}(k_0, k') = V_{L'0}^{\alpha}(k', k_0)$$

and because the free-particle propagators ( $P/e$ ) are more negative than the Bethe-Goldstone propagators ( $Q/e^N$ ). The result is that, for phase-shift-equivalent potentials, the right-hand side of (5-6) represents a repulsive correction term in the  $G$  matrix that varies from potential to potential. The magnitude of the repulsive correction (5-6) depends on the off-energy-shell behavior of  $V$ . If  $V$  has large off-energy-shell matrix elements, this repulsive correction becomes large. In particular, if the off-energy-shell matrix elements are large for intermediate states with  $k' \leq k_F + K$ , the repulsive term (5-6) becomes especially large, because the Pauli  $Q$  operator is less than unity for these intermediate states. In the cases illustrated in Figures 27 and 28,  $(k_F + K)$  corresponds to about  $2.2F^{-1}$ .

The correction term (5-6) is largely determined by Fourier components up to  $(k_F + K)$ . Since the tensor force is primarily responsible for scattering to intermediate states with momenta less than  $(k_F + K)$  (Figure 25), the repulsive correction term (5-6) is very sensitive to the strength of the tensor force. This sensitivity accounts for the large differences in the  ${}^3S_1$  potential energies between potentials with strong tensor forces and those with weak tensor forces. The central-force matrix elements contribute repulsively to (5-6), but these contributions are smaller than those due to the tensor force, because the central force

mainly scatters to intermediate states where the Pauli Q operator is unity. Consequently, the strength of the tensor force becomes the critical factor in determining the magnitude of (5-6) and nuclear binding energies. Also, the repulsive corrections due to the tensor force increase with density because the number of states for which  $k' < (k_F + K)$  increases more rapidly than the volume of the Fermi sphere. For a very strong tensor force this effect shows up as a minimum in the  $^3S_1$  curve at a fairly low density. This property appears most clearly in the  $^3S_1$  curve for the Reid potential. The minimum point of the  $^3S_1$  curve largely determines the saturation density for a given potential.

From the previous discussion we note that the Pauli Q operator in the nuclear medium suppresses some of the attraction from the low Fourier components that is present when two-particles freely interact. Most of these low Fourier components result from the tensor interaction. The interrelation between the Pauli Q operator and the tensor force is thus chiefly responsible for nuclear saturation.

The roles of P waves, D waves, and higher partial waves are relatively minor ones in accounting for the differences in binding energies of nearly phase-shift-equivalent potentials. The approximate Serber property of nuclear forces results in near cancellation of P waves at collision energies of importance in nuclear matter. For D waves, the differences in potential energies among the potentials studied are mainly attributable to different fits to the D-wave phase-shifts. For higher partial waves, the OPEP interaction pretty well fixes the potential energies, at least to within about 1 MeV.<sup>87</sup> Moreover, the approximate Serber property and the two-nucleon phase-shifts approximately determine the potential energies for  $L > 0$ .

So far we have been considering nearly phase-shift-equivalent potentials. To isolate the role of short-range correlations and off-energy-shell effects, we should consider exactly phase-shift-equivalent potentials.

#### E. A Canonical Transformation to Generate Phase-Shift-Equivalent Potentials

A unitary or canonical transformation suggested to us by F. Coester<sup>37</sup> provides us with a means of generating an infinite number of phase-shift-equivalent potentials with varying smoothness. This transformation eliminates the problem of phase-shift fitting when one wants to study the effects of short-range correlations with two or more potential models. We now describe this transformation. We also present some calculations with this transformation. The results of these calculations confirm our previous observations about nuclear binding energies and smoothness.

To generate a set of phase-shift-equivalent potentials, we consider a short-ranged unitary operator  $U$ . When acting on a two-body wave function,  $U$  transforms  $\psi$  to  $\bar{\psi}$  by the relation  $\bar{\psi}(\vec{r}) = U\psi(\vec{r})$ . Because  $U$  is canonical, i.e.  $U \cdot U^\dagger = 1$ ,  $U$  preserves the orthonormality of states. Since  $U$  is short-ranged, it does not alter the asymptotic forms of the two-body scattering wave functions, i.e.,  $\bar{\psi}(\vec{r}) \underset{r \rightarrow \infty}{\sim} \psi(\vec{r})$ . Because of this asymptotic property, the scattering phase-shifts and mixing coefficients are unaltered. Under the transformation  $U$  the Hamiltonian  $H$  transforms to  $\bar{H}$ , where  $\bar{H} = UHU^\dagger$ . We may then define the transformed potential  $\bar{V}$  by

$\bar{V} = \bar{H} - T$ . Because  $U$  is a canonical, short-ranged operator for the two-body system, the potentials  $\bar{V}$  and  $V$  give the same phase-shifts and energy spectra in the two-body problem. The transformation  $V \rightarrow \bar{V}$ , however, does not correspond to a canonical transformation in the many-body system. The potentials  $V$  and  $\bar{V}$ , when substituted into the Bethe-Goldstone equation, do not give the same binding energies of nuclear matter. Since  $U$  alters the short-range part of the two-nucleon wave functions, we may employ  $U$  to study the effects of short-range correlations in nuclear matter.

The particular transformation we choose for  $U$  is

$$U = I - 2\Lambda , \quad (5-7)$$

where  $\Lambda$  is a short-ranged projection operator, i.e.  $\Lambda^2 = \Lambda = \Lambda^+$ . This is by no means a unique transformation, but rather one that will serve our purpose to generate a family of phase-shift-equivalent potentials. We will employ these potentials to test our ideas about smoothness and its relation to nuclear binding energies. We further allow  $\Lambda$  to have the partial-wave decomposition

$$\Lambda(\vec{r}, \vec{r}') = \sum_{LL', \alpha M T_3} \Lambda_{LL'}^\alpha(r, r') \tilde{y}_L^\alpha(\vec{r}) \tilde{y}_{L'}^{\alpha M+}(\vec{r}') , \quad (5-8)$$

where we choose

$$\Lambda_{LL'}^\alpha(r, r') = g_L^\alpha(r) g_{L'}^\alpha(r') \delta_{LL'} . \quad (5-9)$$

The unitarity condition becomes

$$\int_0^\infty r'^2 dr' g_L^\alpha(r')^2 = 1.$$

With this transformation the two-body wave functions transform to

$$\psi_{LL}^{\alpha}(r) = \psi_{LL}^{\alpha}(r) - 2g_L^{\alpha}(r) \int_0^{\infty} r'^2 dr' g_L^{\alpha}(r') \psi_{LL}^{\alpha}(r') .$$

Again, the transformation we have chosen is not unique. We note that the transformation (5-9) is chosen because it does not transform a wave function  $\psi$  that does not have tensor coupling to one that does have tensor coupling. If tensor coupling occurs for  $\psi$ , we may use the function  $g_L^{\alpha}(r)$  to alter the non-asymptotic part of the coupled wave function as well as the non-asymptotic part of the uncoupled wave function. The transformation chosen allows us to control the off-energy-shell behavior of the central and tensor parts of the nuclear interaction. Phase-shift-equivalent potentials, therefore, can be generated that give different wound integrals in nuclear matter.

In our calculations we choose

$$g_L^{\alpha}(r) = \frac{e^{-\alpha_0 r}}{N} (1 - \beta_0 r) \delta_{LO} \quad (5-10)$$

for the  $^3S_1 + ^3D_1$  eigenchannel. Here  $N$  is a normalization constant. By adjusting the parameters  $\alpha_0$  and  $\beta_0$ , we can vary the short-range correlations in  $\psi_{00}^{\alpha}(r)$  and  $\psi_{20}^{\alpha}(r)$ . The variations in the short-range part of  $\psi_{00}^{\alpha}(r)$  and  $\psi_{20}^{\alpha}(r)$  are reflected by a variation in the wound integrals  $\kappa_{00}$  and  $\kappa_{20}$  in nuclear matter. The variation in  $\kappa_{20}$  is small because  $\psi_{20}^{\alpha}(r)$  does not have strong correlations; therefore, our choice mainly succeeds in varying  $\kappa_{00}$ . The main goal of our calculation becomes to study nuclear binding energies as a function of  $\kappa_{00}$ . We employ the Reid soft-core potential as a starting potential.

An alternate choice for (5-10) is

$$g_L^{\alpha}(r) = g_L(r) \delta_{L2} . \quad (5-11)$$

This transformation would alter  $\kappa_{22}$  and  $\kappa_{02}$  in nuclear matter. Since we have found that  $\kappa_{02}$  plays a critical role in nuclear saturation, the transformation (5-11) becomes a worthy avenue for future investigation.<sup>91</sup>

## 1. Results

The results of our calculations with the transformation (5-9,10) appear in Figure 26. Table XV shows the parameters  $\alpha_0, \beta_0$  and the wound integral  $\kappa_{00}$  for each case shown in Figure 29. In Figure 30 we present the functions  $F_{00}^{110}(k)$  for each case in Figure 29.

The results in Figure 29 confirm the relation of less binding with larger wound integrals. In our most extreme case, case 3, where  $\kappa_{00} = .1263$ , drastic underbinding occurs. Cases 1 and 2 are also consistent with our previous results, although large differences in binding do not occur because we are varying  $\kappa_{00}$  instead of  $\kappa_{02}$ . In case 1 the wound integral  $\kappa_{00}$  is about .015 smaller than the Reid value; accordingly, the potential in case 1 gives about 1 MeV more binding than the Reid potential at  $k_F = 1.5$ . In case 2 the wound integral is about .015 larger than the Reid value; here the potential gives about 3 MeV less binding than the Reid potential.

If one examines the wave-function defects in Figure 30, only in case 3 are the Fourier components below  $2.2F^{-1}$  large. This result explains the drastic overbinding in case 3. In fact, the Fourier components below  $2.2F^{-1}$  in case 3 are slightly larger than those of  $F_{02}(k)$  for the Reid potential (see Figure 28). The central force in case 3 actually simulates the saturating effect of a strong tensor force. The importance of low Fourier components in nuclear saturation is confirmed by case 3.

TABLE XI.

Parameters and wound integrals for phase-shift equivalent potentials.

Case	$\alpha_o(F^{-1})$	$\beta_o(F^{-1})$	$K_{00}$
1	4.33	1.25	.0256
2	16.00	12.00	.0537
3	10.00	6.00	.1263
REID			.0385

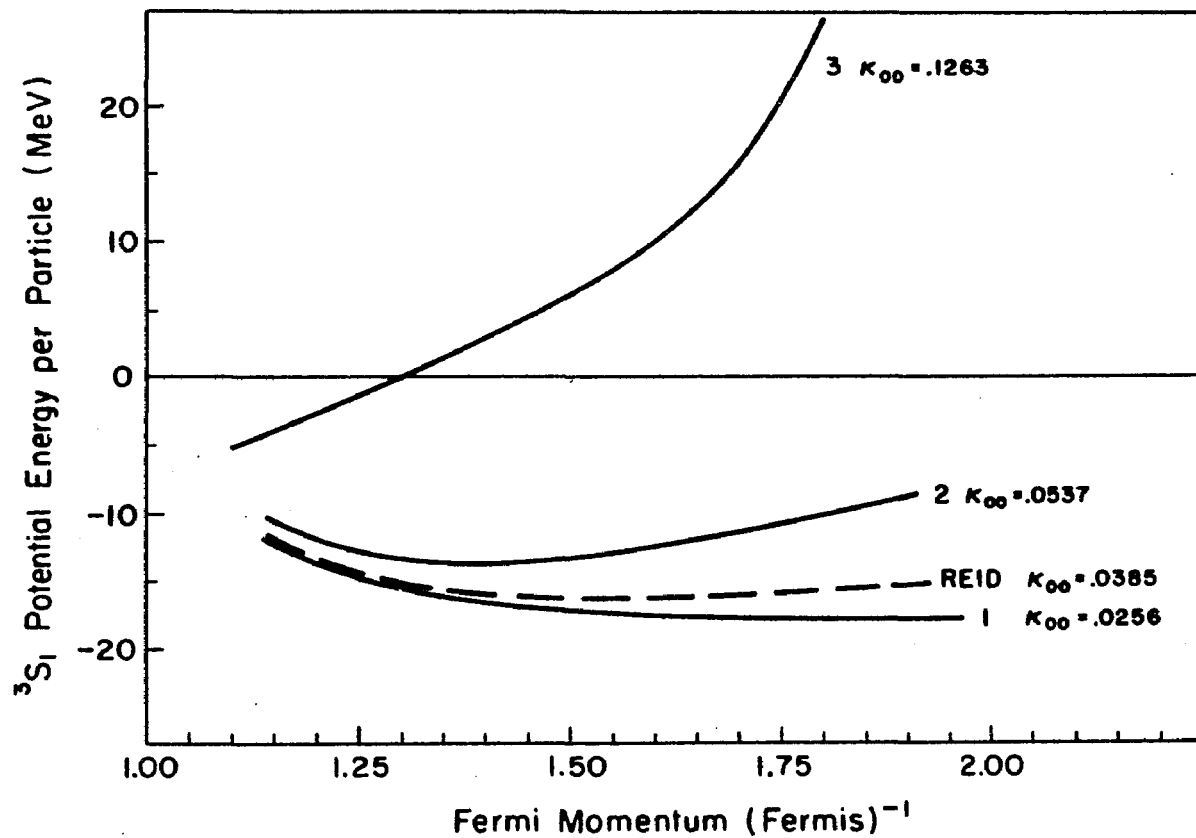


Figure 29. The  $^3S_1$  potential energies for phase-shift equivalent potentials: The parameters  $\alpha_o$  and  $\beta_o$  for each case appear in Table XV.

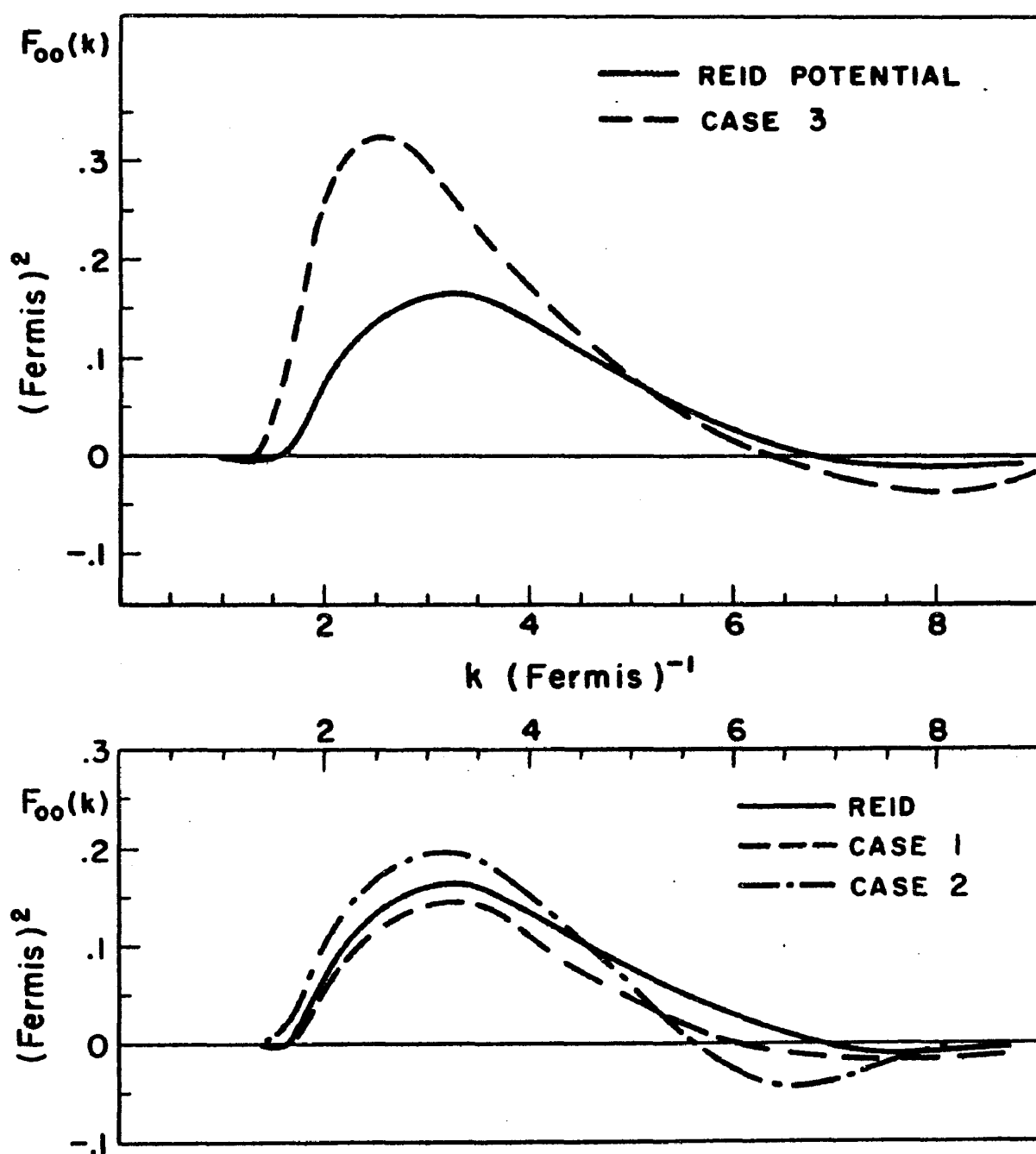


Figure 30.  $F_{00}^\alpha(k)$  for the  ${}^3S_1 + {}^3D_1$  eigenchannel for phase-shift equivalent potentials.

In the course of our calculations we came across a case where a smaller wound integral actually led to less binding. However, the wave-function defect  $\chi_{00}(r)$  for this case had wild oscillations. We rejected this case as being unphysical. This case requires further study.

The main conclusion obtained from our calculations with phase-shift-equivalent potentials is that the two-body-scattering data does not fix the binding energy of nuclear matter to any great degree.<sup>92</sup> The importance of off-energy-shell effects are best exemplified in case 3. This case also demonstrates the repulsive effect of large Fourier components for  $k \lesssim 2F^{-1}$ .

As a future problem one could employ the transformation (5-11) instead of (5-10). Larger effects than the ones we obtained would probably result because (5-11) would vary  $\kappa_{02}$ . As we have seen previously, the strength of the tensor force for incident S waves, which is measured by  $\kappa_{02}$ , largely accounts for the saturating properties of nuclear potentials.

The canonical transformation (5-7) is a very handy tool in studying short-range correlations. Its usefulness is not limited to nuclear matter; the transformation is also applicable to nuclear-structure calculations, the three-body problem, and nuclear reactions.

#### F. Sensitivity of Binding Energies to the Particle Spectrum

Up to this point all of our calculations employ a free "particle" spectrum. Presently the free-particle spectrum choice is believed to be correct;<sup>59</sup> however, future refinements in summing three-body diagrams may lead to a new prescription for the particle spectrum.<sup>93</sup> Also, the

physical picture of a particle immediately above the Fermi sea not interacting with the particles inside the Fermi sea is somewhat unreasonable and difficult for some investigators to accept.<sup>94</sup> In the following calculations we indicate how sensitive binding energies are to the particle spectrum. We do not claim that the particle spectrum we choose is better than the free-particle choice. The only claim is that nuclear-binding energies are sensitive to the particle spectrum for momenta between  $k_\gamma = k_F$  and  $k_\gamma = 2k_F$  and that this sensitivity largely results from the properties of the tensor force. Our calculations indicate that a careful treatment of the tensor force is necessary in the summation of three-body diagrams.

To check the sensitivity of binding energies to the particle spectrum, we replace the free-particle spectrum with a quadratic function of  $k_\gamma$ , i.e.,  $E(k_\gamma) = A + Bk_\gamma^2$ , for  $k_\gamma$  between  $k_F$  and  $2k_F$ . We fix the gap  $\Delta$  between the hole spectrum and the particle spectrum at  $k_\gamma = k_F$ , and fix the single-particle energy at  $k_\gamma = 2k_F$  to  $E(2k_F)$ . These parameters —  $\Delta$  and  $E(2k_F)$  — fix the parameters  $A$  and  $B$ . Figure 31 illustrates this particle spectrum.

The particle spectrum we choose requires us to re-examine the problem of angular dependence. To resolve this problem we make the further approximation that the particles are either excited to intermediate states with both momenta between  $k_F$  and  $2k_F$ , or both particles are excited to intermediate states with momenta above  $2k_F$ . In Appendix D2 we show how this approximation eliminates angular dependence on the direction of the center-of-mass momentum. We also explain in Appendix D2 why this approximation is reasonable. The resulting particle spectrum becomes, in relative and center-of-mass coordinates,

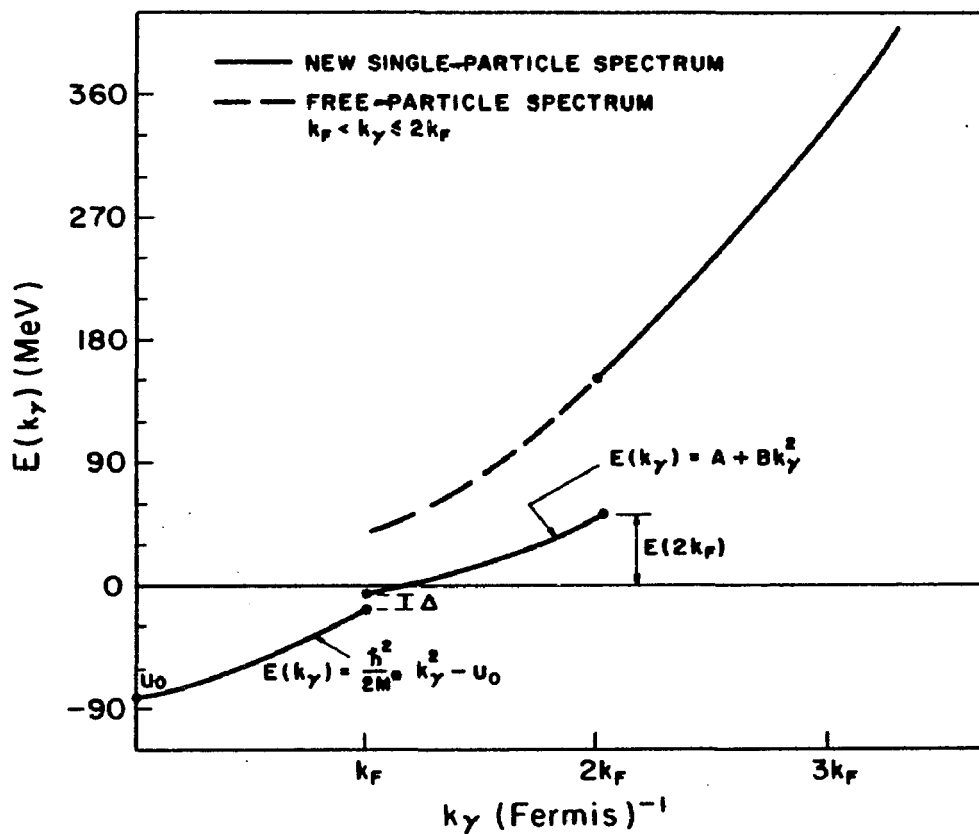


Figure 31. The altered particle spectrum: Definition of the parameters  $\Delta$  and  $E(2k_F)$ . Here  $k_F = 1.36F^{-1}$ ,  $U_0 = 80$  MeV and  $M^*/M = 0.6$ .

$$\vec{E}(k', k) = 2A + 2B(k'^2 + k^2) \text{ for } k'^2 + k^2 \leq 4k_F^2$$

$$= \frac{\hbar^2}{M} (k'^2 + k^2) \text{ for } k'^2 + k^2 > 4k_F^2 .$$

In our calculation of the sensitivity of binding energies to the particle spectrum, we include potential-energy contributions from only the  $^1S_0$ ,  $^1D_2$  and  $^3S_1 + ^3D_1$  eigenchannels. Since great precision is not required here, only a 10-point Laguerre integration routine is used to invert the Bethe-Goldstone equation. The potential used is the Reid soft-core potential. We determine the hole-spectrum parameters  $M^*$  and  $U_0$  reasonably self-consistently; however, we do not attach any self-consistency criterion to the values  $\Delta$  and  $E(2k_F)$ , since we do not know which three-body diagrams we want to cancel.<sup>93</sup>

Figures 32-34 show the sensitivity of nuclear-binding energies to the particle spectrum. For the choice of parameters  $\Delta \approx 9.0$  MeV and  $E(2k_F) \approx 0.0$  MeV, an approximately 8 MeV gain in binding occurs over the free-particle-spectrum case. Almost all of this extra binding comes from the  $^3S_1 + ^3D_1$  state. The potential energies in the  $^1S_0$  and  $^1D_2$  states are very close to their free-particle-spectrum values. While the binding energies are sensitive to the particle spectrum, the saturation densities change little. Even with the altered particle spectrum, the Reid potential saturates at nearly the correct density.

While the  $^3S_1$  state becomes substantially more attractive, the  $^1S_0$  potential energies are slightly less attractive with the new particle spectrum than for the free-particle-spectrum case. To explain the appreciable gain in binding of the  $^3S_1$  state, and the slight loss of binding in the  $^1S_0$  state, we must look at the gaps between the hole

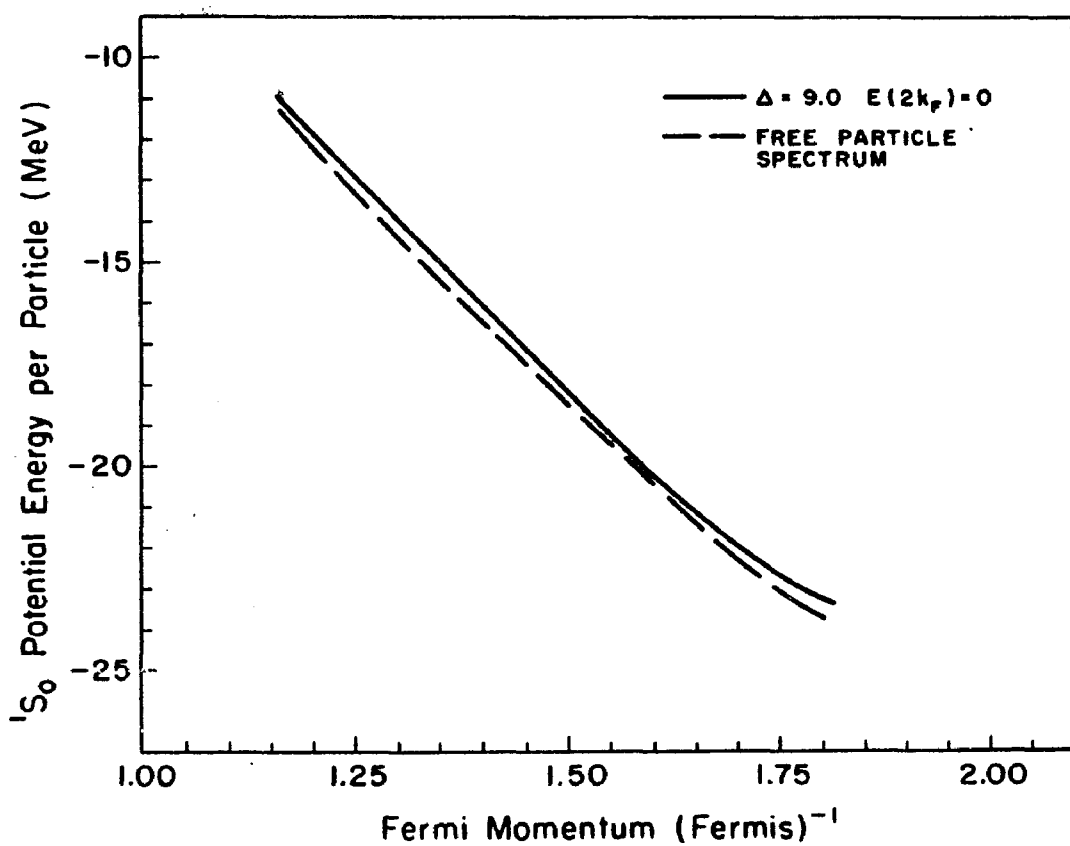


Figure 32. Comparison of the  $^1S_0$  potential energy contributions in nuclear matter for the altered particle spectrum and free-particle spectrum cases.

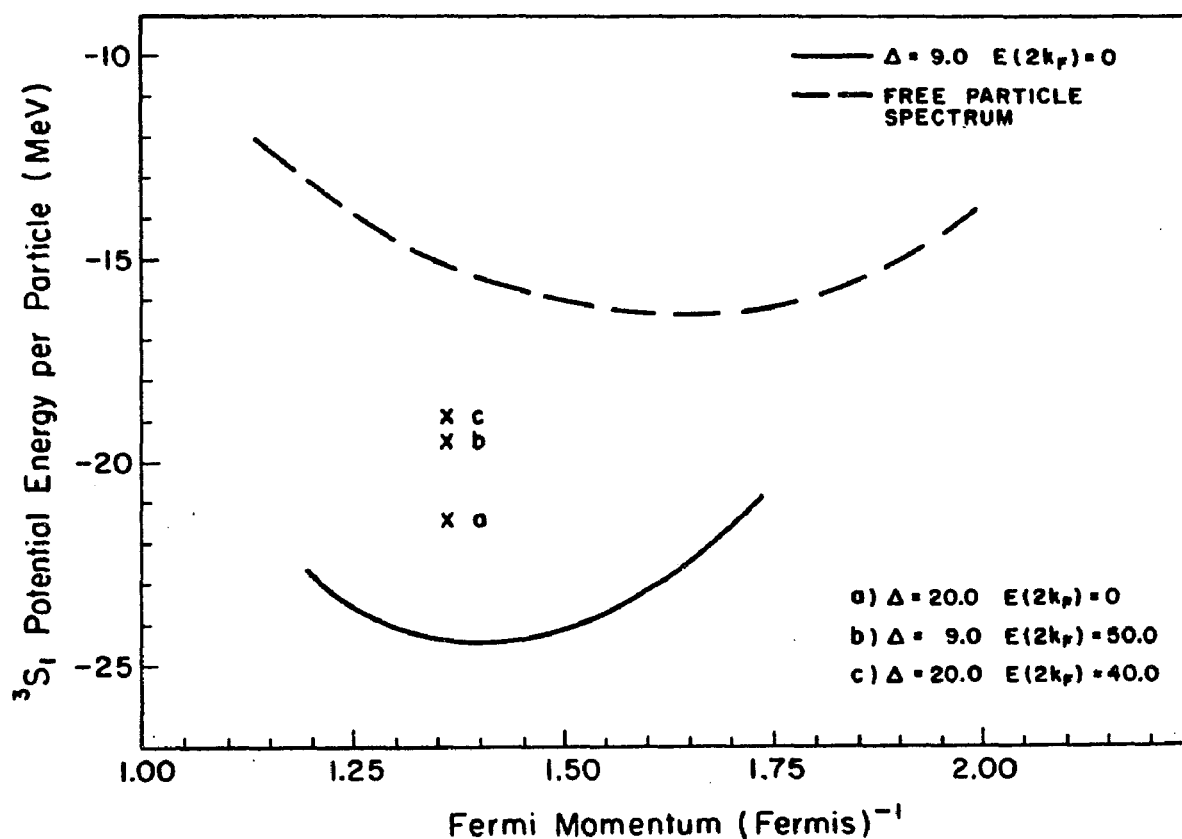


Figure 33. Comparison of the  $^3S_1$  potential energy contributions in nuclear matter for the altered particle spectrum and free-particle spectrum cases: The crosses represent the  $^3S_1$  potential energies at  $k_F = 1.36F^{-1}$  for various parameters of  $\Delta$  and  $E(2k_F)$ .

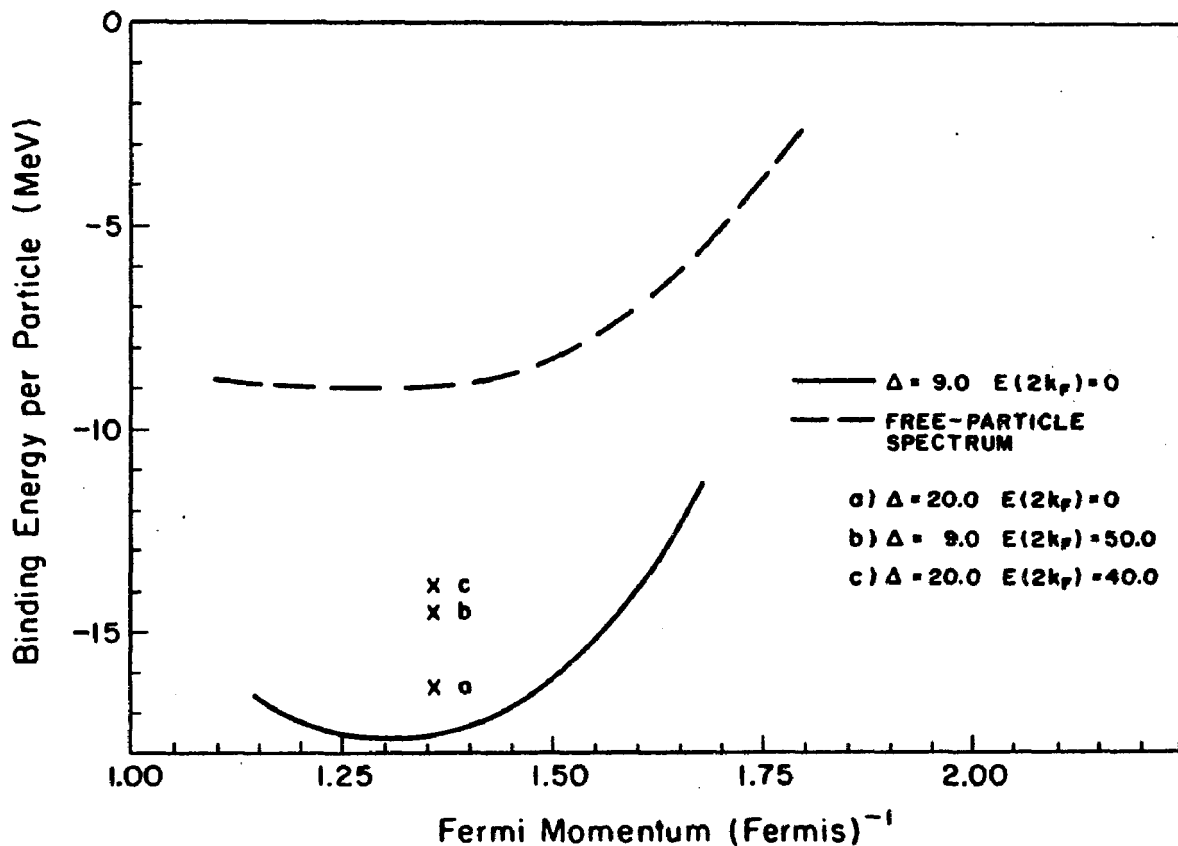


Figure 34. Comparison of the total binding energy of nuclear matter for the altered particle spectrum and free-particle spectrum cases. The crosses represent the total binding energy at  $k_F = 1.36 F^{-1}$  for various parameters of  $\Delta$  and  $E(2k_F)$ . Only the potential energy contributions from the  $^1S_0$ ,  $^1D$ , and  $^3S_1 + ^3D_1$  eigenchannels are included in the total binding energies.

energies and the particle energies. These gaps determine the energy propagators in the Bethe-Goldstone equation.

With the particle-spectrum parameters  $\Delta = 9.0$  MeV and  $E(2k_F) = 0.0$  MeV, the particle-state energies between  $k_F$  and  $2k_F$  become considerably less than they would be in the free-particle case. The gaps between the hole energies and the particle energies for intermediate states between  $k_F$  and  $2k_F$  become correspondingly smaller. The smaller energy gaps lead to larger propagators  $\frac{Q(k', K)}{e^>(k', K) - e^<(k', K)}$  for  $k'^2 + K^2 < 4k_F^2$ . In fact, the energy gap between the hole spectrum and the particle spectrum at  $k_\gamma = k_F$ , assuming a free particle spectrum, is of the order of 60 MeV. The gap in the altered spectrum is only 9 MeV. The larger propagators with the new particle spectrum generate larger attractive contributions to the G matrix from terms like the second-order term

$$-\frac{2}{\pi} \int \frac{k'^2 dk' v_{OL}^{\alpha^2}(k_0, k') Q(k', K)}{e^>(k', K) - e^<(k_0, K)} \quad (5-12)$$

The overall effect of the altered particle spectrum on the total binding energy is increased attraction over the free-particle case. This larger attraction also appears in the form of a deeper hole spectrum. Table XVI gives the nearly self-consistent hole-spectrum parameters  $M^*$  and  $U_0$  for various values of  $\Delta$  and  $E(2k_F)$ . In all cases the hole spectrum becomes slightly deeper and flatter. The new choice of particle spectrum has the indirect effect of widening the gap slightly between the self-consistent hole spectrum and the particle spectrum for  $k_\gamma > 2k_F$  over the free-particle case. Figure 35 illustrates this point. The new particle spectrum has the

TABLE XVI.

Self consistent hole spectrum parameters for various  
choices of particle spectrum.

$\Delta$ (MeV)	$E(2k_F)$ (MeV)	$M^*/M$	$U_0$ (MeV)
9.00	0.00	.663	96.90
9.00	50.00	.617	91.10
20.00	0.00	.650	93.78
20.00	40.00	.620	90.11

indirect effect of decreasing the energy propagators in (5-12) for  $k'^2 + K^2 > 4k_F^2$ . The total effect of altering the particle spectrum between  $k_\gamma = k_F$  and  $k_\gamma = 2k_F$  is to greatly magnify the attractive contributions of the form (5-12) from intermediate states for which  $k'^2 + K^2 < 4k_F^2$  and slightly diminish the attractive contributions for  $k'^2 + K^2 > 4k_F^2$ .

Because the tensor force scatters predominantly to intermediate states for which  $k'^2 + K^2 < 4k_F^2$ , the new choice of the particle spectrum accounts for the large additional attraction in the  $^3S_1$  state over the free-particle-spectrum case. The central force scatters predominantly to states for which  $k'^2 + K^2 > 4k_F^2$ ; consequently, the  $^1S_0$  contributions become slightly less attractive than in the free-particle-spectrum case.

In our calculations of the binding energy of nuclear matter with an altered particle spectrum, we do not claim that the values  $\Delta = 9.0$  MeV and  $E(2k_F) = 0.0$  have any special significance. In Figures 33 and 34 we indicate the values of the binding energy per particle and  $^3S_1$  potential energies for several other choices of  $\Delta$  and  $E(2k_F)$ . In all cases the additional binding occurs in the  $^3S_1$  state as one narrows the average gap between the hole spectrum and the particle spectrum for momenta between  $k_F$  and  $2k_F$ .

The results we have just discussed indicate that the difference between the binding energy of the Reid soft-core potential and the semi-empirical mass formula could conceivably be due to an incorrect choice of the particle spectrum. Our calculations do not prove that the free particle choice is incorrect, but rather points out an ambiguity in Brueckner theory. The best choice of the particle spectrum is intimately

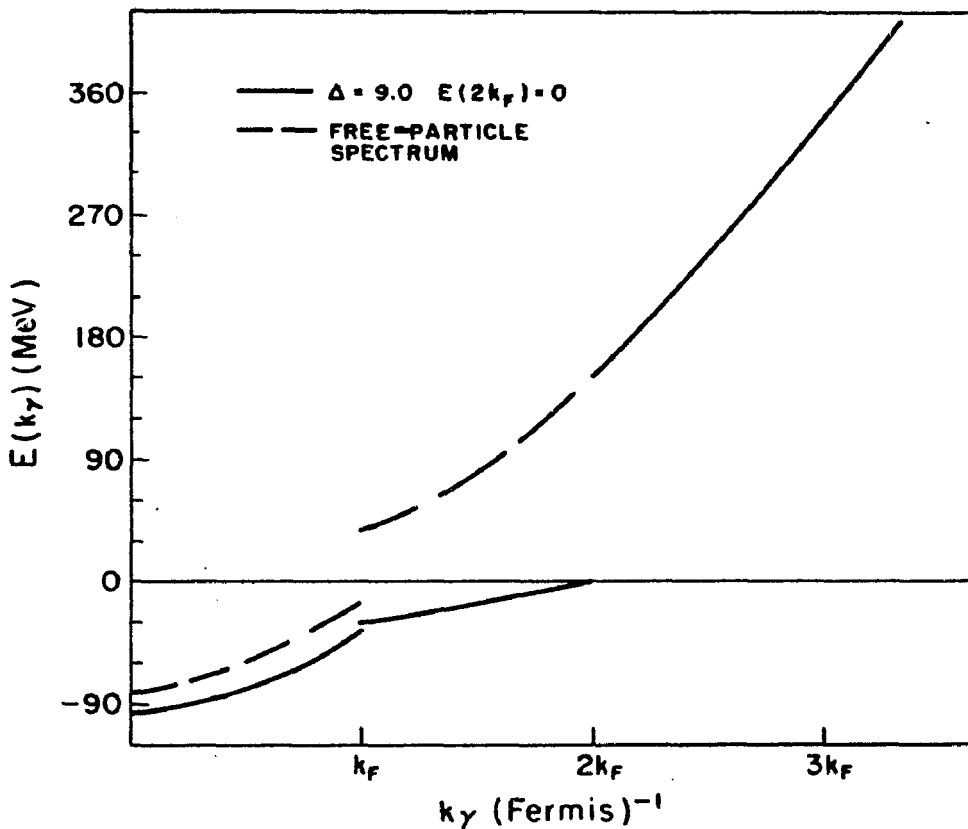


Figure 35. Comparison of the full single-particle spectrums for the altered particle spectrum and free-particle spectrum cases; The hole-spectrum parameters are determined self-consistently in each case. Here  $k_F = 1.36F^{-1}$ . Note the size of the gaps between the hole spectrum and particle spectrum in each case.

related to the study of three-body cluster diagrams. The eventual determination of the best particle spectrum could resolve much of the difference between the binding energy of the Reid potential and experiment. In the study of three-body cluster diagrams, it also appears that the tensor force plays a more important role than the short-range repulsion. Studies of three-body diagrams, therefore, should take into account the properties of the tensor interaction more precisely than they have in the past.

## VI. CONCLUSIONS

The ability to fit the experimental phase-shifts with smooth potentials has been demonstrated by the excellent phase-shifts fits of the smooth potentials A and B in the  $^3S_1 + ^3D_1$  eigenchannel. The introduction of velocity dependence into the central and tensor parts of the two-nucleon interaction apparently supplies the freedom necessary to generate smooth two-nucleon wave functions and fit the experimental data on the energy shell. Strong short-range correlations and strong tensor forces are necessary only if one is limited to static potentials to fit the S-wave phase parameters. In particular, the introduction of non-local tensor forces allows smooth two-nucleon wave functions to be generated in the  $^3S_1 + ^3D_1$  eigenchannel where convergence of perturbation theory is usually unsatisfactory. The total higher-order corrections in the  $^3S_1$  potential energy for nuclear matter come to only 3% for force A and 10% for force B. These figures suggest that the convergence rate in Hartree-Fock theory for either force is excellent. Unfortunately, this convergence leads to binding energies that disagree considerably with the semi-empirical mass formula.

The price paid for smoothness is overbinding and too high a saturation density in nuclear matter. The overbinding comes almost exclusively from the  $^3S_1$  state where the tensor force enters. The orderly behavior of nuclear binding energies with the wound integral  $\mu_{02}$  indicates that the overbinding of forces A and B is not an accident. The degree of overbinding in these smooth potentials suggests that smooth potentials cannot even qualitatively reproduce the correct nuclear binding energies.

Our investigations demonstrate that strength of the tensor force in the  $^3S_1 + ^3D_1$  eigenchannel is the most crucial factor in nuclear saturation. The importance of the tensor force results from the tensor force scattering to intermediate states with lower momenta than to those to which a central force scatters. The tensor force contributes large Fourier components to the nuclear wave functions for all momenta up to about  $6.0F^{-1}$ , with very large contributions at lower momenta where the Pauli Q operator is less than unity. The interplay between the Pauli Q operator and the Fourier components up to about  $2.2F^{-1}$  is a crucial factor in nuclear saturation. The central part of the two-nucleon interaction, for potentials with strong short-range repulsions, gives fairly large Fourier components for  $2.2F^{-1} \lesssim k' \lesssim 6.0F^{-1}$ ; however, the components in the important region up to  $2.2F^{-1}$  are rather small. Our main conclusion is that nuclear saturation requires strong tensor forces rather than strong short-range repulsions.

The wound integral  $\kappa_{02}$  is the most important quantity in determining whether a potential will saturate at near correct density.

The values of  $\kappa_{00}$  in the  $^1S_0$  and  $^3S_1 + ^3D_1$  eigenchannels play lesser roles. The pattern is always increased binding energies and saturation densities with smaller wound integrals.

A wound integral  $\kappa_{02}$  between .05 and .07 usually accompanies nuclear saturation at nearly the correct energy or density. Significantly,  $\kappa_{02} = .057$  for the Bryan-Scott OBEP. The Bryan-Scott potential does saturate very close to the experimental binding energy with  $k_F = 1.58F^{-1}$ . This result implies that the one-boson-exchange-theory of nuclear forces includes the elements necessary for nuclear saturation. Our calculations

for the Bryan-Scott potential suggest that the saturating properties come from the strong tensor force in the OPEP part of the potential.

One puzzling result is that the Reid soft-core potential saturates at nearly the experimental density but with about 6 MeV too little binding compared with the semi-empirical mass formula. Our study of the sensitivity of the nuclear binding energies to the particle spectrum suggests that this discrepancy with experiment could arise from a possibly incorrect assumption of a free-particle spectrum. The  $^3S_1$  state is the only state sensitive to the particle spectrum between  $k_F$  and  $2k_F$ . This sensitivity is attributable to the tensor force scattering to intermediate states just above what is allowed by the Pauli principle. Determination of the best particle spectrum awaits further investigations of three-body cluster diagrams. Clearly, such investigations should not treat the tensor force casually. If the free-particle choice is correct, we must conclude that the very strong tensor force in the Reid potential causes the underbinding.

In dealing with different potential models one has to cope with the problem of how different fits to the two-body data affect nuclear binding energies. To avoid this problem one may employ the canonical transformation described in Section V to generate sets of exactly phase-shift-equivalent potentials. One may use this method to isolate the properties of short-range correlations and off-energy-shell effects in a wide range of problems. This method is not only useful in nuclear matter, but is applicable in studies of the roles of short-range correlations in deuteron properties, the three-body problem, nuclear-structure calculations, and nuclear reactions. The main difficulty in applying the

transformation is the non-locality of the operator  $\Lambda(\vec{r}, \vec{r}')$ . We resolve this difficulty by inverting the Bethe-Goldstone equation in momentum space. Similar techniques could be applied to the other problems mentioned above.

This thesis has shown that the saturation of nuclear matter places a severe constraint on the smoothness of the two-nucleon interaction, especially in regards to the tensor interaction in the  $^3S_1 + ^3D_1$  eigenchannel. The  $^3S_1 + ^3D_1$  eigenchannel is a neutron-proton eigenchannel. Therefore, nuclear saturation mainly restricts the smoothness of the neutron-proton interaction. In problems for which the neutron-proton interaction is unimportant, smooth forces and the Hartree-Fock approach may still prove useful. An example of such a problem is shell-model calculations of the spectra of nuclei with doubly closed shells and a few valence neutrons or a few valence protons.

In nuclear-matter calculations surface effects are excluded. These surface effects are quite important in light nuclei. Therefore, further investigations into the properties of non-locality in the nuclear surface problem are necessary to rule on the applicability of the Hartree-Fock approximation in problems concerning light nuclei. The strong tensor forces necessary to saturate nuclear matter do seem to rule out smooth forces for systems that involve the interactions of large numbers of neutrons and protons. Consequently, the Hartree-Fock approximation does not seem valid for nuclear-structure calculations for heavy nuclei.

The numerical techniques developed in this thesis are applicable to non-local potentials considerably more complicated than the ones we have considered. One class of complicated non-local potentials is the

relativistic one-boson-exchange potentials. We are planning calculations aimed at elucidating the roles of the relativistic parts of the one-boson-exchange potentials in the two-body problem and in nuclear matter.

## APPENDIX A1

### ASYMPTOTIC FORM OF THE TWO-NUCLEON WAVE FUNCTION FOR SCATTERING

Starting from the relation

$$\psi_{LL}^{\alpha}(r) = j_L(k_0 r) \delta_{LL'} - \frac{2}{\pi} P \int_0^{\infty} \frac{k'^2 dk' \cdot R_{LL'}^{\alpha}(k', k_0) j_{L'}(k' r)}{k'^2 - k_0^2} \quad (\text{Al-1})$$

we wish to evaluate  $\psi_{LL}^{\alpha}(r)$  for  $r \rightarrow \infty$ . To employ a convenient principal value contour to evaluate (Al-1), we must change the integrand in (Al-1) to one whose limits are  $\pm\infty$ . To do this we use the relations

$$v_{LL'}^{\alpha}(k', k) = \int_0^{\infty} r^2 dr \ r'^2 dr' j_L(kr) v_{LL'}^{\alpha}(r', r) j_{L'}(k'r') \quad (\text{Al-2})$$

and

$$j_{L'}(-k'r') = (-1)^{L'} j_{L'}(k'r') \quad (\text{Al-3})$$

to derive the relation

$$v_{LL'}^{\alpha}(-k', k) = (-1)^{L'} v_{LL'}^{\alpha}(-k', k) \quad . \quad (\text{Al-4})$$

Substitution of (Al-3) into the Lippmann-Schwinger equation for  $R_{LL'}^{\alpha}(-k', k_0)$  yields

$$\begin{aligned} R_{LL'}^{\alpha}(-k', k_0) &= v_{LL'}^{\alpha}(-k', k_0) - \frac{2}{\pi} P \sum_l \int_0^{\infty} \frac{k'^2 dk \ v_{LL'}^{\alpha}(-k', k) R_{ll}^{\alpha}(k, k_0)}{k'^2 - k_0^2} \\ &= (-1)^{L'} \left[ v_{LL'}^{\alpha}(k', k_0) - \frac{2}{\pi} P \sum_l \int_0^{\infty} \frac{k'^2 dk \ v_{LL'}^{\alpha}(-k', k) R_{ll}^{\alpha}(k, k_0)}{k'^2 - k_0^2} \right]. \end{aligned}$$

Therefore

$$R_{LL'}^{\alpha}(-k', k_0) = (-1)^{L'} R_{LL'}^{\alpha}(k', k_0) \quad . \quad (\text{Al-5})$$

With the application of the relations (Al-3) and (Al-5) to (Al-1), we may rewrite (Al-1) as

$$\downarrow_{LL'}^{\alpha}(r) = j_L(k_0 r) \delta_{LL'} - \frac{P}{\pi} \int_{-\infty}^{\infty} \frac{k'^2 dk' R_{LL'}^{\alpha}(k', k_0) j_{L'}(k' r)}{k'^2 - k_0^2}. \quad (\text{Al-6})$$

To evaluate (Al-6) for  $r \rightarrow \infty$ , we employ the relation

$$j_{L'}(k' r) \underset{r \rightarrow \infty}{\approx} \cos(k' r - (L'+l)\pi/2)/k' r = \frac{1}{2k' r} [e^{i(k' r - (L'+l)\pi/2)} + e^{-i(k' r - (L'+l)\pi/2)}] \quad (\text{Al-7})$$

and rewrite the second term in (Al-6), which we will denote by I, as

$$I = - \frac{P}{2\pi} \int_{-\infty}^{\infty} \frac{k'^2 dk' R_{LL'}^{\alpha}(k', k_0) e^{i(k' r - (L'+l)\pi/2)}}{r(k'^2 - k_0^2)} \\ - \frac{P}{2\pi} \int_{-\infty}^{\infty} \frac{k'^2 dk' R_{LL'}^{\alpha}(k', k_0) e^{-i(k' r - (L'+l)\pi/2)}}{r(k'^2 - k_0^2)}. \quad (\text{Al-8})$$

By changing the variable of integration from  $k' \rightarrow -k'$  in the second term in (Al-8), and employing the relations (Al-3) and  $(-1)^{L'} = e^{-iL'\pi}$ , we can rewrite (Al-8) as one integral whose integrand vanishes on the infinite semi-circle of the upper half complex plane. This integral is

$$I = - \frac{P}{\pi} \int_{-\infty}^{\infty} \frac{k'^2 dk' R_{LL'}^{\alpha}(k', k_0) e^{i(k' r - (L'+l)\pi/2)}}{r(k'^2 - k_0^2)(k' + k_0)}. \quad (\text{Al-9})$$

We now evaluate (Al-9) by employing the principal value contour shown in Figure A-1. We may integrate around the infinite semi-circle in the upper half plane because the integrand in (Al-9) vanishes there due

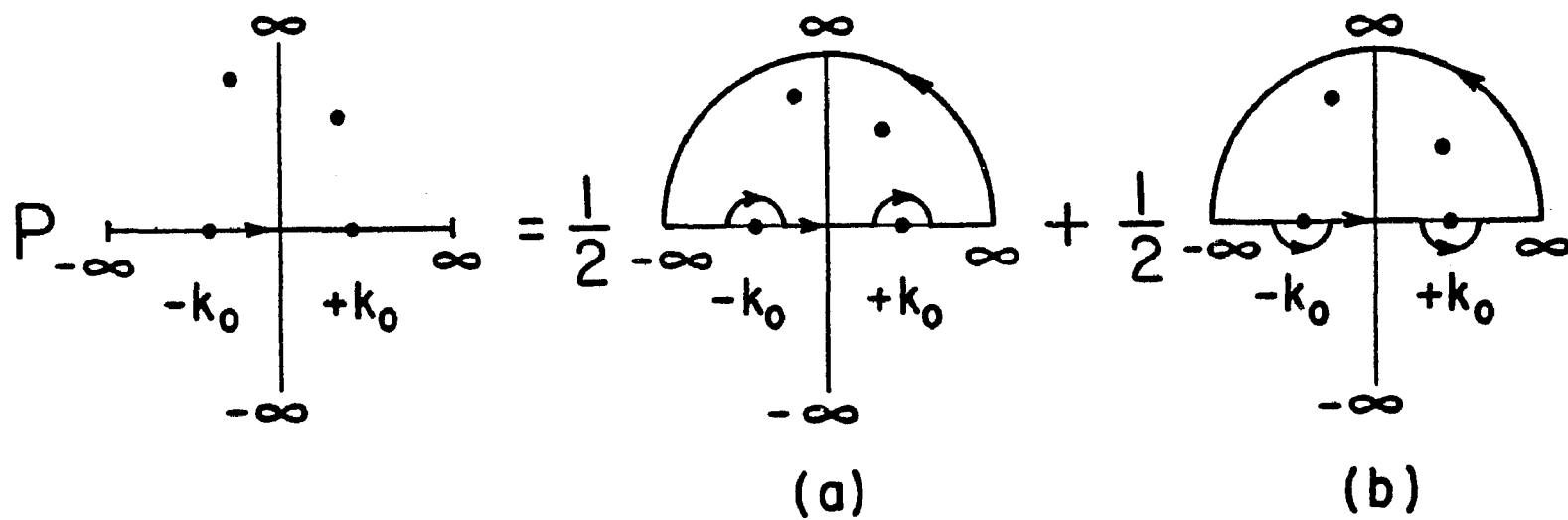


Figure A-1. Integration contour for principal value: The heavy lines with arrows represent integration contours. The dots represent the singularities in the integrand of (Al-9). If  $V$  is short-ranged, the only singularities in (Al-9) on the real axis are at  $k' = \pm k_0$ . Other singularities in Eq. (Al-9) are due to singularities in  $R_{L,L}^{\alpha}(k', k_0)$ , but these singularities are off of the real axis. The contours in (a) and (b) can be closed on the infinite semi-circle of the upper half plane because the integrand in (Al-9) vanishes on this semi-circle.

to the factors  $e^{ikr}$  and  $\frac{1}{k'^2 - k_o^2}$ . Employing Cauchy's theorem, we obtain the result

$$I = -\frac{1}{\pi} \left(\frac{1}{2}\right) 2\pi i \left| \frac{(k' e^{ik'r-i(L'+l)\pi/2}) R_{L'L}^\alpha(k', k_o)}{r(k' - k_o)} \right|_{k'=-k_o}$$

$$= -\frac{1}{\pi} \left(\frac{1}{2}\right) 2\pi i \left| \frac{(k' e^{ik'r-i(L'+l)\pi/2}) R_{L'L}^\alpha(k', k_o)}{r(k' + k_o)} \right|_{k'=k_o}$$

+ terms due to singularities in  $R(k', k_o)$  for  $k'$  off the real axis.

(Al-10)

In (Al-10) the terms due to singularities in  $R_{L'L}^\alpha(k', k_o)$  decay exponentially in  $r$  and vanish in the asymptotic limit. The two remaining terms in (Al-10) result from the singularities at  $\pm k_o$  on the real axis for contour (b) in Figure A-1. Contour (a) does not contribute to (Al-10) because this contour does not enclose the singularities at  $\pm k_o$ .

We can evaluate (Al-10) and employ the relation (Al-5), with the result

$$\begin{aligned} I &= -\frac{i}{2r} ((-1)^{L'} e^{-i(k_o r + (L'+l)\pi/2)} + e^{i(k_o r - (L'+l)\pi/2)}) R_{L'L}^\alpha(k_o, k_o) \\ &= -\frac{i}{2r} (e^{-i(k_o r - L'\pi/2 + \pi/2)} + e^{i(k_o r - L'\pi/2 - \pi/2)}) R_{L'L}^\alpha(k_o, k_o) \\ &= -\frac{1}{2r} (e^{-i(k_o r - L'\pi/2)} + e^{i(k_o r - L'\pi/2)}) R_{L'L}^\alpha(k_o, k_o) \\ &= -\frac{1}{r} \cos(k_o r - L'\pi/2) R_{L'L}^\alpha(k_o, k_o) \end{aligned} \quad . \quad (\text{Al-11})$$

Therefore

$$\psi_{LL'}^{\alpha}(r) \underset{r \rightarrow \infty}{\rightarrow} \frac{\sin(k_0 r - L\pi/2)}{k_0 r} \delta_{LL'} - \frac{1}{r} \cos(k_0 r - L'\pi/2) R_{LL'}^{\alpha}(k_0, k_0) . \quad (\text{Al-12})$$

For uncoupled channels we may identify

$$R_{LL'}^{\alpha}(k_0, k_0) = -\tan \delta_L^{\alpha}(k_0)/k_0$$

and obtain the asymptotic expression

$$\psi_{LL'}^{\alpha}(r) \underset{r \rightarrow \infty}{\rightarrow} \frac{\sin(k_0 r - L\pi/2 + \delta_L^{\alpha})}{k_0 r \cos \delta_L^{\alpha}} . \quad (\text{Al-13})$$

The quantity  $\delta_L^{\alpha}$ , therefore, is simply the scattering phase-shift in channel  $\alpha$ .

For coupled channels, according to the Blatt-Biedenharn parametrization, the eigenphase-shifts  $\delta_{J-1}^{\alpha}$ ,  $\delta_{J+1}^{\alpha}$ , and the mixing coefficient  $e^{\alpha}$  are related to the asymptotic wave function by

$$\psi_{LL'}^{\alpha}(r) \underset{r \rightarrow \infty}{\rightarrow} \sum_l \frac{\tilde{w}_{Ll}^{\alpha}(r) U_{lL'}}{\cos \delta_l^{\alpha}(k_0)}$$

where  $\tilde{w}_{Ll}^{\alpha}(r)$  is the "standard" real solution. The asymptotic form of the standard solution is given by

$$\tilde{w}_{Ll}^{\alpha}(r) \underset{r \rightarrow \infty}{\rightarrow} U_{lL'}^{\alpha} \sin(k_0 r - L'\pi/2 + \delta_L^{\alpha})$$

where  $U_{lL'}^{\alpha}$  is given by the matrix

$$U = \begin{pmatrix} \cos^{\alpha} & \sin^{\alpha} \\ -\sin^{\alpha} & \cos^{\alpha} \end{pmatrix}$$

Therefore, the standard solutions have the asymptotic forms

$$\tilde{w}_{J-1,J-1}^{\alpha}(r) \rightarrow \cos^{\alpha} \sin(k_0 r - (J-1)\pi/2 + \delta_{J-1}^{\alpha})$$

$$\tilde{w}_{J+1,J-1}^{\alpha}(r) \rightarrow \sin^{\alpha} \sin(k_0 r - (J-1)\pi/2 + \delta_{J-1}^{\alpha})$$

$$\tilde{w}_{J+1,J+1}^{\alpha}(r) \rightarrow \cos^{\alpha} \sin(k_0 r - (J+1)\pi/2 + \delta_{J+1}^{\alpha})$$

$$\tilde{w}_{J-1,J+1}^{\alpha}(r) \rightarrow -\sin^{\alpha} \sin(k_0 r - (J+1)\pi/2 + \delta_{J+1}^{\alpha})$$

The U matrices relate to the S matrix by

$$S_{LL}^{\alpha} = \sum_l U_{Ll}^{T\alpha} e^{2i\delta_l^{\alpha}} U_{lL}^{\alpha}$$

APPENDIX A2  
LAGUERRE INTEGRATION POINTS AND WEIGHTS FOR N > 15

The Laguerre integration formula is

$$\int_0^{\infty} f(x) dx \approx \sum_{i=1}^N w_i f(x_i)$$

where  $x_i$  is the  $i^{th}$  zero of the Laguerre polynomial  $L_N(x)$ , and the weight is given by

$$w_i = \frac{e^{x_i}}{x_i} \left[ \frac{N!}{L_N'(x_i)} \right]^2$$

where

$$L_N'(x_i) = \left. \frac{d}{dx} L_N(x) \right|_{x=x_i}$$

To determine the zeroes of  $L_N(x)$ , we evaluated  $L_N(x)$  at a large number of points and searched for the zeroes by a method similar to Newton-Raphson iteration. We obtained the following zero points and weights for  $N = 20, 25, 35$  and  $45$ . The results are accurate to 5 significant figures.

$N = 20$

i	$x_i$	$w_i$
1	.07540	.18108
2	.37213	.42256
3	.91568	.66691
4	1.7073	.91535

## N = 20 continued

i	x <sub>1</sub>	w <sub>1</sub>
5	2.7492	1.1695
6	4.0489	1.4313
7	5.6152	1.7030
8	7.4590	1.9870
9	9.5944	2.2866
10	12.039	2.6058
11	14.814	2.9498
12	17.949	3.3254
13	21.479	3.7423
14	25.452	4.2142
15	29.933	4.7625
16	35.013	5.4217
17	40.833	6.2540
18	47.620	7.3873
19	55.811	9.1513
20	66.524	12.902

## N = 25

1	.05670	.14555
2	.29901	.33935
3	.73591	.53474
4	1.3692	.73223
5	2.2013	.93262
6	3.2357	1.1370

## N = 25 continued

i	x <sub>i</sub>	w <sub>i</sub>
7	4.4765	1.3457
8	5.9291	1.5605
9	7.5999	1.7824
10	9.4967	2.0128
11	11.629	2.2535
12	14.008	2.5066
13	16.647	2.7745
14	19.563	3.0604
15	22.775	3.3684
16	26.309	3.7038
17	30.194	4.0738
18	34.471	4.4884
19	39.191	4.9621
20	44.422	5.5174
21	50.264	6.1933
22	56.865	7.0496
23	64.466	8.2312
24	73.534	10.076
25	85.260	14.035

## N = 35

1	.04073	.10454
2	.21469	.24354
3	.52801	.38322

## N = 35 continued

i	$x_i$	$w_i$
4	.98139	.52368
5	1.5757	.66520
6	2.3122	.80806
7	3.1924	.95259
8	4.2181	1.0991
9	5.3194	1.2480
10	6.7150	1.3996
11	8.1917	1.5544
12	9.8250	1.7129
13	11.619	1.8755
14	13.578	2.0428
15	15.706	2.2156
16	18.011	2.3995
17	20.498	2.5805
18	23.175	2.7746
19	26.050	2.9779
20	29.134	3.1920
21	32.438	3.4186
22	35.976	3.6598
23	39.763	3.9182
24	43.819	4.1972
25	48.166	4.5013
26	52.832	4.8359
27	57.851	5.2090
28	63.266	5.6315

## N = 35 continued

i	$x_i$	$w_i$
29	69.135	6.1192
30	75.534	6.6965
31	82.571	7.4038
32	90.409	8.3133
33	99.313	9.5748
34	109.80	11.576
35	123.17	15.908

## N = 45

1	.03178	.08156
2	.16747	.18994
3	.41177	.29871
4	.76501	.40785
5	1.2276	.51749
6	1.8002	.62776
7	2.4834	.73880
8	3.2781	.85076
9	4.1853	.96379
10	5.2061	1.0780
11	6.3419	1.1937
12	7.5941	1.3110
13	8.9644	1.4300
14	10.455	1.5510
15	12.067	1.6742
16	13.804	1.7999

## N = 45 continued

i	$x_i$	$w_i$
17	15.668	1.9283
18	17.662	2.0597
19	19.788	2.1944
20	22.052	2.3329
21	24.455	2.4754
22	27.004	2.6225
23	29.702	2.7747
24	32.555	2.9325
25	35.569	3.0966
26	38.751	3.2678
27	42.107	3.4470
28	45.648	3.6353
29	49.381	3.8339
30	53.319	4.0443
31	57.474	4.2684
32	61.861	4.5084
33	66.498	4.7672
34	71.403	5.0482
35	76.603	5.3562
36	82.127	5.6972
37	88.011	6.0795
38	94.303	6.5147
39	101.06	7.0200
40	108.37	7.6214

## N = 45 continued

i	x <sub>i</sub>	w <sub>i</sub>
41	116.35	8.3622
42	125.17	9.3202
43	135.12	10.657
44	146.74	12.790
45	161.46	17.437

## APPENDIX B1

### G MATRIX ELEMENTS FOR A SINGLE SEPARABLE POTENTIAL

The analytic expression for the G matrix element  $G_{00}(k; k, k_0)$  for the potential

$$v_{00}(k, k_0) = -g_0(k)g_0(k_0)$$

is given by

$$G_{00}(k; k, k_0) = -g_0(k)g_0(k_0) \left[ 1 - \frac{2}{\pi} \int \frac{k'^2 dk' Q(k', k) g_0^2(k')}{e^{>}(k', k) - e^{<}(k_0, k)} \right]^{-1}. \quad (\text{Bl-1})$$

For the choice

$$g_0(k) = \frac{\alpha}{(k^2 + a^2)} \quad (\text{Bl-2})$$

we may substitute  $g_0(k)$  into Eq. (Bl-1) and obtain

$$\begin{aligned} G_{00}(k, k_0) &= \frac{-\alpha^2}{(k^2 + a^2)(k_0^2 + a^2)} \left[ 1 - \frac{2}{\pi} \alpha^2 \int_0^\infty \frac{k'^2 dk' Q(k', k)}{(k'^2 + b)(k'^2 + a^2)^2} \right]^{-1} \\ &= \frac{-\alpha^2}{(k^2 + a^2)(k_0^2 + a^2)} \left[ 1 - \frac{\alpha^2}{\pi k} \int_{\sqrt{k_F^2 - k^2}}^{k_F + k} dk' \frac{[(k^2 - k_F^2)k' + k'^3]}{(k'^2 + a^2)^2 (k'^2 + b)} \right. \\ &\quad \left. + 2\alpha^2 \int_{k_F + k}^\infty \frac{k' dk'}{(k'^2 + a^2)^2 (k'^2 + b)} \right]^{-1} \quad (\text{Bl-3}) \end{aligned}$$

where

$$b \equiv k^2 \left( 1 - \frac{M}{M^*} \right) - k'^2 \frac{M}{M^*} + \frac{2MU_0}{\hbar^2} .$$

The evaluation of Eq. (B1-3) is straightforward, but quite lengthy. We shall merely state the result:

$$G_{00}(k, k_0) = \frac{-\alpha^2}{(k^2 + a^2)(k_0^2 + a^2)} [1 - \frac{2}{\pi} I(k_0, K)]^{-1}$$

where

$$\begin{aligned} I(k_0, K) = & \frac{\alpha^2}{2K} [(K^2 - k_F^2) \{ p_1(k_F + K, a^2, b) - p_2(\sqrt{k_F^2 - K^2}, a^2, b) \} \\ & + p_3(k_F + K, a^2, b) - p_3(\sqrt{k_F^2 - K^2}, a^2, b)] + \alpha^2 [q(a^2, b) \\ & - p_2(k_F + K, a^2, b)] \end{aligned}$$

The function  $p_i(x, y, z)$  are given by

$$p_i(x, a^2, b) = \frac{1}{(b-a^2)} [f_{i2}(x, a^2) - \frac{1}{(b-a^2)} \{ f_{i1}(x, a^2) - f_{i1}(x, b) \}]$$

and

$$\begin{aligned} q(a^2, b) = & \frac{\pi}{2(b-a^2)} \left[ \frac{1}{2a} + \frac{a}{(b-a^2)} \right] \quad \text{if } b < 0 \\ = & \frac{\pi}{2(b-a^2)} \left[ \frac{1}{2a} + \frac{a-\sqrt{b}}{b-a^2} \right] \quad \text{if } b > 0 \end{aligned}$$

Finally, the functions  $f_{ij}(x, y)$  are given by the indefinite integrals

$$f_{ij}(x, y) = \int \frac{x^i dx}{(x^2 + y)^j} \quad :$$

$$\begin{aligned}
 f_{01}(x,y) &= \frac{1}{\sqrt{y}} \arctan \frac{x}{\sqrt{y}} \quad \text{if } y > 0 \\
 &= \frac{1}{2\sqrt{-y}} \ln \left| \frac{y+x\sqrt{-y}}{y-x\sqrt{-y}} \right| \quad \text{if } y < 0 \\
 &= \frac{1}{x} \quad \text{if } y = 0
 \end{aligned}$$

$$f_{02}(x,y) = \frac{x}{2y(x^2+y)} + \frac{1}{2y} f_{01}(x,y)$$

$$f_{11}(x,y) = \frac{1}{2} \ln(x^2+y)$$

$$f_{12}(x,y) = -\frac{1}{2(x^2+y)}$$

$$f_{21}(x,y) = x-y f_{01}(x,y)$$

$$f_{22}(x,y) = -\frac{x}{2(x^2+y)} + \frac{1}{2} f_{01}(x,y)$$

$$f_{31}(x,y) = \frac{1}{2} x^2 - y f_{11}(x,y)$$

$$f_{32}(x,y) = \frac{1}{2} \ln(x^2+y) - y f_{12}(x,y) = f_{11}(x,y) - y f_{12}(x,y) .$$

APPENDIX B2  
THE SINGLE PARTICLE SPECTRUM

According to the prescription of BBP, the best choice for  $\langle \mu | U | \mu \rangle$  is given by

$$\langle \mu | U | \mu \rangle = \sum_{\nu < A} \langle \mu \nu | G | \mu \nu - \nu \mu \rangle \quad \text{for } \mu < A \quad . \quad (\text{B2-1})$$

We substitute the relation (3-11) into (B2-1) and employ the relation

$$\sum_{\nu < A} \rightarrow \sum_{s_\nu t_\nu} \sum_{t_\nu = -\frac{1}{2}}^{\frac{1}{2}} \frac{(2\pi)^3}{\Omega} \int d^3 k_\nu \quad ,$$

along with the partial wave decomposition of  $G_{LL'}^\alpha(K; k_o, k_o)$ , to obtain

$$\begin{aligned} \langle \mu | U | \mu \rangle &= \frac{2\lambda}{\pi} \sum_{s_\nu t_\nu} \sum_{\substack{LL' \alpha \\ MT_3}} \int_{k_\nu < k_F} d^3 k_\nu \langle \omega_\mu \omega_\nu | G_{LL'}^\alpha(K; k_o, k_o) \tilde{y}_L^{OM}(\hat{k}_o) \\ &\quad [\tilde{y}_L^{OM+}(\hat{k}_o) | \omega_\nu \omega_\mu \rangle - \tilde{y}_L^{OM+}(-\hat{k}_o) | \omega_\nu \omega_\mu \rangle] \end{aligned} \quad (\text{B2-2})$$

where  $\lambda = \frac{\hbar^2}{M}$  and where we denote  $|\omega_\mu \rangle = |s_\mu t_\mu\rangle$ . The momenta  $\vec{K}$  and  $\vec{k}_o$  are the center-of-mass and relative momenta of a two particle state  $|\mu \nu \rangle$ . To simplify Eq. (B2-2) we note that, because of the exchange properties of the momentum, spin and isospin coordinates,

$$\begin{aligned} \tilde{y}_L^{OM+}(-\hat{k}_o) | \omega_\nu \omega_\mu \rangle &= \sum_{M_L M_S} \langle M_L M_S | C_{L'S} | JM \rangle Y_{L'M_L}^* (-\hat{k}_o) | S_M S \rangle \\ &\quad \langle S_M S | C_{\frac{1}{2}\frac{1}{2}} | s_\nu s_\mu \rangle \langle T T_3 | C_{\frac{1}{2}\frac{1}{2}} | t_\nu t_\mu \rangle | T T_3 \rangle \end{aligned}$$

$$\begin{aligned}
&= (-1)^{L'+S+T} \sum_{M_L M_S} \langle M'_L M_S | C_{L'S} | JM \rangle Y^*_{L'M'}(\hat{k}_o) | S M_S \rangle \\
&\quad \langle S M_S | C_{\frac{1}{2}\frac{1}{2}} | s_\mu s_\nu \rangle | TT_3 \rangle \langle TT_3 | C_{\frac{1}{2}\frac{1}{2}} | t_\mu t_\nu \rangle \\
&= (-1)^{L'+S+T} \tilde{y}_{L'}^{OM}(\hat{k}_o) | w_\mu w_\nu \rangle .
\end{aligned}$$

If the summation in  $L, L', \alpha$  is restricted to the allowed eigenstates of the two-body system, Eq. (B2-2) becomes

$$\begin{aligned}
\langle \mu | U | \mu \rangle &= \frac{4\lambda}{\pi} \sum_{s_\nu t_\nu} \sum_{LL' \alpha M T_3} \int d^3 k_\nu \langle w_\mu w_\nu | G_{LL'}^\alpha(K; k_o, k_o) \\
&\quad \tilde{y}_{L'}^{OM}(\hat{k}_o) \tilde{y}_{L'}^{OM+}(\hat{k}_o) | w_\mu w_\nu \rangle
\end{aligned} \tag{B2-3}$$

To eliminate the isospin indices in (B2-3), we use charge independence of  $G$  to expand (B2-3) to

$$\begin{aligned}
\langle \mu | U | \mu \rangle &= \frac{4\lambda}{\pi} \sum_{s_\nu} \sum_{LL' \alpha M T_3} \langle s_\mu s_\nu | \int d^3 k_\nu G_{LL'}^\alpha(K; k_o, k_o) \\
&\quad y_L^{OM}(\hat{k}_o) y_{L'}^{OM+}(\hat{k}_o) \sum_{t_\nu T_3} \langle t_\mu t_\nu | C_{\frac{1}{2}\frac{1}{2}} | TT_3 \rangle \langle TT_3 | C_{\frac{1}{2}\frac{1}{2}} | t_\mu t_\nu \rangle | s_\mu s_\nu \rangle
\end{aligned} \tag{B2-4}$$

One can easily verify the relation

$$\sum_{t_\nu T_3} |\langle t_\mu t_\nu | C_{\frac{1}{2}\frac{1}{2}} | TT_3 \rangle|^2 = \frac{(2T+1)}{2} ,$$

which reduces (B2-4) to

$$\langle \mu | U | \mu \rangle = \frac{2\lambda}{\pi} \sum_{s_\nu} \sum_{LL' \alpha M} (2T+1) \langle s_\mu s_\nu | \int d^3 k_\nu G_{LL'}^\alpha(K; k_o, k'_o) y_L^\alpha(k_o) y_{L'}^{\alpha M}(k_o) | s_\mu s_\nu \rangle . \quad (B2-5)$$

We expand (B2-5) in terms of Legendre functions and Clebsch-Gordan coefficients. The resulting expression becomes

$$\begin{aligned} \langle \mu | U | \mu \rangle &= \frac{2\lambda}{\pi} \sum_{LL' \alpha M} (2T+1) \int d^3 k_\nu G_{LL'}^\alpha(K; k_o, k'_o) \\ &\quad \sum_{M_L M_S} \langle JM | C_{LS} | M_L M_S \rangle \langle JM | C_{L'S} | M_L M_S \rangle Y_{LM_L}(k_o) Y_{LM_L}^*(k_o) \\ &\quad \langle S M_S | C_{\frac{1}{2}\frac{1}{2}} | s_\mu s_\nu \rangle \langle s_\mu s_\nu | C_{\frac{1}{2}\frac{1}{2}} | S M_S \rangle . \quad (B2-6) \end{aligned}$$

We can now employ the relations

$$\begin{aligned} \sum_{s_\nu} \langle S M_S | C_{\frac{1}{2}\frac{1}{2}} | s_\mu s_\nu \rangle \langle s_\mu s_\nu | C_{\frac{1}{2}\frac{1}{2}} | S M_S \rangle \\ = \sum_{s_\nu} \langle S -M_S | C_{\frac{1}{2}\frac{1}{2}} | -s_\mu s_\nu \rangle \langle -s_\mu s_\nu | C_{\frac{1}{2}\frac{1}{2}} | S -M_S \rangle , \end{aligned}$$

and  $\langle -M_L -M_S | C_{LS} | J -M \rangle = (-1)^{L+S-J} \langle M_L M_S | C_{LS} | JM \rangle$ , to rewrite (B2-6) as

$$\begin{aligned} \langle \mu | U | \mu \rangle &= \frac{\lambda}{\pi} \sum_{LL' \alpha M} (2T+1) \int d^3 k_\nu G_{LL'}^\alpha(K; k_o, k'_o) \sum_{M_L M_S} \langle JM | C_{LS} | M_L M_S \rangle \\ &\quad \langle JM | C_{L'S} | M_L M_S \rangle [ \langle S M_S | C_{\frac{1}{2}\frac{1}{2}} | s_\mu s_\nu \rangle \langle s_\mu s_\nu | C_{\frac{1}{2}\frac{1}{2}} | S M_S \rangle \\ &\quad Y_{LM_L}(k_o) Y_{LM_L}^*(k_o) + (-1)^{L+L'+2S-2J} \langle S M_S | C_{\frac{1}{2}\frac{1}{2}} | -s_\mu s_\nu \rangle \\ &\quad \langle -s_\mu s_\nu | C_{\frac{1}{2}\frac{1}{2}} | S M_S \rangle Y_{LM_L}(k_o) Y_{LM_L}^*(k_o) ] . \quad (B2-7) \end{aligned}$$

By conservation of parity  $(-1)^{L+L'+2S-2J} = 1$ . We also employ the relation

$$Y_L^{M_L}(\hat{k}_o) = (-1)^{M_L} Y_L^{M_L}(\hat{k}_o)$$

to re-express Eq. (B2-7) as

$$\begin{aligned} \langle \mu | U | \mu \rangle &= \frac{\lambda}{\pi} \sum_{LL' \alpha M} (2T+1) \int d^3 k_v G_{LL'}^\alpha(K; k_o, k_o) \sum_{M_L M_S} \sum_{s_\mu s_v} \langle S M_S | C_{\frac{1}{2}\frac{1}{2}} | s_\mu s_v \rangle \\ &\quad \langle s_\mu s_v | C_{\frac{1}{2}\frac{1}{2}} | S M_S \rangle \langle JM | C_{LS} | M_L M_S \rangle \langle M_L M_S | C_{L'S} | JM \rangle \\ &\quad Y_L^{M_L}(\hat{k}_o) Y_{L'}^{M_{L'}}(\hat{k}_o) . \end{aligned} \quad (B2-8)$$

The orthonormality of the Clebsch-Gordan coefficients reduces (B2-8) to

$$\begin{aligned} \langle \mu | U | \mu \rangle &= \frac{\lambda}{\pi} \sum_{LL' \alpha M} (2T+1) \sum_{M_L M_S} \langle JM | C_{LS} | M_L M_S \rangle \langle JM | C_{L'S} | M_L M_S \rangle \\ &\quad Y_L^{M_L}(\hat{k}_o) Y_{L'}^{M_{L'}}(\hat{k}_o) \int d^3 k_v G_{LL'}^\alpha(K; k_o, k_o) \end{aligned} \quad (B2-9)$$

Application of the relations

$$\sum_{MM_S} \langle M_L M_S | C_{LS} | JM \rangle \langle JM | C_{L'S} | M_L M_S \rangle = \frac{2J+1}{2L+1} \delta_{LL'}$$

and

$$\sum_{M_L} Y_{LM_L}(\hat{k}_o) Y_{LM_L}^*(\hat{k}_o) = \frac{2L+1}{4\pi} P_L(0) = \frac{2L+1}{4\pi}$$

reduces (B2-9) to

$$\langle \mu | U | \mu \rangle = U(k_\mu) = \frac{\lambda}{4\pi^2} \sum_{L\alpha} (2J+1)(2T+1) \int_{k_v < k_f} d^3 k_v G_{LL'}^\alpha(K; k_o, k_o) . \quad (B2-10)$$

We note that  $\langle \mu | U | \mu \rangle$  only depends on the magnitude of  $\vec{k}_\mu$ . All spin, isospin and directional dependence has vanished. This result is consistent with our assumption in Section III that  $U$  only depends on the magnitude of  $\vec{k}_\mu$ .

The integration in Eq. (B2-10) is over all  $k_v$  in the Fermi sea. We may change the integral over  $k_v$  to one over center of mass and relative coordinates by employing the relation

$$\int_{k_\mu = \text{const}} d^3 k_v = \frac{8}{k_\mu} \int k_o K dk dk_o d\varphi \quad (\text{B2-11})$$

where  $\varphi$  is the azimuthal angle between  $\vec{k}_\mu$  and  $\vec{k}_o$ . Equation (B2-11) may be derived from the Jacobian

$$J = \begin{vmatrix} \partial k_{vx}/\partial k_o & \partial k_{vx}/\partial K & \partial k_{vx}/\partial \varphi \\ \partial k_{vy}/\partial k_o & \partial k_{vy}/\partial K & \partial k_{vy}/\partial \varphi \\ \partial k_{vz}/\partial k_o & \partial k_{vz}/\partial K & \partial k_{vz}/\partial \varphi \end{vmatrix}$$

for

$$k_{vx} = k_{\mu x} - 2k_o \sin\theta \cos\varphi$$

$$k_{vy} = k_{\mu y} - 2k_o \sin\theta \sin\varphi$$

$$k_{vz} = k_{\mu z} - 2k_o \cos\theta$$

$$\text{where } \cos\theta = \vec{k}_\mu \cdot \vec{k}_o / k_\mu k_o = (-K^2 + k_\mu^2 + k_o^2) / 2k_o k_\mu .$$

Substitution of  $J$  into

$$\int_{k_\mu = \text{const}} d^3 k_v = \int J dk_o dk d\varphi$$

results in (B2-11). We may integrate over the angle  $\phi$  to reduce (B2-11) to

$$U(k_\mu) = \frac{4\lambda}{\pi k_\mu} \sum_{L\alpha} (2J+1)(2T+1) \int k_o K dk dk_o G_{LL}^\alpha(K_o, k_o, k_o) . \quad (B2-12)$$

We now have to consider limits of integration. From inspection of Figure 4, one may verify that the limits of integration are

$$|k_\mu - k_o| \leq K < k_\mu + k_o \quad \text{for} \quad k_o \leq (k_F - k_\mu)/2$$

$$\frac{k_F - k_\mu}{2} \leq K \leq \sqrt{\frac{k_F^2 + k_\mu^2}{2} - k_o^2} \quad \text{for} \quad \frac{(k_F - k_\mu)}{2} \leq k_o \leq \frac{(k_F + k_\mu)}{2} .$$

Therefore, the full expression for  $U(k_\mu)$  becomes

$$U(k_\mu) = \frac{4\lambda}{\pi k_\mu} \sum_{L\alpha} (2J+1)(2T+1) \left[ \int_0^{\frac{k_F - k_\mu}{2}} k_o dk_o \int_{|k_\mu - k_o|}^{k_\mu + k_o} K dk G_{LL}^\alpha(K; k_o, k_o) \right. \\ \left. + \int_{\frac{k_F - k_\mu}{2}}^{\frac{k_F + k_\mu}{2}} \int_{|k_\mu - k_o|}^{\sqrt{\frac{k_F^2 + k_\mu^2}{2} - k_o^2}} K dk G_{LL}^\alpha(K; k_o, k_o) \right] . \quad (B2-13)$$

APPENDIX B3  
TOTAL BINDING ENERGY OF NUCLEAR MATTER

The expression for the total binding energy for nuclear matter is given by

$$E = T + \frac{1}{2} \sum_{\mu\nu < A} \langle \mu\nu | G | \mu\nu - v\mu \rangle .$$

Employing the relation for the single-particle energies

$$\langle \mu | U | \mu \rangle = \sum_{v < A} \langle \mu v | G | \mu v - v\mu \rangle ,$$

we may rewrite the total energy as

$$\begin{aligned} E &= T + \frac{1}{2} \sum_{\mu < A} \langle \mu | U | \mu \rangle \\ &= T + \frac{1}{2} \frac{\Omega}{(2\pi)^3} \sum_{s_\mu t_\mu} \int d^3 k_\mu U(k_\mu) . \end{aligned} \quad (B3-1)$$

Applications of spin and charge independence of  $U(k_\mu)$  and (B2-10) yield

$$E = T + \frac{\lambda \Omega}{16\pi^5} \sum_{L\alpha} (2J+1)(2T+1) \int d^3 k_\mu d^3 k_\nu G_{LL}^\alpha(k; k_o, k_o) . \quad (B3-2)$$

We may replace  $\Omega$  in (B3-2) with

$$\Omega = \frac{A}{\rho} = \frac{3\pi^2}{2k_F^3} ,$$

which yields

$$E = T + \frac{3\lambda A}{32\pi^2 k_F^3} \sum_{L\alpha} (2J+1)(2T+1) \int d^3 k_\mu d^3 k_\nu G_{LL}^\alpha(K; k_o, k_o) . \quad (B3-3)$$

We can rewrite (B3-3) in center of mass and relative coordinates as

$$E = T + \frac{3}{4} \frac{\lambda}{\pi^3} \frac{A}{k_F^3} \sum_{L\alpha} (2J+1)(2T+1) \int_{k_\mu, k_\nu < k_F} d^3 k_o d^3 K G_{LL}^\alpha(K; k_o, k_o) . \quad (B3-4)$$

Equation (B3-4) follows from (B3-3) and

$$\int d^3 k_\mu d^3 k_\nu = 8 \int d^3 k_o d^3 K . \quad (B3-5)$$

The angular domain of integration must be such that

$$k_\mu^2 = K^2 + k_o^2 + 2k_o K \cos \theta_{\vec{k}_o \vec{K}} < k_F^2$$

and

$$k_\nu^2 = K^2 + k_o^2 - 2k_o K \cos \theta_{\vec{k}_o \vec{K}} < k_F^2 ,$$

which implies

$$|\cos \theta_{\vec{k}_o \vec{K}}| \leq \frac{k_F^2 - K^2 - k_o^2}{2Kk_o} .$$

Therefore,

$$\begin{aligned} -1 &\leq \cos \theta_{\vec{k}_o \vec{K}} \leq 1 \text{ for } K < k_F - k_o \\ -\left(\frac{k_F^2 - K^2 - k_o^2}{2Kk_o}\right) &\leq \cos \theta_{\vec{k}_o \vec{K}} \leq \frac{k_F^2 - K^2 - k_o^2}{2Kk_o} \text{ for } k_F - k_o \leq K \leq \sqrt{k_F^2 - k_o^2} . \end{aligned} \quad (B3-6)$$

One may obtain the limits on  $K$  and  $k_o$  by inspection of Figure 6.

These limits are

$$\begin{aligned} 0 &\leq k_o \leq k_F \\ 0 &\leq K \leq \sqrt{k_F^2 - k_o^2} \end{aligned} \quad (B3-7)$$

Substitution of the limits (B3-6) and (B3-7) yields the expression for the total binding energy

$$\begin{aligned} E = T + \frac{3 \lambda A}{\pi^2 k_F^3} \sum_{L\alpha} (2J+1)(2T+1) \left[ 4\pi \int_0^{k_F} k_o^2 dk_o \int_0^{k_F - k_o} k^2 dk G_{LL}^\alpha(K; k_o, k_o) \right. \\ \left. + 2\pi \int_0^{k_F} k_o^2 dk_o \int_{k_F - k_o}^{\sqrt{k_F^2 - k_o^2}} \frac{(k_F^2 - K^2 - k_o^2)^2}{K k_o} G_{LL}^\alpha(K; k_o, k_o) \right]. \quad (B3-8) \end{aligned}$$

APPENDIX C1  
MATRIX ELEMENTS FOR GAUSSIAN POTENTIALS

For the potential terms in Section IVB the matrix elements  $v_{LL'}^{\alpha}(k, k')$  are given by

$$v_{LL'}^{\alpha}(k, k') = U_{LL'}^{\alpha}(k, k') A_{LL'}^{JS} .$$

For the local central, spin-orbit, and tensor terms

$$U_{LL'}^{\alpha}(k, k') = \int_0^{\infty} r^2 dr j_L(kr) v_1(r) j_{L'}(k'r)$$

and

$$\begin{aligned} A_{LL'}^{JS} &= \langle y_L^{\alpha} | y_{L'}^{\alpha} \rangle = \delta_{LL'} \quad \text{for the central term ,} \\ &= \langle y_L^{\alpha} | \vec{L} \cdot \vec{S} | y_{L'}^{\alpha} \rangle = \frac{J(J+1)-L(L+1)-S(S+1)}{2} \delta_{LL'} \end{aligned}$$

for the spin orbit term. For the tensor force

$$\begin{aligned} A_{LL'}^{JS} &= \langle y_L^{\alpha} | S_{12} | y_{L'}^{\alpha} \rangle , \quad \text{or} \\ A_{LL'}^{JS} &= 0 \quad \text{if } S = 0 \\ &= 2 \quad \text{if } S = 1, L = L' = J \\ &= \frac{-2(J-1)}{2J+1} \quad \text{if } S = 1, L = L' = J - 1 \\ &= \frac{-2(J+2)}{2J+1} \quad \text{if } S = 1, L = L' = J + 1 \\ &= \frac{6\sqrt{J(J+1)}}{2J+1} \quad \text{if } S = 1, L = J - 1, L' = J + 1 \quad \text{or} \\ &\quad L = J + 1, L' = J - 1 . \end{aligned}$$

For the velocity dependent terms,  $V_P$  and  $V_{TPP}$ , the matrix elements become:

$$V_{LL}^{\alpha}(k, k') = \frac{1}{2}[C(\hbar^2 k^2) + C(\hbar^2 k'^2)]U_{LL}^{\alpha}(k, k')A_{LL}^{JS},$$

where  $A_{LL}^{JS}$  and  $U_{LL}^{\alpha}$  are defined as before.

For the  $V_{TPP}$  force

$$V_{TPP} = \frac{1}{2}[V(r)S_{12}(\hat{p})C(p^2) + C(p^2)S_{12}(\hat{p})V(r)] \quad (Cl-1)$$

We first consider the first term in the brackets. We consider

$$V(\vec{k}, \vec{k}') = \langle \vec{k}|V(r)S_{12}(\hat{p})C(p^2)|\vec{k}' \rangle .$$

Since  $|k'\rangle$  is an eigenvector of  $\hat{p}$ ,

$$\begin{aligned} V(\vec{k}, \vec{k}') &= C(\hbar^2 k'^2) \langle \vec{k}|V(r)|\vec{k}' \rangle S_{12}(\vec{k}') \\ &= C(\hbar^2 k'^2) S_{12}(\vec{k}') \left( \frac{2}{\pi} \right) \frac{\hbar^2}{M} \sum_{LM} U_{LL}^{\alpha}(k, k') Y_L^{LM}(\vec{k}) Y_L^{+LM}(k') \end{aligned} \quad (Cl-2)$$

since  $V(r)$  alone is a central force. To evaluate  $S_{12}(k') Y_L^{+LM}(k')$ , we can rewrite this term as

$$S_{12}(k') Y_L^{+LM}(k') = \sum_{L'} \langle y_L^{\alpha}|S_{12}|y_{L'}^{\alpha} \rangle Y_L^{+LM}(k') .$$

Therefore

$$\begin{aligned} V(\vec{k}, \vec{k}') &= C(\hbar^2 k'^2) \left( \frac{2}{\pi} \right) \frac{\hbar^2}{M} \sum_{LL', LM} \langle y_L^{\alpha}|S_{12}|y_{L'}^{\alpha} \rangle \\ &\quad U_{LL}^{\alpha}(k, k') Y_L^{LM}(\vec{k}) Y_L^{+LM}(k') . \end{aligned}$$

If we include the Hermitian conjugate term,

$$v(\vec{k}, \vec{k}') = \frac{2}{\pi} \frac{\hbar^2}{M} \sum_{LL', \alpha M} \langle y_L^\alpha | s_{12} | y_{L'}^\alpha \rangle y_L^{\alpha M}(\vec{k}) y_{L'}^{\alpha M}(\vec{k}')$$

$$\frac{1}{2} [C(\hbar^2 k'^2) U_{LL'}^{xx}(k, k') + C(\hbar^2 k^2) U_{L'L'}^{xx}(k, k')] .$$

We may identify

$$v_{LL'}^{xx}(k, k') = \frac{1}{2} i^{(L-L')} [C(\hbar^2 k'^2) U_{LL'}^{xx}(k, k') + C(\hbar^2 k^2) U_{L'L'}^{xx}(k, k')] A_{LL'}^{JS} \quad (Cl-3)$$

where  $A_{LL'}^{JS}$  is defined previously for a tensor force. The  $s_{12}(\vec{p})$  force is the only force we consider for which  $v_{LL'}^{xx}(k, k')$  is not proportional to  $U_{LL'}^{xx}(k, k')$  for  $L \neq L'$ .

#### Forms for $U_{LL'}^{xx}(k, k')$ for Gaussians

For all terms except the tensor terms, the radial forms we have chosen are  $v_i(r) = v_i e^{-a_i^2 r^2}$ . The radial integral we must evaluate is

$$U_{LL'}^{xx}(k, k') \propto \int_0^\infty r^2 dr j_L(kr) e^{-a_i^2 r^2} j_{L'}^{(1)}(k' r) \equiv I_{LL'}^{(1)}(k, k') . \quad (Cl-4)$$

This integral is given analytically in reference<sup>95</sup> as

$$I_{LL'}^{(1)}(k, k') = \frac{\sqrt{\pi}}{4a^3} e^{-(k^2+k'^2)/4a^2} i_L\left(\frac{kk'}{2a^2}\right) , \quad (Cl-5)$$

where  $i_L(z)$  is a modified spherical Bessel function of the first kind.

For  $L = 0, 1, 2$  these functions are given by

$$i_0(z) = \sinh z / z$$

$$i_1(z) = -\sinh z / z^2 + \cosh z / z$$

$$i_2(z) = (3/z^2 + 1/z)\sinh z - 3/z^2 \cosh z .$$

In programming, we employed the recursion relation

$$i_{L+1}(z) = i_{L-1}(z) - (2L+1)i_L(z)/z \quad (Cl-6)$$

to obtain  $i_{L+1}(z)$  for  $L \geq 2$ .

Because the  $V_{TPP}$  term involves  $U_{LL}$  for  $r^2 x$  Gaussian, we also had to evaluate

$$I_{LL}^{(2)}(k, k') = \int r^2 dr J_L(kr) r^2 e^{-a^2 r^2} J_L(k'r) . \quad (Cl-7)$$

One may evaluate this integral by noting from Equation (Cl-4)

that

$$I_{LL}^{(2)}(k, k') = -\frac{\partial}{\partial a^2} I_{LL}^{(1)}(k, k') .$$

Therefore, we can differentiate (Cl-5) to obtain

$$I_{LL}^{(2)}(k, k') = \frac{\sqrt{\pi}}{8a^5} e^{-(k^2+k'^2)} \left[ \left( 3 - \frac{k^2+k'^2}{2a^2} \right) i_L\left(\frac{kk'}{2a^2}\right) - \frac{kk'}{a^2} i'_L\left(\frac{kk'}{2a^2}\right) \right] \quad (Cl-8)$$

where  $i'_L(z) = \frac{d}{dz} i_L(z)$  and  $z = kk'/2a^2$ . Again, for  $L \geq 2$  we obtained  $i'_{L+1}(z)$  by differentiating the recursion relation (Cl-6).

The remaining integral for us to evaluate is

$$I_{L, L+2}^{(2)}(k, k') = \int_0^\infty r^2 dr J_L(kr) r^2 e^{-a^2 r^2} J_{L+2}(k'r) . \quad (Cl-9)$$

To evaluate  $I_{L,L+2}^{(2)}(k,k')$  we apply the recursion relation

$$j_{L+1}(y) = \frac{L}{y} j_L(y) - \frac{d}{dy} j_L(y)$$

twice to obtain

$$j_{L+2}(y) = \left[ \frac{L(L+2)}{y^2} - \frac{(2L+1)}{y} \frac{d}{dy} + \frac{d^2}{dy^2} \right] j_L(y) . \quad (Cl-10)$$

We then set  $y = k'r$  to rewrite (Cl-10) as

$$j_{L+2}(k'r) = \left[ \frac{L(L+2)}{k'^2 r^2} - \frac{(2L+1)}{k'^2 r^2} \frac{\partial}{\partial k'} + \frac{1}{r^2} \frac{\partial^2}{\partial k'^2} \right] j_L(k'r) .$$

Equation (Cl-9) thus reduces to

$$I_{L,L+2}^{(2)}(k,k') = \left[ \frac{L(L+2)}{k'^2} - \frac{(2L+1)}{k'} \frac{d}{dk'} + \frac{d^2}{dk'^2} \right] I_{L,L}^{(1)}(k,k') . \quad (Cl-11)$$

With the relation  $\frac{d}{dk'} = \frac{1}{2} \frac{k'}{a^2} \frac{d}{dz}$ , differentiation of (Cl-5) reduces (Cl-11) to

$$\begin{aligned} I_{L,L+2}^{(2)}(k,k') &= \frac{\sqrt{\pi}}{4a^3} e^{-(k^2+k'^2)/4a^2} \left[ \left( \frac{L(L+2)}{k'^2} + \frac{L}{a^2} + \frac{k'^2}{4a^4} \right) i_L(z) \right. \\ &\quad \left. - \left( \frac{[2L+1]k}{2k'a^2} + \frac{kk'}{2a^4} \right) i'_L(z) + \frac{k^2}{4a^4} i''_L(z) \right] , \end{aligned} \quad (Cl-12)$$

where again  $i'_L(z) = \frac{d}{dz} i_L(z)$  and  $z = kk'/2a^2$ . We employ the differential equation

$$z^2 i_L''(z) + 2zi_L'(z) - [z^2 + L(L+1)] i_L(z) = 0$$

to evaluate  $i_L''(z)$ .

Equations (C1-5), (C1-8), and (C1-12) provide analytic forms for the radial integrals necessary to evaluate the matrix elements of the potential model in Section IV. With these analytic forms, the matrix elements are evaluated very rapidly on modern computers.

## APPENDIX C2

### EVALUATION OF THE RADIAL INTEGRALS NECESSARY FOR THE REID AND BRYAN-SCOTT POTENTIALS

The radial integrals necessary to evaluate the matrix elements of the Reid and Bryan-Scott potentials are of the following three types:

$$I_{LL'}^{(1)}(k, k') = \int_0^{\infty} r^2 dr j_L(kr) \frac{e^{-mr}}{r} j_{L'}(k'r) \quad (C2-1)$$

$$I_{LL'}^{(2)}(k, k') = \int_0^{\infty} r^2 dr j_L(kr) \left( \frac{m}{r} + \frac{1}{r^2} \right) \frac{e^{-mr}}{r} j_{L'}(k'r) \quad (C2-2)$$

and

$$I_{LL'}^{(3)}(k, k') = \int_0^{\infty} r^2 dr j_L(kr) \left( m^2 + \frac{3m}{r} + \frac{3}{r^2} \right) \frac{e^{-mr}}{r} j_{L'}(k'r). \quad (C2-3)$$

For a given  $L, L'$ ,  $k, k'$  only two of the  $I_{LL'}^{(1)}(k, k')$  are linearly independent.

The integral  $I_{LL'}^{(1)}(k, k')$  is simply given by<sup>96</sup>

$$I_{LL'}^{(1)}(k, k') = \frac{1}{2kk'} Q_L(z) \quad (C2-4)$$

where  $z = \frac{k^2 + k'^2 + m^2}{2kk'}$  and  $Q_L(z)$  is a Legendre function of the second kind. For  $L \leq 2$ ,  $Q_L(z)$  is given by

$$Q_0(z) = \frac{1}{2} \ln \left( \frac{z+1}{z-1} \right)$$

$$Q_1(z) = \frac{z}{2} \ln \left( \frac{z+1}{z-1} \right) - 1$$

$$Q_2(z) = \left( \frac{3z^2-1}{4} \right) \ln \left( \frac{z+1}{z-1} \right) - \frac{3z}{2} .$$

For  $L > 2$  we used the recursion relation

$$(L+1)Q_{L+1}(z) = (2L+1)z Q_L(z) - LQ_{L-1}(z) . \quad (C2-5)$$

To evaluate  $I_{LL}^{(2)}(k, k')$ , we apply the relation

$$-\left(\frac{m}{r} + \frac{1}{r^2}\right) \frac{e^{-mr}}{r} = \frac{1}{r} \frac{d}{dr} \frac{e^{-mr}}{r} \quad \text{to (C2-2).}$$

We then integrate by parts, employ various recursion relations between the spherical Bessel functions, and obtain

$$I_{LL}^{(2)}(k, k') = \frac{1}{2(2L+1)} (Q_{L+1}(z) - Q_{L-1}(z)) .$$

By a similar procedure, we employ the fact that

$$\left(m^2 + \frac{3m}{r} + \frac{3}{r^2}\right) \frac{e^{-mr}}{r} = r \frac{d}{dr} \frac{1}{r} \frac{d}{dr} \frac{e^{-mr}}{r}$$

to derive

$$I_{LL+2}^{(3)}(k, k') = \frac{k'^2 Q_{L+2}(z) + k^2 Q_L(z)}{2kk'} - Q_{L+1}(z) .$$

To evaluate  $I_{LL+2}^{(1)}(k, k')$ , we use the result in reference<sup>97</sup> that

$$I_{02}^{(1)}(k, k') = \frac{1}{4kk'3} \left[ 6kk' + \frac{1}{2}(3m^2 + k^2 - 3k'^2) \ln\left(\frac{z+1}{z-1}\right) + 6mk' \left( \text{Arc tan } \frac{m}{k+k'} - \text{Arc tan } \frac{m}{k-k'} \right) \right]. \quad (C2-6)$$

We then apply the recursion relations

$$\frac{kr}{2L+3} [j_{L+2}(kr) + j_L(kr)] = j_{L+1}(kr)$$

and

$$\frac{k'r}{2L+5} [j_{L+1}(k'r) + j_{L+3}(k'r)] = j_{L+2}(k'r)$$

to the integral

$$\int_0^\infty r dr j_{L+1}(kr) \frac{e^{-mr}}{r} j_{L+2}(k'r)$$

to obtain the relation

$$\begin{aligned} \frac{k}{2L+3} (I_{LL+2}^{(1)}(k, k') + I_{L+2, L+2}^{(1)}(k, k')) \\ = \frac{k'}{2L+5} (I_{L+1, L+1}^{(1)}(k, k') + I_{L+1, L+3}^{(1)}(k, k')). \end{aligned}$$

We thus get the recursion relation

$$I_{L+1, L+3}^{(1)} = \left( \frac{2L+5}{2L+3} \right) \frac{k}{k'} \left( I_{LL+2}^{(1)}(k, k') + \frac{Q_{L+2}(z)}{2kk'} \right) - \frac{Q_{L+1}(z)}{2kk'} . \quad (C2-7)$$

Since  $I_{02}^{(1)}(k, k')$  is known, we can determine  $I_{13}^{(1)}(k, k')$ , etc. Now that  $I_{LL}^{(1)}(k, k')$ ,  $I_{LL}^{(2)}(k, k')$ ,  $I_{LL+2}^{(1)}(k, k')$  and  $I_{LL+2}^{(3)}(k, k')$  are known, we may obtain  $I_{LL}^{(3)}(k, k')$  and  $I_{LL+2}^{(2)}(k, k')$  by linear combinations of the known integrals.

APPENDIX D1  
 CANCELLATION OF CERTAIN OPEP CONTRIBUTIONS  
 IN THE REID SOFT-CORE POTENTIAL

We consider the cancellation of the potential energy contributions for certain pairs of states in the Reid soft core potential. These pairs of states are characterized by  $V = V_{OPEP}$  and have quantum numbers

$$S = 1, L = \ell, J = \ell + 1 \text{ and } T = 0(1)$$

for one state and

$$S = 1, L = \ell + 1, J = \ell \text{ and } T = 1(0)$$

for the other. The contribution  $U_L^\sigma(k_o)$  to the ground-state binding energy from the momentum  $k_o$  in the state  $L\sigma$  is proportional to, in the Hartree-Fock approximation,

$$U_L^\sigma(k_o) \propto (2J+1)(2T+1) v_{LL}^{\sigma OPEP}(k_o, k_o) \quad (D1-1)$$

where

$$v_{OPEP} = v_\pi \vec{\tau}_1 \cdot \vec{\tau}_2 \left[ \vec{\sigma}_1 \cdot \vec{\sigma}_2 + s_{12}(\hat{r}) \left( 1 + \frac{3}{mr} + \frac{3}{m^2 r^2} \right) \right] \frac{e^{-mr}}{mr} \quad . \quad (D1-2)$$

Since  $\vec{\tau}_1 \cdot \vec{\tau}_2$  has eigenvalues -3 for  $T = 0$  and 1 for  $T = 1$ , we note that  $(2T+1)\vec{\tau}_1 \cdot \vec{\tau}_2$  are equal in magnitude but opposite in sign for the two states involved. We drop these factors, as well as the constant factor  $v_\pi$ . For cancellation to occur, the contributions to the expression

$$v_{LL}^{\sigma OPEP}(k_o, k_o)$$

where

$$v = (2J+1) \left[ \vec{\sigma}_1 \cdot \vec{\sigma}_2 + S_{12}(\hat{r}) \left( 1 + \frac{3}{mr} - \frac{3}{m^2 r^2} \right) \right] \frac{e^{-mr}}{mr}$$

for the two states involved must be equal. We first consider the state where  $S = 1$ ,  $L = \ell$ ,  $J = \ell + 1$ . First, for  $S = 1$ ,  $\vec{\sigma}_1 \cdot \vec{\sigma}_2$  has an eigenvalue of +1. We further employ the relations

$$\int_0^\infty r^2 dr j_L(kr) \frac{e^{-mr}}{r} j_L(k'r) = \frac{1}{2kk'} Q_L(z) \quad (D1-3)$$

and

$$\begin{aligned} & \int_0^\infty r^2 dr j_L(kr) \left( m^2 + \frac{3m}{r} + \frac{3}{r^2} \right) \frac{e^{-mr}}{r} j_L(k'r) \\ &= -\frac{3}{2(2L+1)} [Q_{L+1}^{(z)} - Q_{L-1}^{(z)}] + \frac{m^2 Q_L}{2kk'} \end{aligned} \quad (D1-4)$$

where

$$z = \frac{k' + k^2 + m^2}{2kk'}$$

and  $Q_L(z)$  is a Legendre function of the second kind.

First, we evaluate  $v_{LL}^\alpha(k_o, k_o)$  for the state where  $S = 1$ ,  $L = \ell$ , and  $J = \ell + 1$ . The result is

$$v_{\ell\ell}^\alpha(k_o, k_o) = (2\ell+1) \left[ \left( 1 - \frac{2\ell}{2\ell+3} \right) \frac{Q_\ell}{2k_o^2} + \frac{3\ell Q_{\ell+1}}{(2\ell+1)(2\ell+3)m^2} - \frac{3\ell Q_{\ell-1}}{m^2(2\ell+1)(2\ell+3)} \right]. \quad (D1-5)$$

We have made use of the relation

$$\begin{aligned} \langle y_{LS}^{JM} | S_{12} | y_{LS}^{JM} \rangle &= \frac{-2(J-1)}{2J+1} \quad \text{for } L = J - 1 \\ &= \frac{-2(J+2)}{2J+1} \quad \text{for } L = J + 1 . \end{aligned}$$

Now (Dl-5) may be rewritten

$$v_{ll}^{\alpha}(k_o, k_o) = \frac{-3l}{(2l+1)m^2} Q_{l-1} + \frac{3}{2k_o^2} Q_l + \frac{3l}{(2l+1)m^2} Q_{l+1} . \quad (\text{Dl-6})$$

Application of the recursion relation

$$(L+1)Q_{L+1}(z) = (2L+1)z Q_L(z) - LQ_{L-1}(z) \quad (\text{Dl-7})$$

reduces Eq. (Dl-6) to

$$v_{ll}^{\alpha}(k_o, k_o) = \left( \frac{3}{2k_o^2} - \frac{3z}{m^2} \right) Q_l(z) + \frac{3}{m^2} Q_{l+1}(z) . \quad (\text{Dl-8})$$

Because  $z = \frac{2k_o^2 + m^2}{2}$ , we can rewrite (Dl-8) as

$$v_{ll}^{\alpha}(k_o, k_o) = \frac{3}{m^2} [Q_{l+1}(z) - Q_l(z)] . \quad (\text{Dl-9})$$

Employing the same procedure for the  $S = 1$ ,  $L = l + 1$ ,  $J = l$  state, we obtain

$$v_{ll}^{\alpha}(k_o, k_o) = - \frac{3(l+2)}{(2l+3)m^2} Q_l - \frac{3}{2k_o^2} Q_{l+1} + \frac{3(l+2)}{(2l+3)m^2} Q_{l+2} . \quad (\text{Dl-10})$$

The recursion relation (Dl-7) enables us to express  $Q_{l+2}(z)$  in terms of  $Q_l$  and  $Q_{l+1}$ . The resulting expression for  $v_{ll}^{\alpha}(k_o, k_o)$  becomes

$$v_{ll}^{\alpha}(k_o, k_o) = - \frac{3}{m^2} Q_l - \left( \frac{3}{2k_o^2} - \frac{3z}{m^2} \right) Q_{l+1} ,$$

which can be rewritten

$$v_{LL}^{\alpha}(k_0, k_0) = \frac{3}{m^2} [Q_{\ell+1}(z) - Q_{\ell}(z)] . \quad (\text{D1-11})$$

By Equations (D1-9) and (D1-11), the quantities  $v_{LL}^{\alpha}(k_0, k_0)$  are equal for the  $S = 1, L = \ell, J = \ell + 1$  and  $T = 0(1)$  and  $S = 1, L = \ell + 1, J = \ell$  and  $T = 1(0)$  states. Their contributions to  $v_{LL}^{\alpha \text{ OPEP}}(k_0, k_0)$  are equal and opposite because of the  $(2T+1)\vec{\tau}_1 \cdot \vec{\tau}_2$  factor. This property accounts for the cancellation of the  ${}^3G_5 - {}^3H_4$ ,  ${}^3H_6 - {}^3I_5$ , and  ${}^3I_7 - {}^3J_6$  potential energies for the OPEP part of the Reid potential, and for the near cancellation of the  ${}^3F_4 - {}^3G_3$  pair.

APPENDIX D2  
ELIMINATION OF ANGULAR DEPENDENCE IN THE  
ALTERED SINGLE PARTICLE SPECTRUM

We consider the particle spectrum

$$E(k_\mu) = A + B k_\mu^2 \quad \text{for } k_F < k_\mu \leq 2k_F$$

$$= \frac{\lambda}{2} k_\mu^2 \quad \text{for } k_\mu > 2k_F \text{ where } \lambda = \frac{\hbar^2}{2M} .$$

We then consider two particles with momenta  $\vec{k}_\mu$  and  $\vec{k}_v$  where both  $k_\mu, k_v > k_F$ . We define the usual center-of-mass and relative coordinates and write  $E(k_\mu)$  and  $E(k_v)$  as

$$E(k_\mu) = A + B(\vec{k} + \vec{k}')^2 \quad \text{for } k_F < k_\mu \leq 2k_F$$

$$= \frac{\lambda}{2} (\vec{k} + \vec{k}')^2 \quad \text{for } k_\mu > 2k_F$$

$$E(k_v) = A + B(\vec{k} - \vec{k}')^2 \quad \text{for } k_F < k_v \leq 2k_F$$

$$= \frac{\lambda}{2} (\vec{k} - \vec{k}')^2 \quad \text{for } k_v > 2k_F .$$

In the energy denominators, the summation  $E(k_\mu) + E(k_v)$  appears. If both  $k_\mu$  and  $k_v$  are between  $k_F$  and  $2k_F$ , we may write the sum as

$$E(k_\mu) + E(k_v) = 2A + 2B(k^2 + k'^2) = E^>(k', k),$$

If both  $k_\mu, k_v > 2k_F$

$$E(k_\mu) + E(k_v) = \lambda(k^2 + k'^2) = E^>(k', k) . \quad (D2-1)$$

In both of these cases the sum  $E(k_\mu) + E(k_\nu)$  does not depend on the angle between  $\vec{k}$  and  $\vec{k}'$ . However, in the case that

$$k_F < k_\mu \leq 2k_F$$

$$k_\nu > 2k_F$$

the sum becomes

$$E(k_\mu) + E(k_\nu) = A + \frac{\lambda}{2} + (B + \frac{\lambda}{2})(K^2 + k'^2) + (B - \frac{\lambda}{2})Kk' \cos\theta_{\vec{k}\vec{k}'} . \quad (D2-2)$$

We may pursue two alternatives at this point to eliminate the angular dependence in (D-2). One alternative is to angle average  $E(k_\mu) + E(k_\nu)$  for a given  $K, k'$ . This procedure is similar to that of the angle average approximation of  $Q$ . A second alternative is to merely assume that both  $k_\mu$  and  $k_\nu$  are between  $k_F$  and  $2k_F$  or both are above  $2k_F$ . In terms of center of mass and relative momenta, the necessary conditions for both momenta to be between  $k_F$  and  $2k_F$  becomes

$$k_F^2 < K^2 + k'^2 \leq 4k_F^2 ;$$

for both  $k_\mu, k_\nu > 2k_F$ , the necessary condition becomes

$$K^2 + k'^2 \geq 4k_F^2.$$

Our assumption that either both  $k_\mu, k_\nu$  are between  $k_F$  and  $2k_F$ , or both are above  $2k_F$  implies that

$$\begin{aligned} E(k_\mu) + E(k_\nu) &\approx E^>(k, k') = 2A + 2B(K^2 + k'^2) \text{ for } K^2 + k'^2 < 4k_F^2 \\ &= \lambda(K^2 + k'^2) \quad \text{for } K^2 + k'^2 > 4k_F^2 . \quad (D2-3) \end{aligned}$$

To be sure, there are cases where either  $k^2 + k'^2 > 4k_F^2$  or  $k^2 + k'^2 < 4k_F^2$ , and  $k_F < k_\mu \leq 2k_F$  and  $k_\nu > 2k_F$ . We ignore these cases with the argument that the exact sum  $E(k_\mu) + E(k_\nu)$  is sometimes less than  $E^>(k, k')$  as defined in (D2-3), and sometimes it is more. On the average, however, (D2-3) should be a good approximation to  $E(k_\mu) + E(k_\nu)$  because the cases where (D2-3) underestimates the true sum should roughly cancel the cases where (D2-3) overestimates the true sum. The approximation (D2-3) is the one we employ because it is simpler than the angle average procedure.

## REFERENCES

1. R. A. Bryan and B. L. Scott, Phys. Rev. 135, B434 (1964).
2. R. A. Bryan and B. L. Scott, Phys. Rev. 164, 1215 (1967).
3. R. A. Bryan and B. L. Scott, Phys. Rev. 177, 1435 (1969).
4. A. E. S. Green and R. D. Sharma, Phys. Rev. Letters 14, 380 (1965).
5. A. E. S. Green and T. Sawada, Rev. Mod. Phys. 39, 594 (1967).
6. L. Ingber, Ph.D. Thesis, University of California, San Diego (1967).
7. A. M. Green, Nucl. Phys. 33, 218 (1962).
8. M. Razavy, G. Field, and J. S. Levinger, Phys. Rev. 125, 269 (1962).
9. We often refer to the terms "local", "non-local", "static", and "velocity-dependent" potentials. Local potentials can be expressed as  $V = V(\vec{r})$ , while non-local potentials cannot be so expressed. Static potentials may have linear momentum dependence, i.e.  $\vec{L} \cdot \vec{S}$  forces; therefore, strictly speaking, static potentials may not be local. Velocity dependent potentials have at least quadratic momentum dependence. We often refer to non-local and velocity-dependent potentials interchangeably. Likewise, we often refer to static and local potentials interchangeably. Potentials that have different static forms in each eigenchannel, like the Reid potentials, we classify as static.
10. K. A. Brueckner, C. A. Levinson, and H. M. Mahmoud, Phys. Rev. 95, 217 (1954); K. A. Brueckner, Phys. Rev. 97, 1353 (1955).
11. K. A. Brueckner and J. L. Gammel, Phys. Rev. 109, 1023 (1958).
12. K. A. Brueckner and K. S. Masterson, Jr., Phys. Rev. 128, 2267 (1962).
13. H. Kummel, J. H. E. Mattauch, W. Thiele and A. H. Wapstra, Nucl. Phys. 81, 129 (1966). Also see Reference 30 for other references. All

## References continued

- references mentioned in reference 30 give values close to -16 MeV per particle.
14. B. H. Brandow, Ph.D. thesis, Cornell University (1964). Reference 30 also gives other references. Sprung,in reference 30,concludes that the correct Fermi momentum is  $1.35 \pm .1F^{-1}$ .
  15. J. Da Providencia, Nucl. Phys. 40, 321 (1963).
  16. F. Tabakin, Ann. Phys. (N.Y.) 30, 51 (1964).
  17. R. Jastrow, Phys. Rev. 81, 165 (1951).
  18. J. L. Gammel, R. S. Christian and R. M. Thaler, Phys. Rev. 105, 311 (1957).
  19. J. L. Gammel and R. M. Thaler, Prog. Elem. Particle and Cosmic Ray Phys. 5, 99 (1960); J. L. Gammel and R. M. Thaler, Phys. Rev. 107, 291 and 1337 (1958).
  20. A. K. Kerman, J. P. Svenne and F. M. H. Villars, Phys. Rev. 147, 710 (1966).
  21. W. H. Bassichis, A. K. Kerman and J. P. Svenne, Phys. Rev. 160, 746 (1967).
  22. A. K. Kerman and M. K. Pal, Phys. Rev. 162, 970 (1967).
  23. C. W. Lee and E. Baranger, Nucl. Phys. 79, 385 (1966); D. M. Clement and E. Baranger, Nucl. Phys. 81, 241 (1966); D. M. Clement, Ph.D. thesis, University of Pittsburgh (1967).
  24. D. M. Clement, F. J. D. Serduke and I. R. Afnan, C.N.L. Internal Report, Theoretical 111 (1969) (unpublished).
  25. K. E. Lassila, M. H. Hull, Jr., H. M. Ruppel, F. A. McDonald and G. Breit, Phys. Rev. 126, 881 (1962).

## References continued

26. T. Hamada and I. D. Johnston, Nucl. Phys. 34, 382 (1962).
27. R. V. Reid, Ph.D. thesis, Cornell University (1968).
28. M. Razavy, Phys. Rev. 130, 1091 (1963).
29. C. N. Bressel, Ph.D. thesis, M.I.T. (1965);  
 C. Bressel, A. Kerman and L. Lamon, Bull. Am. Phys. Soc. 10, 584  
 (1965);  
 C. Bressel, A. Kerman and B. Rouben, to be published in Nucl. Phys.
30. D. W. Sprung, paper delivered at the International Conference on  
 Atomic Masses, Winnipeg (1967).
31. A. Kallio and B. D. Day, Nucl. Phys. A124, 177 (1969).
32. F. Tabakin and K. T. R. Davies, Phys. Rev. 150, 793 (1966).
33. A. Scotti and D. Wong, Phys. Rev. 138, B145 (1965).
34. R. S. McKean, Jr., Phys. Rev. 125, 1399 (1962).
35. N. Hoshizaki, S. Otsuki, S. Sawada, T. Ueda, W. Watari and M.  
 Yonezawa, Progr. Theoret. Phys. (Kyoto) 32, 380 (1964).
36. B. H. Brandow, Phys. Rev. 152, 863 (1966).
37. F. Coester, private communication. Also see:  
 H. Ekstein, Phys. Rev. 117, 1590 (1960) and  
 G. A. Baker, Jr., Phys. Rev. 128, 1485 (1962).
38. S. Okubo and R. E. Marshak, Ann. Phys. (N.Y.) 4, 166 (1958) define  
 the most general two-nucleon potential in terms of the position,  
 momentum, spin, and isospin operators. This formulation and the  
 matrix formulation  $V_{LL}^{\alpha}(k, k')$  of the most general two-nucleon inter-  
 action are equivalent.
39. J. M. Blatt and L. C. Biedenharn, Phys. Rev. 86, 399 (1952).

## References continued

40. For coupled channels, the Lippmann-Schwinger equation becomes two sets of two coupled integral equations. The first set couples the solutions for  $R_{J-1, J-1}^\alpha(k, k_0)$  with those of  $R_{J+1, J-1}^\alpha(k, k_0)$ , while the second set couples the solutions for  $R_{J-1, J+1}^\alpha(k, k_0)$  with those of  $R_{J+1, J+1}^\alpha(k, k_0)$ .
41. R. G. Newton, Scattering Theory of Waves and Particles (McGraw-Hill Book Co., New York, (1966)); M. Bertera et al., Nucl. Phys. Al13, 625 (1968).
42. M. Scadron and S. Weinberg, Phys. Rev. 133B, 1589 (1964) provide an alternative to matrix inversion for solving the Lippmann-Schwinger equation for potentials with a bound state. Their method, however, is not as direct as the one we describe.
43. M. Wada, Progr. Theor. Phys. 37, 763 (1967).
44. P. S. Signell, Progr. Theor. Phys. 22, 492 (1959).
45. M. H. Kalos and R. H. Dalitz, Phys. Rev. 100, 1515 (1955).
46. H. P. Noyes, Phys. Rev. Letters 15, 538 (1965). The method used in this paper to eliminate the singularity at  $k' = k_0$  in the Lippmann-Schwinger equation is essentially the same as in references 43-45. Our method is slightly different and more direct.
47. M. Abramowitz and I. A. Stegun, Handbook of Mathematical Functions (National Bureau of Standards Applied Mathematics Series 55, Washington, D. C., 1965), 3rd Printing, p. 890, 923; H. E. Salzer and R. Zucker, Bull. Am. Math. Soc. Volume 55, No. 10, 1004 (1949). The latter reference has the correct expression for the LaGuerre weights, while the former reference has an incorrect expression on p. 890.

## References continued

48. The methods used in references 43-46 eliminate the singularity at  $k' = k_0$  by defining  $N_{LL}^{\alpha}(k, k_0) = D_L^{\alpha}(k_0)R_{LL}^{\alpha}(k, k_0)$  and deriving a non-singular integral equation for N. This method is a two-step process because once N is determined, D must be calculated to determine R. Our method is more direct because we solve for R in one step. The methods in references 43-46 also restrict  $k_0$  to be one of the grid points.
49. G. E. Brown, A. D. Jackson and T. T. S. Kuo (to be published) verify the accuracy and convergence of the direct matrix inversion method, which we suggested to them.
50. J. Goldstone, Proc. Roy. Soc. (London) A239, 267 (1957).
51. H. A. Bethe, B. H. Brandow and A. G. Petschek, Phys. Rev. 129, 225 (1963). We refer to this paper as BBP.
52. N. M. Hugenholtz, Physica 23, 481 (1957). This paper shows that the contribution to the ground-state energy of diagrams with n unlinked parts is approximately proportional to  $A^n$ .
53. Here  $\omega$  is equal to the starting energy  $E_\mu + E_\nu$ . For this case,  $\omega$  is said to be on the energy shell. Higher order terms in the Brueckner-Goldstone expansion involve off-energy-shell propagation, i.e.,  $\omega$  may not be equal to the starting energy.
54. L. C. Gomez, J. D. Walecka and V. F. Weisskopf, Ann. Phys. (N.Y.) 3, 241 (1958). This paper gives a particularly clear explanation of "healing".
55. R. Rajaraman, Phys. Rev. 131, 1244 (1963).
56. H. A. Bethe, Phys. Rev. 138, B804 (1965).
57. B. D. Day, Rev. Mod. Phys. 39, 719 (1967).

## References continued

58. L. D. Faddeev and Z. Eksperim, Soviet Phys.-JETP 12, 1014 (1961).
59. G. Dahl, E. Ostgaard and B. Brandow, Nucl. Phys. A124, 481 (1969).
60. R. Rajaraman and H. A. Bethe, Rev. Mod. Phys. 39, 745 (1967).
- Consult this paper for other references.
61. B. S. Bhaker and R. J. McCarthy, Phys. Rev. 169, 1343 (1967).
62. B. H. Brandow, Rev. Mod. Phys. 39, 771 (1967);  
     E. Ostgaard (to be published) indicates that for liquid He<sup>3</sup>,  $\kappa \approx .25$ .
63. E. J. Irwin, Ph.D. thesis, Cornell University (1963).
64. E. L. Lomon and M. McMillan, Ann. Phys. (N.Y.) 23, 439 (1963).
65. The class of hole-bubble diagrams is the class of diagrams cancelled by the proper choice of the hole-spectrum, according to BBP. The class of hole-bubble diagrams, therefore, is not included in calculations of the contributions of three-body diagrams.
66. The -1 MeV contribution of three-body diagrams is rather small considering that the first order potential energy for the Reid hard-core potential is -33 MeV. With  $.15 \leq K \leq .20$  a 5 to 7 MeV contribution from three-hole-line diagrams would have been expected. Actually, the -1 MeV total results from the near cancellation of fairly large attractive and repulsive terms. Whether this near cancellation is peculiar to hard-core potentials is not known. Further investigations of three-body terms for potentials other than hard-core potentials are necessary. Also, the -1 MeV figure resulted from certain assumptions concerning the tensor force. Since the tensor force (we shall see) is quite important in nuclear saturation, a more careful treatment of the tensor force is essential for the accurate evaluation of three-body terms.

## References continued

67. S. Coon and J. Dabrowski. Phys. Rev. 140, B287 (1965).
68. S. A. Moszkowski and B. L. Scott, Ann. Phys. (N.Y.) 11, 225 (1960).
69. H. S. Köhler, Ann. Phys. (N.Y.) 16, 375 (1961).
70. We could reduce our error in calculating the G matrix by dividing the infinite integration grid into two regions - one for  $\sqrt{k_F^2 - k'^2} \leq k' \leq k_F + K$  and one for  $k' > k_F + K$ . We then could apply an integration formula to each grid, sum, and matrix invert. This procedure would require us to calculate the entire matrix  $V_{LL}^\alpha(k, k')$  for different sets of values of  $k, k'$  for each different value of  $K$  that appears in the calculation. Because we obtained very accurate total binding energies without resorting to this procedure, we rejected it as too costly.
71. R. J. McCarthy and H. S. Köhler, Nucl. Phys. A99, 55 (1967).
72. H. S. Köhler and R. J. McCarthy, Nucl. Phys. A106, 313 (1967).
73. L. Puzikov, R. Rydin and J. Smorodinsky, Nucl. Phys. 3, 436 (1957).
74. R. E. Seamon, K. A. Friedman, G. Breit, R. D. Haracz, J. M. Holt and A. Prakash, Phys. Rev. 165, 1579 (1968).
75. There are indications that the formula  $e_1(k) \approx \sqrt{2} Qk^2$  gives better results for the deuteron electric quadrupole moment  $Q$  than the earlier formula  $e_1(k) = \sqrt{2} (1 - k_B r_{\text{ot}})^2 Qk^2$ . The reliability of either formula, however, has not been fully proven and our electric quadrupole moments are subject to future correction.
76. The errors in the measurement of the phase-parameters in reference 74 are given in the Yale phase-parameterization, while we employ the Blatt-Biedenharn phase-parameterization. The uncertainty in  $\rho_1$

## References continued

- in the Yale parameterization is .017 for 0-69 MeV, .022 for 69-155 MeV, .115 for 155-275 MeV, and .1321 for 275-350 MeV. The uncertainties in  $\epsilon_1$  are probably of the same order as the uncertainties in  $p_1$ .
77. C. W. Nestor, K. T. R. Davies, S. J. Krieger and M. Baranger, Nucl. Phys. 113, 14 (1968).
78. In our nuclear matter studies, we employ the Reid soft-core potential, where available for  $J \geq 3$  because of its accurate phase-shift fits. Otherwise, we employ the OPEP tail of the Reid soft-core potential.
79. W. B. Riesenfeld and K. M. Watson, Phys. Rev. 104, 492 (1956); N. Fukuda and R. Newton, Phys. Rev. 103, 1558 (1956).  
 One kind of phase-shift approximation in nuclear matter consists of replacing  $G_{LL}^{\alpha}(k, k_0, k_0)$  with  $R_{LL}^{\alpha}(k_0, k_0)$  in the evaluation of the total binding energy. This approximation handles the hard-core properly, but ignores the Pauli exclusion principle.
80. A. Kallio, Phys. Letters 18, 51 (1965).
81. J. P. Elliott, H. A. Mavromatis and E. A. Sanderson, Phys. Letters 24B, 358 (1967).
82. K. Appel, Z. Physik 219, 447 (1969).
83. Sometimes we refer to  $F_{LL}^{\alpha}(k)$  as the Fourier transform of the wave function defect, or just the wave-function defect. The function  $F_{LL}^{\alpha}(k)$  is related to the wave-function defect in momentum space by
- $$F_{LL}^{\alpha}(k) = \frac{\pi}{2} k \chi_{LL}^{\alpha}(k).$$

## References continued

84. In all figures the following abbreviations are used:  
A-Force A, B-Force B, R-Reid soft-core potential, BS-Bryan-Scott potential, AP-Appel potential.
85. An alternate way to handle higher partial waves is the phase-shift approximation. See reference 87.
86. P. C. Bhargava and D. W. L. Sprung, Ann. Phys. (N.Y.) 42, 222 (1967).
87. D. W. L. Sprung, P. K. Banerjee, A. M. Jopko and M. K. Srivastava, McMaster University preprint (1969), calculate the contributions for  $J \geq 3$  in the phase-shift approximation. Their total comes to  $.7 \pm .25$  MeV instead of their previous 2.26 MeV total. Their new result disagrees with our result by 1 to 1.5 MeV, most of which comes from the  $^3D_3$  state contribution. The disagreement in the  $^3D_3$  state results comes about because the OPEP does not satisfactorily reproduce the experimental two-body data in the  $^3D_3$  state.
88. While there may be some evidence for the existence of the  $\sigma_1$  meson, the  $\sigma_0$  is thought to be a means of simulating the S-wave two-pion continuum and excited isobar ( $N^*$ ) effects.
89. We have found this approximation is accurate to within 2 MeV.
90. J. Hamilton and W. S. Woolcock, Rev. Mod. Phys. 35, 737 (1963). This paper gives a value of 14.7 for  $g_\pi^2$  as determined from pion-nucleon scattering. The pion mass in the Bryan-Scott potential is fixed at 138.7 MeV, which is very close to the experimental value.
91. We really should have used this transformation to change  $x_{02}$  instead of  $x_{20}$  to see large changes in the binding energy. Future investigations along these lines are planned.